Copyright

by

Rhutesh Kishorkant Shah

2006

The Dissertation Committee for Rhutesh Kishorkant Shah Certifies that this is the approved version of the following dissertation:

Polymer – Layered Silicate Nanocomposites by Melt Processing

Committee:

Donald R. Paul, Supervisor

Benny D. Freeman

Issac C. Sanchez

Peter F. Green

Desiderio Kovar

Polymer – Layered Silicate Nanocomposites by Melt Processing

by

Rhutesh Kishorkant Shah, B.E.; M.S.

Dissertation

Presented to the Faculty of the Graduate School of

The University of Texas at Austin

in Partial Fulfillment

of the Requirements

for the Degree of

Doctor of Philosophy

The University of Texas at Austin

May 2006

To my father, late Dr. Kishorkant J. Shah, and brother, late Mr. Purvesh K. Shah

Acknowledgements

It has been an eventful journey of four and a half years, during which I have learned a lot and have hopefully contributed a “positive delta” towards the advancement of the field of Polymer Nanocomposites. I am thankful to my advisor, Prof. Don Paul, for introducing me to this fascinating research area and for guiding me through the entire process. His encouragement and constructive criticisms have played a major role not only in this work but in the overall development of my research aptitude. I would also like to express my gratitude to Dr. Benny Freeman, Dr. Issac Sanchez, Dr. Peter Green, and Dr. Desiderio Kovar for serving on my committee and providing useful input at various times.

The work presented in this thesis is a result of several industrial, academic, and personal collaborations. I have had the good fortune of working closely with Southern Clay Products (SCP), Chevron Phillips Chemical Company (CPCC), and Inhance-Fluoroseal Inc. on different projects. The personnel at SCP, with their technical support and prompt supply of custom-designed organoclays, have been a strong ally right from the beginning. In particular, I sincerely appreciate the advice and friendship of Dr. Douglass Hunter and the experimental support of Tony Gonzales, Ben Knesek, and Randy Chapman. Special thanks go to Rajendrakumar (Raj) Krishnaswamy of Chevron Phillips Chemical Company. A former colleague of mine, Raj has been a great collaborator, friend, and guide over the last decade.

Members of the Don Paul research group have been fun to work with, and I have thoroughly enjoyed their companionship and little eccentricities. My discussions and, in some cases, joint projects, with Tim Fornes, Piljoon Yoon, Hyuk-Soo Lee, Do Hoon Kim, Shuichi Takahashi, Florencia Chavarria, Sachio Hotta, Lili Cui, and Holly Stretz have yielded several novel and fruitful ideas. Tim, in particular, was a big help in the initial stages of my Ph.D. program. His camaraderie and alacrity made my transition from industry to graduate school a lot smoother than what I had expected. Besides these, the friendships developed with John Wind, John Sanchez, Jijun Huang, Attaso Khamwichit, Parag Shah, Dmitry Krapchetov, Bharadwaj Narayanan, Megha Surve, and Karthik Sundaram have also resulted in many memorable experiences.

Last, but not least, I am grateful to my parents not only for their love and encouragement, but also for the innumerous sacrifices they have made for my education since childhood. I will always remain indebted to them.

Polymer – Layered Silicate Nanocomposites by Melt Processing

Publication No._____

Rhutesh Kishorkant Shah, Ph.D.

The University of Texas at Austin, 2006

Supervisor: Donald R. Paul

Polymer-layered silicate nanocomposites formed from the organically modified clay mineral montmorillonite and related materials have attracted a great deal of technological and scientific interest in the past decade. These composites offer the promise of greatly improved mechanical, thermal, and barrier properties over those of the matrix polymer owing to the nanoscale reinforcement and constraints of the polymer caused by dispersing the one nanometer thick, high aspect ratio aluminosilicate (clay) layers. The central scientific issue is how to achieve a high level of dispersion, and ultimately full exfoliation of the clay platelets within the polymer matrix since this is necessary to realize the large filler aspect ratios. Although several factors play a role in organoclay exfoliation, it seems to be largely dependent upon a complex array of interactions between the polymer matrix and the organoclay.

Recently, there has been a strong commercial drive for producing such nanocomposites from low cost polymers like polyolefins. Unfortunately, polyolefins are highly inefficient at exfoliating the organoclays by themselves, since there is no favorable interaction with the polar aluminosilicate surface of the clay. Hence, the principal goal of

this research work was to explore the various routes to improve polyolefin-organoclay interactions, and thus, organoclay exfoliation in these systems. Three mutually exclusive strategies were employed to achieve this objective. First, the polyolefin matrix was made more polar by several techniques viz., surface treating the polyolefin particles, grafting of maleic anhydride on the polyolefin backbone, copolymerizing with polar monomers like methacrylic acid, and incorporating ionic groups (ionomers). These modifications resulted in significant improvements in organoclay exfoliation. Second, the organoclay structure was engineered to improve polyolefin-organoclay compatibility. It was determined that surfactants whose structure lead to more shielding of the silicate surface or increased alkyl material within the organoclay galleries result in improved levels of exfoliation. Finally, the melt processing conditions were fine tuned to generate optimum amounts of shear, and reduce thermal degradation of the surfactant during the preparation of nanocomposites. Once sufficient levels of organoclay exfoliation were attained, these materials were tested for barrier film applications.

Table of Contents

List of Tables xiii

List of Figures xv

Chapter 1: Introduction 1

Background 1

Preparation of Nanocomposites 3

Characterization 4

Dissertation scope and organization 6

References 8

Chapter 2: Experimental - Materials and Techniques 12

Materials 12

Experimental 17

Melt Processing 17

Testing and Characterization 19

Evaluation of Mechanical Properties 19

Wide Angle X-ray Scattering (WAXS) 20

Transmission Electron Microscopy and Particle Analysis 20

References 22

Chapter 3: Nylon 6 Nanocomposites Prepared by a Melt Mixing Masterbatch Process 23

Experimental 25

Results and Discussion 29

Mechanical Properties 29

Characterization 33

Processability 40

Conclusions 44

References 45

Chapter 4: Polyethylene-Organoclay Nanocomposites: Effect of Matrix Modification on Organoclay Exfoliation 47

Experimental 48

Results 50

HDPE vs. HDPE-g-MA 50
Morphology 50
Mechanical properties 52
LDPE vs. poly(ethylene-co-methacrylic acid) 53
Morphology 53
Mechanical properties 55
LDPE vs. poly(ethylene-co-methacrylic acid) ionomer 58
Morphology 58
Mechanical properties 61
Conclusions 64
References 64

Chapter 5: Comparison of nanocomposites made from sodium, zinc, and lithium ionomers of poly(ethylene-co-methacrylic acid) 66
Experimental 66
Results 68
Processability and rheology 68
TEM and particle analysis 72
Mechanical properties 78
WAXS analysis 84
Discussion 87
Conclusions 90
References 91

Chapter 6: Nanocomposites from fluoro-oxygenated polyethylene: a novel route to organoclay exfoliation 93
Experimental 93
Results and Discussion 95
Morphological Characterization using TEM and Particle Analysis 95
WAXS Analysis of Nanocomposites 101
Mechanical Properties 105
Conclusions and future work 108
References 109

Chapter 7: Nanocomposites from Ethylene/ Methacrylic acid Ionomers: Effect of Surfactant Structure on Morphology and Properties 110
Experimental 111
Results 113
Stress-Strain Analysis 113
Effect of the number of long alkyl groups 117
Effect of hydroxy-ethyl versus methyl groups 121
Effect of the length of the surfactant alkyl tail 124
Effect of the level of organic loading (MER comparison) 127
Saturated tallow effects 129
Effect of quaternary vs. tertiary ammonium treatments 131
WAXS Analysis 132
Izod Impact measurements 135
Discussion 136
Conclusions 141
References 142

Chapter 8: Organoclay degradation in melt processed polyethylene nanocomposites 143
Experimental 144
Results 146
Organoclay degradation characterized by WAXS analysis 146
Effect of organoclay degradation on mechanical properties 151
Thermogravimetric analysis (TGA) of pristine organoclays 154
Discussion 160
Conclusions 164
References 165

Chapter 9: Blown films of nanocomposites prepared from LDPE and poly(ethylene-co-methacrylic acid) ionomers 167
Experimental 167
Results and discussion 169
Rheology of nanocomposites 169
Visual morphology of blown-films 170
Mechanical properties of blown-films 170

Tensile modulus 172
Tensile stress at break 176
Tensile strain at break 179
Puncture resistance 182
Resistance to tear propagation 183
Barrier properties 186
Steady-state gas permeation properties 186
Comparison of permeation data with theoretical models 191
Conclusions 194
References 195
Chapter 10: Conclusions and recommendations 197
Conclusions 198
Recommendations 201
Modifications of polyethylene 201
Organoclay structure 202
Processability 203
Morphology of the base (unmodified) polyethylene 204
References 205
Bibliography 207
Vita 214

List of Tables

Table 2.1 Polymers used in this research work....13

Table 2.2 Organoclays used in this study. 16

Table 3.1 Summary of nylon 6/ $M_3C_{18})_1$ organoclay nanocomposites prepared in this study....28

Table 3.2 Selected mechanical properties of nylon 6/$M_3(C_{18})_1$ organoclay nanocomposites....31

Table 3.3 Relative melt viscosity....41

Table 4.1 Polymers used in this study....48

Table 4.2 Selected mechanical properties of nanocomposites prepared from HDPE and HDPE-g-MA....52

Table 4.3 Select mechanical properties of nanocomposites prepared from LDPE and Nucrel® polymers. 56

Table 5.1 Results of particle analysis....74

Table 5.2 Selected mechanical properties of nanocomposites prepared by melt mixing $M_2(HT)_2$ organoclay and ionomers of poly(ethylene-co-methacrylic acid) 79

Table 6.1 Particle analysis results....97

Table 6.2 Selected mechanical properties of nanocomposites prepared in this study....104

Table 7.1 Select mechanical properties of nanocomposites formed from Surlyn® 8945 and various organoclays....114

Table 8.1 Amount of surfactant loss from $M_3(HT)_1$ organoclay during nanocomposite extrusion and thermogravimetric analysis of the organoclay.....160

Table 9.1 Selected mechanical properties of the blown-films examined in this study 171

Table 9.2 Improvement in tensile modulus of blown-films prepared from nanocomposites of LDPE and poly(ethylene-co-methacrylic acid) containing 3 wt% MMT relative to modulus of blown films produced using identical processing conditions from the corresponding unfilled polymers. 174

Table 9.3 Gas permeability data of selected blown films evaluated in this study 187

Table 9.4 Particle aspect ratio calculated by comparison of experimental permeation data with the two composite theories.....193

List of Figures

Figure 1.1 Atomic structure of sodium montmorillonite 2

Figure 1.2 Ion exchange reaction between sodium montmorillonite clay and an amine surfactant producing an organophilic clay (organoclay).....3

Figure 1.3 TEM and WAXD characterization of polymer organoclay composites with different morphologies.....5

Figure 2.1 Molecular structure of organic ammonium ion surfactants exchanged onto montmorillonite clay. The symbols M = methyl, H = hydrogen, T = tallow, (HT) = hydrogenated tallow, (HE) = 2-hydroxy-ethyl, and C^* = coconut oil.....15

Figure 2.2 Overview of the experimental process.....17

Figure 2.3 Illustration of the X-ray beam path and the location of TEM samples.....20

Figure 3.1 Schematic of the strategy employed for preparing nylon 6 based nanocomposites with good exfoliation and processability. 25

Figure 3.2 Comparison of tensile modulus of nanocomposites prepared from high molecular weight (HMW) nylon 6 and trimethyl-hydrogenated tallow quaternary ammonium chloride ($M_3(HT)_1$) versus octadecyltrimethyl ammonium chloride ($M_3(C_{18})_1$). 26

Figure 3.3. (a) Effect of montmorillonite content on the tensile modulus of nanocomposites prepared from four masterbatches containing different MMT concentrations (b) Tensile modulus of nanocomposites containing 2.0 wt% MMT (triangles) , 4.0 wt% MMT (circles), and 6.5 wt% MMT (squares are plotted as a function of the MMT content of the masterbatch they were made from (bottom axis). Data for nanocomposites made directly from HMW nylon 6 only (unfilled symbols) and LMW nylon 6 only (gray symbols) are plotted versus the top axis for comparison. 30

Figure 3.4 Yield strength of nanocomposites containing 2.0 wt% MMT (triangles), and 4.0 wt% MMT (circles) are plotted as a function of the MMT content of the masterbatch they were made from (bottom axis). Data for nanocomposites made directly from HMW nylon 6 only (unfilled symbols) and LMW nylon 6 only (gray symbols) are plotted versus the top axis for comparison. 32

Figure 3.5 Elongation at break of nanocomposites containing 2.0 wt% MMT (triangles), 4.0 wt% MMT (circles), and 6.5 wt% MMT (squares) are plotted as a function of the MMT content of the masterbatch they were made from (bottom axis), measured at crosshead speeds of (a) 0.51 cm/min and (b) 5.1 cm/min. Data for nanocomposites made directly from HMW nylon 6 only (unfilled symbols) and LMW nylon 6 only (gray symbols) are plotted versus the top axis for comparison. 34

Figure 3.6 WAXD patterns for $M_3(C_{18})_1$ organoclay and $M_3(C_{18})_1$ organoclay nanocomposite masterbatches based on HMW nylon 6 containing 20, 14, 8.25, and 6.5 wt% montmorillonite. The curves are shifted vertically for clarity. 35

Figure 3.7 WAXD patterns for $M_3(C_{18})1$ organoclay nanocomposites containing (a) ~ 2 wt% (b) ~4 wt%, and (c) ~6.5 wt% montmorillonite based on HMW nylon 6, LMW nylon 6, and a diluted masterbatch. WAXD patterns of organoclay and the parent masterbatch (~20 wt% MMT) are plotted for comparison. The curves are shifted vertically for clarity. 38

Figure 3.8 TEM micrographs of nanocomposites containing ~2.0 wt% montmorillonite based on (a) HMW nylon 6, (b) HMW masterbatch containing ~20 wt% montmorillonite diluted down with LMW, and (c) LMW nylon 6.....39

Figure 3.9 Brabender torque at 10 min (steady state), for nylon 6-montmorillonite nanocomposites containing ~2.0 and ~6.5 wt% montmorillonite, prepared by diluting HMW nylon 6 masterbatches with LMW nylon 6. The torque values for HMW-LMW nylon 6 mixes (no organoclay added) are plotted for comparison. 41

Figure 3.10 The trade-off between tensile modulus and Brabender torque, a measure of melt viscosity or processability, of nylon 6-montmorillonite nanocomposites containing (a) 2.0 wt% MMT, and (b) 6.5 wt% MMT prepared using a masterbatch approach. 43

Figure 4.1 TEM micrographs of nanocomposites prepared from $M_2(HT)_2$-95 organoclay and (a) unmodified HDPE, and (b) maleic anhydride grafted HDPE (HDPE-g-MA). The concentration of MMT in both cases is ~5 wt%. 51

Figure 4.2 WAXS patterns of nanocomposites prepared from $M_2(HT)_2$-95 organoclay and the two HDPE based matrices. The concentration of MMT in both cases is ~5 wt%. X-ray pattern of $M_2(HT)_2$-95 organoclay is plotted for comparison. The curves are shifted vertically for clarity. 51

Figure 4.3 (a) Tensile modulus, and (b) Relative modulus of nanocomposites prepared from unmodified HDPE and maleic anhydride grafted HDPE (HDPE-g-MA).....53

Figure 4.4 WAXS patterns of $M_2(HT)_2$-95 organoclay based nanocomposites prepared from LDPE and two ethylene/methacrylic acid copolymers (Nucrels®).....54

Figure 4.5 Tensile modulus of nanocomposites prepared from LDPE and Nucrel® 0403 plotted as a function of their montmorillonite content.....57

Figure 4.6 Relative modulus of nanocomposites prepared from Nucrel® 0903, and Nucrel® 0403 plotted as a function of their montmorillonite concentration.....57

Figure 4.7 TEM micrographs of nanocomposites prepared from LDPE and Surlyn® 8945 ionomer using a one-tailed organoclay (a, d), two-tailed organoclay (b, e), and a three-tailed organoclay (c,f).....59

Figure 4.8 WAXS patterns of nanocomposites prepared from LDPE and Surlyn® 8945 ionomer using a one-tailed organoclay, $M_3(HT)_1$, a two-tailed organoclay, $M_2(HT)_2$-95, and a three-tailed organoclay, $M_1(C_{16})_3$. The curves are shifted vertically for clarity. 62

Figure 4.9 Tensile modulus of nanocomposites prepared from (a) LDPE and (b) Surlyn® 8945 ionomer using one-tailed, two-tailed, and three-tailed organoclays. 63

Figure 4.10 Relative modulus of nanocomposites prepared from LDPE and the ionomer using a one-tailed organoclay, $M_3(C_{16})_1$, and a three-tailed organoclay, $M_1(C_{16})_3$. 63

Figure 5.1 The electrical current drawn by the extruder motor during extrusion of the various nanocomposites based on ionomers of ethylene/methacrylic acid copolymers. The feed (polymer + organoclay) rate in all cases is 800 g/hr. 69

Figure 5.2 The axial forces generated by (a) the ionomers, and (b) nanocomposites containing 10 wt% MMT prepared from these ionomers, when sheared at 190 ^oC using a screw speed of 100 rpm in a DSM micro-compounder. 71

Figure 5.3 TEM micrographs of nanocomposites prepared from $M_2(HT)_2$-95 organoclay and (a) lithium, (b) sodium, and (c) zinc ionomers of poly(ethylene-co-methacrylic acid). The concentration of MMT in all three cases is ~5 wt%. Sections were microtomed from the core portion of an Izod bar in a plane parallel to the flow direction but perpendicular to the major face.....73

Figure 5.4 Histograms of MMT particle length obtained by analyzing TEM micrographs of nanocomposites containing ~5 wt% MMT prepared from (a) lithium, (b) sodium, and (c) zinc ionomers of poly(ethylene-co-methacrylic acid). 75

Figure 5.5 Histograms of MMT particle thickness obtained by analyzing TEM micrographs of nanocomposites containing ~5 wt% MMT prepared from (a) lithium, (b) sodium, and (c) zinc ionomers of poly(ethylene-co-methacrylic acid). 76

Figure 5.6 Representative stress-strain diagrams of nanocomposites prepared from $M_2(HT)_2$ organoclay and (a) lithium, (b) sodium, and (c) zinc ionomers of poly(ethylene-co-methacrylic acid). 80

Figure 5.7 (a) Tensile modulus and (b) Relative modulus of nanocomposites prepared from lithium, sodium, and zinc ionomers of poly(ethylene-co-methacrylic acid). 82

Figure 5.8 Elongation at break measured at a crosshead speed of 5.1 cm/min for nanocomposites prepared from lithium, sodium, and zinc ionomers of poly(ethylene-co-methacrylic acid).....84

Figure 5.9 WAXS patterns of nanocomposites prepared from $M_2(HT)_2$ organoclay and the three ionomers. The concentration of MMT in all cases is ~5 wt%. X-ray pattern of the $M_2(HT)_2$ organoclay is plotted for comparison, and is shifted vertically for clarity. The dotted vertical line shows the position of the d_{001} peak of the organoclay. 85

Figure 5.10 WAXS patterns of nanocomposites prepared from $M_2(HT)_2$ organoclay and (a) lithium, (b) sodium, and (c) zinc ionomers of poly(ethylene-co-methacrylic acid). The dotted vertical line showing the position of the d_{001} peak of the $M_2(HT)_2$ organoclay is included for comparison. The curves are shifted vertically for clarity.....86

Figure 5.11 Schematic of the proposed ion-exchange process between the ionomer and the organoclay which subsequently leads to a reduction in the d-spacing of the nanocomposites prepared from the lithium ionomer. 90

Figure 6.1 TEM micrographs of nanocomposites prepared from $M_2(HT)_2$-95 organoclay and (a) unmodified HDPE, (b) surface treated HDPE (ST-HDPE), and (c) maleic anhydride grafted HDPE (HDPE-g-MA). The concentration of MMT in all three cases is ~5 wt%. 96

Figure 6.2 Histograms of MMT particle length obtained by analyzing TEM micrographs of nanocomposites containing ~5 wt% MMT prepared from (a) unmodified HDPE, (b) surface treated HDPE (ST-HDPE), and (c) maleic anhydride grafted HDPE (HDPE-g-MA). 98

Figure 6.3 Histograms of MMT particle thickness obtained by analyzing TEM micrographs of nanocomposites containing ~5 wt% MMT prepared from (a) unmodified HDPE, (b) surface treated HDPE (ST-HDPE), and (c) maleic anhydride grafted HDPE (HDPE-g-MA). 99

Figure 6.4 WAXS patterns of nanocomposites prepared from $M_2(HT)_2$ organoclay and the three HDPE based matrices. The concentration of MMT in all cases is ~5 wt%. X-ray pattern of the $M_2(HT)_2$ organoclay is plotted for comparison. The curves are shifted vertically for clarity. 102

Figure 6.5 WAXS patterns of nanocomposites prepared from $M_2(HT)_2$ organoclay and (a) unmodified HDPE (b) surface treated HDPE (ST-HDPE), and (c) maleic anhydride grafted HDPE (HDPE-g-MA). X-ray pattern of the $M_2(HT)_2$ organoclay is plotted for comparison. The curves are shifted vertically for clarity. 103

Figure 6.6 (a) Tensile modulus, and (b) Relative modulus of nanocomposites prepared from unmodified HDPE, surface treated HDPE (ST-HDPE), and maleic anhydride grafted HDPE (HDPE-g-MA). 106

Figure 6.7 Elongation at break measured at crosshead speeds of (a) 0.51 cm/min and (b) 5.1 cm/min for nanocomposites prepared from unmodified HDPE, surface treated HDPE (ST-HDPE), and maleic anhydride grafted HDPE (HDPE-g-MA). 107

Figure 6.8 Izod impact strength of (a) gate end, and (b) far end samples of nanocomposites prepared from unmodified HDPE, surface treated HDPE (ST-HDPE), and maleic anhydride grafted HDPE (HDPE-g-MA). 108

Figure 7.1 Organoclays used to evaluate the effect of structural variations of the amine cations on nanocomposite morphology and properties 112

Figure 7.2 Stress-strain diagrams of nanocomposites prepared from poly(ethylene-co-methacrylic acid) ionomer and (a) $(HE)_2M_1C^*_1$ and (b) $M_2(HT)_2$-140 organoclays measured at a crosshead speed of 5.1 cm/min. 115

Figure 7.3 Variation in the 'experimental strain hardening coefficient' α with clay concentration for nanocomposites prepared from $(HE)_2M_1C^*_1$ and $M_2(HT)_2$-140 organoclays. 116

Figure 7.4 TEM micrographs comparing the morphology of nanocomposites prepared from (a) a one-tailed organoclay, $M_3(HT)_1$, (b) two- tailed organoclay, $M_2(HT)_2$-95, (c) one-tailed organoclay, $M_3(C_{16})_1$, and (d) three tailed organoclay, $M_1(C_{16})_3$. The concentration of MMT in all cases is 2.5 wt%. 118

Figure 7.5 (a) Tensile modulus, (b) yield strength, and (c) elongation at break of nanocomposites of poly(ethylene-co-methacrylic acid) ionomer showing the effect of the number of organoclay alkyl tails on nanocomposite mechanical properties. 119

Figure 7.6 Schematic illustration of the proposed differences in interactions between the polymer and the organoclay in the case of a one-tailed organoclay ($M_3(HT)_1$), and a two-tailed organoclay ($M_2(HT)_2$). 120

Figure 7.7 TEM micrographs showing the morphology of nanocomposites formed from poly(ethylene-co-methacrylic acid) ionomer and the organoclays $(HE)_2M_1T_1$ and M_3T_1. The concentration of MMT in both cases is 5.0 wt%. 122

Figure 7.8 (a) Tensile modulus, (b) yield strength, and (c) elongation at break of nanocomposites of poly(ethylene-co-methacrylic acid) ionomer showing the effect of 2-hydroxy-ethyl versus methyl groups on nanocomposite mechanical properties. 123

Figure 7.9 Schematic illustration of proposed interactions between the silicate surface and the amine surfactants in the case of $(HE)_2M_1T_1$ and M_3T_1 organoclays. 124

Figure 7.10 TEM micrographs showing the morphology of nanocomposites formed from poly(ethylene-co-methacrylic acid) ionomer and the organoclays $(HE)_2M_1T_1$ and $(HE)_2M_1C^*_1$. The concentration of MMT in both cases is 5.0 wt%. 125

Figure 7.11 (a) Tensile modulus, (b) yield strength, and (c) elongation at break of nanocomposites of poly(ethylene-co-methacrylic acid) ionomer showing the effect of the length of the alkyl tail on nanocomposite mechanical properties. 126

Figure 7.12 TEM micrographs showing the morphology of nanocomposites formed from poly(ethylene-co-methacrylic acid) ionomer and the organoclays $M_2(HT)_2$-95 and $M_2(HT)_2$-140. The concentration of MMT in both cases is 2.5 wt%. 128

Figure 7.13 (a) Tensile modulus, (b) yield strength, and (c) elongation at break of poly(ethylene-co-methacrylic acid) ionomer showing the effect of MER loading on nanocomposite mechanical properties.....128

Figure 7.14 TEM micrographs showing the morphology of nanocomposites formed from poly(ethylene-co-methacrylic acid) ionomer and the organoclays $M_3(HT)_1$ and M_3T_1. The concentration of MMT in both cases is 2.5 wt%. 130

Figure 7.15 (a) Tensile modulus and (b) yield strength of nanocomposites of poly(ethylene-co-methacrylic acid) ionomer showing the effect of alkyl saturation on nanocomposite mechanical properties.....130
Figure 7.16 (a) Tensile modulus and (b) yield strength of nanocomposites of poly(ethylene-co-methacrylic acid) ionomer showing the effect of quaternary vs. tertiary amines on nanocomposite mechanical properties. 131
Figure 7.17 WAXD patterns of the skin (surface) of injection molded nanocomposites formed from poly(ethylene-co-methacrylic acid) ionomer and various organoclays. The concentration of MMT in all cases is 5.0 wt%. Curves are shifted vertically for clarity. 133
Figure 7.18 WAXD patterns of the skin (surface) of nanocomposites formed from poly(ethylene-co-methacrylic acid) ionomer (full curves) and the corresponding organoclays used to prepare them (dotted curves). The concentration of MMT in all cases is 5.0 wt%. The curves are shifted vertically for clarity. 134
Figure 7.19 WAXD patterns of the core of nanocomposites formed from poly(ethylene-co-methacrylic acid) ionomer and various organoclays. The concentration of MMT in all cases is 5.0 wt%. The curves are shifted vertically for clarity.....134
Figure 7.20 Izod impact strength as a function of montmorillonite content for nanocomposites formed from poly(ethylene-co-methacrylic acid) ionomer and $(HE)_2M_1T_1$ organoclay.....136

Figure 7.21 Relative modulus (E/E_m) as a function of MMT content for nanocomposites formed from poly(ethylene-co-methacrylic acid) ionomer and various organoclays. 137
Figure 7.22 Tensile modulus versus organoclay d-spacing for nanocomposites formed from poly(ethylene-co-methacrylic acid) ionomer and various organoclays. 138
Figure 7.23 Izod impact strength versus organoclay d-spacing for nanocomposites formed from poly(ethylene-co-methacrylic acid) ionomer and various organoclays at (a) 2.5 wt% MMT and (b) 10 wt% MMT 139
Figure 7.24 Yield strength versus tensile modulus for nanocomposites formed from poly(ethylene-co-methacrylic acid) ionomer and various organoclays 140
Figure 8.1 WAXS patterns of injection molded samples of LDPE nanocomposites prepared from (a) $M_3(HT)_1$ and (b) $M_2(HT)_2$ organoclays at various extrusion temperatures (ET). X-ray scans of the organoclays are also plotted for comparison. The concentration of MMT in all cases is about 5 wt%. The curves are shifted vertically for clarity.....147
Figure 8.2 WAXD patterns of injection molded samples of LDPE nanocomposites with different montmorillonite contents prepared from (a) $M_3(HT)_1$ and (b) $M_2(HT)_2$ organoclays. The extrusion temperature in all cases is 200 °C. The curves are shifted vertically for clarity.....150

Figure 8.3 Relative modulus (E/E_m) as a function of the extrusion temperature for LDPE (LD 621) nanocomposites prepared from $M_3(HT)_1$ and $M_2(HT)_2$ organoclays. The concentration of MMT in all cases is about 5 wt%.....151

Figure 8.4 Relative modulus (E/E_m) of LD 621- $M_2(HT)_2$ nanocomposites (left axis) is plotted as a function of the extrusion temperature. The data for the melt flow rate of LD 621 (right axis) is plotted against temperature to demonstrate the change in the melt viscosity of the matrix polymer over the same range of temperature. 153

Figure 8.5 Relative modulus (E/E_m) of LDPE-$M_2(HT)_2$ nanocomposites as a function of the melt index of the matrix polymers from which they are formed. Note that there are slight differences in MMT content in the materials that partly account for the trend shown. ...153

Figure 8.6 Isothermal TGA results for pre-dried $M_3(HT)_1$ organoclay obtained in air and nitrogen at 200 °C. 155

Figure 8.7 Isothermal TGA results of (a) $M_3(HT)_1$, (b) $M_2(HT)_2$ and (c) $M_1(C_{16})_3$ organoclays obtained in nitrogen at various temperatures. 156

Figure 8.8 Isothermal TGA results showing the weight percent of surfactant loss from $M_3(HT)_1$, $M_2(HT)_2$ and $M_1(C_{16})_3$ organoclays at (a) 150 °C, (b) 200 °C and (c) 240 °C under nitrogen atmosphere. 157

Figure 8.9 Isothermal TGA results showing the absolute mass loss for $M_3(HT)_1$, $M_2(HT)_2$ and $M_1(C_{16})_3$ organoclays at (a) 150 °C, (b) 200 °C and (c) 240 °C under nitrogen atmosphere. 158

Figure 8.10 Comparison of the surfactant loss from $M_3(HT)_1$ organoclay during nanocomposite extrusion and during thermogravimetric analysis of the organoclay at 200 °C and 240 °C. 161

Figure 8.11 WAXD patterns of injection molded samples of LDPE and polypropylene nanocomposites prepared from $M_3(HT)_1$ organoclay at 200 °C and 240 °C. X-ray scans of $M_3(HT)_1$ and M_4 (tetra methyl ammonium) organoclays are plotted for comparison. The concentration of MMT in all cases is about 5 wt%. The curves are shifted vertically for clarity.....163

Figure 9.1 Complex viscosity of the unfilled polymers and nanocomposites prepared from (a) LDPE, (b) a sodium ionomer of poly(ethylene-co-methacrylic acid), Surlyn® 8945.....170

Figure 9.2 Tensile modulus of blown-films prepared from LDPE and $M_2(HT)_2$-140 organoclay plotted as a function of the montmorillonite content: (a) films with 2:1 BUR tested along the machine direction, (b) films with 2:1 BUR tested along the transverse direction, (c) films with 3:1 BUR tested along the machine direction, (d) films with 3:1 BUR tested along the transverse direction. The X-axis has been extended beyond zero in all graphs for clarity. The dotted lines are trend lines (linear regression lines), and are included to serve as visual guides. 172

Figure 9.3 Tensile modulus of blown-films prepared from Surlyn® ionomer and $M_2(HT)_2$-140 organoclay plotted as a function of the montmorillonite content: (a) films with 2:1 BUR tested along the machine direction, (b) films with 2:1 BUR tested along the transverse direction, (c) films with 3:1 BUR tested along the machine direction, (d) films with 3:1 BUR tested along the transverse direction. The X-axis has been extended beyond zero in all graphs for clarity. 173

Figure 9.4 Tensile stress at break of blown-films prepared from LDPE and $M_2(HT)_2$-140 organoclay plotted as a function of the montmorillonite content: (a) films with 2:1 BUR tested along the machine direction, (b) films with 2:1 BUR tested along the transverse direction, (c) films with 3:1 BUR tested along the machine direction, (d) films with 3:1 BUR tested along the transverse direction. The X-axis has been extended beyond zero in all graphs for clarity. 178

Figure 9.5 Tensile stress at break of blown-films prepared from Surlyn® ionomer and $M_2(HT)_2$-140 organoclay plotted as a function of the montmorillonite content: (a) films with 2:1 BUR tested along the machine direction, (b) films with 2:1 BUR tested along the transverse direction, (c) films with 3:1 BUR tested along the machine direction, (d) films with 3:1 BUR tested along the transverse direction. The X-axis has been extended beyond zero in all graphs for clarity. The dotted lines are trend lines (linear regression lines), and are included to serve as visual guides.....179

Figure 9.6 Tensile strain at break of blown-films prepared from LDPE and $M_2(HT)_2$-140 organoclay plotted as a function of the montmorillonite content: (a) films with 2:1 BUR tested along the machine direction, (b) films with 2:1 BUR tested along the transverse direction, (c) films with 3:1 BUR tested along the machine direction, (d) films with 3:1 BUR tested along the transverse direction. The X-axis has been extended beyond zero in all graphs for clarity. The dotted lines are trend lines (linear regression lines), and are included to serve as visual guides. 180

Figure 9.7 Tensile strain at break of blown-films prepared from Surlyn® ionomer and $M_2(HT)_2$-140 organoclay plotted as a function of the montmorillonite content: (a) films with 2:1 BUR tested along the machine direction, (b) films with 2:1 BUR tested along the transverse direction, (c) films with 3:1 BUR tested along the machine direction, (d) films with 3:1 BUR tested along the transverse direction. The X-axis has been extended beyond zero in all graphs for clarity. The dotted lines are trend lines (linear regression lines), and are included to serve as visual guides.....181

Figure 9.8 Dart impact strength of blown-films prepared from LDPE and $M_2(HT)_2$-140 organoclay plotted as a function of the montmorillonite content: (a) films with 2:1 BUR, (b) films with 3:1 BUR. The X-axis has been extended beyond zero in all graphs for clarity. The dotted lines are trend lines (linear regression lines), and are included to serve as visual guides.....182

Figure 9.9 Dart impact strength of blown-films prepared from Surlyn® ionomer and $M_2(HT)_2$-140 organoclay plotted as a function of the montmorillonite content: (a) films with 2:1 BUR, (b) films with 3:1 BUR. The X-axis has been extended beyond zero in all graphs for clarity. The dotted lines are trend lines (linear regression lines), and are included to serve as visual guides. 183

Figure 9.10 Tear strength of blown-films prepared from LDPE and $M_2(HT)_2$-140 organoclay plotted as a function of the montmorillonite content: (a) films with 2:1 BUR tested along the machine direction, (b) films with 2:1 BUR tested along the transverse direction, (c) films with 3:1 BUR tested along the machine direction, (d) films with 3:1 BUR tested along the transverse direction. The X-axis has been extended beyond zero in all graphs for clarity. The dotted lines are trend lines (linear regression lines), and are included to serve as visual guides. 184

Figure 9.11 Tear strength of blown-films prepared from Surlyn® ionomer and $M_2(HT)_2$-140 organoclay plotted as a function of the montmorillonite content: (a) films with 2:1 BUR tested along the machine direction, (b) films with 2:1 BUR tested along the transverse direction, (c) films with 3:1 BUR tested along the machine direction, (d) films with 3:1 BUR tested along the transverse direction. The X-axis has been extended beyond zero in all graphs for clarity. The dotted lines are trend lines (linear regression lines), and are included to serve as visual guides. 185

Figure 9.12 Relative permeability (P/P_o) plotted as a function of the montmorillonite content of the nanocomposite films prepared from (a) LDPE, and (b) Surlyn® 8945 ionomer. 189

Figure 9.13. Effect of draw down ratio on the barrier properties of blown films prepared from nanocomposites based on LDPE.....190

Figure 9.14 The reciprocal tortuosity factor predicted by two theories as a function of αø. Horizontal lines correspond to experimental values for each gas computed from permeability. Plot (a) is for LDPE nanocomposite with a montmorillonite content of ø = 0.0033, plot (b) is for LDPE nanocomposites with a montmorillonite content of ø = 0.0099, plot (c) is for the Surlyn ionomer nanocomposites with a montmorillonite content of ø = 0.0034, and plot (d) is for the Surlyn ionomer nanocomposite with a montmorillonite content of ø = 0.0104. 192

Chapter 1: Introduction

Polymer-layered silicate nanocomposites represent an emerging filler technology wherein 1 nm thick layered aluminosilicate platelets are used as the reinforcing filler in a polymer matrix [1, 2]. These platelets have high aspect ratios (~ 50-500), large surface areas, and high moduli (~178 GPa) which helps in enhancing a wide range of matrix properties, viz., stiffness and strength [3-6], gas barrier properties [7, 8], dimensional stability [5, 6, 9], solvent and UV resistance [10-12], and flame retardancy [13, 14]. These property enhancements are obtained at extremely low filler concentrations (2-5 vol%), a fraction of what is typically needed in conventional composite materials (10-30 vol%), thus, leading to the development of new, light weight, high performance materials. Recently, there have been published reports of the commercial applications in the automobile industry of such nanocomposites based on nylon 6 and polypropylene [15-17].

BACKGROUND

Polymer layered silicate nanocomposites are typically derived from sodium montmorillonite, which is a member of the 2:1 layered smectite family of clays. These clays consist of a three layered structure as shown in Figure 1. The outer tetrahedral layers containing Si and O atoms are fused to an inner octahedral layer of Al and Mg atoms that are bonded to oxygen or hydroxyl groups. Due to the isomorphous substitution of divalent Mg for trivalent Al, an electrostatic imbalance is created within the clay, resulting in an excess negative charge. The excess negative charge is

counterbalanced by the adsorption of cations like Na+ or Ca++. The thickness of a sodium montmorillonite platelet is approximately 0.96 nm, while its lateral dimensions range from a few nanometers to possibly microns. These platelets are stacked together to form bundles which are of the order of a few microns.

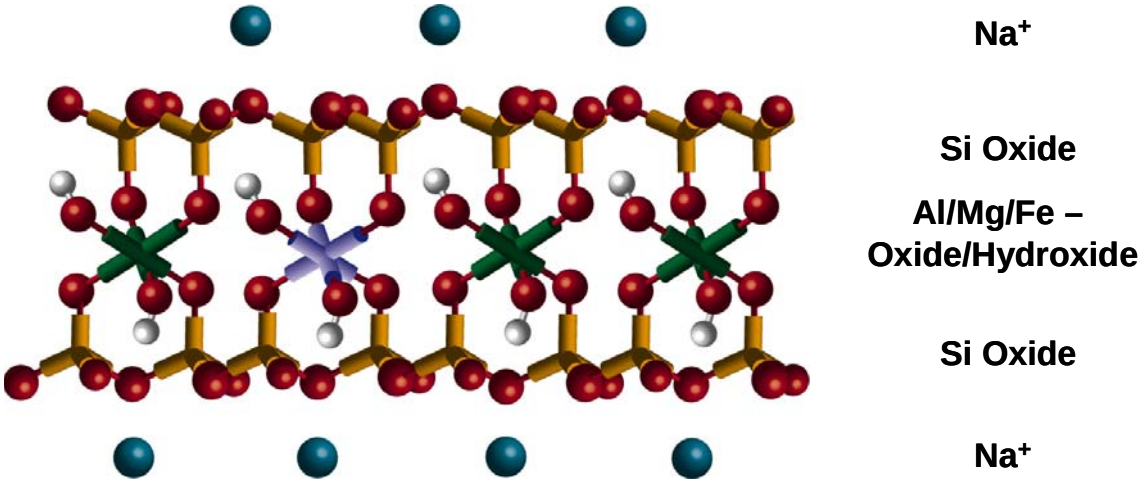

Figure 1.1 Atomic structure of sodium montmorillonite

The central scientific issue is how to delaminate these 1 nm thick aluminosilicate platelets from the bundles and disperse them uniformly in the polymer matrix since this is necessary to achieve large filler aspect ratios which in turn lead to the property enhancements listed above. The first step in this direction is to make the hydrophilic native smectites more organophilic using surfactants. The most commonly used surfactants are quarternary ammonium based cationic surfactants, although, the use phosphonium [18-20] or imidazolium [21-25] based cationic surfactants has also been reported in the literature. When alkyl ammonium surfactants are used, the sodium ions of

sodium montmorillonite are exchanged with alkyl ammonium ions to form a swollen hybrid structure known as 'organoclay' as shown in Figure 2.

Despite the fact that an organoclay is easier to exfoliate than native sodium montmorillonite, additional steps are required to improve organoclay exfoliation in a polymer matrix. The necessary experimental approaches may include (i) optimization of preparation conditions, (ii) selection of appropriate amine surfactants and, (iii) chemical modification of the polymer matrix to improve matrix-organoclay compatibility.

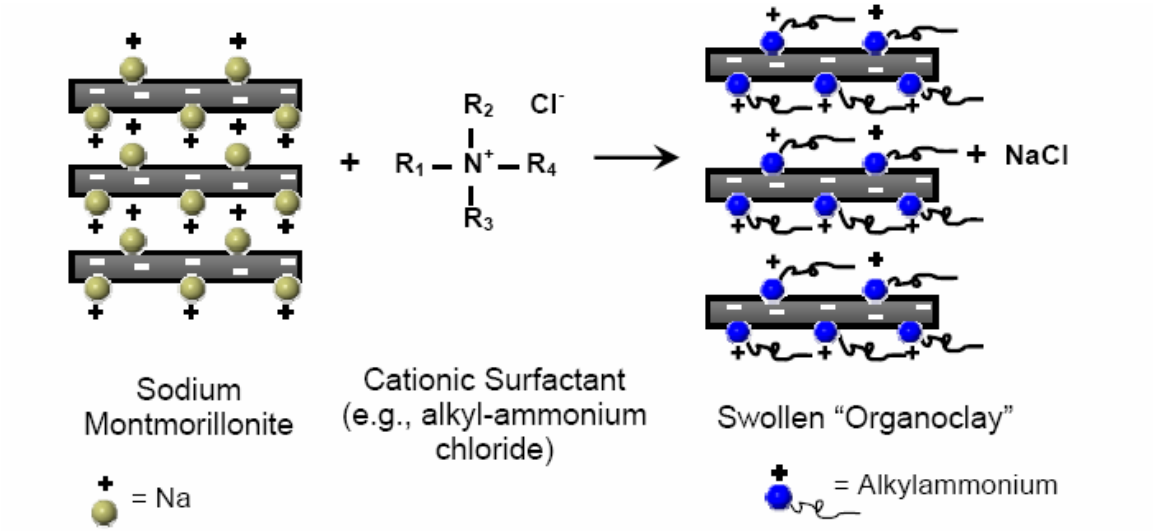

Figure 1.2 Ion exchange reaction between sodium montmorillonite clay and an amine surfactant producing an organophilic clay (organoclay).

Preparation of Nanocomposites

Various techniques have been employed for preparing nanocomposites. These include in situ polymerization [26-29], emulsion polymerization [30, 31], sol-gel templating [32, 33], solid state pulverization [34, 35], melt processing [5, 36, 37], etc. Of these, melt processing is becoming increasingly attractive due to its versatility and

compatibility with existing processing infrastructure. It also shifts the production of nanocomposites further downstream, thereby giving the end-use manufacturers added degrees of freedom with regard to final product specification (e.g., selection of polymer grade, choice of organoclay, level of reinforcement, etc.). Hence, all nanocomposites investigated in this research were prepared using melt processing techniques, the details of which are provided in Chapter 2.

Characterization

The level of exfoliation (or the lack of it) in a clay-polymer composite is most commonly characterized using wide angle X-ray scattering (WAXS), transmission electron microscopy (TEM), and stress-strain analysis. Figure 1.3 illustrates the typical WAXS patterns and their respective transmission electron micrographs for the three broad classifications of nanocomposites: immiscible, intercalated, and exfoliated. In the case of an immiscible system (alternatively known as a microcomposite), where the polymer does not intercalate within the organoclay galleries, the X-ray pattern remains unchanged from that of the pure organoclay. For intercalated composites, where small amounts of polymer diffuse into the organoclay galleries without completely disrupting the ordered structure of the clay bundles, the X-ray pattern reveals a broad intense peak which has shifted to the left (corresponding to larger d-spacings) as compared to that of the pure organoclay. WAXS of exfoliated composites do not show a characteristic basal reflection, since most of the silicate layers are delaminated and uniformly distributed in the polymer matrix.

As one would expect, stress-strain analysis of injection molded nanocomposites also provide a useful comparison between the levels of organoclay exfoliation achieved in various composites. The average particle aspect ratio in a well exfoliated system is higher than that in a less exfoliated system, and this is reflected in the modulus measurements, where a higher increase in stiffness is observed in the case of the former as compared to the latter.

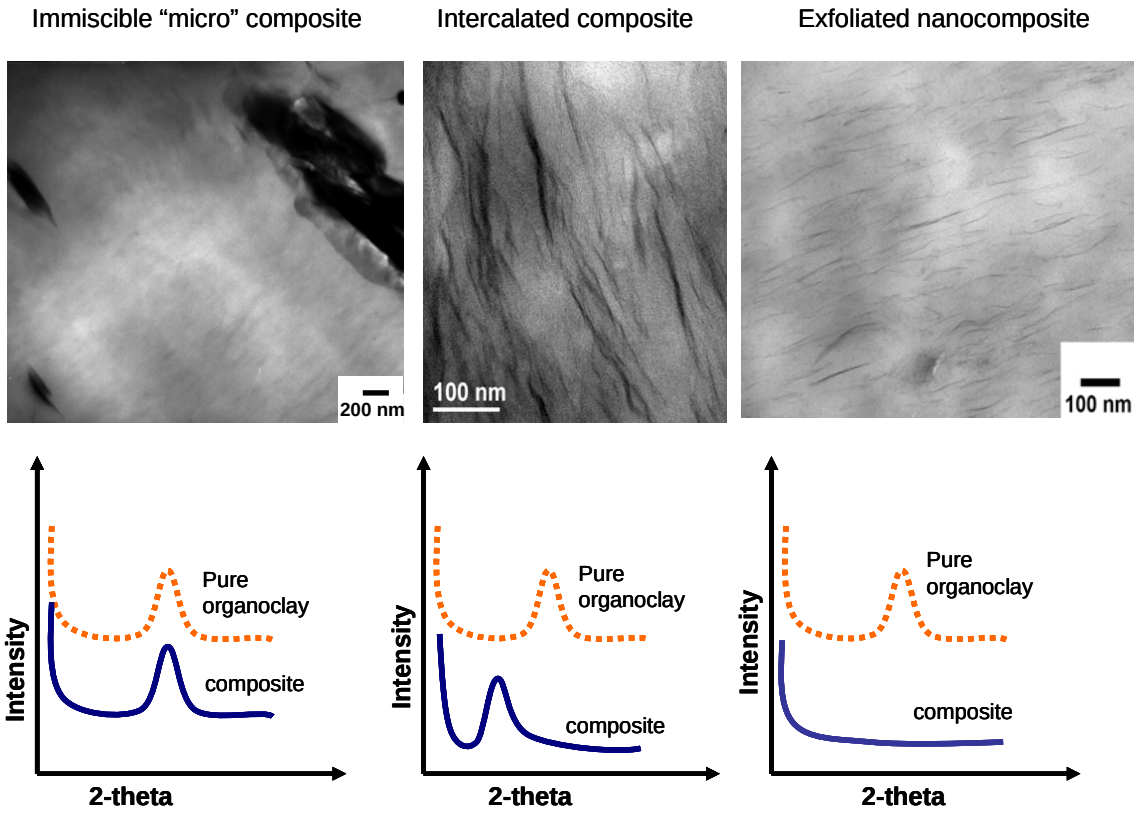

Figure 1.3 TEM and WAXD characterization of polymer organoclay composites with different morphologies

Nylon 6 was the first [38] and is one of the few polymers which readily form well-exfoliated nanocomposites [5, 27, 36]. Although modification of the nylon 6 matrix is not required, research has shown that the choice of the surfactant [39, 40] and processing conditions [41] significantly affect its ability to exfoliate organoclays. On the other hand, non-polar polymers like polyolefins seem incapable of exfoliating the organoclays by themselves, and so, it is necessary to optimize the polymer and organoclay chemistry in addition to processing conditions in order to improve exfoliation.

DISSERTATION SCOPE AND ORGANIZATION

This research was aimed at addressing a number of fundamental and practical issues associated with the formation and applications of polymer-organoclay nanocomposites prepared by melt processing. In the initial stages, efforts were concentrated on polyamide based nanocomposites; however, later on the focus was shifted to nanocomposites prepared from polyethylene type materials. A major part of the investigation was dedicated to improving organoclay exfoliation in these matrices, and exploring the effects of material chemistry and processing conditions on the morphology and properties of such composites. The overall goal was to develop a better understanding of the matrix filler interactions in these systems, which could eventually lead to the formation of well exfoliated nanocomposites on a commercial scale for a variety of applications.

This dissertation is divided into ten chapters. Chapter 2 gives an overview of the experimental techniques employed to form and characterize the nanocomposites investigated in this study. Depending upon the objective and the matrix polymer, there

were slight variations in these techniques, and these variations are described in the corresponding chapters. Chapter 3 deals with nanocomposites prepared from nylon 6. A two-step masterbatch process to improve organoclay exfoliation and processability of nylon 6 - organoclay nanocomposites is presented. Chapters 4 through 7 detail the various routes explored to improve organoclay exfoliation in polyethylene. First, the polarity of polyethylene was increased by several techniques viz., grafting of maleic anhydride on the polyolefin backbone, copolymerizing with polar monomers like methacrylic acid, and incorporating ionic groups (ionomers). The effects of these changes in matrix polymer chemistry on the morphology and properties of the nanocomposites formed are described in Chapter 4. Encouraged by the level of organoclay dispersion observed in nanocomposites prepared from a sodium ionomer of poly(ethylene-co-methacrylic acid), further investigations were made to determine the role played by the type of neutralizing cation (sodium vs. lithium vs. zinc) on organoclay exfoliation. Results of these investigations are detailed in Chapter 5. In Chapter 6 we present a novel approach to improve organoclay dispersion in polyethylene. The polyethylene particles were subjected to an oxidative surface treatment, which resulted in the formation of polar groups like hydroxyls and carboxylates on their surface. The details of the surface treatment method and its effects on nanocomposite properties are summarized in that chapter. Chapter 7 is devoted to understanding the relationship between the organoclay structure and the morphology and physical properties of nanocomposites prepared from poly(ethylene-co-methacrylic acid) ionomers. Specific comparisons among organic amine surfactants that are commercially available are made by addressing structural variations one issue at a time. The effects of processing

temperature on organoclay degradation and subsequently on the mechanical properties of the nanocomposites were also examined. The results of these examinations along with a comparison of the thermal stability of various organoclays are presented in Chapter 8. Once the optimum processing conditions were established, and the organoclay structure engineered to maximize the polyolefin-organoclay compatibility, nanocomposites with acceptable levels of exfoliation were prepared on a large scale from LDPE and poly(ethylene-co-methacrylic acid) ionomers. These were subsequently blown into films of different thicknesses under a variety of conditions. The effect of the film blowing conditions and film thickness on the mechanical and barrier properties of the nanocomposite films are discussed in Chapter 9. Finally, Chapter 10 summarizes the overall conclusions of the research work undertaken, and includes suggestions for future work.

REFERENCES

[1] Ray SS, Okamoto M. Progress in Polymer Science 2003;28(11):1539-641.

[2] Alexandre M, Dubois P. Mater Sci Eng, R 2000;R28(1-2):1-63.

[3] Usuki A, Koiwai A, Kojima Y, Kawasumi M, Okada A, Kurauchi T, Kamigaito O. J Appl Polym Sci 1995;55(1):119-23.

[4] Wang Z, Pinnavaia TJ. Chem Mater 1998;10(12):3769-71.

[5] Liu L, Qi Z, Zhu X. J Appl Polym Sci 1999;71(7):1133-38.

[6] Lan T, Pinnavaia TJ. Chem Mater 1994;6(12):2216-19.

[7] Messersmith PB, Giannelis EP. J Polym Sci, Part A: Polym Chem 1995;33(7):1047-57.

[8] Yano K, Usuki A, Okada A, Kurauchi T, Kamigaito O. J Polym Sci, Part A: Polym Chem 1993;31(10):2493-8.

[9] Gu A, Kuo S-W, Chang F-C. J Appl Polym Sci 2001;79(10):1902-10.

[10] Kojima Y, Usuki A, Kawasumi M, Okada A, Kurauchi T, Kamigaito O. J Appl Polym Sci 1993;49(7):1259-64.

[11] Lincoln DM, Vaia RA, Sanders JH, Phillips SD, Cutler JN, Cerbus CA. Polym Mater Sci Eng 2000;82:230-1.

[12] Huang J-C, Zhu Z-k, Yin J, Qian X-f, Sun Y-Y. Polymer 2001;42(3):873-7.

[13] Gilman JW. Appl Clay Sci 1999;15(1-2):31-49.

[14] Vaia RA, Price G, Ruth PN, Nguyen HT, Lichtenhan J. Appl Clay Sci 1999;15(1-2):67-92.

[15] Garces JM, Moll DJ, Bicerano J, Fibiger R, McLeod DG. Adv Mater (Weinheim, Ger) 2000;12(23):1835-9.

[16] Rose J. Modern Plastics 2001;(October 2001):37.

[17] Editors. Modern Plastics 2005;(September 2005)

[18] Maiti P, Yamada K, Okamoto M, Ueda K, Okamoto K. Chemistry of Materials 2002;14(11):4654-61.

[19] Zhu J, Morgan AB, Lamelas FJ, Wilkie CA. Chemistry of Materials 2001;13(10):3774-80.

[20] Kim MH, Park CI, Choi WM, Lee JW, Lim JG, Park OO, Kim JM. Journal of Applied Polymer Science 2004;92(4):2144-50.

[21] Awad WH, Gilman JW, Nyden M, Harris RH, Sutto TE, Callahan J, Trulove PC, DeLong HC, Fox DM. Thermochimica Acta 2004;409(1):3-11.

[22] Bottino FA, Fabbri E, Fragala IL, Malandrino G, Orestano A, Pilati F, Pollicino A. Macromolecular Rapid Communications 2003;24(18):1079-84.

[23] Davis CH, Mathias LJ, Gilman JW, Schiraldi DA, Shields JR, Trulove P, Sutto TE, Delong HC. Journal of Polymer Science, Part B: Polymer Physics 2002;40(23):2661-6.

[24] Gilman JW, Awad WH, Davis RD, Shields J, Harris RH, Jr., Davis C, Morgan AB, Sutto TE, Callahan J, Trulove PC, DeLong HC. Chemistry of Materials 2002;14(9):3776-85.

[25] Wang ZM, Chung TC, Gilman JW, Manias E. Journal of Polymer Science, Part B: Polymer Physics 2003;41(24):3173-87.

[26] Kawasumi M, Kohzaki M, Kojima Y, Okada A, Kamigaito O. United States Patent 4810734; 1989. [Assigned to Toyota Motor Co., Japan]

[27] Usuki A, Kojima Y, Kawasumi M, Okada A, Fukushima Y, Kurauchi T, Kamigaito O. J Mater Res 1993;8(5):1179-84.

[28] Kojima Y, Usuki A, Kawasumi M, Okada A, Kurauchi T, Kamigaito O. J Polym Sci, Part A: Polym Chem 1993;31(7):1755-8.

[29] Weimer MW, Chen H, Giannelis EP, Sogah DY. J Am Chem Soc 1999;121(7):1615-6.

[30] Lee DC, Jang LW. J Appl Polym Sci 1998;68(12):1997-2005.

[31] Lee DC, Jang LW. J Appl Polym Sci 1996;61(7):1117-22.

[32] Gregar KC, Winans RE, Botto RE. US Patent 5308808; 1994. [Assigned to (United States Dept. of Energy, USA).]

[33] Carrado KA, Xu L. Chem Mater 1998;10(5):1440-5.

[34] Torkelson JM, Lebovitz A, Kasimatis K, Khait K. US Patent 2003-701067, 2005096422; 2005. [Assigned to (Material Sciences Corporation, USA)]

[35] Torkelson JM, Lebovitz AH, Kasimatis K, Khait K. WO Patent 2003-US34892, 2004043663; 2004. [Assigned to (Material Sciences Corporation, USA)]

[36] Christiani BR, Maxfield M. United States Patent 5747560; 1998. [Assigned to Allied Signal]

[37] Vaia RA, Ishii H, Giannelis EP. Chem Mater 1993;5(12):1694-6.

[38] Okada A, Fukushima Y, Kawasumi M, Inagaki S, Usuki A, Sugiyami S, Kurauchi T, Kamigaito O. United States Patent 4739007; 1988. [Assigned to Toyota Motor Co., Japan]

[39] Fornes TD, Yoon PJ, Hunter DL, Keskkula H, Paul DR. Polymer 2002;43(22):5915-33.

[40] Fornes TD, Hunter DL, Paul DR. Macromolecules 2004;37(5):1793-8.

[41] Dennis HR, Hunter DL, Chang D, Kim S, White JL, Cho JW, Paul DR. Polymer 2001;42(23):9513-22.

Chapter 2: Experimental - Materials and Techniques

An overview of the experimental techniques employed to form and characterize the nanocomposites investigated in this study is presented in this chapter. At times, depending upon the research objective, there were slight variations in these techniques; these variations are described in the corresponding chapters.

MATERIALS

Although nanocomposites prepared from both, polyamide and polyethylene type materials were examined in this investigation, the majority of the efforts were focused on studying the morphology and properties of nanocomposites prepared from polyethylene and structurally modified/ copolymers of polyethylene. A list of the polymers used in this research work is presented in Table 2.1.

Table 2.1 Polymers used in this research work

Polymer class	Polymer grade	Commercial designation	Supplier	Select specifications
Polyamides	Nylon 6 (Low mol. wt.)	Capron® 8202	Honeywell	M_n = 16,400 MI = 23 g/10 min
	Nylon 6 (High mol. wt.)	Capron® B135WP	Honeywell	M_n = 29,300 MI = 1.2 g/10 min
Polyethylenes	High density polyethylene	HiD 9055	Chevron Phillips Chem.	Density = 0.95 g/cc MI = 55.0 g/10 min
	Low density polyethylene	LD 621	Exxon Mobil	Density = 0.919 g/cc MI = 1.9 g/10 min
	Low density polyethylene	Novapol® LF-Y819-A	Nova Chemicals	Density = 0.919 g/cc MI = 0.75 g/10 min
	Low density polyethylene	Novapol® LF-0219-A	Nova Chemicals	Density = 0.919 g/cc MI = 2.3 g/10 min
	Low density polyethylene	Novapol® LC-0717-A	Nova Chemicals	Density = 0.917 g/cc MI = 7.0 g/10 min
Modified polyethylenes	Maleic anhydride grafted polyethylene	Fusabond® E MB265D	Du Pont	Density = 0.95 g/cc MI = 12.3 g/10 min
	Surface treated polyethylene	Inhance® HD-1800	Fluor-Seal Intl. L. P.	Density = 0.95 g/cc MI = 50 g/10 min
Acid copolymers	Poly(ethylene-co-methacrylic acid)	Nucrel® 0903	Du Pont	MI = 2.6 g/10 min Methacrylic acid: 8.9 mol%
	Poly(ethylene-co-methacrylic acid)	Nucrel® 0403	Du Pont	MI = 3.2 g/10 min Methacrylic acid: 3.9 mol%
Ionomers	Sodium ionomer of Poly(ethylene-co-methacrylic acid)	Surlyn® 8920	Du Pont	MI = 0.9 g/10 min Methacrylic acid: 5.53 mol% Neutralization: 44.1% Sodium content 1.78 wt%
	Sodium ionomer of Poly(ethylene-co-methacrylic acid)	Surlyn® 8940	Du Pont	MI = 2.8 g/10 min Methacrylic acid: 5.81 mol% Neutralization: 27.0% Sodium content 1.14 wt%
	Sodium ionomer of Poly(ethylene-co-methacrylic acid)	Surlyn® 8945	Du Pont	MI = 4.0 g/10 min Methacrylic acid: 5.59 mol% Neutralization: 39.0% Sodium content 1.58 wt%
	Lithium ionomer of Poly(ethylene-co-methacrylic acid)	Surlyn® 7940	Du Pont	MI = 2.66 g/10 min Methacrylic acid: 5.45 mol% Neutralization: ~ 40 % Lithium content 0.52 wt%
	Zinc ionomer of Poly(ethylene-co-methacrylic acid)	Surlyn® 9945	Du Pont	MI = 4.1 g/10 min Methacrylic acid: 5.50 mol% Neutralization: ~ 40 % Zinc oxide content 3.70 wt%

The organically modified clays were generously donated by Southern Clay Products and were used as received. These were prepared by an ion exchange reaction between sodium montmorillonite (Na-MMT) and a variety of amine surfactants. The amine surfactants used for preparing the organoclays are derived from natural products like coconut, palm and tallow oils, and were provided to Southern Clay Products by Akzo Nobel. The molecular structures of the amine surfactants used in this study are presented in Figure 2.1. A simple nomenclature system has been adopted to describe these structures in a concise manner, i.e., M for methyl, H for hydrogen, (HE) for 2-hydroxy-ethyl, C^* for coconut oil (predominantly C_{12} chains), T for tallow (predominantly C_{18} chains), and HT for hydrogenated tallow oil (saturated). Procedural details of the cation exchange reaction between the onium ions and Na-MMT are provided by Fornes et al.[1]. A brief description of the organoclays used in this study is presented in Table 2.2.

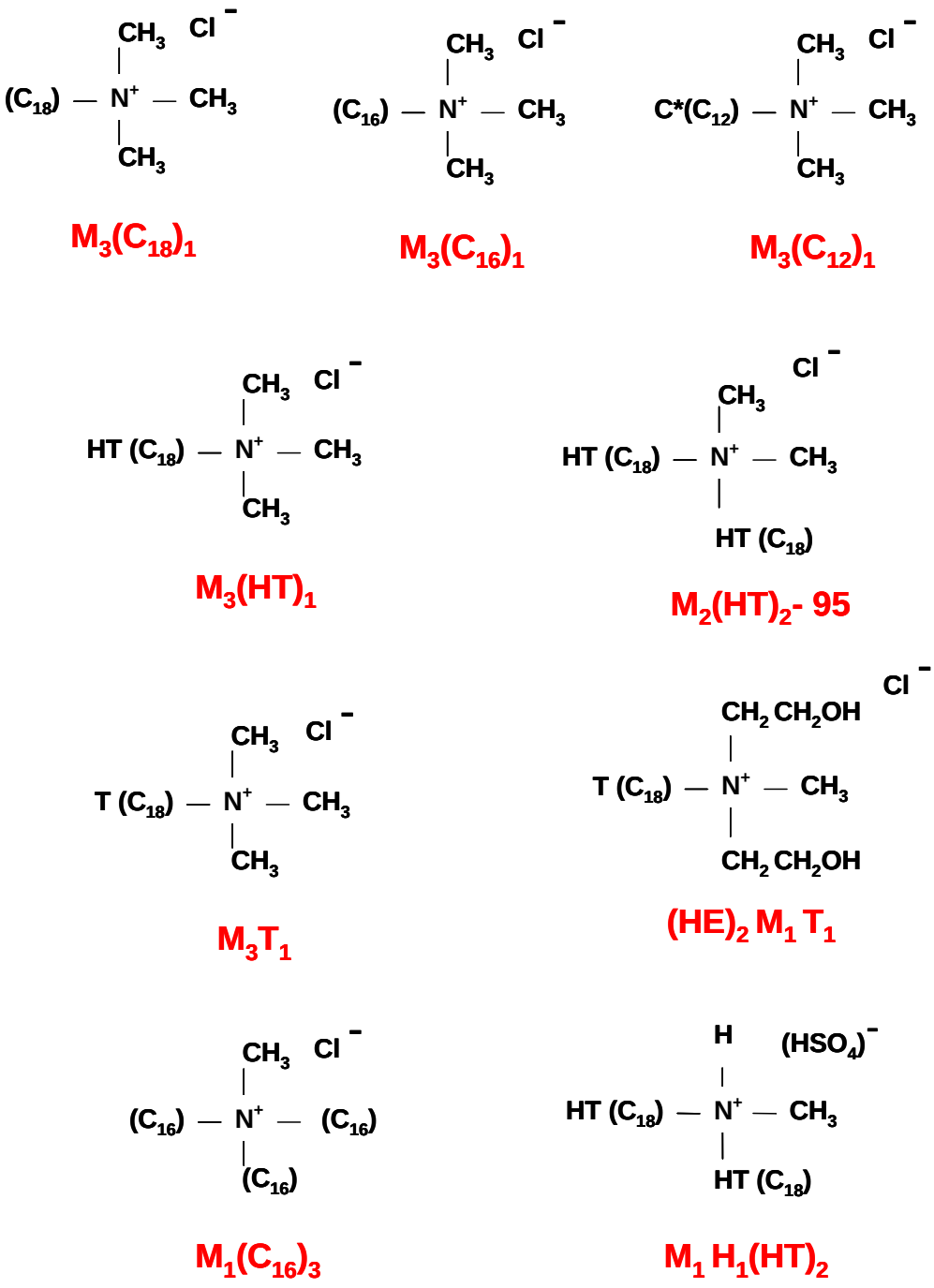

Figure 2.1 Molecular structure of organic ammonium ion surfactants exchanged onto montmorillonite clay. The symbols M = methyl, H = hydrogen, T = tallow, (HT) = hydrogenated tallow, (HE) = 2-hydroxy-ethyl, and C* = coconut oil.

Table 2.2 Organoclays used in this study.

Organoclay	SCP designation	Chemical structure	Organic loading[b] (MER)	Organic content[c] (wt%)	d_{001} spacing[d] (Å)
$M_3(HT)_1$	Experimental	Trimethyl hydrogenated-tallow ammonium montmorillonite	95	29.6	18.0
$M_3(C_{18})_1$	Experimental	Octadecyl trimethyl ammonium montmorillonite	95	29.8	18.1
$M_3(C_{16})_1$	Experimental	Hexadecyl trimethyl ammonium montmorillonite	100	27.5	17.9
$M_2(HT)_2$-95	Cloisite® 20A[a]	Dimethyl bis(hydrogenated-tallow) ammonium montmorillonite	95	39.6	25.5
$M_2(HT)_2$-140	Cloisite® 6A[a]	Dimethyl bis(hydrogenated-tallow) ammonium montmorillonite	140	48.0	35.1
$M_1(C_{16})_3$	Experimental	Methyl trihexadecyl ammonium montmorillonite	100	43.4	29.3
$(HE)_2M_1C_1$*	Experimental	bis(2-hydroxy-ethyl)methyl coco ammonium montmorillonite	95	26.4	14.4
$(HE)_2M_1T_1$	Cloisite® 30B[a]	bis(2-hydroxy-ethyl)methyl tallow ammonium montmorillonite	90	31.5	17.7
M_3T_1	Experimental	Trimethyl tallow quaternary ammonium montmorillonite	95	29.1	17.5
$M_1H_1(HT)_2$	Experimental	Dimethyl hydrogenated-tallow ammonium montmorillonite	95	38.4	24.3

[a] Cloisite® is a registered trademark of Southern Clay Products, Inc.

[b] Organic loading describes the number of milliequivalents of amine salt used per 100 g of clay (MER) during the cation exchange reaction with sodium montmorillonite

[c] The wt% of organic component on the final organoclay was determined by high temperature residual ash measurements.

[d] The basal spacing corresponds to the characteristic Bragg reflection peak (d_{001}) obtained from a powder WAXS scan of the organoclay.

EXPERIMENTAL

All nanocomposites investigated in this study were prepared using melt processing techniques. A broad outline of the experimental procedure used for the preparation and characterization of nanocomposites is given in Figure 2.2

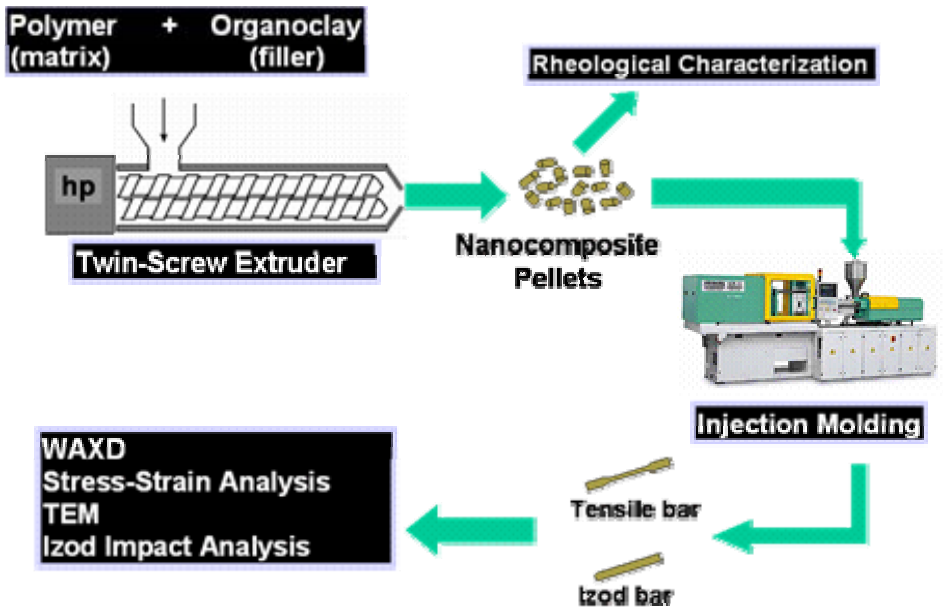

Figure 2.2 Overview of the experimental process

Melt Processing

Polymer and organoclay were melt-mixed in a twin screw extruder at a temperature slightly above melt temperature of the polymer. Nanocomposites were formed as a result of the combined effect of shear, chemical interactions between the polymer and organoclay, and diffusion of the polymer melt into the clay galleries. Prior to melt processing, the polymers were dried in a vacuum oven for a minimum of 16

hours. Most of the compounding was done in a Haake, co-rotating, intermeshing twin screw extruder (diameter = 30 mm, L/D = 10) using a screw speed of 280 rpm, and a feed rate of 800-1200 g/hr. Whenever possible, the amount of montmorillonite in the nanocomposite was confirmed by placing pre-dried nanocomposite pellets in a furnace at 900 °C for 45 minutes and weighing the remaining ash. The results were corrected for loss of structural water [2, 3]. The percent MMT in the final nanocomposite was calculated from

$$\% \text{ MMT} = \%\text{MMT}_{ash}/0.935 \qquad (2.1)$$

where, $\%\text{MMT}_{ash}$ is the weight of the residue left after incineration relative to the original nanocomposite weight.

In some studies, rheological characterization of the nanocomposites was done using a Brabender Plasticorder or a DSM microcompounder. In a Brabender rheometer, the melt viscosity is characterized by the torque required to mix a constant mass of polymer (or nanocomposite) at a fixed speed at a given temperature. On the other hand, the DSM microcompounder, when operated under recycle mode, measures the axial force exerted on the twin-screws by the polymer melt when operated at a fixed speed, at a given temperature. A comparison of the Brabender torque (or DSM axial force) of different nanocomposites measured under identical conditions provides a useful measure of their relative melt viscosities.

Tensile specimens (ASTM D638) and Izod specimens (ASTM D256) were prepared by injection molding using and Arburg Allrounder 305-210-700 injection

molding machine. After molding, the samples were immediately sealed in a polyethylene bag and placed in a vacuum desiccator for a minimum of 24 hours prior to testing.

Testing and Characterization

Evaluation of Mechanical Properties

Tensile tests were conducted at room temperature according to ASTM D696 using an Instron model 1137 machine equipped with digital data acquisition capabilities. Modulus was measured using an extensiometer at a crosshead speed of 0.51 cm/min. The yield strength of polyamide nanocomposites was measured at a cross head speed of 0.51 cm/min. while their elongation at break was measured at both low and high speeds (0.51 and 5.1 cm/min.). Polyethylene type materials are a lot more ductile than polyamides. Hence, for composites prepared from such polymers, elongation at break, yield strength and tensile strength at break were measured at a crosshead speed of 5.1 cm/min. Typically, data from six specimens were averaged to determine the tensile properties.

Notched Izod impact tests were performed at room temperature using a TMI Izod tester (6.8 J hammer and 3.5 m/s impact velocity) according to ASTM D256. It is a common practice to cut the Izod bars into half (to generate more samples) and average the impact strength data from the "gate end" (the end from which molten polymer enters the mold during injection molding) and the "far end". However, in multi-component systems, morphological differences can lead to significant differences between the impact strength measured at the gate end and the far end of a sample [4]. Hence, in this study, the impact strength data from four samples each from the gate end and the far end of the bar were averaged separately.

Wide Angle X-ray Scattering (WAXS)

WAXS experiments were conducted in the reflection mode using a Sintag XDS 2000 diffractometer with an incident X-ray wavelength of 1.542 Å at a scan rate of 1.0 °/min. The analysis was performed at room temperature on injection molded Izod bars. The specimens were oriented such that the incident beam reflected off the major face as shown in Figure 2.3.

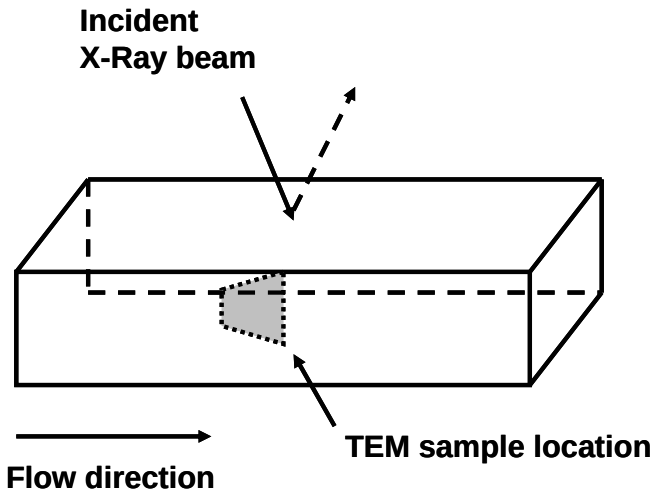

Figure 2.3 Illustration of the X-ray beam path and the location of TEM samples

Transmission Electron Microscopy and Particle Analysis

Samples for TEM analysis were taken from the core portion of an Izod bar parallel to the flow direction but perpendicular to the major face as shown in Figure 2.3. Ultra-thin sections approximately 50 nm in thickness were cut with a diamond knife using a Reichert-Jung Ultracut E microtome. Polyamide nanocomposite samples were

microtomed at -40 °C, while nanocomposites prepared from polyethylene type materials were microtomed at -65 °C. Sections were collected on 300 mesh grids and subsequently dried with filter paper. These were then examined using a JEOL 2010F TEM equipped with a Field Emission Gun at an accelerating voltage of 120 kV.

The negative films containing the electron micrographs were electronically scanned and converted into gray scale tagged-image file format (TIFF) image files. In order to conduct quantitative analysis on these images, the TIFF files were opened in Adobe Photoshop, where the dimensions of the dispersed platelets and agglomerates were traced over into an overlapped blank layer. Two separate tracings were done for each TEM picture, one contained the lengths of the particles, and the other one contained their thicknesses. The resulting black and white layer files were then imported into an image analysis software, SigmaScan Pro, which analyzed the traced particles, assigned a numerical label to each of them, and exported their characteristic dimensions to a different file. Since two different tracings were used for measuring the lengths and thicknesses of the particles, each particle got assigned two different numerical labels. This made it extremely difficult to match the length of a given particle with its thickness, and thus, calculate its aspect ratio. Hence, in this study, the aspect ratio of the particles for any given nanocomposite was determined by dividing its average particle length by its average particle thickness [5-7].

REFERENCES

[1] Fornes TD, Yoon PJ, Hunter DL, Keskkula H, Paul DR. Polymer 2002;43(22):5915-33.

[2] Fornes TD, Yoon PJ, Keskkula H, Paul DR. Polymer 2001;42(25):9929-40.

[3] Van Olphen H. *An introduction to clay colloid chemistry: for clay technologists, geologists, and soil scientists*. 2nd ed. 1977, New York: Wiley. xviii, 318.

[4] Huang JJ, Keskkula H, Paul DR. Polymer 2004;45(12):4203-15.

[5] Fornes TD, Paul DR. Polymer 2003;44(17):4993-5013.

[6] Chavarria F, Paul DR. Polymer 2004;45(25):8501-15.

[7] Lee H-s, Fasulo PD, Rodgers WR, Paul DR. Polymer 2005;46(25):11673-89.

Chapter 3: Nylon 6 Nanocomposites Prepared by a Melt Mixing Masterbatch Process

The initial and one of the most well-known research works in polymer-organoclay nanocomposites was done by the Toyota research group in the late eighties using Nylon 6 as a matrix polymer. Since then, nanocomposites have been prepared from a number of polymers, but few exhibit a level of organoclay exfoliation that matches that of nylon 6 based composites. Even with nylon 6, seemingly insignificant material specifications, viz., polymer molecular weight, end group concentrations, etc. have a remarkable effect on the morphology and properties of the nanocomposites formed [1, 2] . Melt processing studies with nylon 6 have revealed that high molecular weight grades of nylon 6 (hereafter referred to as HMW nylon 6 or sometimes simply HMW) lead to higher levels of exfoliation of montmorillonite (MMT) based organoclays than do low molecular weight (LMW) grades of nylon 6 [1, 3]. This is believed to be a result of the higher shear stresses generated by the HMW grade caused by its higher melt viscosity. On the other hand, LMW grades process much faster than the HMW grades in certain operations like injection molding. From a commercial standpoint, it is desirable to achieve similar exfoliation with LMW grades or 'injection molding grades' as seen in the HMW grades, since product throughput is essential for the economical manufacturing of injection-molded parts.

Hence, the objective of this study is to develop a viable means of achieving good exfoliation in nylon 6 with improved melt processability. This is done using a two step process: In the first, masterbatches of HMW nylon 6 with different clay contents are

prepared by melt processing using a twin-screw extruder. Second, these masterbatches are then diluted with LMW nylon 6 under the same melt processing conditions mentioned above to produce nanocomposites with 2%, 4% and 6.5% MMT. The premise underlying this strategy is to get good exfoliation in HMW nylon 6 and then reduce the viscosity by dilution with LMW nylon 6 while preserving the exfoliation obtained in HMW. From an economic standpoint, it is desirable to make the HMW masterbatches as concentrated in MMT as possible since it would lower the manufacturing and distribution costs. Also, a more concentrated masterbatch would result in a higher LMW/HMW ratio on dilution, which would lead to improved melt processability. The question is what is the upper limit of MMT concentration in the HMW nylon 6 masterbatch that can be formed for implementation of this strategy from a processing point of view? Can one get good exfoliation at high MMT contents in HMW nylon 6 and, if so, can it be preserved after dilution with LMW nylon 6? These questions are addressed in this study. The effects of the clay content of the masterbatches on the morphology and physical properties of the final nanocomposites are examined using wide-angle x-ray diffraction (WAXD), transmission electron microscopy (TEM), and stress-strain analysis. In addition, these data are compared to that of equivalent nanocomposites prepared by direct melt processing from HMW and LMW nylon 6 (no masterbatches used). A schematic of the strategy described above is presented in Figure 3.1

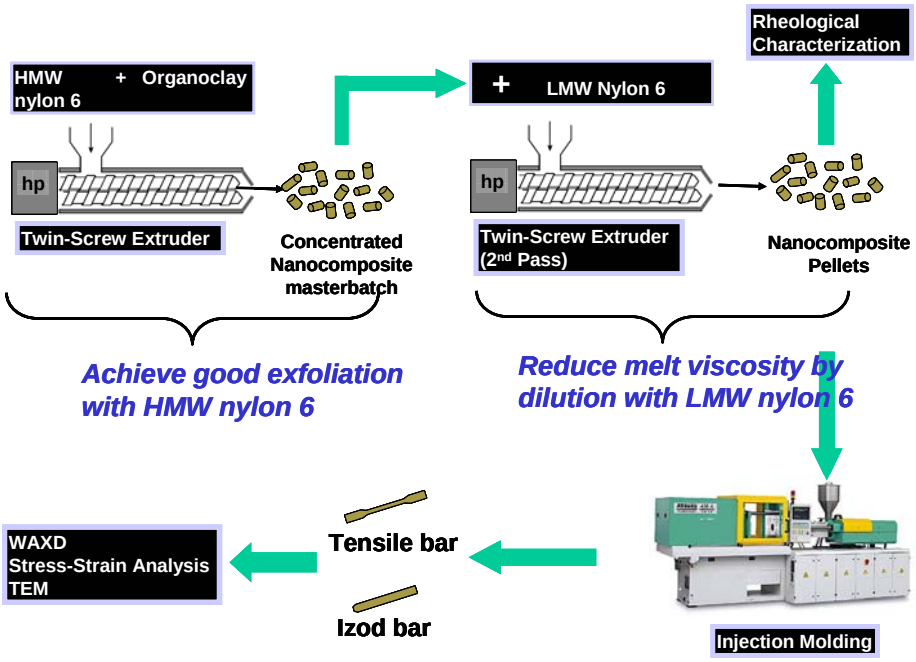

Figure 3.1 Schematic of the strategy employed for preparing nylon 6 based nanocomposites with good exfoliation and processability.

EXPERIMENTAL

Two commercial grades of nylon 6 from Honeywell, a high molecular weight grade, HMW (M_n = 29,300), and a low molecular weight grade, LMW (M_n = 16,400), were used. The organically modified clay was prepared by a cation exchange reaction between sodium montmorillonite (Na-MMT) and octadecyltrimethyl ammonium chloride (Arquad 18-50® quat), designated here as $M_3(C_{18})_1$. Specifications of the polymers and the organoclay are given in Chapter 2. The choice of the organoclay used was based on a recent study of the effect of organoclay structure on clay exfoliation in nylon 6 nanocomposites made by melt processing [4] which revealed that greater exfoliation could be achieved using surfactants with (i) one long alkyl tail on the ammonium ion

rather than two and (ii) methyl groups on the amine rather than 2-hydroxy-ethyl groups. In prior studies in this lab, trimethyl-hydrogenated tallow quaternary ammonium chloride, $M_3(HT)_1$, was used [4, 5]; however, due to supply constraints, $M_3(C_{18})_1$ was used instead in this study. A comparison of the tensile modulus of nylon 6 nanocomposites prepared using these two organoclays shows nearly equivalent performance (see Figure 3.2). The yield strength and ductility of samples prepared using these two organoclays were also found to be similar.

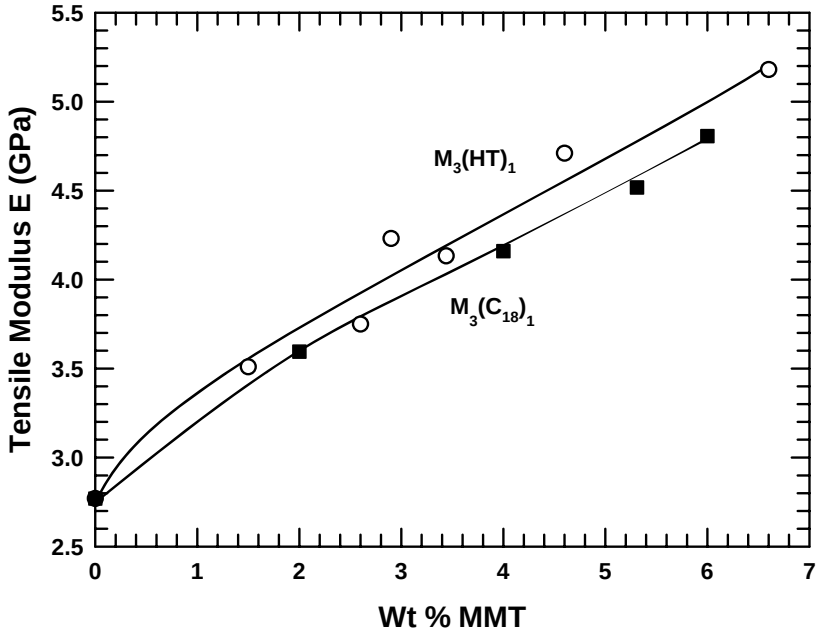

Figure 3.2 Comparison of tensile modulus of nanocomposites prepared from high molecular weight (HMW) nylon 6 and trimethyl-hydrogenated tallow quaternary ammonium chloride ($M_3(HT)_1$) versus octadecyltrimethyl ammonium chloride ($M_3(C_{18})_1$).

As mentioned above, a two-step process was used to prepare nanocomposites of the desired montmorillonite content. In the first step, masterbatches containing 20, 14 and 8.25 wt% MMT (28.5, 19.9 and 11.7 wt% organoclay respectively) were prepared by melt blending the organoclay and HMW nylon 6 in a Haake co-rotating, intermeshing twin screw extruder as described in Chapter 2. The barrel temperature was set at 240 ºC; whereas, the screw speed and feed-rate were set at 280 rpm and 1200 g/h respectively. The low melt strength of the extrudate caused problems in forming a strand which coupled with pelletizing difficulties arising form high hardness of the solidified strand prohibited use of higher organoclay contents in the masterbatch. Each of the masterbatches was then diluted with LMW nylon 6 using the same processing conditions to produce nanocomposites with 2, 4 and 6.5 wt% MMT. In addition to these, a HMW masterbatch containing 4 wt% MMT was also diluted down to 2 wt% MMT with LMW nylon 6. Prior to extrusion, all the polyamides (in steps 1 and 2) and masterbatches (in step 2) were dried in a vacuum oven at 80 ºC for a minimum of 16 h. For comparison, nylon 6 nanocomposites with 2, 4 and 6.5 wt% MMT were prepared from the HMW only and LMW only materials using the same organoclay and processing conditions mentioned above. These were passed through the extruder twice so that they have the same thermal and shear history as nanocomposites made from masterbatches. The amount of montmorillonite (MMT) in each batch was confirmed by incinerating the nanocomposites in a furnace as described in Chapter 2. A summary of the blends prepared is given in Table 3.1.

Table 3.1 Summary of nylon 6/ $M_3C_{18})_1$ organoclay nanocomposites prepared in this study

MMT Content (wt%)	Matrix/ Starting material	Comments
20.0	HMW nylon 6	Masterbatch
14.0	HMW nylon 6	Masterbatch
8.25	HMW nylon 6	Masterbatch
6.5	HMW nylon 6	For comparison
4.0	HMW nylon 6	Masterbatch/ For comparison
2.0	HMW nylon 6	For comparison
0.0	HMW nylon 6	For comparison
6.5	LMW nylon 6	For comparison
4.0	LMW nylon 6	For comparison
2.0	LMW nylon 6	For comparison
0.0	LMW nylon 6	For comparison
6.5	20% Masterbatch	Diluted with LMW nylon 6
4.0	20% Masterbatch	Diluted with LMW nylon 6
2.0	20% Masterbatch	Diluted with LMW nylon 6
6.5	14% Masterbatch	Diluted with LMW nylon 6
4.0	14% Masterbatch	Diluted with LMW nylon 6
2.0	14% Masterbatch	Diluted with LMW nylon 6
6.5	8.25% Masterbatch	Diluted with LMW nylon 6
4.0	8.25% Masterbatch	Diluted with LMW nylon 6
2.0	8.25% Masterbatch	Diluted with LMW nylon 6
2.0	4.0% Masterbatch	Diluted with LMW nylon 6

The samples were injection molded using a barrel temperature of 260 ºC, mold temperature of 75 ºC, injection pressure of 70 bar and holding pressure of 35 bar. The nanocomposites were characterized using WAXS, TEM and stress-strain analysis as described in Chapter 2. The data revealed standard deviations of the order of 4-5% for modulus, 2% for yield strength and 5-25% for elongation at break values. The

rheological characterization was done in a Brabender Plasticorder with a 60 ml mixing head and standard rotors. A constant mass of 58 g for each sample was mixed at 240 °C at 70 rpm for 15 minutes. The melt viscosity characterized by the Brabender torque plateaued after 7-9 minutes of operation. The torque values at 10 minutes are reported here for each sample.

RESULTS AND DISCUSSION

Mechanical Properties

Figure 3.3 shows the tensile modulus of nylon 6 nanocomposites made by the masterbatch process. For clarity, the moduli are plotted as a function of both the montmorillonite content of the final nanocomposites, Figure 3.3(a), and the montmorillonite content of the masterbatches, Figure 3.3(b). The corresponding values for nanocomposites prepared directly from HMW and LMW nylon 6 are also plotted for comparison. As expected [1, 6], stiffness of nylon 6 improves substantially with the addition of organoclay and although there is not much difference between the moduli of virgin HMW and LMW nylon 6, the moduli of nanocomposites based on HMW nylon 6 are 10-15% higher than that of nanocomposites based on LMW nylon 6. Stiffness values of all samples prepared using the masterbatch approach fall between that of the equivalent HMW and LMW nanocomposite samples. It is interesting to note that the moduli of samples prepared from 4 and 8.25 wt% masterbatches are much closer to those of the corresponding samples prepared from HMW nylon 6 only. Also, there is not much difference between the moduli of equivalent samples made from the 14 and 20 wt% masterbatches.

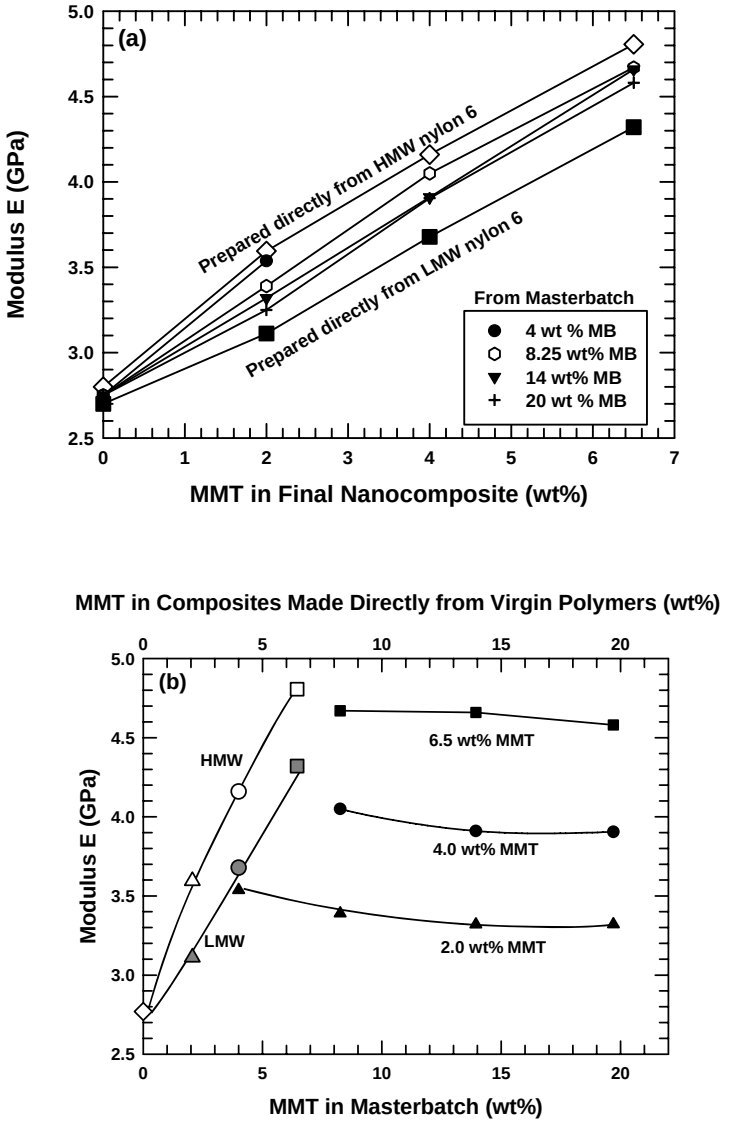

Figure 3.3. (a) Effect of montmorillonite content on the tensile modulus of nanocomposites prepared from four masterbatches containing different MMT concentrations (b) Tensile modulus of nanocomposites containing 2.0 wt% MMT (triangles) , 4.0 wt% MMT (circles), and 6.5 wt% MMT (squares are plotted as a function of the MMT content of the masterbatch they were made from (bottom axis). Data for nanocomposites made directly from HMW nylon 6 only (unfilled symbols) and LMW nylon 6 only (gray symbols) are plotted versus the top axis for comparison.

Table 3.2 Select mechanical properties of nylon 6/$M_3(C_{18})_1$ organoclay nanocomposites

MMT in final nanocomposite (wt%)*	Mechanical Property	HMW	LMW	MMT in masterbatch (wt%) *			
				20%	14%	8.25%	4%
0.0%	Tensile Modulus (GPa)	2.77	2.78				
	Yield Strength (MPa)	67.0	67.3				
	Elongation at Break at 0.51cm/min (%)	273	205				
	Elongation at Break at 5.1cm/min (%)	136	24.6				
2.0%	Tensile Modulus (GPa)	3.60	3.11	3.32	3.32	3.39	3.54
	Yield Strength (MPa)	85.2	73.5	74.5	75.9	79.7	79.7
	Elongation at Break at 0.51cm/min (%)	201	84.0	127	141	146	169
	Elongation at Break at 5.1cm/min (%)	85.3	13.6	26.1	27.6	30.7	44.7
4.0%	Tensile Modulus (GPa)	4.16	3.68	3.91	3.91	4.05	
	Yield Strength (MPa)	88.8	76.5	79.8	79.6	81.2	
	Elongation at Break at 0.51cm/min (%)	67.0	16.1	11.5	11.7	26.1	
	Elongation at Break at 5.1cm/min (%)	39.8	9.57	8.71	7.46	10.5	
6.5%	Tensile Modulus (GPa)	4.81	4.32	4.58	4.66	4.67	
	Yield Strength (MPa)	93.1	74.7**	79.3**	77.9**	81.4**	
	Elongation at Break at 0.51cm/min (%)	3.19	2.81	2.94	2.82	2.96	
	Elongation at Break at 5.1cm/min (%)	3.60	3.10	2.94	3.32	2.89	

*Masterbatches were prepared from HMW nylon 6 and were diluted down to the desired MMT content with LMW nylon 6.
** Tensile strength at break, i.e., samples failed before reaching the yield point.

Table 3.2 summarizes the moduli and other mechanical properties of the virgin materials, nanocomposites prepared by direct melt processing (no masterbatches used), and nanocomposites prepared from masterbatches. Figure 3.4 shows the yield strength as a function of the montmorillonite content of masterbatches for nanocomposites with 2 and 4 wt% MMT loading. Yield strength data for nanocomposites containing 6.5 wt% MMT are not available since all samples (except for the HMW based composites) failed before reaching the yield point. As before, yield strength data for nanocomposites based on virgin HMW and LMW nylon 6 are plotted for comparison. Once again, the yield strengths of the nanocomposites prepared using the masterbatch process are between those of equivalent nanocomposites prepared by direct melt processing of pure HMW or LMW nylon 6.

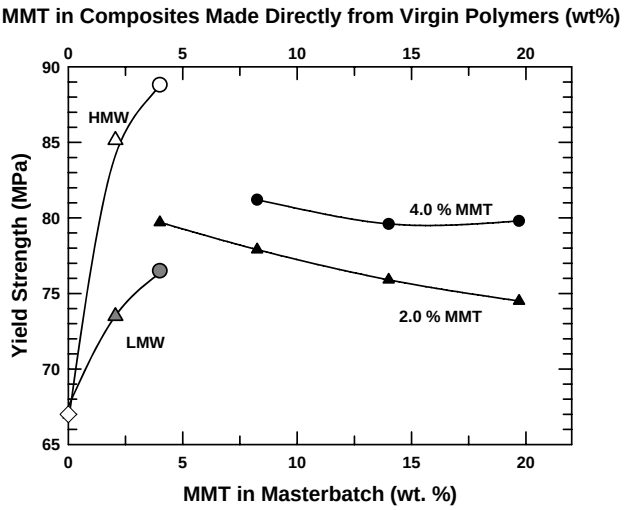

Figure 3.4 Yield strength of nanocomposites containing 2.0 wt% MMT (triangles), and 4.0 wt% MMT (circles) are plotted as a function of the MMT content of the masterbatch they were made from (bottom axis). Data for nanocomposites made directly from HMW nylon 6 only (unfilled symbols) and LMW nylon 6 only (gray symbols) are plotted versus the top axis for comparison.

The relationship between the montmorillonite content of the masterbatch and elongation at break for the different nanocomposites is shown in Figure 3.5 for two rates of extension. As observed in prior studies [1, 6], the virgin polyamides are very ductile at a test rate of 0.51 cm/min, but increasing the clay content sacrifices ductility. The drop in ductility with increasing organoclay content is much steeper for the LMW based composites than with HMW nylon 6 based composites (Table 3.2). It is interesting to note, that composites with 2 wt% MMT prepared by the masterbatch process, maintain reasonable levels of ductility. Elongation at break values of samples prepared from the 20 wt% masterbatch are 50% higher than corresponding samples prepared directly from LMW nylon 6 while those prepared from the 4 wt% masterbatch are more than twice that for samples prepared directly from LMW nylon 6. The degree of improvement for nanocomposites containing 4 wt% MMT prepared by masterbatch dilution is not as pronounced as those with 2 wt% MMT. At higher montmorillonite concentrations of 6.5 wt%, the ductility is seriously compromised across the board and there is not much difference in the elongation at break values between samples based on the different grades of nylon 6 or those made from masterbatches. On increasing the testing speed to 5.1 cm/min (Figure 3.5(b)), similar trends are seen, but the absolute levels of elongation at break values are significantly lower.

Characterization

Figure 3.6 compares the WAXD patterns for the $M_3(C_{18})_1$ organoclay and the $M_3(C_{18})_1$/ HMW masterbatches with different montmorillonite contents. The organoclay pattern reveals an intense peak at around $2\theta = 4.9°$, corresponding to a basal spacing of

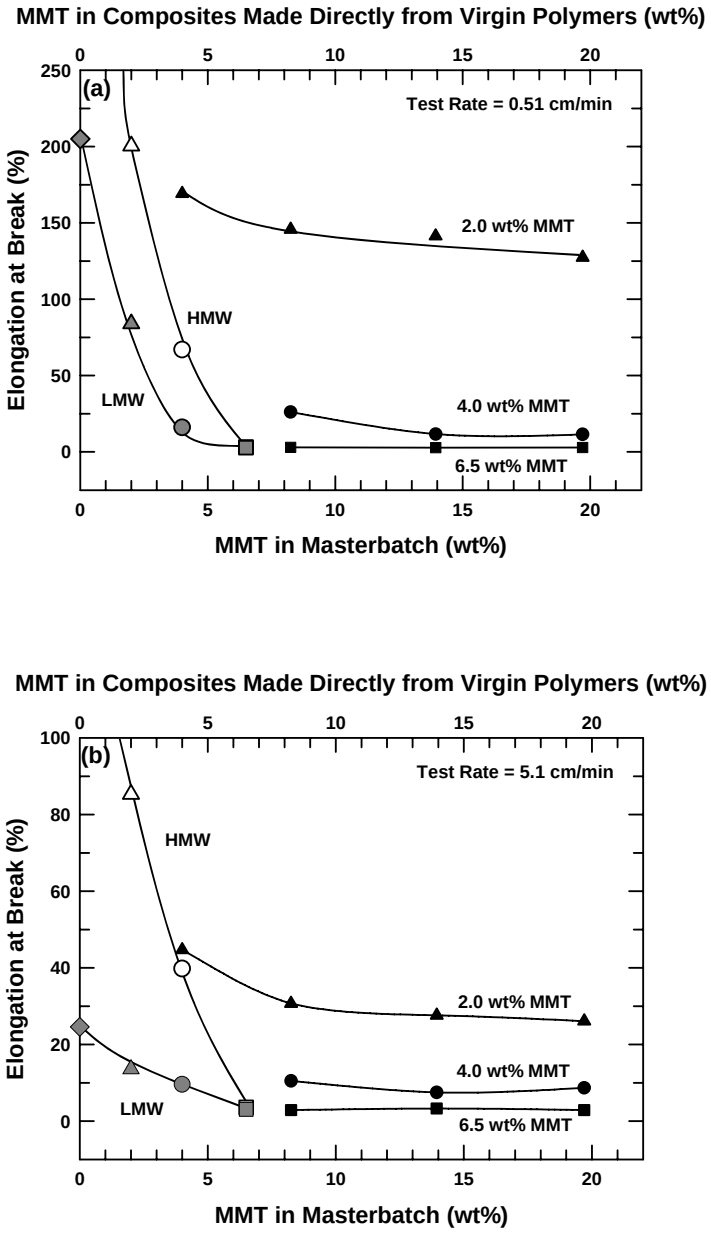

Figure 3.5 Elongation at break of nanocomposites containing 2.0 wt% MMT (triangles), 4.0 wt% MMT (circles), and 6.5 wt% MMT (squares) are plotted as a function of the MMT content of the masterbatch they were made from (bottom axis), measured at crosshead speeds of (a) 0.51 cm/min and (b) 5.1 cm/min. Data for nanocomposites made directly from HMW nylon 6 only (unfilled symbols) and LMW nylon 6 only (gray symbols) are plotted versus the top axis for comparison.

18.1 Å. The X-ray pattern for the masterbatch with 4.0 wt% MMT does not show a characteristic basal reflection; this is indicative of a homogeneous exfoliated structure. On the other hand, patterns for the 20 and 14% masterbatches reveal a low broad peak that suggests these systems have a mixed morphology consisting of regions of intercalated clay tactoids and regions of exfoliated clay platelets. The WAXD pattern of the masterbatch with 8.25 wt% MMT does not show a distinct peak; however, there is a slight hint of curvature, which could be interpreted as an extremely broad peak indicating that the system is almost exfoliated. This agrees well with the mechanical property results that show nanocomposites formed from masterbatches containing 4 and 8.25 wt% MMT have stiffness similar to the corresponding nanocomposites based on HMW nylon 6 while the nanocomposites based on masterbatches containing 14 and 20 wt% MMT have lower modulus values.

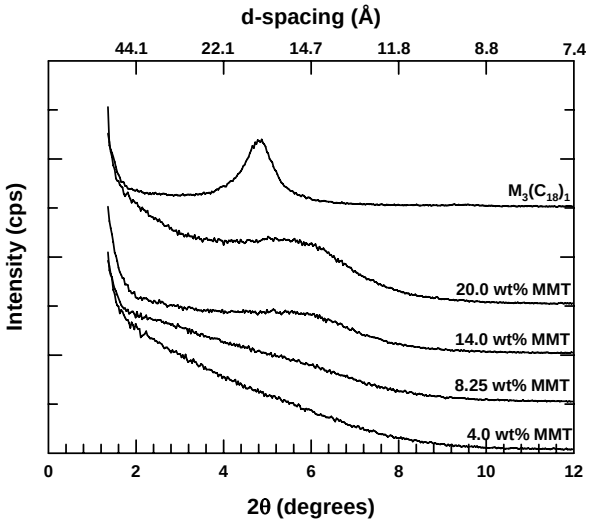

Figure 3.6 WAXD patterns for $M_3(C_{18})_1$ organoclay and $M_3(C_{18})_1$ organoclay nanocomposite masterbatches based on HMW nylon 6 containing 20, 14, 8.25, and 6.5 wt% montmorillonite. The curves are shifted vertically for clarity.

Figure 3.7 compares WAXD scans of nanocomposites with three different MMT levels that were formed from HMW and LMW nylon 6 only with those formed by dilution of a masterbatch containing 20% MMT. Composites formed from the masterbatch containing 20 wt% MMT were selected for this comparison because they require the greatest dilution with LMW nylon 6 and, thus, offer the greatest ease of processing. X-ray patterns of the organoclay and the parent masterbatch are also shown in each figure for comparison. As expected [1, 6], the WAXD scans of the HMW nylon 6 composites are devoid of any characteristic peaks, which is consistent with the well-exfoliated character of these systems; whereas, the nanocomposites prepared from LMW nylon 6 show a distinct broad peak indicative of the presence of intercalated clay tactoids. The X-ray patterns of the masterbatch-based nanocomposites have a characteristic peak similar to that of the parent masterbatch. However, the intensity of this peak is lower than both that of the nanocomposite based on LMW nylon 6 and the parent masterbatch suggesting a greater degree of exfoliation than observed in the latter two. These results support the mechanical property results which show the masterbatch-based composites have better properties than comparable LMW nylon 6 based composites.

Careful observation of the WAXD patterns reveals shifts in the peak position for the nanocomposites and masterbatches relative to that of the pristine organoclay. These shifts apparently reflect the net result of two counteracting phenomena occurring concurrently during melt processing, viz., intercalation of the clay galleries by the matrix polymer and degradation of the organic component of the organoclay. TGA studies have shown that the organic component of organoclays begins to breakdown at temperatures as

low as 180 °C. The thermal degradation of alkyl ammonium montmorillonite organoclays has been discussed in detail by Xie et al. [7, 8] and VanderHart et al. [9, 10]. More degradation may occur in the masterbatch owing to viscous heat dissipation from the combined effects of higher filler levels and higher melt viscosity of the virgin HMW nylon 6. This would explain the shift of the peak to the right corresponding to a reduction of the interlayer spacing by 2-5 Å compared to the pure organoclay. In the case of LMW-based nanocomposites with low filler concentration, the amount of degradation is believed to be considerably less and the intercalation of polymer into the clay galleries prevails since the peak shifts to the left corresponding to an increase in the d-spacing of the organoclay stacks by 1-3 Å. A detailed analysis on organoclay exfoliation and the relative thermal stabilities of various organoclays is presented in Chapter 8.

The TEM micrographs of nanocomposites formed from the $M_3(C_{18})_1$ organoclay and nylon 6 shown in Figure 3.8 provide a more direct visualization of the degree of exfoliation of these materials. The micrograph of the HMW nylon 6 nanocomposite, Figure 3.8(a), reveals a well-exfoliated structure; whereas, the LMW nylon 6 nanocomposite, Figure 3.8(c), reveals partial exfoliation with areas containing exfoliated platelets plus some tactoids. The TEM image of the masterbatch-based nanocomposites, Figure 3.8(b) also showed a mixed morphology; however, the unexfoliated clay stacks were fewer in number and smaller in size than those found in LMW nanocomposite micrographs. These results are in good agreement with the WAXD and mechanical property data.

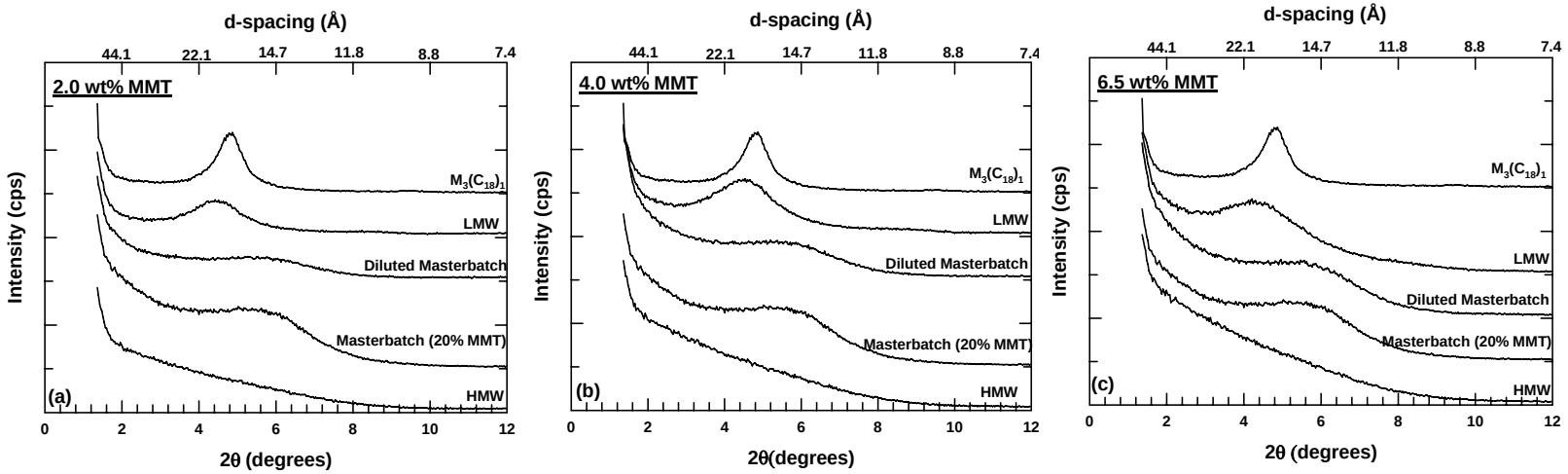

Figure 3.7 WAXD patterns for $M_3(C_{18})1$ organoclay nanocomposites containing (a) ~ 2 wt% (b) ~4 wt%, and (c) ~6.5 wt% montmorillonite based on HMW nylon 6, LMW nylon 6, and a diluted masterbatch. WAXD patterns of organoclay and the parent masterbatch (~20 wt% MMT) are plotted for comparison. The curves are shifted vertically for clarity.

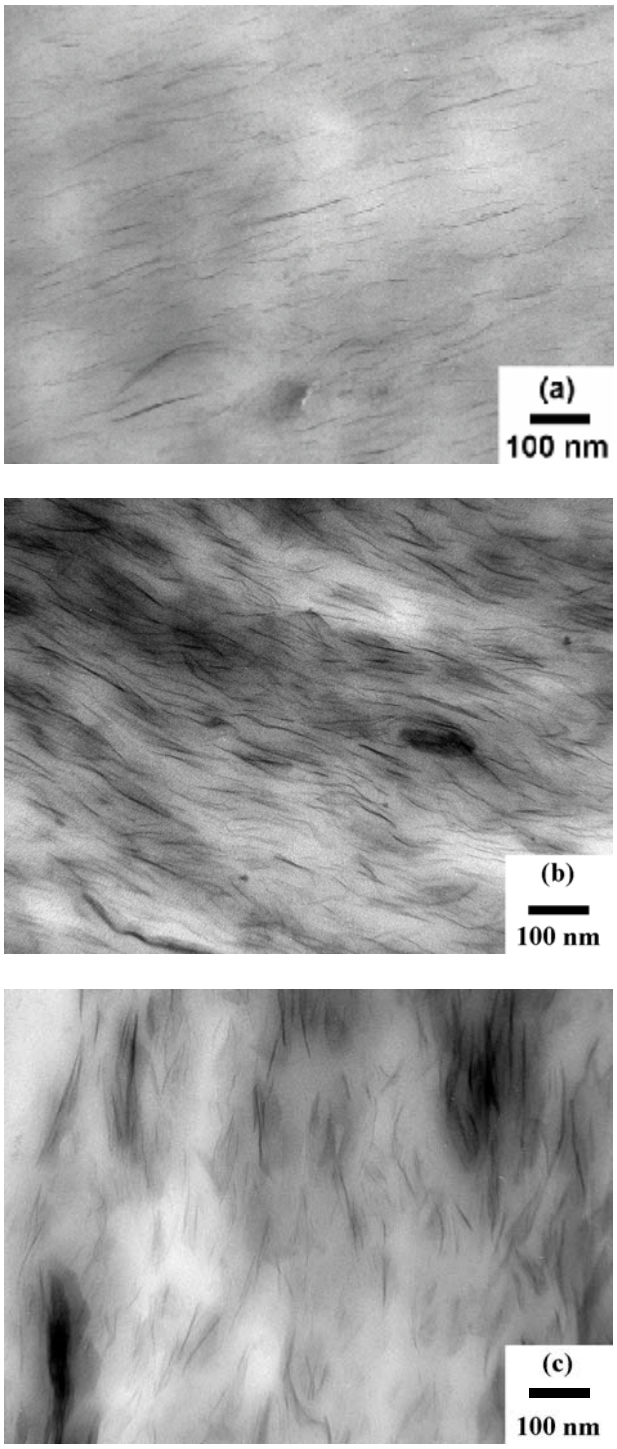

Figure 3.8 TEM micrographs of nanocomposites containing ~2.0 wt% montmorillonite based on (a) HMW nylon 6, (b) HMW masterbatch containing ~20 wt% montmorillonite diluted down with LMW, and (c) LMW nylon 6

Processability

Figure 3.9 compares the Brabender torques of virgin HMW and LMW nylon 6, their blends, and nanocomposites based on them. The torque for HMW nylon 6 is about three times higher than that for LMW nylon 6, with the HMW-LMW nylon 6 blends in between. The addition of $M_3(C_{18})_1$ organoclay does not result in large changes in the torque values. The relative gains in processability are presented in Table 3.3. Contrary to expectation, addition of small amounts of organoclay (2 wt% MMT) results in a slight reduction in the torque relative to the nylon 6 mixture for most compositions. At higher montmorillonite loadings (6.5%), the torque for LMW nylon 6 increases by ~40% over that of virgin LMW nylon 6; however, a small decrease is observed for HMW nylon 6. These trends in the Brabender torque values reflect two opposing phenomena. The addition of montmorillonite tends to increase the matrix melt viscosity and, thus, the torque; however, degradation of the organic component of the organoclay leads to matrix molecular weight degradation, which lowers the Brabender torque as recently described by Fornes et al. [11]. That study concluded that for a given organoclay, the level of polymer molecular weight reduction was greatest for nanocomposites based on high molecular weight nylon 6 materials owing to the greater exposure of the surfactant to the nylon 6 caused by increased levels of organoclay exfoliation. Similar matrix degradation has been reported for nanocomposites based on poly(ethylene terepthalate) (PET) [12] and polycarbonate [13] prepared by melt processing. At 2% MMT loading, the viscosity effects of matrix degradation apparently exceed the intrinsic increase caused by addition of montmorillonite, thus, shifting the curve lower. At higher loadings (6.5%), the viscosity enhancement gained by the addition of montmorillonite, evidently exceeds the

reduction resulting from polymer degradation in LMW nylon 6. On the other hand, at the same high loadings in HMW nylon 6, the two effects seem to offset each other resulting in little change in the torque values.

Table 3.3 Relative melt viscosity

Nanocomposite	HMW : LMW ratio	Brabender torque[a] [N-m]	Relative melt viscosity
2.0 wt% MMT			
From HMW	100 : 0	9.2	1.00
From masterbatch containing 4.00% MMT	48.5: 51.5	5.5	0.60
From masterbatch containing 8.25% MMT	23.5 : 76.5	4.0	0.43
From masterbatch containing 20% MMT	6.6: 93.4	3.5	0.38
From LMW	0 : 100	3.1	0.34
6.5 wt% MMT			
From HMW	100 : 0	9.7	1.00
From masterbatch containing 8.25% MMT	72.7 : 27.3	7.2	0.74
From masterbatch containing 20% MMT	25.6 : 74.4	4.7	0.48
From LMW	0 : 100	4.9	0.51

[a] Torque was measured at 240 ^{o}C temperature after 10 minutes of operation

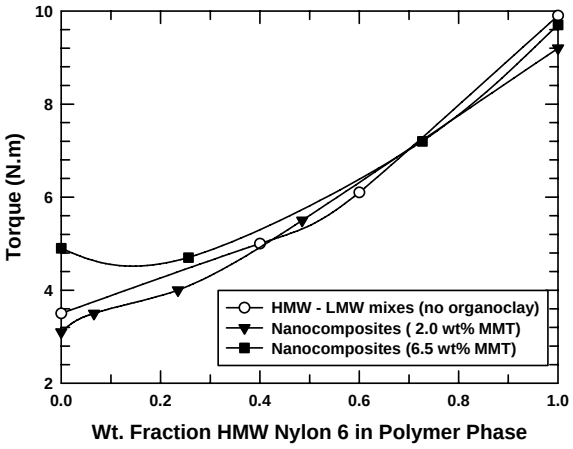

Figure 3.9 Brabender torque at 10 min (steady state), for nylon 6-montmorillonite nanocomposites containing ~2.0 and ~6.5 wt% montmorillonite, prepared by diluting HMW nylon 6 masterbatches with LMW nylon 6. The torque values for HMW-LMW nylon 6 mixes (no organoclay added) are plotted for comparison.

Figure 3.10 shows the tradeoff between processability as quantified by the Brabender torque and tensile modulus of the nanocomposites based on nylon 6 for two MMT loading levels. As shown in Figure 3.10(a), the relationship between the melt viscosity and the tensile modulus of nanocomposites is not linear. By using a masterbatch that has a lower montmorillonite content (< 8.25 wt%), a significant reduction in melt viscosity (Brabender torque) is achieved over HMW based nanocomposites for a relatively smaller penalty in modulus. A further increase in the MMT content of the masterbatch results in a marginal reduction in the melt viscosity but causes the modulus to drop precipitously. Nanocomposites with a higher montmorillonite concentration (6.5 wt%) display similar trends as shown in Figure 3.10(b).

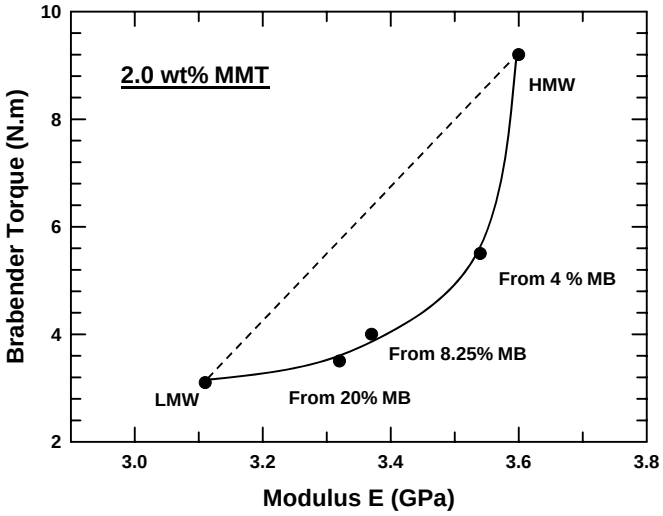

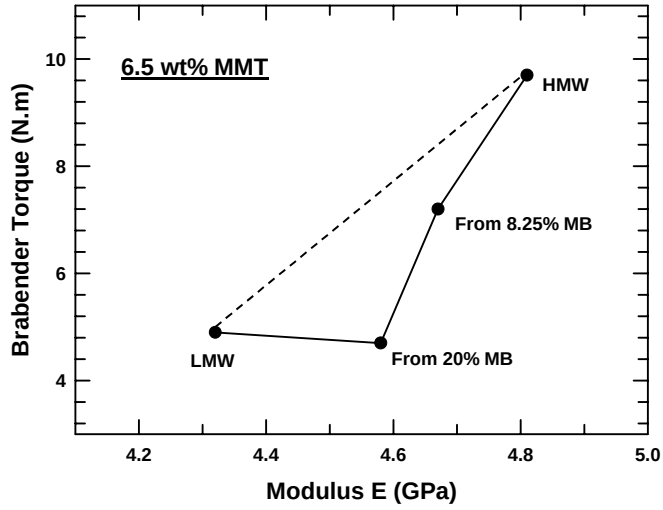

Figure 3.10 The trade-off between tensile modulus and Brabender torque, a measure of melt viscosity or processability, of nylon 6-montmorillonite nanocomposites containing (a) 2.0 wt% MMT, and (b) 6.5 wt% MMT prepared using a masterbatch approach.

CONCLUSIONS

A two-step masterbatch process for preparing nylon 6 nanocomposites that provides good exfoliation and low melt viscosities (for shorter cycle times in injection molding) has been investigated. In the first step, masterbatches of high molecular weight (HMW) nylon 6 with different clay contents were prepared by melt processing to get good exfoliation. In the second step, the masterbatch was diluted with low molecular weight (LMW) nylon 6 to the desired MMT content to reduce the melt viscosity. It was difficult to produce masterbatches containing more than 20 wt% MMT (or 28.5 wt% organoclay) owing to problems of stranding the extrudate arising from its lower melt strength and of pelletizing the solidified strand because of its hardness.

Masterbatches containing 4 and 8.25 wt% MMT were quite well exfoliated, and nanocomposites prepared by diluting them with LMW nylon 6 exhibited properties close to those seen with composites based on HMW nylon 6 alone. On the other hand, masterbatches containing 14 and 20 wt% MMT, were not so well exfoliated; however, mechanical property, TEM and WAXD analysis of nanocomposites prepared by diluting these masterbatches revealed better exfoliation than corresponding nanocomposites prepared directly from LMW nylon 6.

A distinct trade-off between the tensile modulus of these nanocomposites and the reduction of melt viscosity was observed. Nanocomposites prepared from HMW masterbatches that have a lower MMT concentration (< 8.25 wt%), offer a significant decrease in melt viscosity over those prepared directly from HMW nylon 6, for a small reduction in modulus. On increasing the MMT content of the masterbatch further, the tradeoff becomes less favorable. However, if it is absolutely necessary to have

throughput rates similar to LMW nylon 6, the use of nanocomposites prepared from a more concentrated masterbatch (> 8.25 wt%) could offer up to a 10% improvement in modulus over nanocomposites prepared from LMW nylon 6 only.

While two extrusion steps were used in this work, the concept illustrated could be implemented in a single extrusion through the use of larger twin-screw extruders that have downstream feed ports. In this case, the organoclay and HMW nylon 6 would be fed to the hopper while LMW nylon 6 could be injected in a downstream feed port.

REFERENCES

[1] Fornes TD, Yoon PJ, Keskkula H, Paul DR. Polymer 2001;42(25):9929-40.

[2] Fornes TD. Ph.D. Thesis, The University of Texas at Austin, 2003.

[3] Fornes TD, Yoon PJ, Keskkula H, Paul DR. Polymer 2002;43(7):2121-2.

[4] Fornes TD, Yoon PJ, Hunter DL, Keskkula H, Paul DR. Polymer 2002;43(22):5915-33.

[5] Yoon PJ, Fornes TD, Paul DR. Polymer 2002;43(25):6727-41.

[6] Chavarria F, Paul DR. Polymer 2004;45(25):8501-15.

[7] Xie W, Gao Z, Pan W-P, Hunter D, Singh A, Vaia R. Chem Mater 2001;13(9):2979-90.

[8] Xie W, Gao Z, Liu K, Pan WP, Vaia R, Hunter D, Singh A. Thermochimica Acta 2001;367-368:339-50.

[9] VanderHart DL, Asano A, Gilman JW. Macromolecules 2001;34(12):3819-22.

[10] VanderHart DL, Asano A, Gilman JW. Chem Mater 2001;13(10):3796-809.

[11] Fornes TD, Yoon PJ, Paul DR. Polymer 2003;44(24):7545-56.

[12] Matayabas Jr. JC, Turner SR. In: Polymer-clay nanocomposites, T.J. Pinnavaia and G.W. Beall, editors. Wiley: New York: 2000. p. 207.

[13] Yoon PJ, Hunter DL, Paul DR. Polymer 2003;44(18):5341-54.

Chapter 4: Polyethylene-Organoclay Nanocomposites: Effect of Matrix Modification on Organoclay Exfoliation

Recently there has been a strong commercial drive for producing organoclay based nanocomposites from low cost polymers like polyolefins. Unfortunately, unlike nylon 6, polyolefins are highly inefficient at exfoliating the organoclays by themselves, since there are no favorable interactions with the polar aluminosilicate surface of the clay. Hence, the use of an appropriate compatibilizer or chemical modification of the polymer matrix is required to attain acceptable levels of organoclay exfoliation.

The objective of this study is to evaluate the effects of matrix modification on the morphology and mechanical properties of polyethylene based nanocomposites. In an effort to improve the polarity of the polymer, and, thus, the polymer-organoclay interactions, three different modifications of polyethylene were employed. The level of organoclay exfoliation attained in nanocomposites based on these polymers was compared to equivalent nanocomposites prepared from unmodified polyethylene. In the first comparison, nanocomposites prepared from maleic anhydride grafted high density polyethylene (MA-g-HDPE) are evaluated against those prepared from high density polyethylene (HDPE). This approach is well-developed for polypropylene based systems including numerous commercial applications in the automotive industry [1-3]. In the second comparison, nanocomposites prepared from ethylene-methacrylic acid copolymers are evaluated against low density polyethylene (LDPE). Methacrylic acid by itself is a fairly polar monomer, and it imparts its polarity to the copolymer when it is copolymerized with ethylene. For the third comparison, ionomers, prepared by

neutralizing some of the acid groups of ethylene-methacrylic acid copolymers to form sodium, zinc, lithium or magnesium salts are evaluated against LDPE. Besides improving the toughness of the polymer, the ionic groups offer the possibility of favorable interactions with the organoclay. Transmission electron microscopy, wide angle X-ray scattering, and stress-strain analysis are used to evaluate the nanocomposite morphology and physical properties.

EXPERIMENTAL

A list of the polymers used in this study is given in Table 4.1.

Table 4.1 Polymers used in this study

Polymer	Commercial Designation	Selected Specifications
Low density polyethylene	LD 621 (Exxon Mobil)	Density = 0.919 g/cc MI = 1.9 g/10 min
High density polyethylene	HiD 9055 (Chevron Phillips Chemical Company)	Density = 0.95 g/cc MI = 55.0 g/10 min
Maleic anhydride grafted polyethylene	Fusabond® E MB265D	Density = 0.95 g/cc MI = 12.3 g/10 min
Poly(ethylene-co-methacrylic acid)	Nucrel® 0903	MI = 2.6 g/10 min Methacrylic acid: 8.9 mol%
Poly(ethylene-co-methacrylic acid)	Nucrel® 0403	MI = 3.2 g/10 min Methacrylic acid: 3.9 mol%
Sodium ionomer of Poly(ethylene-co-methacrylic acid)	Surlyn® 8945	MI = 4.5 g/10 min Methacrylic acid: 5.59 mol% Neutralization: 39.0% Sodium content 1.58 wt%

Specific comparisons made between these polymers are presented below:

(i) Effect of grafting of maleic anhydride on the polyethylene backbone

HiD 9055 vs. Fusabond® E MB265D

(ii) Effect of copolymerization with methacrylic acid

LD 621 vs. Nucrel® 0403
LD 621 vs. Nucrel® 0903

(iii) Effect of copolymerization with methacrylic acid and presence of ionic groups

LD 621 vs. Surlyn® 8945

The organoclays used in this study are given below. Their molecular structures and other pertinent details are included in Figure 2.1 and Table 2.2.

(i) $M_3(HT)_1$: One-tailed organoclay

(ii) $M_3(C_{16})_1$: One-tailed organoclay

(iii) $M_2(HT)_2$-95: Two-tailed organoclay

(iv) $M_1(C_{16})_3$: Three-tailed organoclay

Melt compounded composites were prepared using a Haake, co-rotating, intermeshing twin screw extruder using a barrel temperature of 200 ^oC, a screw speed of 280 rpm, and a feed rate of 1200 g/hr. The polymer was dried in a vacuum oven at 65 ^oC for a minimum of 48 hours prior to compounding while the organoclays were used as received. The samples were injection molded using a barrel temperature of 220 ^oC, mold temperature of 45 ^oC, injection pressure of 70 bar and a holding pressure of 40 bar. The nanocomposites were characterized using WAXS, TEM, and stress-strain analysis as described in chapter 2.

RESULTS

HDPE vs. HDPE-g-MA

Morphology

Fig. 4.1 shows TEM micrographs comparing the morphology of nanocomposites formed from HDPE and HDPE-g-MA using $M_2(HT)_2$-95 organoclay (5 wt% MMT). The nanocomposite from HDPE-g-MA (Fig. 4.1(b)) exhibits a much higher level of clay exfoliation and distribution compared to the one made from unmodified HDPE (Fig. 4.1(a)). The micrograph of nanocomposites prepared from the former reveal a pattern of uniformly dispersed single platelets along with a few thin bundles comprised of 2-3 platelets. On the other hand, the morphology of HDPE/ $M_2(HT)_2$-95 nanocomposites mostly revealed micron-sized tactoids of the organoclay .

Figure 4.2 compares the WAXS scans of the $M_2(HT)_2$-95 organoclay and its nanocomposites prepared by melt mixing with HDPE, and HDPE-g-MA, respectively. The organoclay pattern reveals an intense peak at around $2\theta = 3.46°$, corresponding to a basal spacing of 25.5 Å. The X-ray pattern for the HDPE-g-MA based nanocomposites does not show a characteristic basal reflection which is often interpreted as a sign of complete exfoliation. However, we believe that this lack of an X-ray peak is the result of a combination of high levels of dispersion and a more random orientation of clay particles rather than indicating a completely exfoliated morphology. The TEM analyses support this hypothesis. The X-ray scan for HDPE based nanocomposites reveal a distinct peak indicative of the presence of unexfoliated clay tactoids. The peak position is the same as that of the pristine organoclay, which suggests that the organoclay interplatelet distances were unaltered during the formation of these composites.

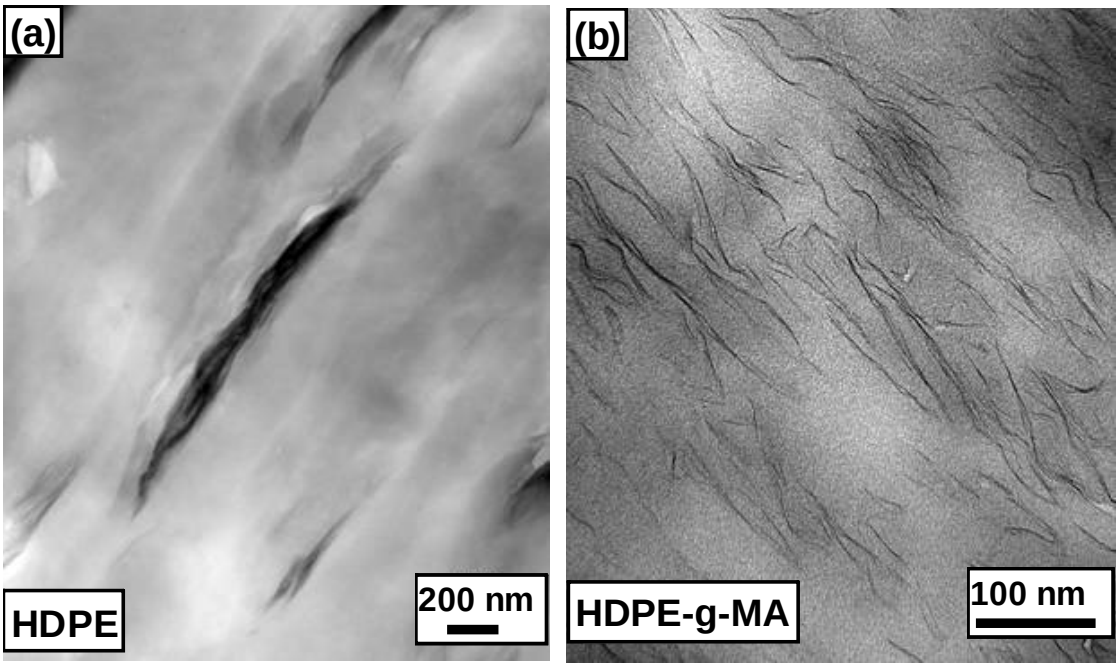

Figure 4.1 TEM micrographs of nanocomposites prepared from $M_2(HT)_2$-95 organoclay and (a) unmodified HDPE, and (b) maleic anhydride grafted HDPE (HDPE-g-MA). The concentration of MMT in both cases is ~5 wt%.

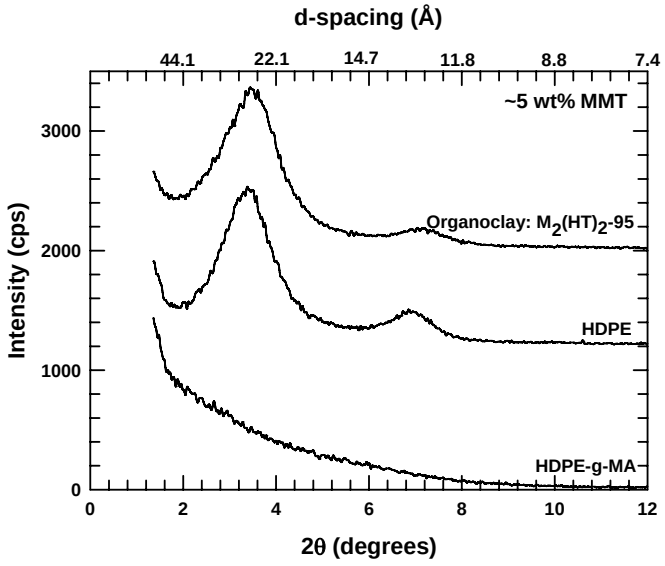

Figure 4.2 WAXS patterns of nanocomposites prepared from $M_2(HT)_2$-95 organoclay and the two HDPE based matrices. The concentration of MMT in both cases is ~5 wt%. X-ray pattern of $M_2(HT)_2$-95 organoclay is plotted for comparison. The curves are shifted vertically for clarity.

Mechanical properties

Selected mechanical properties of nanocomposites prepared from HDPE, and HDPE-g-MA using $M_2(HT)_2$-95 organoclay are listed in Table 4.2. Fig. 4.3(a) compares the tensile modulus of the different nanocomposites as a function of their montmorillonite content. To account for the differences between the moduli of the two matrices, the relative improvement in stiffness achieved by melt mixing these polymers with $M_2(HT)_2$-95 organoclay is presented in Fig. 4.3(b). It is clear that the increase in modulus observed in nanocomposites prepared from HDPE-g-MA is much stronger than that observed in nanocomposites prepared from unmodified HDPE.

Table 4.2 Selected mechanical properties of nanocomposites prepared from HDPE and HDPE-g-MA

Polymer	Clay loading (wt% MMT)	Modulus E (GPa)	Relative modulus E/E_m	Tensile strength (0.51 cm/min) (MPa)	Elongation at break	
					(0.51 cm/ min) (%)	(5.1 cm/ min) (%)
HDPE	0.00	0.595	1.000	15.6	333.7	88.8
HDPE	2.25	0.678	1.139	16.3	15.7	12.1
HDPE	5.20	0.768	1.291	16.3	12.5	8.9
HDPE-g-MA	0.00	0.803	1.000	18.3	> 400	> 400
HDPE-g-MA	2.25	1.141	1.421	21.8	> 400	328.7
HDPE-g-MA	4.97	1.399	1.742	23.6	40.9	7.1

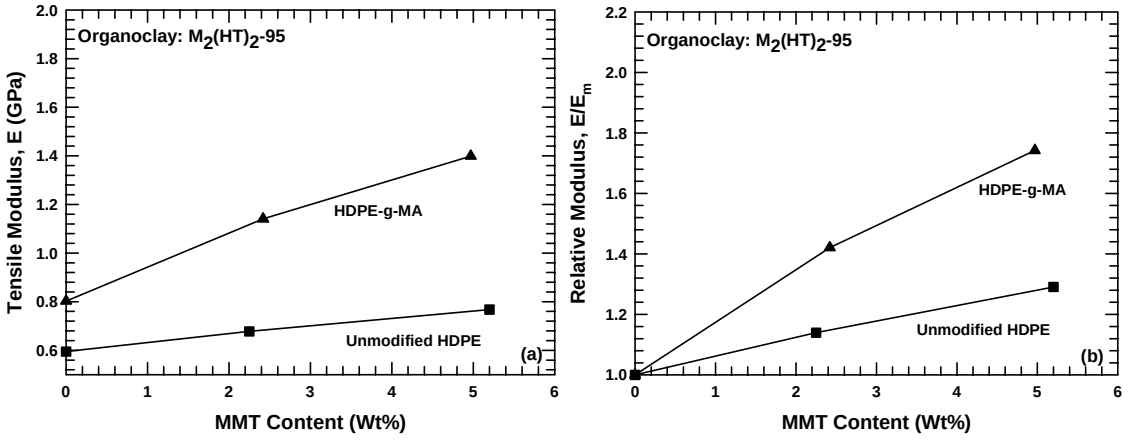

Figure 4.3 (a) Tensile modulus, and (b) Relative modulus of nanocomposites prepared from unmodified HDPE and maleic anhydride grafted HDPE (HDPE-g-MA).

Based upon the results of stress-strain analysis, transmission electron microscopy, and WAXS, it is clear that the grafting of maleic anhydride onto the polyethylene backbone results in a significant improvement the ability of the polymer to exfoliate the $M_2(HT)_2$-95 organoclay.

LDPE vs. poly(ethylene-co-methacrylic acid)

Morphology

WAXS scans of nanocomposites containing 2.5 wt% MMT prepared from LDPE and the two ethylene/methacrylic acid copolymers are presented in Fig. 4.4. X-ray diffraction pattern of $M_2(HT)_2$-95 organoclay is also included for comparison. The peak position in the WAXS pattern of the nanocomposite prepared from LDPE shifts to lower d-spacings compared to that of the organoclay. This is a result of surfactant degradation that occurs when the nanocomposites are processed at a temperature of 200 ^{o}C. A

detailed treatise on this phenomenon is presented in Chapter 8. The peak position in the X-ray pattern of the nanocomposite prepared from Nucrel® 0403 also shifts to a lower d-spacing compared to that of the organoclay; however, the shift in the peak position is not as significant as the one observed for LDPE- $M_2(HT)_2$-95 composite. In contrast, the WAXS peak of the nanocomposite prepared from Nucrel® 0903 shift to higher d-spacings compared to that of the organoclay. One reason for such an observation is the intercalation of polymers and/or low molecular weight oligomers present in the matrix polymer. However, that may not be the only reason [4, 5].

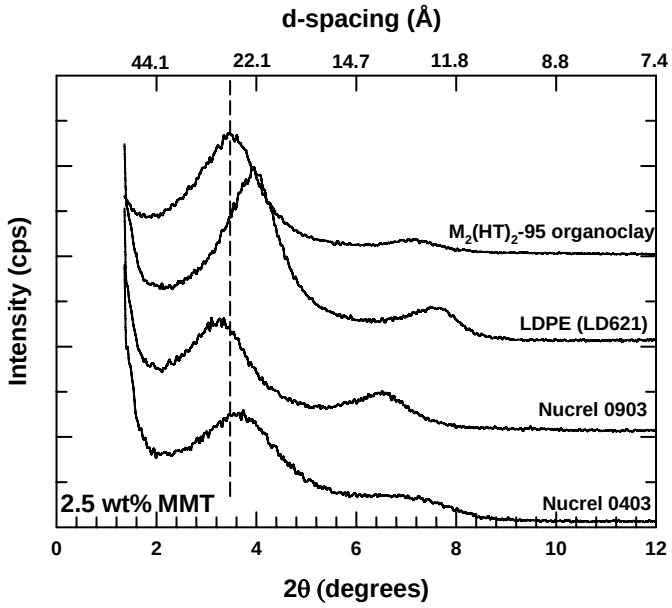

Figure 4.4 WAXS patterns of $M_2(HT)_2$-95 organoclay based nanocomposites prepared from LDPE and two ethylene/methacrylic acid copolymers (Nucrels®).

It is difficult to comment on the level of organoclay exfoliation in the three matrices based upon the results of the WAXS alone. For a thorough understanding of the nanocomposite morphology, TEM analysis of the samples is required. Such analyses are currently in progress.

Mechanical properties

Selected mechanical properties of the unfilled polymers and their nanocomposites are tabulated in Table 4.3. Tensile modulus data of nanocomposites prepared my melt mixing LDPE, and Nucrel® 0403 with a one-tailed organoclay, $M_3(HT)_1$, and a two-tailed organoclay, $M_2(HT)_2$-95, are presented in Fig. 4.5. It is clear that with both polymers the level of reinforcement achieved is higher with $M_2(HT)_2$-95 organoclay is significantly greater than that achieved with $M_3(HT)_1$ organoclay. These trends are opposite from those reported for nanocomposites prepared from nylon 6. It appears that unlike nylon 6, these polymers have more affinity for the alkyl tails than the polar surface of the aluminosilicate clays. The two-tailed surfactant not only offers a greater number of alkyl-polymer interactions compared to the one-tailed surfactant, but also shields the surface of the clay better than the latter. The combination of these effects result in a higher level of organoclay exfoliation, and thus, greater reinforcement in nanocomposites prepared from $M_2(HT)_2$-95 organoclay compared to those prepared from $M_3(HT)_1$ organoclay.

A comparison between the modulus of nanocomposites prepared from LDPE and Nucrel® 0403 also provides some interesting insights into the composite morphology. Despite the fact that the two unfilled polymers have very similar modulus values, nanocomposites prepared from Nucrel® 0403 exhibit higher levels of reinforcement compared to equivalent composites prepared from LDPE. Thus, it appears that the presence of small amounts of the polar methacrylic acid groups in the Nucrel® polymer results in an improvement in the level of organoclay exfoliation, and thus, greater reinforcement compared to LDPE.

Table 4.3 Select mechanical properties of nanocomposites prepared from LDPE and Nucrel® polymers.

Polymer (Matrix)	Organoclay	Clay content (wt% MMT)	Tensile modulus, E (MPa)	Relative modulus, E/E_m	Elongation at break (at 5.1 cm/min) (%)
LDPE	None	0.0	114	1.00	108
LDPE	$M_3(HT)_1$	2.5	155	1.36	87
LDPE	$M_3(HT)_1$	5.0	172	1.51	80
LDPE	$M_3(HT)_1$	7.5	194	1.70	73
LDPE	$M_3(HT)_1$	10	218	1.91	67
LDPE	$M_2(HT)_2$-95	2.5	178	1.56	83
LDPE	$M_2(HT)_2$-95	5.0	227	1.99	77
LDPE	$M_2(HT)_2$-95	7.5	280	2.46	70
LDPE	$M_2(HT)_2$-95	10	375	3.29	62
Nucrel® 0403	None	0.0	118	1.00	136
Nucrel® 0403	$M_3(HT)_1$	2.5	151	1.31	120
Nucrel® 0403	$M_3(HT)_1$	5.0	180	1.52	108
Nucrel® 0403	$M_3(HT)_1$	7.5	220	1.86	99
Nucrel® 0403	$M_3(HT)_1$	10	260	2.20	90
Nucrel® 0403	$M_2(HT)_2$-95	2.5	189	1.60	111
Nucrel® 0403	$M_2(HT)_2$-95	5.0	259	2.20	99
Nucrel® 0403	$M_2(HT)_2$-95	7.5	328	2.78	91
Nucrel® 0403	$M_2(HT)_2$-95	10	425	3.60	82
Nucrel® 0903	None	0.0	73	1.00	185
Nucrel® 0903	$M_3(HT)_1$	2.5	112	1.53	176
Nucrel® 0903	$M_3(HT)_1$	5.0	133	1.82	165
Nucrel® 0903	$M_3(HT)_1$	7.5	178	2.44	148
Nucrel® 0903	$M_3(HT)_1$	10	220	3.01	133
Nucrel® 0903	$M_2(HT)_2$-95	2.5	147	2.01	156
Nucrel® 0903	$M_2(HT)_2$-95	5.0	203	2.78	143
Nucrel® 0903	$M_2(HT)_2$-95	7.5	254	3.48	134
Nucrel® 0903	$M_2(HT)_2$-95	10	353	4.83	120

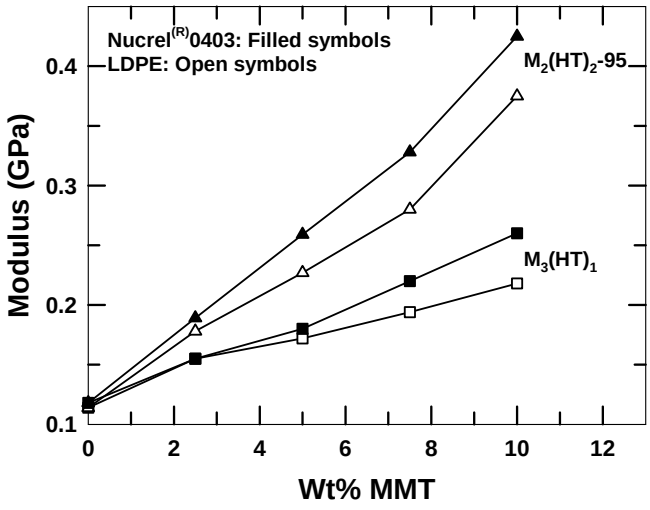

Figure 4.5 Tensile modulus of nanocomposites prepared from LDPE and Nucrel® 0403 plotted as a function of their montmorillonite content.

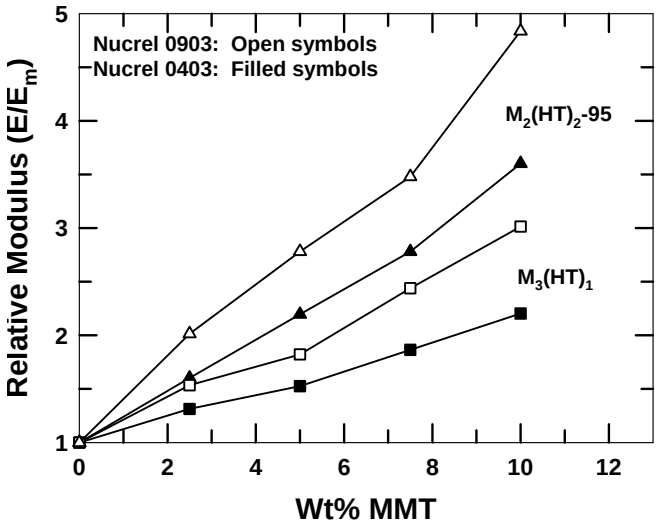

Figure 4.6 Relative modulus of nanocomposites prepared from Nucrel® 0903, and Nucrel® 0403 plotted as a function of their montmorillonite concentration.

To evaluate the effect of methacrylic acid content on the reinforcement efficiency of the nanocomposites prepared from the Nucrel® polymers, relative modulus of the

nanocomposites prepared from Nucrel® 0403 (3.2 MI, 3.9 mole% methacrylic acid), and Nucrel® 0903 (2.6 MI, 8.9 mole% methacrylic acid) are plotted in Fig. 4.6. For both polymers, nanocomposites prepared using $M_2(HT)_2$-95 organoclay show higher levels of reinforcement compared to those prepared from $M_3(HT)_1$. Also, nanocomposites prepared from the copolymer with a higher acid content exhibit greater improvements in stiffness compared to those prepared from the copolymer with a lower acid content. It is not clear whether this observation is a consequence of potentially better organoclay exfoliation in Nucrel® 0903 compared to Nucrel® 0403 or a result of possible differences between the platelet orientation in the two systems, or simply an outcome of the difference between the moduli of the two unfilled polymers (118 MPa vs. 73 MPa). (Composite theory predicts that for a given filler aspect ratio, low-modulus matrices offer greater potential for reinforcement per unit mass of filler than high-modulus matrices due to the larger ratio of filler modulus to matrix modulus [6, 7].) Similar observations are made while comparing mechanical properties of nanocomposites prepared from LDPE and ionomers as described later.

LDPE vs. poly(ethylene-co-methacrylic acid) ionomer

Morphology

TEM micrographs of nanocomposites prepared from LDPE and a sodium ionomer of poly(ethylene-co-methacrylic acid), Surlyn® 8945, are presented in Figure 4.7. Nanocomposites were prepared using a one-tailed organoclay, $M_3(HT)_1$, a two-tailed organoclay, $M_2(HT)_2$-95, and a three-tailed organoclay, $M_1(C_{16})_3$.

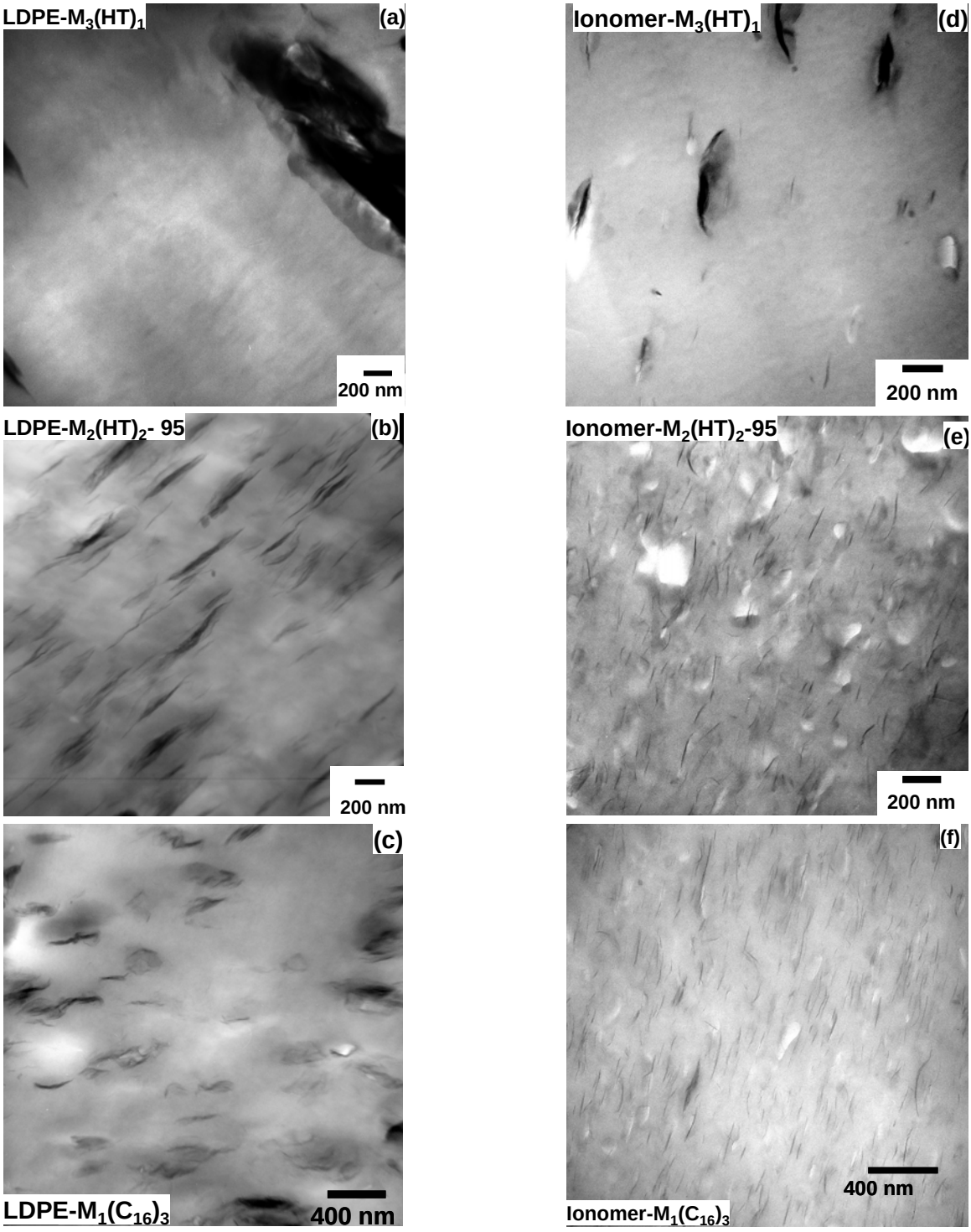

Figure 4.7 TEM micrographs of nanocomposites prepared from LDPE and Surlyn® 8945 ionomer using a one-tailed organoclay (a, d), two-tailed organoclay (b, e), and a three-tailed organoclay (c,f).

Two trends emerge from the six TEM micrographs presented above: (i) In both polymers, LDPE and the ionomer, organoclays with multiple alkyl tails exfoliate better than the organoclay with a single alkyl tail (similar to the observations made in ethylene/methacrylic acid copolymers). (ii) With all three organoclays, the level of exfoliation achieved in the ionomer was higher than that achieved in LDPE. It appears that the presence of the polar methacrylic acid groups and the ionic clusters improves the favorable interactions between the organoclay and the polymer, which subsequently leads to better exfoliation in these systems compared to nanocomposites prepared from LDPE.

The WAXS patterns of nanocomposites prepared from LDPE and the ionomer are shown in Fig. 4.8. All of these patterns show a distinct peak indicative of the presence of unexfoliated tactoids. However, the position of peaks has shifted in different directions with respect to the WAXD patterns of the organoclays from which they were prepared. For nanocomposites prepared from both, LDPE and the ionomer, the X-ray peaks of the composites formed from the one-tailed organoclay, $M_3(HT)_1$, have shifted to lower d-spacings than the organoclay. This is largely due to the thermal degradation of the one-tailed surfactant as described in Chapter 8. WAXS patterns of nanocomposites prepared from another one-tailed organoclay, $M_3(C_{16})_1$, showed similar peak-shifts. XRD patterns of nanocomposites prepared from multiple-tailed organoclays are different for LDPE and the ionomer. While the X-ray patterns of nanocomposites prepared from LDPE and the two-tailed/ three-tailed organoclay show peaks that have shifted to lower d-spacings (compared to those of the organoclays used to prepare them), the X-ray patterns of nanocomposites prepared from the ionomer using the same multiple-tailed organoclays

exhibit peaks that have shifted to higher d-spacings relative to that of the organoclays used to prepare them. As mentioned earlier, this could result from the intercalation of the polymer or some oligomers (that may be present in the polymer) inside the clay galleries. As shown below, in all cases, the peak position is unaffected by the montmorillonite content of the nanocomposite.

Mechanical properties

Tensile modulus of nanocomposites prepared from LDPE and Surlyn® 8945 ionomer are presented in Fig. 4.9. The data are in agreement with the results of TEM analysis presented above, i.e., for both polymers, nanocomposites prepared from $M_1(C_{16})_3$ organoclay exhibit a higher level of reinforcement than the nanocomposites prepared from $M_2(HT)_2$-95 organoclay, which in turn show greater modulus than the nanocomposites prepared from the two one-tailed organoclays. It is not always possible to directly correlate the level of reinforcement achieved to the degree of organoclay exfoliation in two different systems. As shown in Fig. 4.10, nanocomposites prepared from LDPE and the ionomer show similar improvements in modulus over those the unfilled polymer. However, as shown earlier, the level of organoclay exfoliation achieved in the ionomer based nanocomposites is much superior than that observed in LDPE based nanocomposites. Part of the reason for such a discrepancy is the difference between the values of the tensile modulus of the two unfilled polymers. As mentioned earlier, low-modulus matrices offer greater potential for reinforcement per unit mass of filler than high-modulus matrices due to the larger ratio of the filler modulus to the matrix modulus [6-8]. A detailed attempt aimed at explaining such discrepancies is presented in Chapter 5.

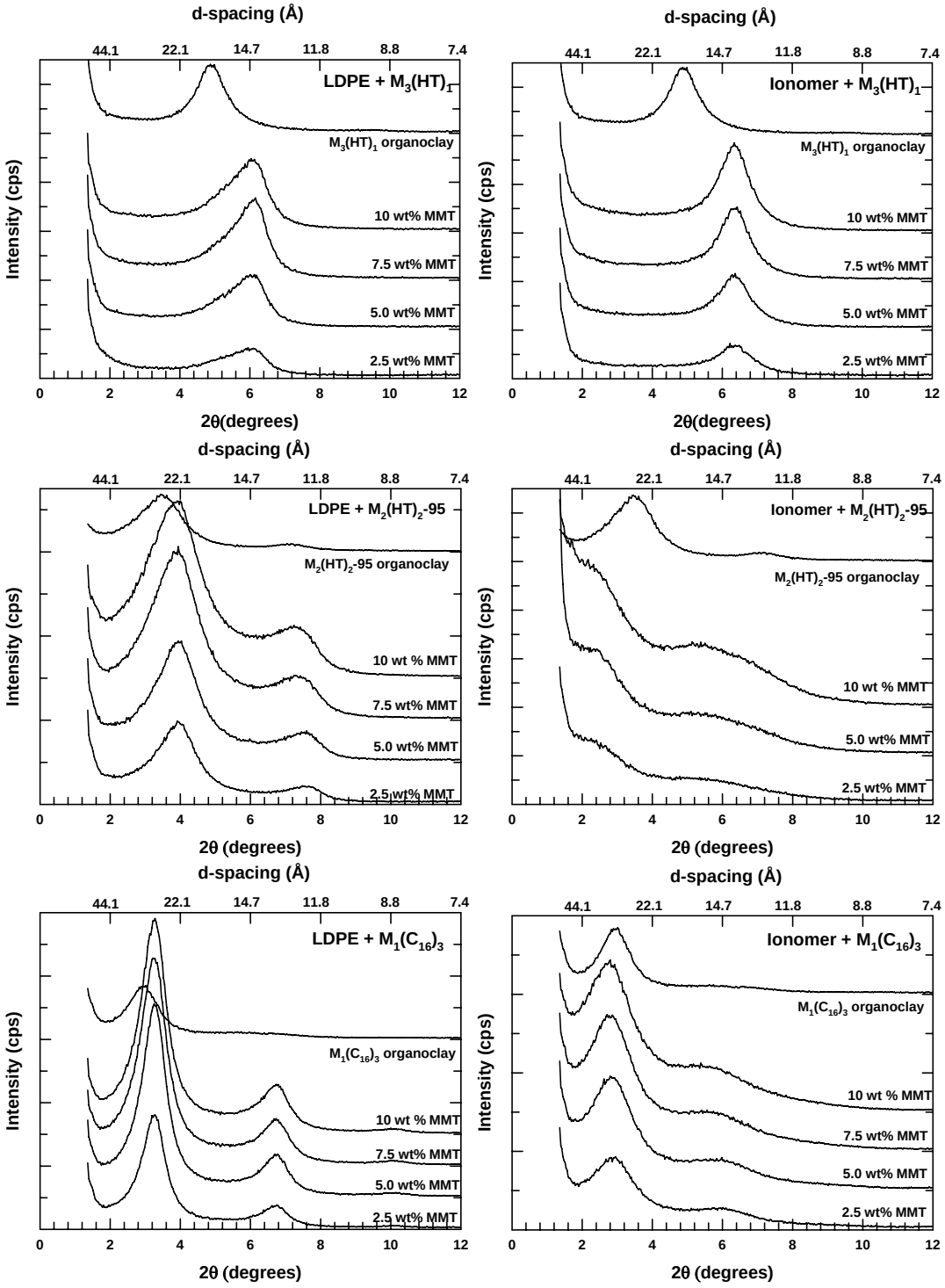

Figure 4.8 WAXS patterns of nanocomposites prepared from LDPE and Surlyn® 8945 ionomer using a one-tailed organoclay, $M_3(HT)_1$, a two-tailed organoclay, $M_2(HT)_2$-95, and a three-tailed organoclay, $M_1(C_{16})_3$. The curves are shifted vertically for clarity.

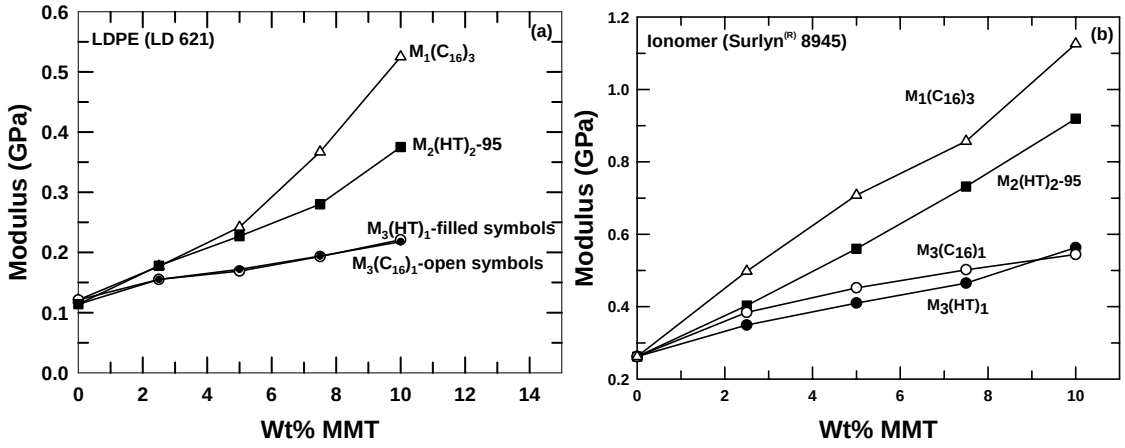

Figure 4.9 Tensile modulus of nanocomposites prepared from (a) LDPE and (b) Surlyn® 8945 ionomer using one-tailed, two-tailed, and three-tailed organoclays.

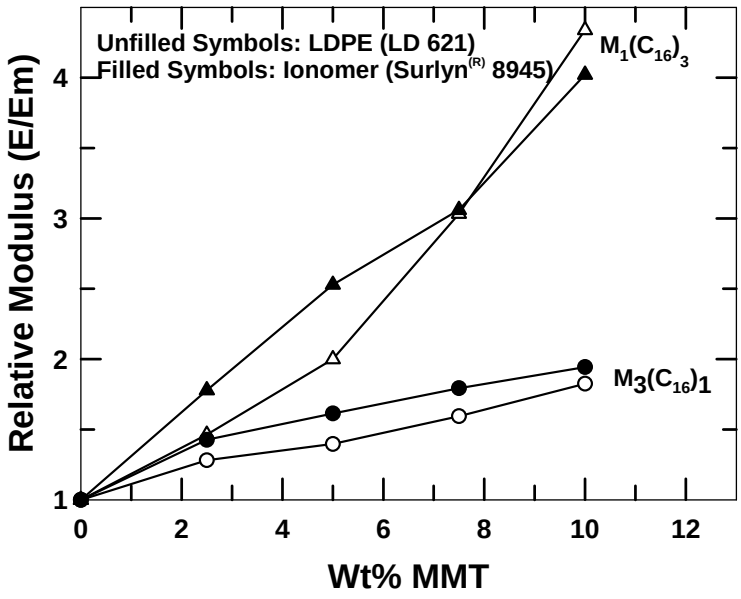

Figure 4.10 Relative modulus of nanocomposites prepared from LDPE and the ionomer using a one-tailed organoclay, $M_3(C_{16})_1$, and a three-tailed organoclay, $M_1(C_{16})_3$.

CONCLUSIONS

The effects of matrix modification on the morphology and mechanical properties of polyethylene based nanocomposites have been examined. In an effort to improve the polarity of the polymer, and thus, the polymer-organoclay interactions, three different modifications of polyethylene were employed. (i) maleic anhydride grafted polyethylene (ii) ethylene-methacrylic acid copolymers, and (iii) an ionomer of poly(ethylene-co-methacrylic acid). The level of organoclay exfoliation and the degree of reinforcement achieved in nanocomposites based on these polymers were compared to equivalent nanocomposites prepared from unmodified polyethylene. All of the three modifications resulted in significant improvements in organoclay exfoliation and/or reinforcement compared to the base polyethylene. Also, for all polymers examined in this study, nanocomposites made from organoclays with multiple alkyl tails exhibit a much better degree of clay exfoliation and distribution compared to those made from one-tailed organoclays.

REFERENCES

[1] Editors. Modern Plastics 2005;(September 2005)

[2] Rose J. Modern Plastics 2001;(October 2001):37.

[3] Lee H-s, Fasulo PD, Rodgers WR, Paul DR. Polymer 2005;46(25):11673-89.

[4] Paul DR, Zeng QH, Yu AB, Lu GQ. Journal of Colloid and Interface Science 2005;292(2):462-8.

[5] Shah RK, Paul DR. Accepted by Polymer

[6] Halpin JC, Finlayson KM, Ashton JE. *Primer on composite materials analysis*. 2nd , rev. / ed. 1992, Lancaster, Pa.: Technomic Pub. Co. xi, 227.

[7] Halpin JC, Kardos JL. Polymer Engineering and Science 1976;16(5):344-52.

[8] Fornes TD, Paul DR. Macromolecules 2004;37(20):7698-709.

Chapter 5: Comparison of nanocomposites made from sodium, zinc, and lithium ionomers of poly(ethylene-co-methacrylic acid)

As described in Chapter 4, ionomers of ethylene/methacrylic acid copolymers are more efficient than the base polyolefin (LDPE) at exfoliating montmorillonite based organoclays. The presence of the pendant ionic groups and the polar methacrylic acid groups in these ionomers potentially creates favorable interactions between the polymer and the aluminosilicate clays, resulting in a much more exfoliated morphology compared to nanocomposites prepared from LDPE. In this study, we examine the effect of the type of neutralizing cation on the exfoliation efficiency in the ion containing polymer and on the morphology and mechanical properties of the nanocomposites formed. Sodium, zinc, and lithium ionomers of poly(ethylene-co-methacrylic) acid were carefully chosen such that all other specifications, viz., melt index, acid content, and degree of neutralization, are comparable. Nanocomposites were prepared by melt mixing these ionomers with an appropriate organoclay in a twin screw extruder. Stress-strain analysis, X-ray scattering (WAXS), and transmission electron microscopy (TEM) coupled with particle analysis were used to evaluate the level of organoclay exfoliation, and appropriate mechanisms have been suggested to explain the differences in the rheology, morphology and properties of these nanocomposites.

EXPERIMENTAL

Three commercial grades of Surlyn® ionomer resins, Surlyn® 7940, 8945, and 9945 were purchased from du Pont. These are lithium, sodium, and zinc salts,

respectively, of poly(ethylene-co-methacrylic acid). As shown in Table 2.1, all three polymers have similar melt indices, acid contents, and degrees of neutralization. Since it was determined that higher levels of organoclay exfoliation could be achieved using surfactants with multiple alkyl tails on the ammonium ion rather than one tail (see Chapter 4, 7), a two-tailed organoclay, $M_2(HT)_2$-95, was chosen as the organoclay for this study. Selected properties of this organoclay are also included in Chapter 2.

Melt compounded composites were prepared using a Haake, co-rotating, intermeshing twin screw extruder using a barrel temperature of 190 ^{o}C, and a screw speed of 280 rpm. The polymers and the organoclays were premixed, and fed to the extruder using a single hopper. Initially, the feed rate was set at 1200 g/hr. However, the high melt viscosities generated in the case of a few nanocomposites based on the zinc ionomer (containing more than 5 wt% MMT) resulted in high values of extruder torque that exceeded the permissible limits of the equipment. Hence, all nanocomposites evaluated in this study were prepared using a lower feed rate of 800 g/hr. Surlyn® materials were dried in a vacuum oven at 65 ^{o}C for a minimum of 48 hours prior to compounding while the organoclays were used as received. In the past, the amount of montmorillonite in nanocomposites prepared from polyethylene and nylon 6 was determined using the incineration techniques described in Chapter 2. It was not possible to employ this technique with these ionomers since the polymer itself resulted in a hard, yellowish-green coating on the inside of the crucible reflecting some complex residue of the inorganic component of the ionomer. The amount of the residue varied from batch to batch rendering this method useless for quantitative analysis. Hence, in order to ensure that a predetermined polymer/ MMT ratio was maintained in all cases, the desired

amounts of clay and polymer were premixed before feeding to the extruder and precautions were taken to minimize any losses of organoclay during the extrusion process.

The samples were injection molded using a barrel temperature of 220 ^{o}C, mold temperature of 45 ^{o}C, injection pressure of 70 bar and a holding pressure of 40 bar. The nanocomposites were characterized using WAXS, TEM, particle analysis, and stress-strain analysis as described earlier. The data revealed standard deviations of the order of 2-7% for modulus, 1-10% for tensile strength at break and, 2-21% for elongation at break. Yield stress data are not reported because the stress-strain behavior of some of the ionomers and their nanocomposites do not show a distinct yield point.

Relative melt viscosities of the polymers and their nanocomposites were determined using a DSM micro-compounder operated under "recycle" mode. A charge of 2.5g of polymer/nanocomposite pellets was mixed separately in the micro-compounder using a constant screw speed of 100 rpm at 190 ^{o}C. The axial force, which is a function of the melt viscosity, was recorded at regular intervals over a 10 minute period.

RESULTS

Processability and rheology

Fig. 5.1 shows the electrical current drawn by the extruder motor while processing the various nanocomposites based on lithium, sodium, and zinc ionomers of poly(ethylene-co-methacrylic acid) at a feed rate of 800 g/hr. At a fixed screw-speed, the current drawn is a function of the torque, which in turn is dependent upon the melt viscosity of the nanocomposite being processed. For nanocomposites prepared from the

lithium ionomer, the current does not change much with clay concentration. For the nanocomposites based on the sodium ionomer, there is a small increase in the current when the clay content is gradually increased from 2.5 wt% MMT to 10.0 wt% MMT. The slightly lower current observed for the nanocomposites made from the sodium ionomer, compared to those formed from the lithium ionomer at low filler concentrations, could be a result of the small difference in the melt indices of the two matrices (4.5 g/10 min. vs. 2.6 g/10 min.). In contrast, the current for the nanocomposites based on the zinc ionomer increases steadily, but significantly, when the montmorillonite content is increased from 2.5 wt% to 10 wt%, which is indicative of a large increase in melt viscosity as the clay content is increased.

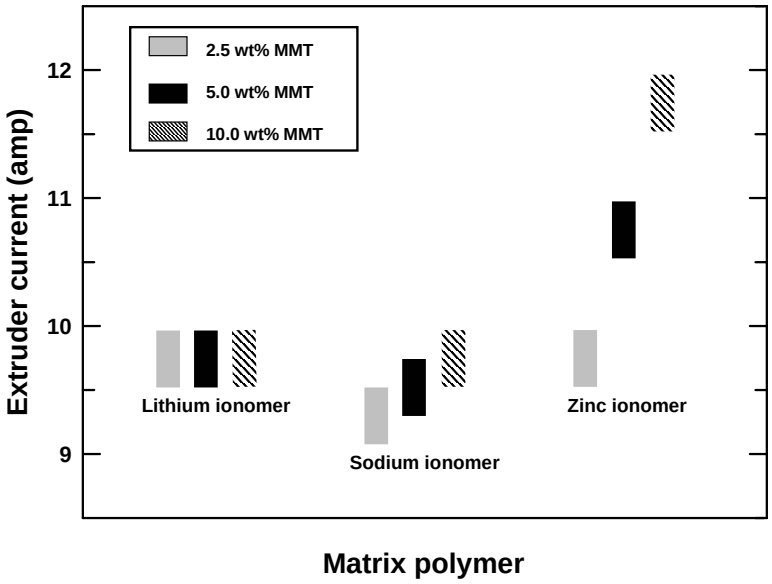

Figure 5.1 The electrical current drawn by the extruder motor during extrusion of the various nanocomposites based on ionomers of ethylene/methacrylic acid copolymers. The feed (polymer + organoclay) rate in all cases is 800 g/hr.

To get a rough idea of the comparative melt viscosities, we decided to measure the relative viscosities of the unfilled polymers and their nanocomposites using a DSM micro-compounder as described in the experimental section. Fig. 5.2(a) compares the axial force generated by the polymer melts when sheared at 190 ^{o}C using a screw speed of 100 rpm in a DSM micro-compounder. Initially (t < 90 seconds), the forces decrease with time for all three ionomers. The differences between the forces generated by the three polymer melts in this region could be attributed to the small differences in their melt indices. Between t = 90 sec. and t = 600 sec., there is little change in the axial force generated by the lithium and sodium ionomer melts; however, the force exerted by the zinc ionomer melt increases steadily to a value which is ~25 % higher than the minimum observed at t < 90 sec. Although, we are not completely sure what causes this increase in the melt viscosity of the zinc ionomers, we believe it is a result of possible formation of anhydrides in the polymer melt. As mentioned in Table 2.1, the degree of neutralization of the ionomers used in this study is about 40%. The remaining unneutralized acid groups are capable of forming anhydrides (with the expulsion of water); these anhydrides could act as branch (and eventually crosslink) points, which could lead to an increase in the melt viscosity of the polymer. Transition metal salts (such as zinc acetate) are well-known to catalyze anhydride formation, just as they act as esterification catalysts. So, it could be that this process is more rapid for Zn ionomers than Li and Na ionomers [1, 2].

The nanocomposites prepared from these ionomers exhibited similar trends as shown in Fig. 2(b). Careful comparison of Fig. 2(a) and 2(b) suggests that, while the axial forces generated by the nanocomposites prepared from sodium and zinc ionomers is higher than those of the corresponding unfilled polymers, the nanocomposite based on

the lithium ionomer produces a smaller viscous force than the lithium ionomer itself. The higher melt viscosities of the sodium and zinc ionomer nanocomposites could be an artifact of organoclay exfoliation in these polymers, while the lower melt viscosity of the Li ionomer nanocomposites could be a consequence of compositional changes of the organoclay that are unique to mixing with the lithium ionomer as described later.

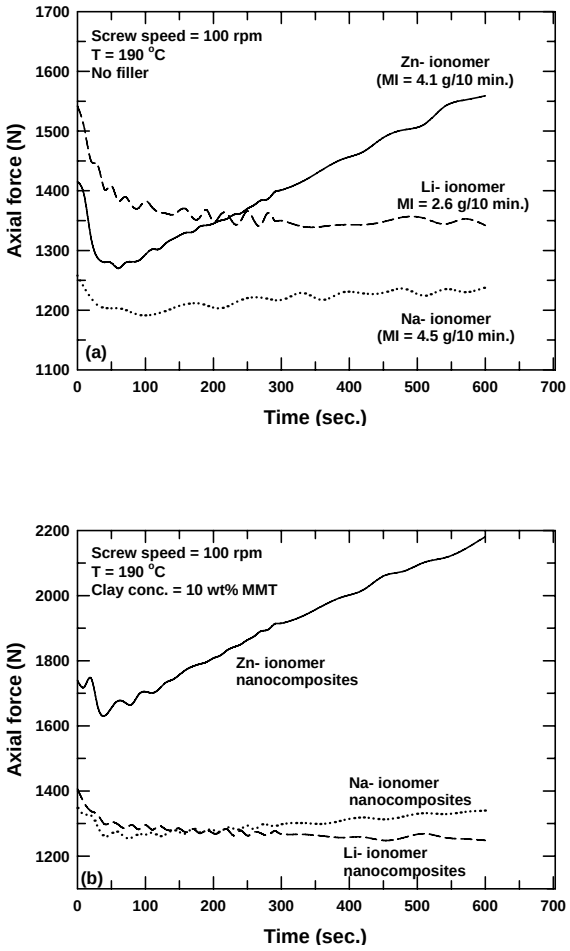

Figure 5.2 The axial forces generated by (a) the ionomers, and (b) nanocomposites containing 10 wt% MMT prepared from these ionomers, when sheared at 190 °C using a screw speed of 100 rpm in a DSM micro-compounder.

TEM and particle analysis

Fig. 5.3 shows TEM micrographs comparing the morphology of nanocomposites formed from $M_2(HT)_2$-95 organoclay and lithium, sodium, and zinc ionomers of poly(ethylene-co-methacrylic acid). The concentration of montmorillonite in all three samples is 5 wt%. Nanocomposites prepared from the sodium ionomer (Fig. 5.3(b)), and the zinc ionomer (Fig. 5.3(c)) exhibit better clay exfoliation or dispersion of the organoclay than the one prepared from the lithium ionomer (Fig. 5.3(a)). The micrographs of nanocomposites prepared from the former two reveal a pattern of uniformly dispersed single platelets along with a few thin stacks comprised of 2-4 platelets. On the other hand, the morphology of the lithium ionomer based nanocomposites revealed a significant number of thicker stacks of platelets.

To provide a quantitative comparison of the level of organoclay exfoliation in the three matrices, particle analysis was conducted on TEM micrographs of nanocomposites using image analysis techniques as described in Chapter 2. Fig. 5.4 shows a series of histograms of MMT particle lengths and pertinent statistical data obtained on nanocomposites containing ~5 wt% MMT prepared from $M_2(HT)_2$-95 organoclay and the three ionomers. The sections were taken parallel to the flow direction but perpendicular to the major face. Similar measurements were conducted for the thickness of clay particles and the results are plotted in Fig 5.5. The filler particles in the nanocomposites prepared from the sodium and the zinc ionomer were shorter and thinner than the ones in the nanocomposites based on the lithium ionomer.

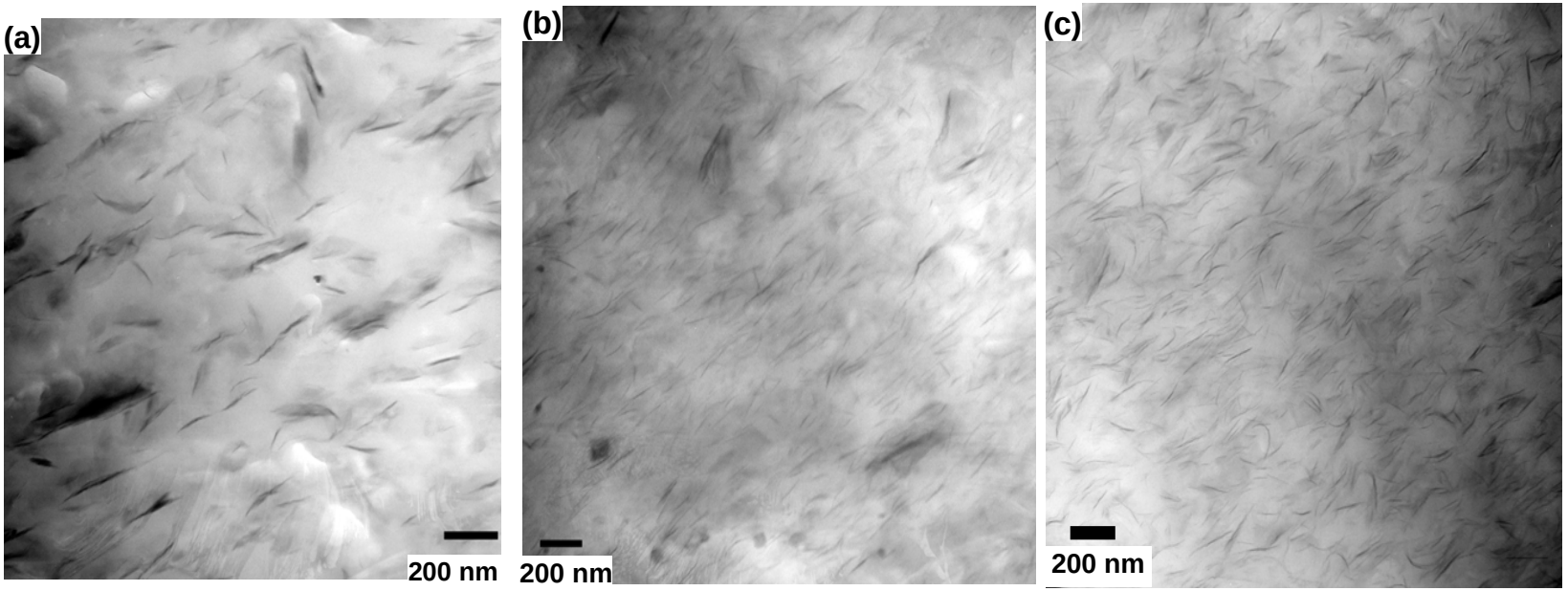

Figure 5.3 TEM micrographs of nanocomposites prepared from $M_2(HT)_2$-95 organoclay and (a) lithium, (b) sodium, and (c) zinc ionomers of poly(ethylene-co-methacrylic acid). The concentration of MMT in all three cases is ~5 wt%. Sections were microtomed from the core portion of an Izod bar in a plane parallel to the flow direction but perpendicular to the major face.

Table 5.1 Results of particle analysis

Organoclay nanocomposites	Total number of particles	Number average particle length, (nm)	Weight average particle length (nm)	Number average particle thickness (nm)	Weight average particle thickness (nm)	Aspect ratio[a]	Aspect ratio[b]
Lithium ionomer (Surlyn® 7940) + 5 wt% MMT	502	163.3	214.7	11.9	25.4	13.7	8.4
Sodium ionomer (Surlyn® 8945) + 5 wt% MMT	762	92.6	119.2	3.5	8.0	26.5	14.9
Zinc ionomer (Surlyn® 9945) + 5 wt% MMT	703	92.7	120.6	3.4	5.5	27.3	21.9

[a] These values of the aspect ratio were computed from the number average platelet lengths and thicknesses.
[b] These values of the aspect ratio were computed from the weight average platelet lengths and thicknesses.

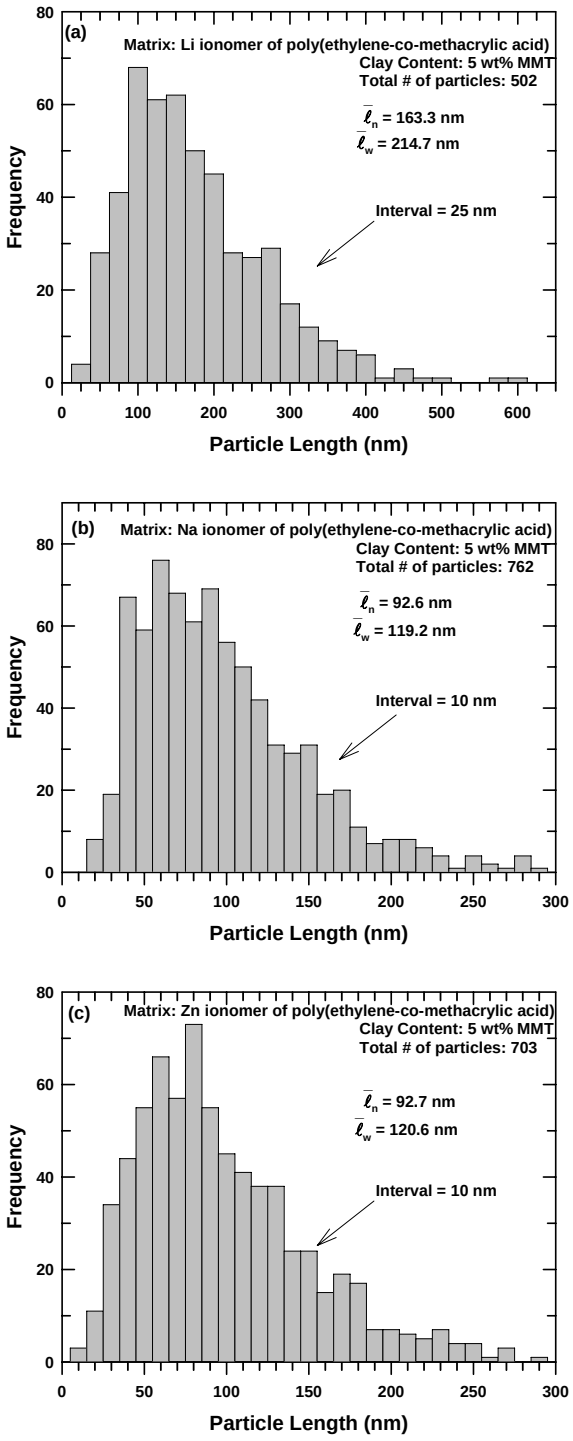

Figure 5.4 Histograms of MMT particle length obtained by analyzing TEM micrographs of nanocomposites containing ~5 wt% MMT prepared from (a) lithium, (b) sodium, and (c) zinc ionomers of poly(ethylene-co-methacrylic acid).

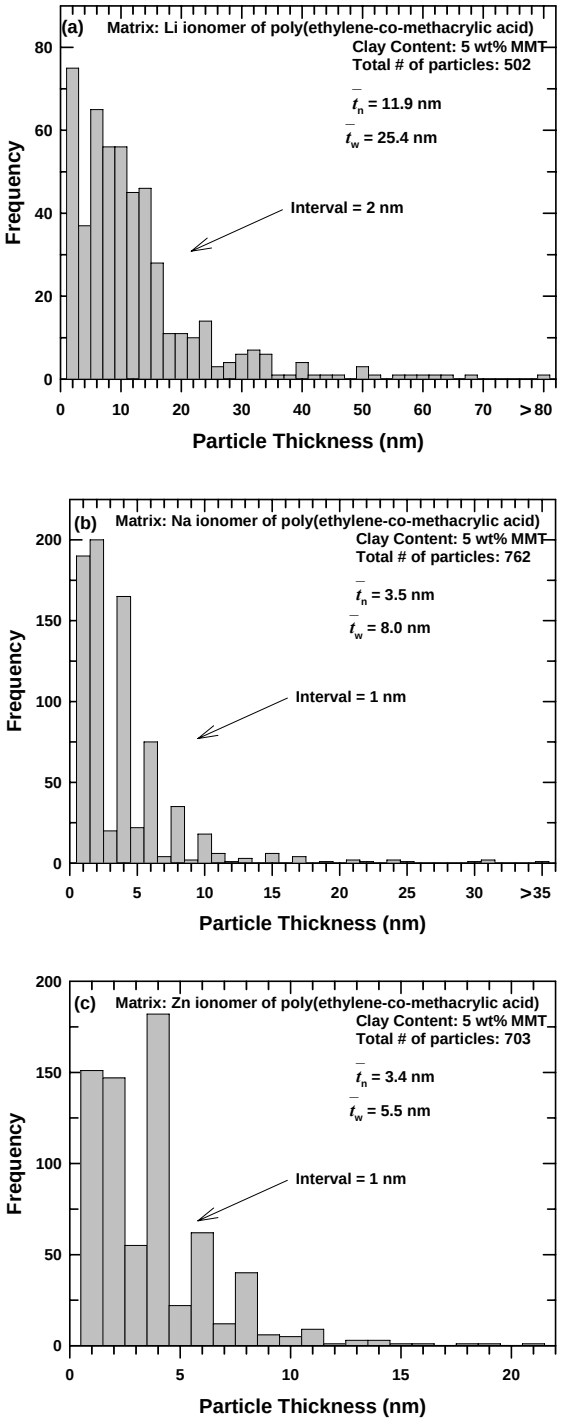

Figure 5.5 Histograms of MMT particle thickness obtained by analyzing TEM micrographs of nanocomposites containing ~5 wt% MMT prepared from (a) lithium, (b) sodium, and (c) zinc ionomers of poly(ethylene-co-methacrylic acid).

The average particle length of ~92 nm calculated in the case of the former two nanocomposites agrees well with the average particle length in well-exfoliated nylon 6 nanocomposites determined using a similar technique [3]. It is interesting to note the greater average particle length in the nanocomposite prepared from the lithium ionomer (163 nm) compared to similar nanocomposites prepared from the sodium and zinc ionomers (92 nm). This could be a result of a partial breakdown of the clay agglomerates comprised of randomly overlaid platelets and the "skewing" of thicker clay bundles as described by Chavarria et al.[4]. The thickness distribution profiles of particles in the nanocomposites prepared from the sodium ionomer and the zinc ionomer appear to be fairly similar, with ~75 % of the particles having a thickness of 4 nm or less. Their average particle thickness (~3.5 nm) was noticeably lower than that calculated for the nanocomposites based on the lithium ionomer (11.9 nm). The aspect ratio of the particles in each nanocomposite was determined by dividing the average particle length by the average particle thickness of the nanocomposite (see Table 5.1). The average particle aspect ratio in the nanocomposites based on the sodium ionomer and the zinc ionomer was calculated to be ~ 27, while that in the nanocomposites based on the lithium ionomer was determined to be ~ 14. Based on TEM evaluation and particle analysis, it can be concluded that, (i) the sodium and the zinc ionomers are much more efficient at exfoliating the $M_2(HT)_2$-95 organoclay than the lithium ionomer, and (ii) there is not much difference in the morphology of the nanocomposites (containing 5 wt% MMT) prepared from the sodium and the zinc ionomer.

Mechanical properties

Selected mechanical properties of the nanocomposites prepared are listed in Table 5.2. However, before we discuss these properties in detail, it is important to highlight the similarities and subtle differences in the stress-strain behavior of these composites. Figure 5.6 displays typical stress-strain diagrams for nanocomposites prepared from $M_2(HT)_2$-95 organoclay and lithium, sodium and zinc ionomers. The stress-strain curves of the unfilled lithium and sodium ionomers reveal a distinct stress maximum followed by a slight drop in the tensile stress after this yield point, corresponding to the onset of necking. This stress drop gradually diminishes as the clay content increases. In contrast, the stress-strain curves of the zinc ionomer and nanocomposites prepared from it do not show a maximum stress or a yield point. The stress-strain curves of almost all polymers/nanocomposites suggest the occurrence of strain hardening. The slope of the plastic region, indicative of the level of strain hardening decreases as the clay content increases.

Table 5.2 Selected mechanical properties of nanocomposites prepared by melt mixing $M_2(HT)_2$ organoclay and ionomers of poly(ethylene-co-methacrylic acid)

Polymer	MMT content (wt%)	Tensile modulus, E (GPa)	Relative modulus, E/E_m	Elongation at break (5.1 cm/min) (%)	Tensile strength at break (5.1 cm/min) (MPa)
Zinc ionomer	0.0	0.176	1.00	172	19.3
Zinc ionomer	2.5	0.314	1.78	116	22.2
Zinc ionomer	5.0	0.447	2.50	85.9	24.2
Zinc ionomer	10.0	0.795	4.51	58.9	29.2
Sodium ionomer	0.0	0.260	1.00	194	21.0
Sodium ionomer	2.5	0.412	1.58	130	22.6
Sodium ionomer	5.0	0.568	2.18	119	25.9
Sodium ionomer	10.0	0.908	3.49	65.6	28.8
Lithium ionomer	0.0	0.292	1.00	136	21.0
Lithium ionomer	2.5	0.407	1.38	116	24.2
Lithium ionomer	5.0	0.491	1.68	104	24.8
Lithium ionomer	10.0	0.676	2.32	98.4	27.2

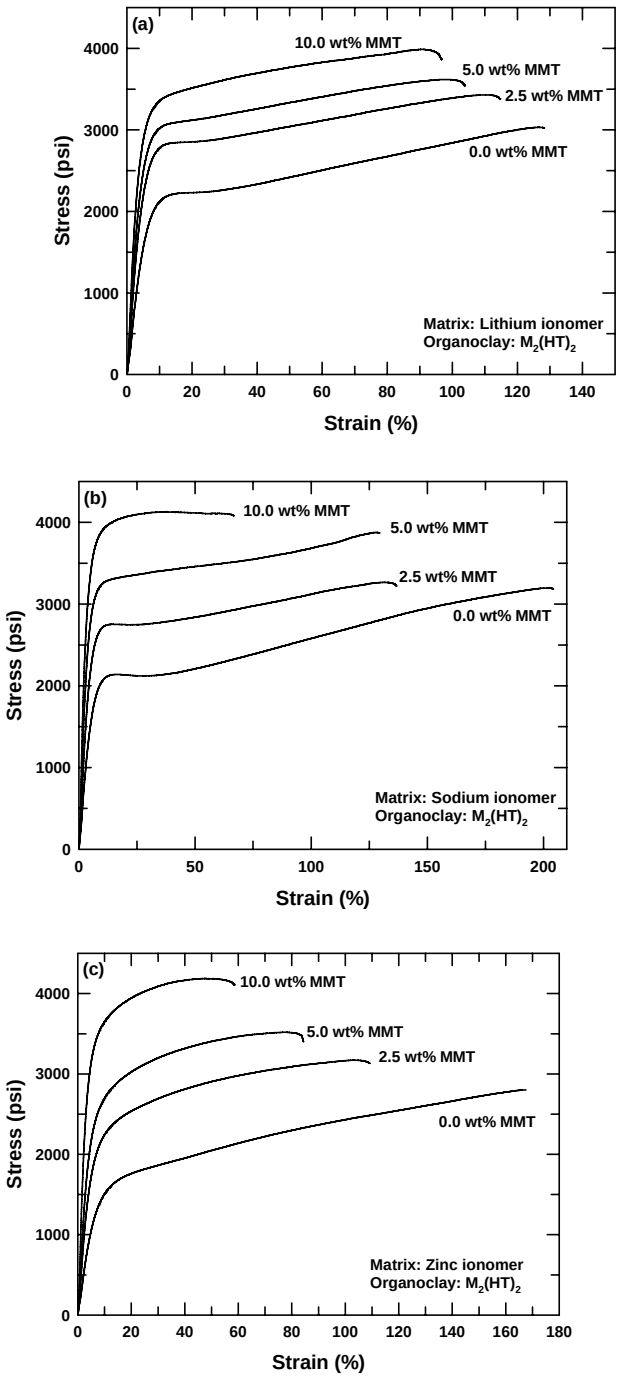

Figure 5.6 Representative stress-strain diagrams of nanocomposites prepared from $M_2(HT)_2$ organoclay and (a) lithium, (b) sodium, and (c) zinc ionomers of poly(ethylene-co-methacrylic acid).

Fig. 5.7(a) compares the tensile moduli of the different nanocomposites as a function of their montmorillonite content. As expected, the stiffness of all ionomers improves substantially with addition of $M_2(HT)_2$-95 organoclay. To get a comparative idea of the improvements in the level of reinforcement achieved, the relative moduli of the nanocomposites are plotted against the montmorillonite content in Fig. 5.7(b). It is clear that the increase in modulus observed in nanocomposites prepared from the sodium and zinc ionomers is much greater than that observed in nanocomposites prepared from the lithium ionomer. However, the level of reinforcement observed in nanocomposites formed from the zinc ionomer seems to be somewhat greater than that seen for those formed from the sodium ionomer. These differences are more pronounced at higher MMT content. Thus, it appears that the moduli data are not in complete agreement with the results of the particle analysis, which revealed similar aspect ratios for the zinc ionomer, and sodium ionomer based nanocomposites containing 5 wt% MMT. We are not completely sure about the cause of this disagreement between the results of the two analytical methods. In principle, some part of this discrepancy could stem from differences between the moduli of the two ionomers (0.176 GPa vs. 0.260 GPa). Composite theory predicts that for a given filler aspect ratio, low-modulus matrices offer greater potential for reinforcement per unit mass of filler than high-modulus matrices due to the larger ratio of filler modulus to the matrix modulus [5, 6]. However, simple calculations using the Halpin-Tsai theory reveal that the discrepancy noted above cannot be fully rationalized in this way [7, 8]. But then again, these calculations are based upon numerous simplifications and assumptions of ideal conditions [7].

Another explanation may stem from some departure from one of the basic premises of composite theory, i.e., the matrix modulus is not altered by the presence of the nano-scale clay particles [5, 6]. It was suggested above that anhydride formation occurs in nanocomposite based on the zinc ionomer but not those containing sodium or lithium. This chemistry might possibly alter the material properties. There seems to be no simple or straightforward way to test such a hypothesis.

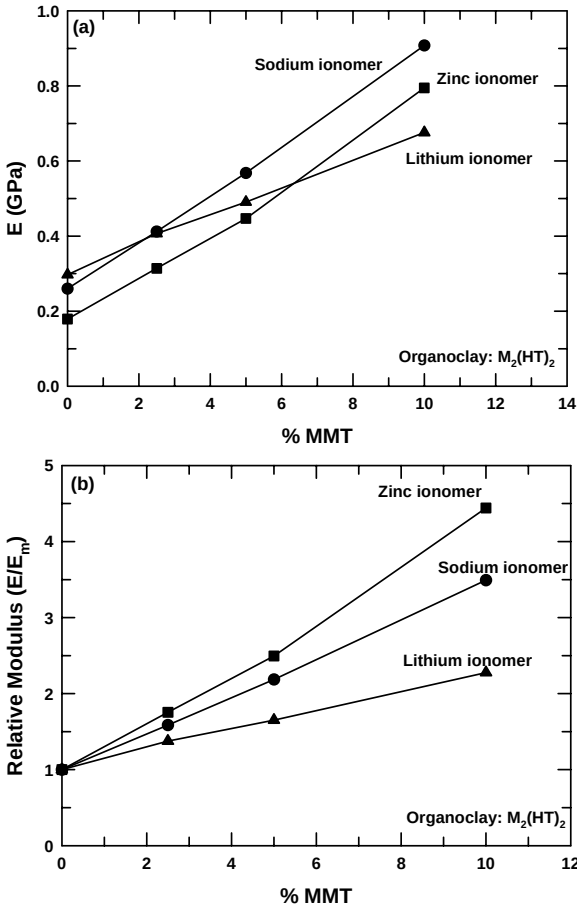

Figure 5.7 (a) Tensile modulus and (b) Relative modulus of nanocomposites prepared from lithium, sodium, and zinc ionomers of poly(ethylene-co-methacrylic acid).

Finally, a certain degree of caution should be exercised when attempting to correlate mechanical properties with morphology determined by TEM since each micrograph provides a snapshot of only a small microscopic area. An extensive particle analysis is needed to fully describe the morphology of the macroscopic sample which is reflected in property measurements like modulus. Particle analysis of such partially exfoliated systems is a tricky job, and both, human and software limitations need to be taken into consideration. This is especially true during analysis of the thicknesses of the particles (a comparison of Fig. 5.4 and Fig. 5.5 reveals that while the length distributions of the particles suggest a uniform gamma distribution, the thickness distribution of the particles do not). Furthermore, any differences in platelet orientation are reflected in the measured value of the modulus, but are not accounted for in the numerical values determined using the particle analysis method employed in this study.

The comparatively smaller improvements in the modulus of the lithium ionomer by addition of the organoclay is a result of the relatively lower levels of organoclay exfoliation in these systems compared to nanocomposites prepared from the zinc and lithium ionomers (as revealed by TEM micrographs). The slightly higher modulus of the unfilled lithium ionomer compared to the other two polymers contributes to some degree to this observation; we propose an additional explanation below.

The relationship between the MMT content of the nanocomposites and their elongation at break is shown in Fig. 5.8. The unfilled ionomers are very ductile, but increasing the clay content sacrifices ductility. The drop in ductility with increasing organoclay is much steeper for the zinc and sodium ionomer based nanocomposites compared to similar nanocomposites prepared from the lithium ionomer. This is

consistent with the higher level of organoclay exfoliation in the sodium and zinc ionomers than in the lithium ionomer.

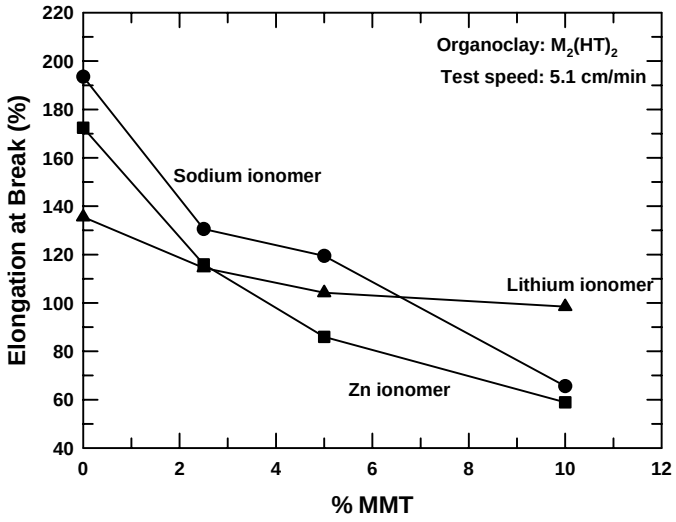

Figure 5.8 Elongation at break measured at a crosshead speed of 5.1 cm/min for nanocomposites prepared from lithium, sodium, and zinc ionomers of poly(ethylene-co-methacrylic acid).

WAXS analysis

Figure 5.9 compares the WAXS scans of the $M_2(HT)_2$-95 organoclay and its nanocomposites prepared by melt mixing with the three ionomer matrices. The organoclay pattern reveals an intense peak at around $2\theta = 3.46^{\circ}$, corresponding to a basal spacing of 25.5 Å. WAXS patterns of all nanocomposites show a distinct peak indicative of the presence of unexfoliated clay tactoids. However, the positions of the peaks for the nanocomposites shift in different directions relative to the peak of the organoclay. The peaks for composites formed from the zinc and sodium ionomers are shifted to higher d-spacings than the organoclay, which according to prevalent understanding suggests the intercalation of mass, e.g., polymer, within the clay galleries. On the other hand, the peak

for the nanocomposite prepared from the lithium ionomer is shifted to the right (lower d-spacings) suggesting loss of mass from the galleries, e.g., loss of surfactant mass by degradation or some other mechanism [9]. A detailed description and a proposed mechanism for this phenomenon resulting from the interactions between the lithium ionomer and the filler are described below.

The position of the peak did not change with organoclay content of the nanocomposites; however, the height of the peak increases as the clay concentration increases as shown in Fig. 5.10. WAXS results for nanocomposites prepared from unmodified polyethylene exhibit similar trends [10].

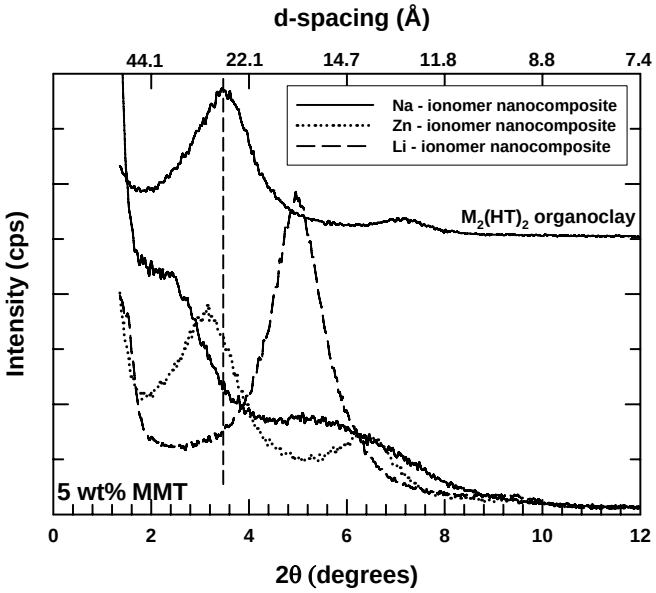

Figure 5.9 WAXS patterns of nanocomposites prepared from $M_2(HT)_2$ organoclay and the three ionomers. The concentration of MMT in all cases is ~5 wt%. X-ray pattern of the $M_2(HT)_2$ organoclay is plotted for comparison, and is shifted vertically for clarity. The dotted vertical line shows the position of the d_{001} peak of the organoclay.

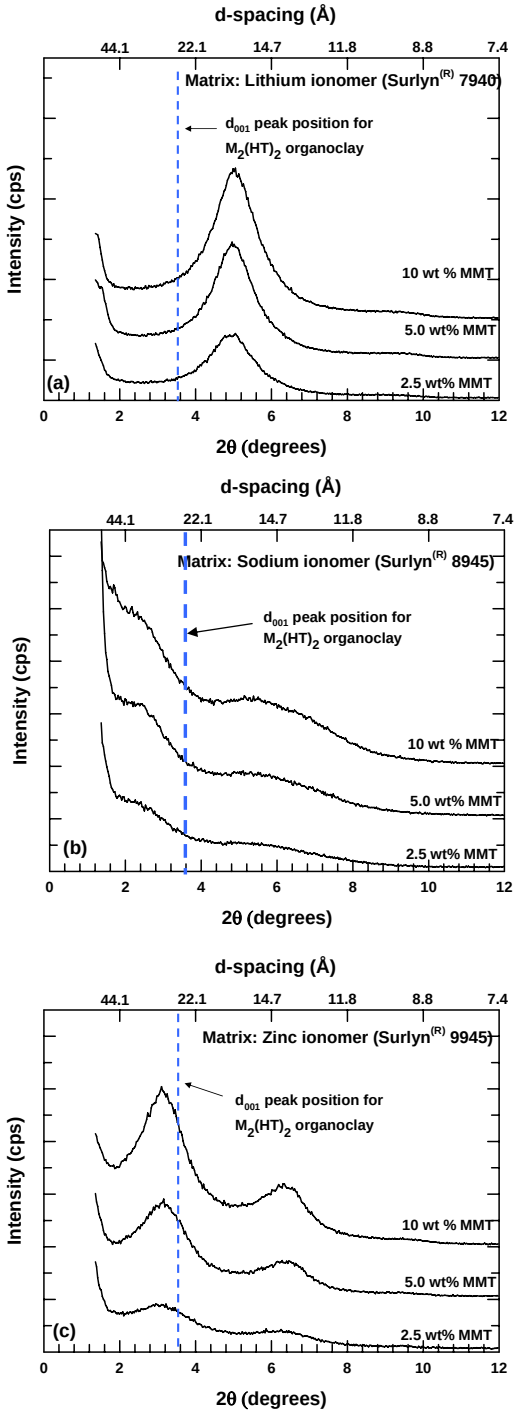

Figure 5.10 WAXS patterns of nanocomposites prepared from $M_2(HT)_2$ organoclay and (a) lithium, (b) sodium, and (c) zinc ionomers of poly(ethylene-co-methacrylic acid). The dotted vertical line showing the position of the d_{001} peak of the $M_2(HT)_2$ organoclay is included for comparison. The curves are shifted vertically for clarity.

DISCUSSION

As described above, a series of polymer-silicate nanocomposites were prepared by melt mixing $M_2(HT)_2$-95 organoclay with lithium, sodium, and zinc ionomers of poly(ethylene-co-methacrylic acid). Three observations merit special consideration: (i) Unlike the nanocomposites prepared from the sodium and the zinc ionomers, the melt viscosity of the nanocomposite prepared from the lithium ionomer was lower than that of the matrix polymer. (ii) Nanocomposites prepared from the zinc and the sodium ionomers exhibited a higher level of organoclay exfoliation compared to equivalent nanocomposites prepared from the lithium ionomer. (iii) WAXS peaks of the nanocomposites prepared from the sodium and the zinc ionomers shifted to the left (higher d-spacing); whereas, those based on the lithium ionomer shifted to the right (lower d-spacing).

The right shift of the WAXS peak of a nanocomposite is indicative of a decrease in the interplatelet spacing of the organoclay and is generally attributed to the loss of mass from the organoclay galleries, e.g., by thermal degradation of the surfactant [9, 11]. The quaternary ammonium surfactants used for preparing the organoclays are known to degrade at the high temperatures required to melt process the nanocomposites. The initial thermal degradation, which is believed to follow a Hoffman elimination mechanism [12-14], begins at temperatures as low as 155-165 ^oC. WAXS patterns of similar nanocomposites prepared from polyethylene [9], polypropylene [9], polystyrene [11], and nylon 66 [4] have also revealed such shifts to the right. For LDPE/ $M_2(HT)_2$-95 nanocomposites, the X-ray peak shifts to 23.2 Å when melt processed at 200 ^oC [9]. Increasing the processing temperature to 240 ^oC results in a further decrease in the

organoclay d-spacing (22 Å). For the nanocomposites prepared from the lithium ionomer at 190 ^{o}C, the organoclay d-spacing is reduced much more significantly (from 25.5 Å to 17.4 Å) compared to that reported for nanocomposites prepared from other polymers using a similar organoclay [9]. It is important to note that WAXS patterns of nanocomposites prepared from the zinc and the sodium ionomers do not reveal such peak shifts. As far as we know, there are no reports of the catalytic effects of the Li^{+} ion on the Hoffman elimination reaction. Thus, it appears that for the nanocomposites based on the lithium ionomer, there may be another mechanism than thermal degradation of the surfactant by the Hoffman elimination reaction involved in the shift of WAXS peak to higher d-spacings.

A possible explanation may involve an ion exchange process between the organoclay and these ionomers, wherein a few of the bulky quaternary ammonium ions of the organoclay are replaced by the smaller metal cations of the ionomers, thus, reducing the d-spacing of the organoclay as shown in Fig. 5.11. The obvious question is why such behavior is only exhibited by the nanocomposites prepared from the lithium ionomer and not by the nanocomposites prepared from the sodium and the zinc ionomers? The answer possibly lies in the smaller size, and the higher reactivity of the lithium cation. The Li^{+} ion has a radius of 0.68 Å compared to 0.74 Å for the Zn^{++} ion and 0.98 Å for the Na^{+} ion. The Li^{+} ion is capable of entering the montmorillonite lattice structure, resulting in an irreversible exchange of quaternary ammonium ions [15-22]. Hofmann and Klemen [15] showed that heating Li^{+} saturated bentonite caused fixation of previously exchangeable Li^{+} ions and a reduction of the Cation Exchange Capacity (CEC) and expandability of the main clay mineral present in bentonite (Hofmann-

Klemen effect). The irreversible exchange of the Li^+ ions could serve as a driving force for the cation exchange process between the organoclay and the ionomer. On the other hand, Zn^{++} and Na^+ ions are not as capable of entering the montmorillonite lattice structure as the Li^+ ions. Emmerich et al. [23, 24], while investigating homoionic forms of montmorillonite heated at 220 ^oC for 20 h, found that the CEC of the Li^+ forms of montmorillonite dropped to 28% of the value observed in an unheated sample. In comparison, the CEC of Zn^{++} form dropped marginally to 91%, and there was no change in the CEC of the Na^+ form. Thus, in the case of nanocomposites prepared from the sodium and the zinc ionomers there is no driving force to promote the cation exchange reaction between the polymer and the organoclay.

The cation exchange process and the relatively lower levels of organoclay exfoliation could also explain why nanocomposites prepared from the lithium ionomer do not show similar improvements in melt viscosity over that of the unfilled ionomer as those revealed by nanocomposites prepared from the sodium and the zinc ionomers. Replacement of the smaller Li^+ cations by bulkier quaternary ammonium cations in the polymer phase should affect the melt rheology of the nanocomposite.

(a) Cation exchange process between the ionomer and the organoclay

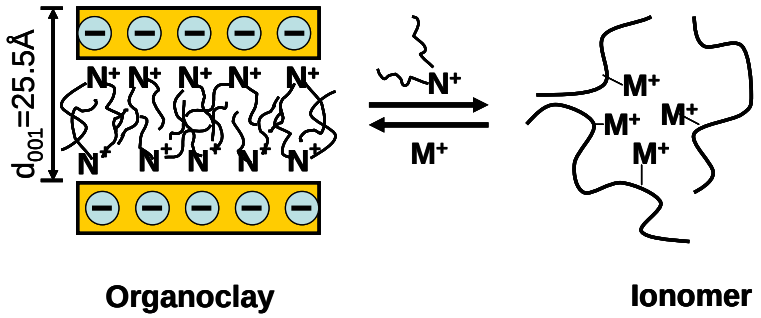

(b) In the case of nanocomposites prepared from the lithium ionomer ($M^+ = Li^+$), the exchanged lithium cation irreversibly enters the MMT lattice structure

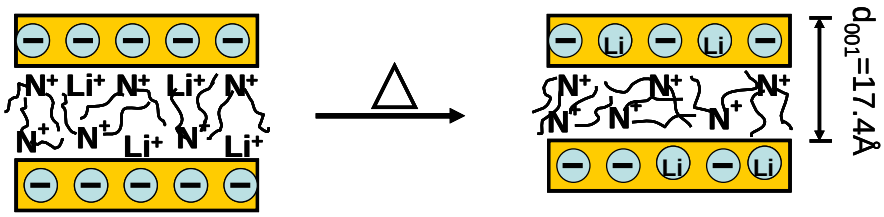

Figure 5.11 Schematic of the proposed ion-exchange process between the ionomer and the organoclay which subsequently leads to a reduction in the d-spacing of the nanocomposites prepared from the lithium ionomer.

CONCLUSIONS

Structure-property relationships for nanocomposites prepared from ionomers of poly(ethylene-co-methacrylic acid) and $M_2(HT)_2$-95 organoclay have been presented here. The effect of the neutralizing cation on the exfoliation efficiency of the polymer was evaluated by comparing the morphology and properties of nanocomposites prepared from sodium, zinc, and lithium ionomers of poly(ethylene-co-methacrylic acid). Based

on transmission electron microscopy and particle analysis of the images, nanocomposites prepared from the zinc and the sodium ionomers show much better exfoliation of the organoclay compared to equivalent nanocomposites prepared from the lithium ionomer. The mechanical properties of the nanocomposites paralleled the TEM observations in this regard. WAXS peaks of the sodium and the zinc ionomer based nanocomposites showed shifts to larger d-spacings relative to the organoclay, suggesting intercalation of polymer species within the organoclay gallery. On the other hand, the WAXS peaks of nanocomposites prepared from the lithium ionomer shifted to lower d-spacings indicating loss of mass from the galleries of the organoclay. Based upon WAXS analysis, mechanical property data, and melt rheology observations, the lower levels of organoclay exfoliation observed in the nanocomposites prepared from the lithium ionomer are suggested to be a result of the irreversible exchange of quaternary ammonium ions for the very small lithium ions that can enter the montmorillonite lattice structure.

REFERENCES

[1] Register RA, *Personal communication*.

[2] Winey KI, *Personal communication*.

[3] Fornes TD, Paul DR. Polymer 2003;44(17):4993-5013.

[4] Chavarria F, Paul DR. Polymer 2004;45(25):8501-15.

[5] Halpin JC, Kardos JL. Polymer Engineering and Science 1976;16(5):344-52.

[6] Halpin JC, Finlayson KM, Ashton JE. *Primer on composite materials analysis*. 2nd , rev. / ed. 1992, Lancaster, Pa.: Technomic Pub. Co. xi, 227.

[7] Fornes TD, Paul DR. Macromolecules 2004;37(20):7698-709.

[8] Stretz HA, Paul DR, Cassidy PE. Polymer 2005;46(11):3818-30.

[9] Shah RK, Paul DR. Accepted by Polymer

[10] Shah RK, Cui L, Williams KL, Bernard B, Paul DR. Accepted by Journal of Applied Polymer Science

[11] Tanoue S, Utracki LA, Garcia-Rejon A, Tatibouet J, Cole KC, Kamal MR. Polymer Engineering and Science 2004;44(6):1046-60.

[12] Xie W, Gao Z, Pan W-P, Hunter D, Singh A, Vaia R. Chem Mater 2001;13(9):2979-90.

[13] Fornes TD, Yoon PJ, Paul DR. Polymer 2003;44(24):7545-56.

[14] Davis R, Gilman J, VanderHart D. Polym Degrad Stab 2003;79:111-21.

[15] Hofmann U, Klemen R. Z anorg Chem 1950;262:95-9.

[16] Madejova J, Bujdak J, Gates WP, Komadel P. Clay Minerals 1996;31(2):233-41.

[17] Madejova J, Bujdak J, Petit S, Komadel P. Clay Minerals 2000;35(5):739-51.

[18] Alvero R, Alba MD, Castro MA, Trillo JM. Journal of Physical Chemistry 1994;98(32):7848-53.

[19] Theng BKG, Hayashi S, Soma M, Seyama H. Clays and Clay Minerals 1997;45(5):718-23.

[20] Calvet R, Prost R. Clays and Clay Minerals, Proceedings of the Conference 1971;19(3):187-91.

[21] Stackhouse S, Coveney PV. Journal of Physical Chemistry B 2002;106(48):12470-7.

[22] Williams J, Purnell JH, Ballantine JA. Catalysis Letters 1991;9(1-2):115-19.

[23] Emmerich K, Madsen FT, Kahr G. Clays and Clay Minerals 1999;47(5):591-604.

[24] Emmerich K, Plotze M, Kahr G. Applied Clay Science 2001;19(1-6):143-54.

Chapter 6: Nanocomposites from fluoro-oxygenated polyethylene: A novel route to organoclay exfoliation

Effect of matrix modification on the exfoliation efficiency of polyethylene was explored in Chapter 4. In this chapter, we present a novel method to improve organoclay exfoliation in polyethylene. The polarity of high density polyethylene, HDPE, was increased by the subjecting the HDPE particles to a fluoro-oxidation process, alternatively known as reactive-gas surface treatment (RGST). These surface treated HDPE particles (ST-HDPE) were then melt mixed with an appropriate organoclay to form nanocomposites with improved levels of exfoliation. Transmission electron microscopy (TEM), wide angle X-ray scattering (WAXS), stress-strain analysis and Izod impact measurements were used to evaluate nanocomposite morphology and physical properties. In addition, these data were compared to that of equivalent nanocomposites prepared from unmodified HDPE and HDPE grafted with maleic anhydride (HDPE-g-MA), the same two polymers described in Chapter 4.

EXPERIMENTAL

As mentioned above, HDPE (HiD 9055), HDPE-g-MA (Fusabond® E MB265D), and ST-HDPE (Inhance® HD-1800) were used in this study. A brief description of these materials is given in Table 2.1. ST-HDPE was prepared by subjecting 18μ HDPE particles to a reactive gas atmosphere containing F_2 and O_2, a process sometimes termed as fluoro-oxidation. This treatment functionalizes the surface such that it has a composition of 10-15 atomic percent fluorine and 10-15 atomic percent oxygen. Surface

functionalities include carboxyl, hydroxyl, and ketone functionalities. These polar groups create a very high surface energy on the particles that is in excess of 60 dynes/cm and enables the particles to be wet by and completely dispersed in water. The treatment essentially follows a free-radical mechanism. Cross-linking of the surface molecules on the particles occurs in concert with the treatment. Besides ST-HDPE, commercially available HDPE (without any modifications) and HDPE-g-MA with similar specifications were also used as matrices in this study for comparison purposes.

Based upon the analyses presented in Chapter 4, $M_2(HT)_2$-95 organoclay was used in this study. Nanocomposites were prepared by melt mixing the polymers with organoclay powder in a Haake, co-rotating, intermeshing twin screw extruder using a barrel temperature of 160 °C, screw speed of 280 rpm, and a feed rate of 1200 g/hr. A low extrusion temperature was selected to reduce organoclay degradation in these nanocomposites [1]. Also, the low extrusion temperature helped increase the melt viscosity of these low molecular weight, injection molding grade polymers. The higher melt viscosity also imparts sufficient melt strength to the extrudate strand for continuous pelletization. Following extrusion, the amount of montmorillonite (MMT) in each nanocomposite was confirmed by the incineration technique described in Chapter 2. Tensile specimens (ASTM D638) and Izod specimens (ASTM D256) were prepared by injection molding using a barrel temperature of 160 ^{o}C, mold temperature of 45 ^{o}C, injection pressure of 40 bar and holding pressure of 40 bar. The nanocomposites were characterized using WAXS, TEM, particle analysis, stress-strain analysis, and Izod impact testing as described in Chapter 2. Standard deviations of the order of 1-5% for

modulus, 0-2% for tensile strength, 0-21% for elongation at break, and 0-20 % for Izod impact strength were observed.

RESULTS AND DISCUSSION

Morphological Characterization using TEM and Particle Analysis

Fig. 6.1 shows TEM micrographs comparing the morphology of nanocomposites formed from $M_2(HT)_2$-95 organoclay and HDPE, ST-HDPE, and HDPE-g-MA matrices. Nanocomposites from ST-HDPE (Fig. 6.1(b)), and HDPE-g-MA (Fig. 6.1(c)) exhibit a much higher level of clay exfoliation and distribution compared to those made from unmodified HDPE (Fig. 6.1(a)). Of the two modifications of the HDPE matrix, HDPE-g-MA seems to exfoliate the organoclays better than ST-HDPE. The micrographs of nanocomposites prepared from the former reveal a pattern of uniformly dispersed single platelets along with a few thin bundles comprising of 2-3 platelets. On the other hand, the morphology of ST-HDPE/ $M_2(HT)_2$-95 nanocomposites, although much more exfoliated than HDPE/ $M_2(HT)_2$-95 nanocomposites, reveal thicker bundles comprising of 5-8 platelets.

To provide a quantitative comparison of the level of organoclay exfoliation in the three matrices, particle analysis was conducted on TEM micrographs of nanocomposites. For best statistical validity, a substantial number of particles (>300) should be analyzed for a given nanocomposite. This was not possible for the poorly exfoliated HDPE/ $M_2(HT)_2$-95 nanocomposites as each of their TEM micrographs barely contained 5-6 large sized agglomerates.

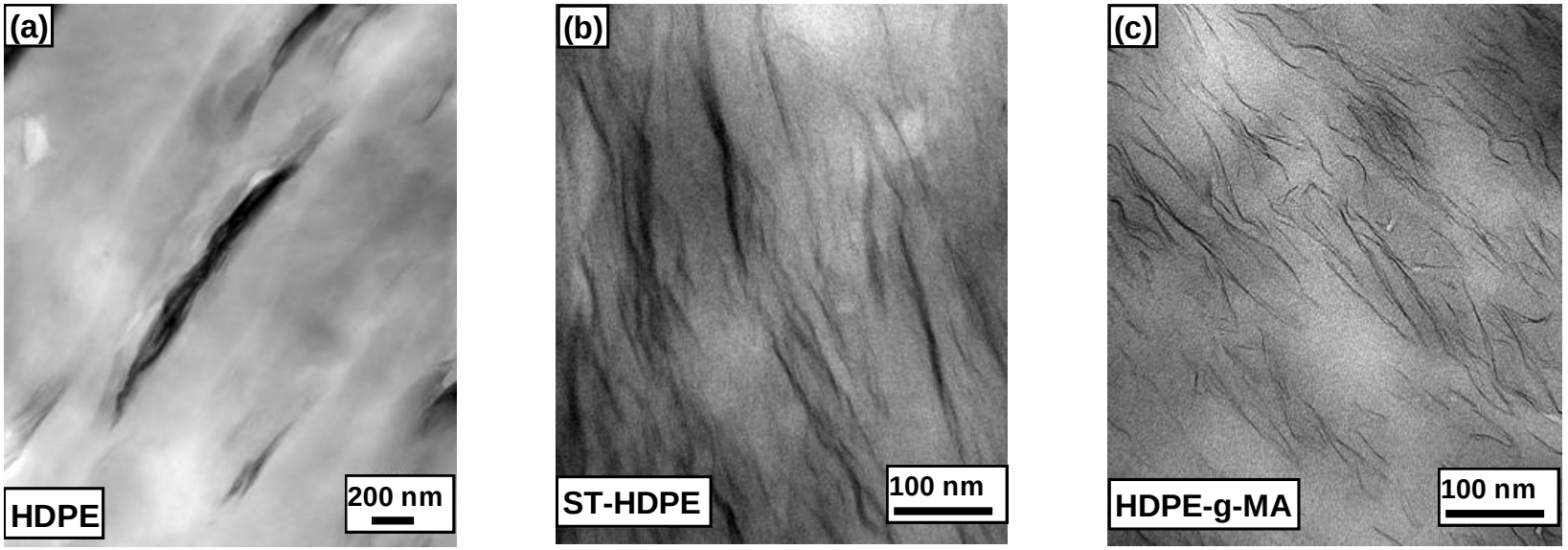

Figure 6.1 TEM micrographs of nanocomposites prepared from $M_2(HT)_2$-95 organoclay and (a) unmodified HDPE, (b) surface treated HDPE (ST-HDPE), and (c) maleic anhydride grafted HDPE (HDPE-g-MA). The concentration of MMT in all three cases is ~5 wt%.

Table 6.1 Particle analysis results

Organoclay nanocomposites	Number of particles analyzed	Number average particle length (nm)	Weight average particle length (nm)	Number average particle thickness (nm)	Weight average particle thickness (nm)	Aspect ratio[a]	Aspect ratio[b]
HDPE + 5.2 wt% MMT	28	548.0	806.8	73.1	130.1	7.5	6.2
ST-HDPE + 5.55 wt% MMT	348	114.5	149.0	6.5	8.8	17.5	17.0
HDPE-g-MA + 4.97 wt% MMT	421	53.0	68.0	1.9	2.7	28.4	25.5

[a] Computed from the number average platelet lengths and thicknesses.
[b] Computed from the weight average platelet lengths and thicknesses.

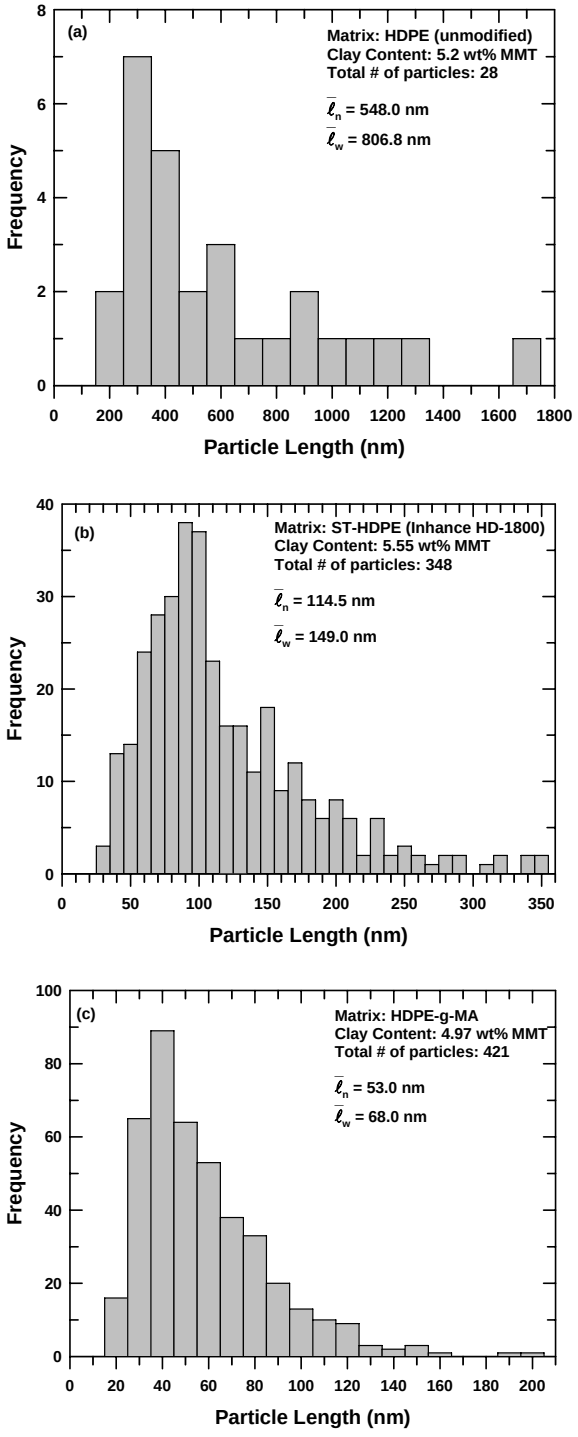

Figure 6.2 Histograms of MMT particle length obtained by analyzing TEM micrographs of nanocomposites containing ~5 wt% MMT prepared from (a) unmodified HDPE, (b) surface treated HDPE (ST-HDPE), and (c) maleic anhydride grafted HDPE (HDPE-g-MA).

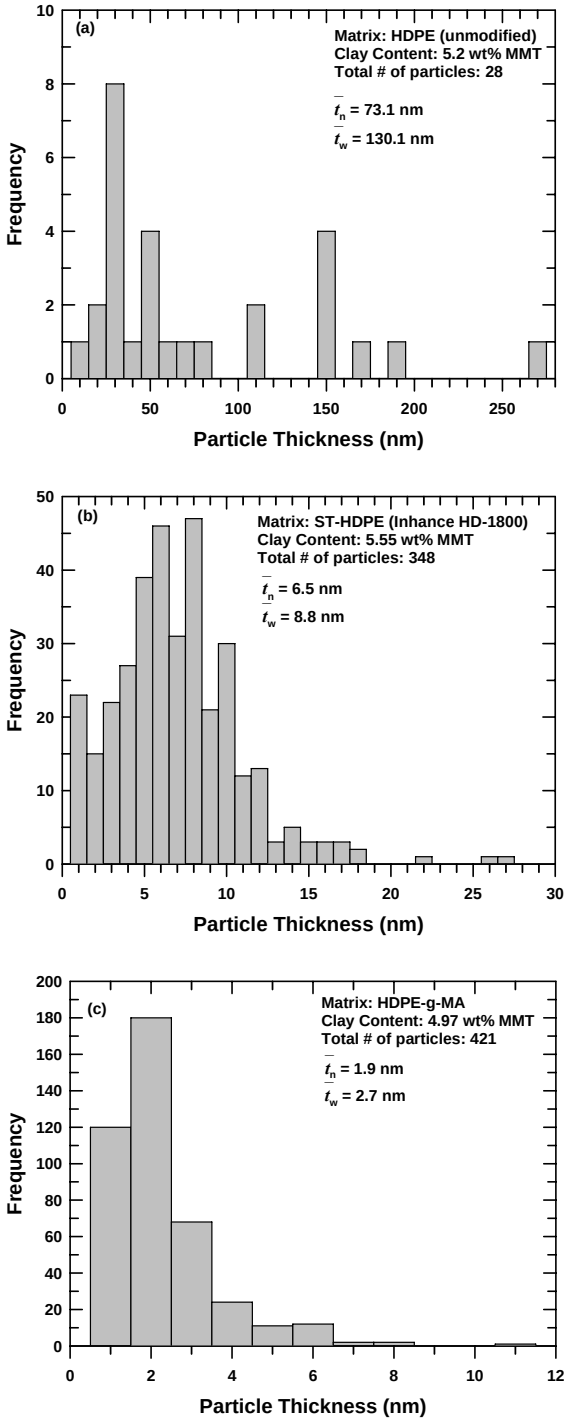

Figure 6.3 Histograms of MMT particle thickness obtained by analyzing TEM micrographs of nanocomposites containing ~5 wt% MMT prepared from (a) unmodified HDPE, (b) surface treated HDPE (ST-HDPE), and (c) maleic anhydride grafted HDPE (HDPE-g-MA).

Hence, for this study, the length and thickness of 28 particles were determined for HDPE/ $M_2(HT)_2$-95 nanocomposites, whereas 348 and 421 particles respectively of ST-HDPE/ $M_2(HT)_2$-95 and HDPE-g-MA/ $M_2(HT)_2$-95 nanocomposites were analyzed using a particle analysis software (see Table 6.1).

Fig. 6.2 shows a series of histograms of MMT particle lengths and pertinent statistical data obtained on nanocomposites containing ~5 wt% MMT prepared from $M_2(HT)_2$-95 organoclay and the three HDPE based matrices. The sections were taken parallel to the flow direction but perpendicular to the major face. Similar measurements were conducted for the thickness of clay particles and the results are plotted in Fig 6.3. As expected, the filler particle size in HDPE-g-MA and ST-HDPE based nanocomposites is much smaller than in HDPE based nanocomposites. The average particle length of 53 nm calculated for HDPE-g-MA nanocomposites agrees well with the average particle length in well-exfoliated nylon 6 nanocomposites determined using a similar technique.[21] The average particle thickness of 1.9 nm for HDPE-g-MA nanocomposites roughly corresponds to the thickness of two montmorillonite platelets and is slightly higher than the 1.5 nm thickness reported for nylon 6 nanocomposites [2]. This suggests that although HDPE-g-MA based nanocomposites reveal a fairly exfoliated morphology, the level of exfoliation is not as high as that seen in nanocomposites prepared from high molecular weight nylon 6. The average thickness of the filler particles in ST-HDPE nanocomposites was calculated to be 6.5 nm which is a little higher than HDPE-g-MA nanocomposite particles but significantly lower than the 73 nm thick particles observed in HDPE based nanocomposites. It is interesting to note the greater average particle length in ST-HDPE nanocomposites as compared to HDPE-g-MA (114 nm vs 53 nm). This

could be the result of partially sheared clay agglomerates and/or the "skewing" of thicker clay bundles as described by Chavarria et al. [2]. The aspect ratio of the particles in each nanocomposite was calculated by dividing the average particle length by the average particle thickness of the nanocomposite (see Table 6.1). Of the three matrices, HDPE-g-MA nanocomposite particles had the highest aspect ratio followed by ST-HDPE while the HDPE composite particles had the lowest aspect ratio. Based upon TEM evaluation and particle analysis, it could be safely concluded that the two matrix modification methods employed in this study significantly improve organoclay dispersion compared to that for a virgin polyethylene matrix. However, it appears that HDPE-g-MA exfoliates the organoclays better than the current version of ST-HDPE.

WAXS Analysis of Nanocomposites

Fig. 6.4 compares the WAXS scans of the $M_2(HT)_2$-95 organoclay and its nanocomposites prepared by melt mixing with three HDPE based matrices. The organoclay pattern reveals an intense peak at around $2\theta = 3.46°$, corresponding to a basal spacing of 25.5 Å. The X-ray pattern for the HDPE-g-MA based nanocomposites does not show a characteristic basal reflection which is often interpreted as a sign of complete exfoliation. However, we believe that this lack of an X-ray peak is the result of a combination of high levels of dispersion and a more random orientation of clay particles rather than indicating a completely exfoliated morphology. The TEM analyses support this hypothesis. The X-ray scan for HDPE based nanocomposites reveal a distinct peak indicative of the presence of unexfoliated clay tactoids. The peak position is the same as that of the pristine organoclay, which suggests that the organoclay interplatelet distances

were unaltered during the formation of these composites. On the other hand, the WAXS peak of the ST-HDPE nanocomposite shifted to a higher d-spacing than the organoclay, which according to prevalent understanding suggests the intercalation of polymer within the clay galleries.

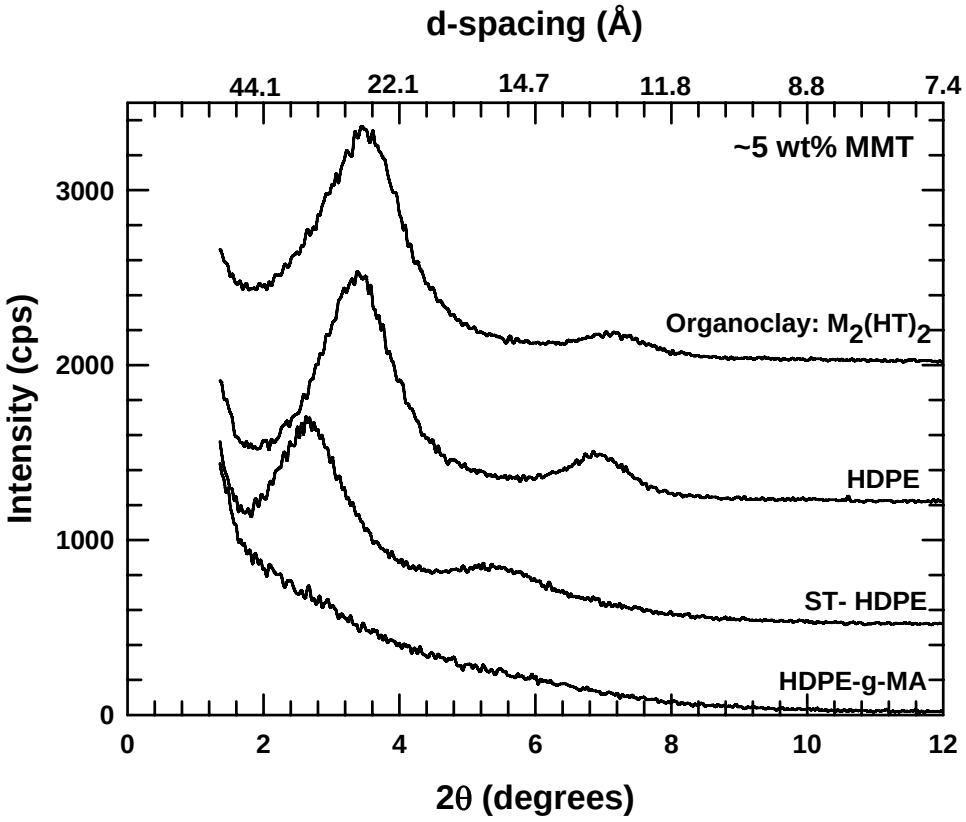

Figure 6.4 WAXS patterns of nanocomposites prepared from $M_2(HT)_2$ organoclay and the three HDPE based matrices. The concentration of MMT in all cases is ~5 wt%. X-ray pattern of the $M_2(HT)_2$ organoclay is plotted for comparison. The curves are shifted vertically for clarity.

The position of the peak (or the lack of it) does not change along with organoclay content of the nanocomposites as shown in Fig. 6.5. Nanocomposites made from LDPE [3] and poly(ethylene-co-methacrylic acid) ionomers [4] exhibit similar trends.

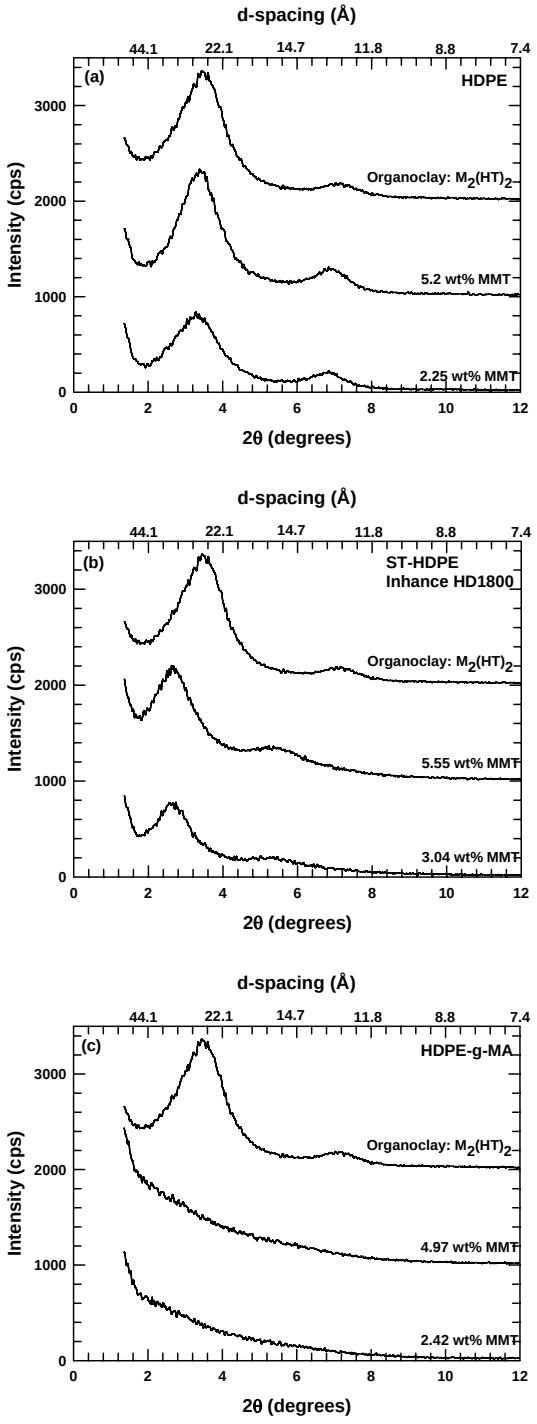

Figure 6.5 WAXS patterns of nanocomposites prepared from $M_2(HT)_2$ organoclay and (a) unmodified HDPE (b) surface treated HDPE (ST-HDPE), and (c) maleic anhydride grafted HDPE (HDPE-g-MA). X-ray pattern of the $M_2(HT)_2$ organoclay is plotted for comparison. The curves are shifted vertically for clarity.

Table 6.2 Selected mechanical properties of nanocomposites prepared in this study

Polymer	Clay loading	Modulus E	Relative modulus E/E_m	Tensile Strength	Elongation at break		Izod impact strength	
	(wt% MMT)	(GPa)		(0.51 cm/min) (MPa)	(0.51 cm/ min) (%)	(5.1 cm/ min) (%)	Gate end (J/m)	Far end (J/m)
HDPE	0.00	0.595	1.000	15.6	333.7	88.8	29.4	28.8
HDPE	2.25	0.678	1.139	16.3	15.7	12.1	20.6	20.6
HDPE	5.20	0.768	1.291	16.3	12.5	8.9	19.6	19.1
ST-HDPE	0.00	0.958	1.000	20.3	12.4	8.9	22.5	21.5
ST-HDPE	3.04	1.466	1.530	21.1	4.0	3.6	12.2	9.8
ST-HDPE	5.55	1.942	2.027	21.1	2.8	2.5	13.7	9.8
HDPE-g-MA	0.00	0.803	1.000	18.3	> 400	> 400	71.25[a]	51.74[a]
HDPE-g-MA	2.25	1.141	1.421	21.8	> 400	328.7	39.8	33.4
HDPE-g-MA	4.97	1.399	1.742	23.6	40.9	7.1	46.3	28.4

[a] Ductile failure. All other samples had brittle failure

Mechanical Properties

Selected mechanical properties of nanocomposites prepared from $M_2(HT)_2$-95 organoclay and the three HDPE based matrices are listed in Table 6.2. Fig. 6.6(a) compares the tensile modulus of the different nanocomposites as a function of their montmorillonite content. To account for the differences between the moduli of the three matrices, the relative improvement in stiffness achieved by melt mixing these polymers with $M_2(HT)_2$-95 organoclay is presented in Fig. 6.6(b). It is clear that the increase in modulus observed in nanocomposites prepared from ST-HDPE, and HDPE-g-MA matrices is much stronger than that observed in nanocomposites prepared from unmodified HDPE. However, the level of reinforcement observed in ST-HDPE based nanocomposites is comparable to, if not better than, that seen in HDPE-g-MA based nanocomposites. Thus, it seems that the moduli data is not in complete agreement with the nanocomposite morphology as revealed by TEM and WAXD analysis. This could be a result of possible differences between the filler orientation in ST-HDPE and HDPE-g-MA based nanocomposites. The tensile modulus of a nanocomposite sample is a function of the level of organoclay exfoliation and the orientation of the aluminosilicate platelets in the direction of the axial force. If the platelet orientation in HDPE-g-MA based nanocomposites is more random than in ST-HDPE based nanocomposites, their tensile moduli would not be as high as what one might expect based upon their filler aspect ratio. This could also explain why the WAXD patterns of HDPE-g-MA based nanocomposites are devoid of any peaks despite the presence of a few “doublets” and “triplets” as revealed by their TEM micrographs. Then again, we are not quite sure as to what could possibly lead to such differences between the filler orientation in the two

composite systems. Hotta et al. [5] reported a similar discrepancy between tensile properties and TEM morphology of nanocomposites prepared from LLDPE, and maleic anhydride grafted LLDPE (LLDPE-g-MA). In his study, nanocomposites prepared from LLDPE-g-MA revealed a very well exfoliated morphology as compared to those prepared from LLDPE. However, the mechanical properties of the two nanocomposite systems did not reflect this large difference in morphology to the extent expected.

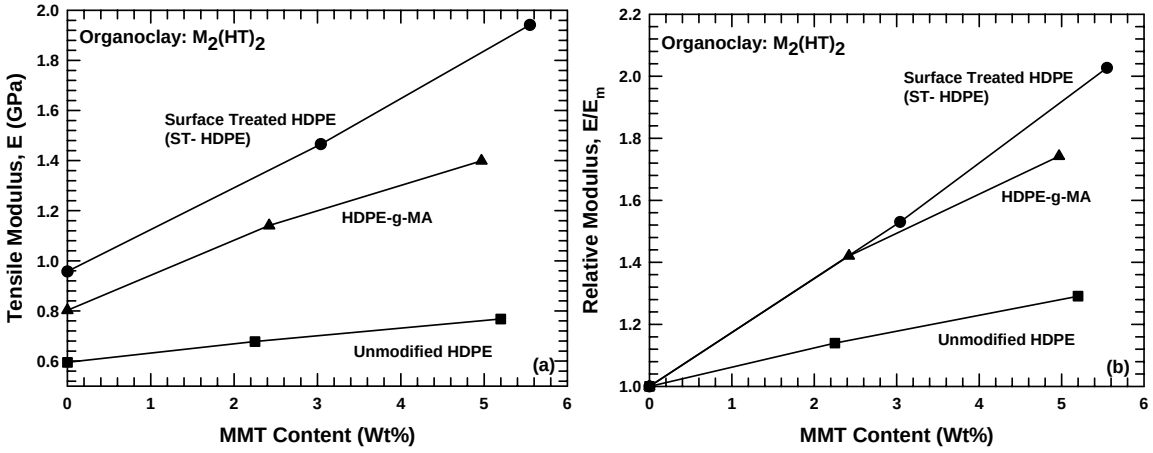

Figure 6.6 (a) Tensile modulus, and (b) Relative modulus of nanocomposites prepared from unmodified HDPE, surface treated HDPE (ST-HDPE), and maleic anhydride grafted HDPE (HDPE-g-MA).

The relationship between the MMT content of the nanocomposites and elongation at break is shown in Fig. 6.7 for two rates of extension. It is interesting to note the differences in the elongation at break values for the three unfilled polymers. The samples prepared from ST-HDPE exhibited much lower ductility as compared to those prepared from unmodified HDPE with similar specifications (~50 MI, 0.95 density). As expected, ductility of all polymers decreased along with an increase in the montmorillonite content.

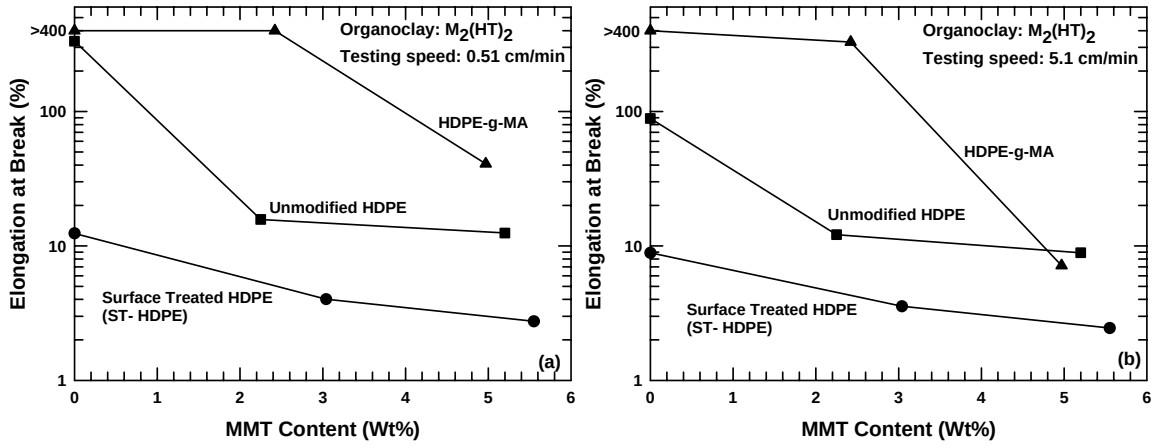

Figure 6.7 Elongation at break measured at crosshead speeds of (a) 0.51 cm/min and (b) 5.1 cm/min for nanocomposites prepared from unmodified HDPE, surface treated HDPE (ST-HDPE), and maleic anhydride grafted HDPE (HDPE-g-MA).

The effects of clay content on room temperature Izod impact behavior of nanocomposites prepared from HDPE, ST-HDPE, and HDPE-g-MA matrices are presented in Fig. 6.8. For all nanocomposites, toughness as judged by Izod deteriorates gradually with increasing clay concentration. There is not much difference between the trends observed in the gate and far end samples. However, the gate end samples do appear to be a little tougher than the far end samples (for both neat polymer and nanocomposites). It is interesting to note that although ST-HDPE and its nanocomposites are significantly less ductile than HDPE and composites made from it, there is not much difference between their Izod impact values. This could be attributed to the differences in moduli of the two sets of materials. Since the Izod measures the energy absorbed during impact, i.e., the area under the resisting force versus displacement curve during the test, the values obtained reflect a net result of opposing effects brought by higher stiffness and lower ductility. In our case, the higher modulus of ST-HDPE and its

nanocomposites somewhat compensates for the lowering effects (in terms of Izod impact strength) caused by their poor ductility (as compared to unmodified HDPE).

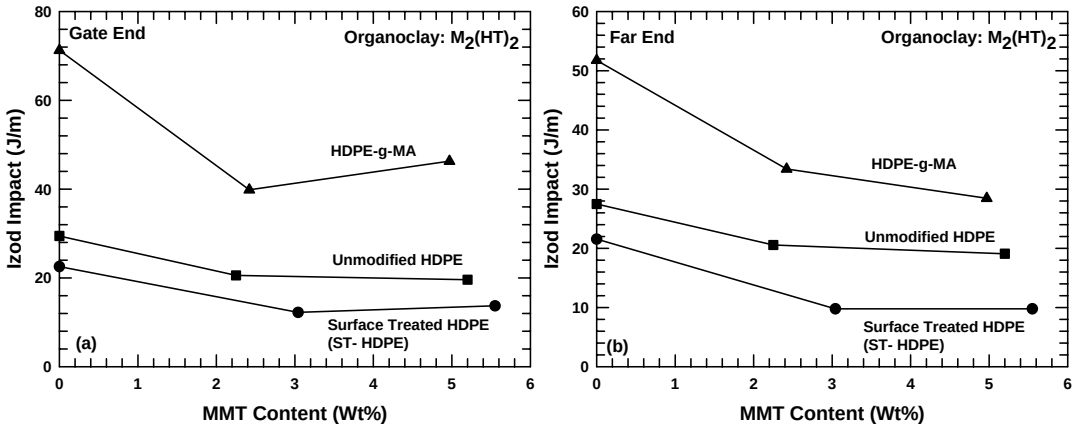

Figure 6.8 Izod impact strength of (a) gate end, and (b) far end samples of nanocomposites prepared from unmodified HDPE, surface treated HDPE (ST-HDPE), and maleic anhydride grafted HDPE (HDPE-g-MA).

CONCLUSIONS AND FUTURE WORK

A novel method to improve organoclay exfoliation in polyethylene has been presented here. The polarity of the HDPE matrix was increased by subjecting the polyethylene particles to a controlled fluoro-oxidation process, thus forming hydroxyl, carboxyl, and ketone functionalities on the surface of the polymer particles. These surface treated HDPE particles (ST-HDPE) were then melt mixed with an appropriate organoclay to form nanocomposites, whose morphology and properties were compared to nanocomposites prepared from unmodified HDPE and maleic anhydride grafted HDPE (HDPE-g-MA). The level of reinforcement observed in ST-HDPE based nanocomposites was comparable to, if not better than, that seen in HDPE-g-MA based nanocomposites. TEM micrographs of HDPE-g-MA and ST-HDPE based nanocomposites revealed a

much more exfoliated morphology as compared to that of nanocomposites prepared from unmodified HDPE. However, the level of exfoliation observed in HDPE-g-MA by TEM was better than that observed in the current version of ST-HDPE.

This was our first effort at using surface treatment as a means to improve organoclay dispersion in polyethylene. It would be interesting to raise the polarity of the particles even further by increasing the intensity of the oxidative treatment, i.e., increasing the thickness of the surface treatment layer of the polyethylene particle. We expect this to further elevate the level of organoclay exfoliation in ST-HDPE. The effect of the molecular weight of ST-HDPE particles on the level of organoclay exfoliation should also be examined using a low melt index (higher molecular weight) ST-HDPE sample. The eventual goal is to use such surface treated particles as compatibilizers (like PE-g-MA) to prepare polyethylene nanocomposites on a commercial scale. From a technical standpoint, this requires the miscibility of the surface treated polyethylene in unmodified polyethylene. If this miscibility could be achieved, then highly concentrated organoclay/HDPE masterbatches, with high levels of exfoliation, could be prepared and subsequently diluted down with unmodified polyethylene (while preserving exfoliation).

REFERENCES

[1] Shah RK, Paul DR. Accepted by Polymer

[2] Chavarria F, Paul DR. Polymer 2004;45(25):8501-15.

[3] Shah RK, Paul DR. In preparation

[4] Shah RK, Hunter DL, Paul DR. Polymer 2005;46(8):2646-62.

[5] Hotta S, Paul DR. Polymer 2004;45(22):7639-54.

Chapter 7: Nanocomposites from Poly(ethylene-co-methacrylic acid) Ionomers: Effect of Surfactant Structure on Morphology and Properties

As discussed in Chapter 4, nanocomposites prepared from ionomers of poly(ethylene-co-methacrylic acid) exhibit a much higher level of organoclay exfoliation than those prepared from polyethylene. The amount of methacrylic acid and the type of neutralizing cation employed have a remarkable impact on the nanocomposite morphology (Chapter 5). The selection of a suitable organoclay is equally critical for producing nanocomposites with excellent exfoliation. Structural aspects of the surfactant like the number and length of alkyl tails, degree of saturation, etc. along with the amount of surfactant loading on the clay may significantly affect the degree of clay exfoliation [1-3]. Prior work [1, 4] has shown that organic modifiers with one long alkyl tail lead to higher levels of organoclay exfoliation in nylon 6 than those having two alkyl tails. This is believed to be the result of the higher affinity that nylon 6 has for the pristine surface of the organoclay than for the largely aliphatic organic modifier. Similar trends were seen in SAN based nanocomposites [3]. On the other hand, nanocomposites made from a non-polar polymer like LLDPE showed completely opposite trends [5], i.e., the two-tailed organoclay formed nanocomposites with better exfoliation and mechanical properties than a one-tailed organoclay.

The objective of this study is to examine the effect of the number of alkyl tails and other aspects of the surfactant structure on the morphology and properties of nanocomposites made from poly(ethylene-co-methacrylic acid) ionomers. Specific

comparisons among organic amine surfactants that are commercially available are made by addressing structural variations one issue at a time. Transmission electron microscopy (TEM), wide angle X-ray scattering (WAXS), stress-strain analysis and Izod impact measurements are used to evaluate nanocomposite morphology and physical properties.

EXPERIMENTAL

A commercial grade sodium ionomer of poly(ethylene-co-methcrylic acid), Surlyn® 8945, was used in the matrix polymer. Specifications of the polymer and the organoclays selected for this study were given in Chapter 2. The organoclays were carefully chosen to explore the effect of the chemical structure of the surfactant on the extent of organoclay exfoliation observed in the corresponding Surlyn® based nanocomposites made using them. These organoclays permit six structural comparisons to be made as shown in Figure 7.1.

Melt compounded composites were prepared using a Haake, co-rotating, intermeshing twin screw extruder using a barrel temperature of 200 ^{o}C, a screw speed of 280 rpm, and a feed rate of 1200 g/hr. The polymer was dried in a vacuum oven at 65 ^{o}C for a minimum of 48 hours prior to compounding while the organoclays were used as received. As mentioned in Chapter 5, it was not possible to confirm the montmorillonite content of the nanocomposites by incineration since the polymer itself resulted in a hard, yellowish green coating on the inside of the crucible reflecting some complex residue of the inorganic component.

The samples were injection molded using a barrel temperature of 220 ^{o}C, mold temperature of 45 ^{o}C, injection pressure of 70 bar and a holding pressure of 40 bar.

The nanocomposites were characterized using WAXS, TEM, stress-strain analysis, and Izod impact testing as described in Chapter 2. The data revealed standard deviations of the order of 1-6% for modulus, 2% for yield strength, 2-22% for elongation at break, and 2-18% for Izod impact values. In order to see if there were any differences between the morphologies of the skin (surface) and the core, two sets of samples were prepared for WAXS analysis. The first set of samples used for studying the morphology of the skin, comprised of unmodified Izod bars of nanocomposites (thickness = 0.125 inches). The second set of samples used for studying the morphology of the core comprised of Izod bars that were milled down to a thickness of 0.065 inches using a Bridgeport® vertical mill. As before, the specimens were oriented such that the incident beam reflected off the major face.

Effect	Organoclays		
Number of Alkyl Tails	$M_3(HT)_1$	*vs.*	$M_2(HT)_2$-95
	$M_3(C_{16})_1$	*vs.*	$M_1(C_{16})_3$
Hydroxy-ethyl vs. Methyl	M_3T_1	*vs.*	$(HE)_2M_1T_1$
MER Loading	$M_2(HT)_2$-95	*vs.*	$M_2(HT)_2$-140
Quaternary vs. Tertiary	$M_2(HT)_2$-95	*vs.*	$M_1H_1(HT)_2$
Length of Alkyl Tail	$(HE)_2M_1T_1$	*vs.*	$(HE)_2M_1C_1$*
Saturation	M_3T_1	*vs.*	$M_3(HT)_1$

Figure 7.1 Organoclays used to evaluate the effect of structural variations of the amine cations on nanocomposite morphology and properties.

RESULTS

Stress-Strain Analysis

Selected mechanical properties of Surlyn® 8945 based nanocomposites prepared with various organoclays are listed in Table 7.1. Differences in the enhancement of mechanical properties achieved with the addition of various organoclays reflect the variation in the extent of exfoliation attained in each of them. However, before we discuss these issues in detail, it is important to highlight the similarities and subtle differences in the stress-strain behavior of composites prepared from these organoclays. As an example, Figure 7.2 displays the stress-strain diagrams for nanocomposites based on $(HE)_2M_1C^*_1$ and $M_2(HT)_2$-140, two clays which cause significantly different degrees of matrix reinforcement. In both cases, at low clay concentrations, there is a distinct drop in the tensile stress after the yield point, corresponding to the onset of necking. This stress drop gradually diminishes as the clay content increases. Noticeably, the slope of the plastic region of the curves, indicative of strain hardening is different in both cases. Metallurgists typically quantify strain hardening by a 'strain hardening coefficient' *n*, defined as the slope of the plastic portion of the true stress-strain curve. However, because of the neck formation in test samples when subjected to uniaxial tension, it is difficult to determine the true stress-strain behavior for most polymer samples. A number of investigators have used non-contacting, imaging methods [6-9] to calculate the dynamic changes in the dimensions of samples during tensile testing and have, thus, determined their true stress-strain behavior. Since our labs are not equipped to perform such analyses, we define here an 'experimental strain hardening coefficient', α, as the slope of the plastic region of the experimental stress-strain curve.

Table 7.1 Select mechanical properties of nanocomposites formed from Surlyn® 8945 and various organoclays

Clay	Loading	Modulus	Yield Strength	Tensile Strenght at Break	Elong. At Break		Izod Impact[b]	
			(2.0 cm/min)	(2.0 cm/min)	(2.0 cm/min)	α[a]	(Far end)	(Gate end)
	(% MMT)	(GPa)	(MPa)	(MPa)	(%)		(J/m)	(J/m)
None	0.0	0.262	14.5	21.3	194	7.31	442	428
$M_3(HT)_1$	2.5	0.349	17.9	21.2	117	6.22	573	601
	5.0	0.410	18.7	21.0	111	4.96	415	572
	7.5	0.465	19.6	22.1	119	3.96	294	491
	10.0	0.563	21.6	23.2	116	3.45	160	394
$M_3(C_{16})_1$	2.5	0.384	18.2	20.7	159	5.85	437	475
	5.0	0.452	18.4	22.3	155	5.37	328	478
	7.5	0.502	18.6	23.2	158	5.29	183	411
	10.0	0.544	19.9	23.6	140	5.26	119	319
$M_2(HT)_2$-95	2.5	0.403	18.9	22.3	127	6.21	572	675
	5.0	0.560	21.0	23.8	111	5.40	419	607
	7.5	0.732	23.8	26.6	72	4.68	109	249
	10.0	0.919	27.6	29.4	65	0.00	22*	43*
$M_2(HT)_2$-140	2.5	0.554	20.0	22.1	132	5.15	547	576
	5.0	0.628	21.7	25.5	131	4.04	162	422
	7.5	0.825	23.8	24.5	93	1.20	43	92
	10.0	1.008	24.1	24.9	42	0.00	17*	25*
$M_1(C_{16})_3$	2.5	0.498	20.4	25.2	148	6.53	641	685
	5.0	0.708	23.6	26.2	116	4.55	296	652
	7.5	0.857	26.7	27.2	63	0.00	95	237
	10.0	1.126	29.4	29.0	48	0.00	24*	98*
$(HE)_2M_1C_1$*	2.5	0.328	15.9	19.6	145	6.60	483	422
	5.0	0.364	16.5	21.6	150	6.44	479	449
	7.5	0.419	17.9	23.4	148	6.46	359	462
	10.0	0.504	19.0	24.1	146	6.09	283	458
$(HE)_2M_1T_1$	2.5	0.396	18.5	22.5	145	6.15	490	587
	5.0	0.559	21.0	23.0	105	4.69	461	530
	7.5	0.708	23.5	25.3	106	4.29	323	439
	10.0	0.853	25.4	26.3	92	2.57	105	241
M_3T_1	2.5	0.385	18.2	22.3	164	6.01	397	408
	5.0	0.444	18.7	23.3	162	5.96	318	479
	7.5	0.489	19.3	22.7	150	5.26	209	460
	10.0	0.533	20.3	22.4	133	4.41	121	401
$M_1H_1(HT)_2$	2.5	0.413	19.0	24.2	180	6.20	536	535
	5.0	0.529	20.1	25.7	197	5.66	429	528
	7.5	0.695	22.0	25.0	174	4.99	304	468
	10.0	0.830	23.3	23.3	105	0.00	50	250

[a] α = Slope of the plastic region of the experimental stress-strain curve
[b] an asterisk (*) denotes brittle failure

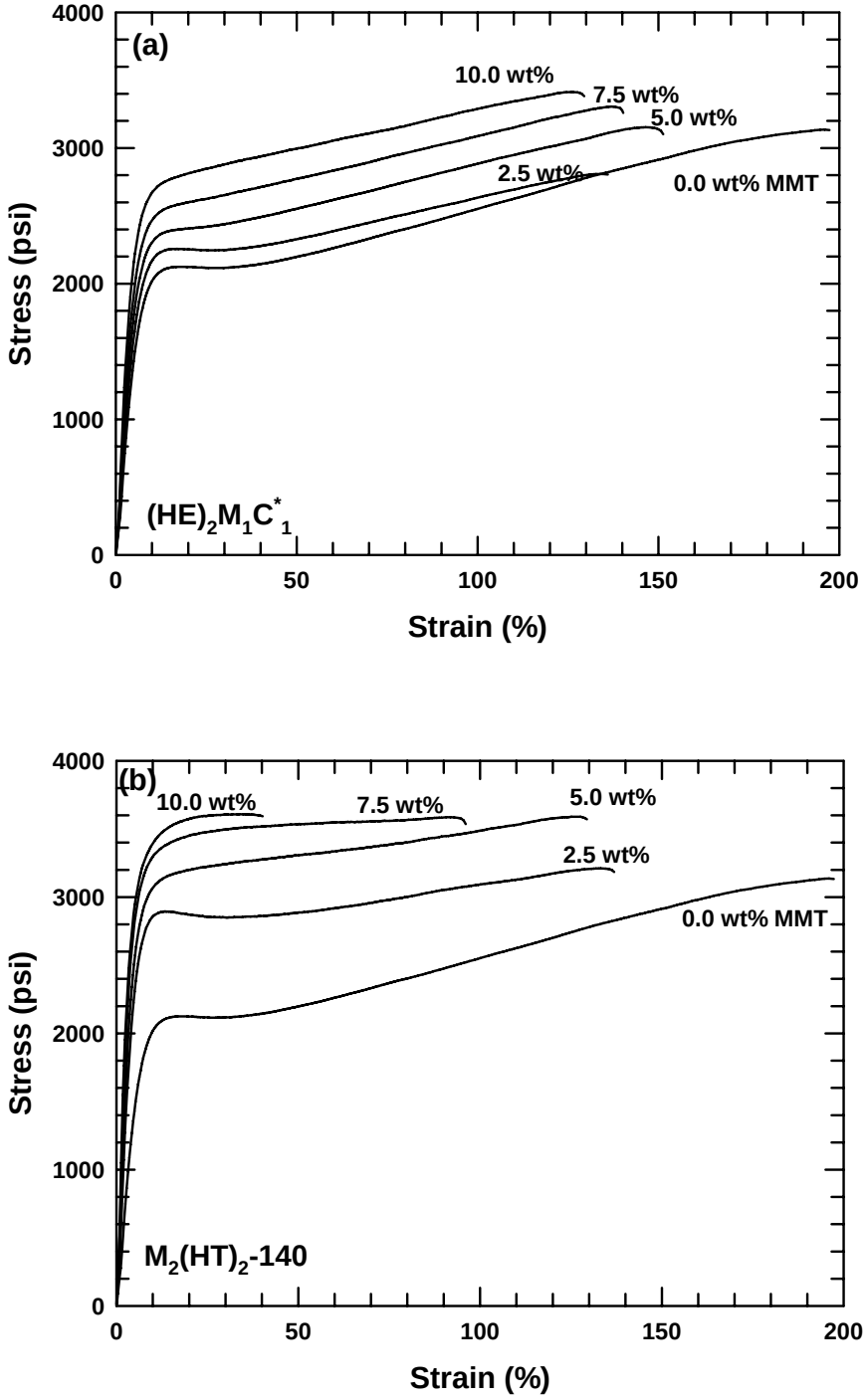

Figure 7.2 Stress-strain diagrams of nanocomposites prepared from poly(ethylene-co-methacrylic acid) ionomer and (a) $(HE)_2M_1C^*_1$ and (b) $M_2(HT)_2$-140 organoclays measured at a crosshead speed of 5.1 cm/min.

We realize that the absolute value of α may differ from that of *n*; however, α should provide a relative tool for comparing strain hardening in different nanocomposites. Figure 7.3 shows the variation in strain hardening along with the clay concentration for $(HE)_2M_1C^*_1$ and $M_2(HT)_2$-140 based nanocomposites. The value of α drops precipitously at higher MMT concentrations for $M_2(HT)_2$-140 based nanocomposites compared to $(HE)_2M_1C^*_1$ based composites. The α values of all nanocomposites made are listed in Table 7.1. It appears that composites made from organoclays that lead to high levels of reinforcement exhibit low degrees of strain hardening and vice versa .

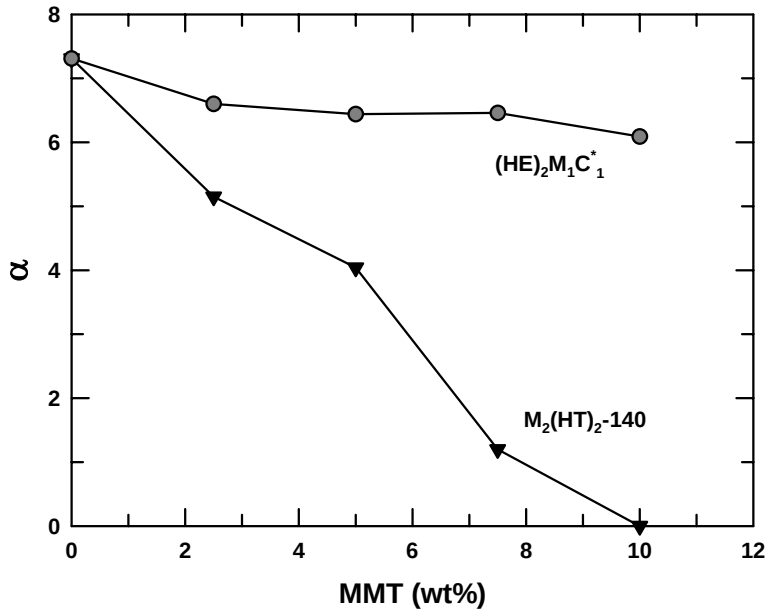

Figure 7.3 Variation in the 'experimental strain hardening coefficient' α with clay concentration for nanocomposites prepared from $(HE)_2M_1C^*_1$ and $M_2(HT)_2$-140 organoclays.

Effect of the number of long alkyl groups on organoclay exfoliation

Figure 7.4 shows TEM micrographs comparing the morphology of nanocomposites formed from Surlyn® 8945 and organoclays with one alkyl tail ($M_3(HT)_1$, $M_3(C_{16})_1$), two alkyl tails ($M_2(HT)_2$-95), and three alkyl tails ($M_1(C_{16})_3$). Nanocomposites from $M_2(HT)_2$-95 (Figure 7.4(b)) exhibit a much better degree of clay exfoliation and distribution compared to those made from $M_3(HT)_1$ (Figure 7.4(a)), which display a large number of unexfoliated clay tactoids. Similarly, the TEM micrograph of a composite made from $M_1(C_{16})_3$ shown in Figure 7.4(d) reveals a higher level of exfoliation than that obtained for a nanocomposite made from a corresponding one-tailed organoclay $M_3(C_{16})_1$ (Figure 7.4(c)).

The TEM analyses clearly corroborate the mechanical property trends of these nanocomposites. Figure 7.5(a) shows that the larger the number of alkyl tails, the higher the level of reinforcement. The increase in modulus on addition of MMT is much stronger for the organoclay with three alkyl tails $M_1(C_{16})_3$, than for one with two alkyl tails, $M_2(HT)_2$-95, which in turn is better than for those with one alkyl tail. There is not much difference between the moduli of the nanocomposites formed from the two one-tailed organoclays, $M_3(HT)_1$ and $M_3(C_{16})_1$. Yield strength data showed similar trends (Figure 7.5(b)). Elongation at break data, presented in Figure 7.5(c), show that the more exfoliated systems ($M_1(C_{16})_3$, $M_2(HT)_2$-95) are less ductile than the one-tailed systems; generally, ductility decreases when stiffness is increased by reinforcement.

Based on the above results, it is concluded that organoclays with multiple long alkyl groups lead to better exfoliation of montmorillonite platelets in these ionomers than organoclays with one long alkyl group when all other aspects of the structure are the

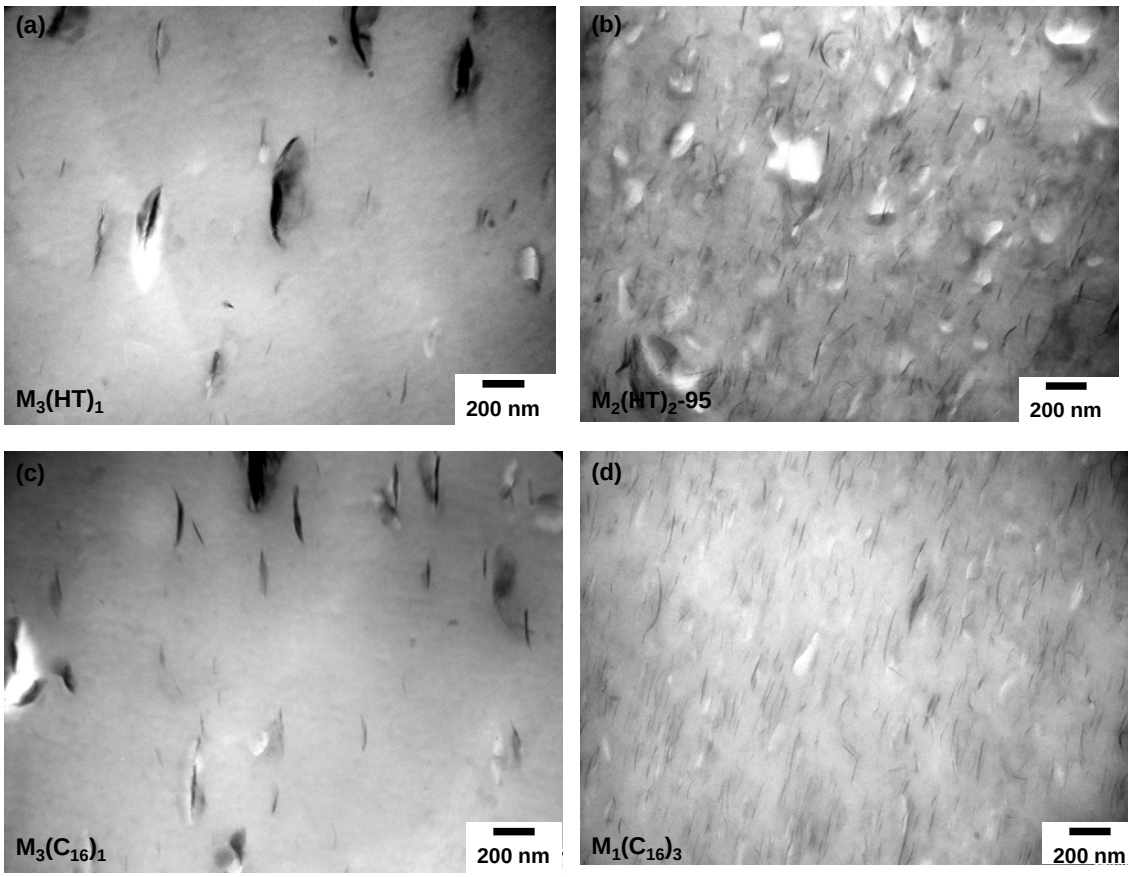

Figure 7.4 TEM micrographs comparing the morphology of nanocomposites prepared from (a) a one-tailed organoclay, $M_3(HT)_1$, (b) two- tailed organoclay, $M_2(HT)_2$-95, (c) one-tailed organoclay, $M_3(C_{16})_1$, and (d) three tailed organoclay, $M_1(C_{16})_3$. The concentration of MMT in all cases is 2.5 wt%.

same. This conclusion is similar to that made for LLDPE nanocomposites [5] but is opposite of that made for nylon 6 nanocomposites; where one alkyl tail leads to much better dispersion of clay than does two tails [4]. It is believed that nylon 6 has a higher affinity for the pristine surface of the organoclay than for the largely aliphatic organic modifier. The one-tailed surfactant leaves a large silicate surface area exposed for interaction with the polyamide and requires the polyamide to mix with fewer alkyl tails;

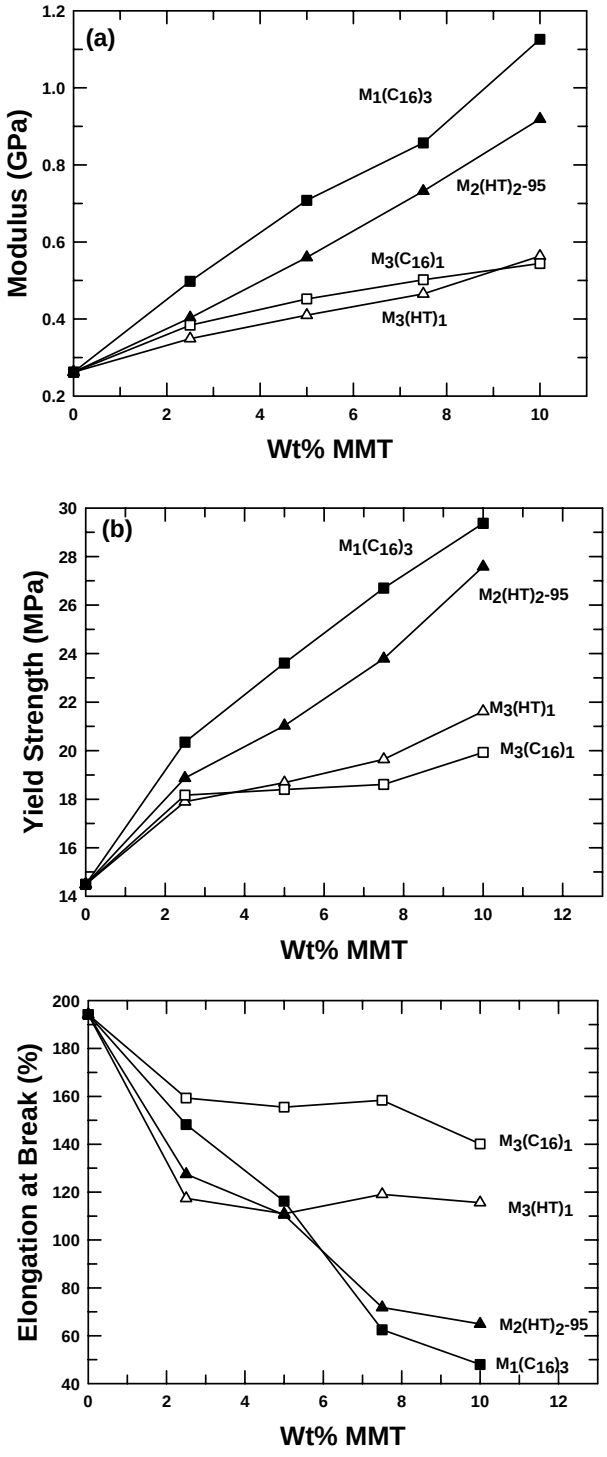

Figure 7.5 (a) Tensile modulus, (b) yield strength, and (c) elongation at break of nanocomposites of poly(ethylene-co-methacrylic acid) ionomer showing the effect of the number of organoclay alkyl tails on nanocomposite mechanical properties.

whereas, the two tailed modifier shields more silicate surface and, thus, precludes desirable interactions between the polyamide and the clay surface, which ultimately limits the degree of organoclay exfoliation. In the case of poly(ethylene-co-methacrylic acid) ionomers, it could be argued that the polymer has a higher affinity for the alkyl tails than the silicate surface. As a result, the larger the number of alkyl tails, the larger is the number of relatively more favorable alkyl-polymer interactions and the more the silicate surface is shielded from the matrix, both of which leads to better exfoliation. This explanation is presented schematically in Figure 7.6. Also, an increase in the number of alkyl tails increases the inter-platelet distances within the clay tactoids and, thus, facilitates easier intercalation of the polymer within the clay galleries.

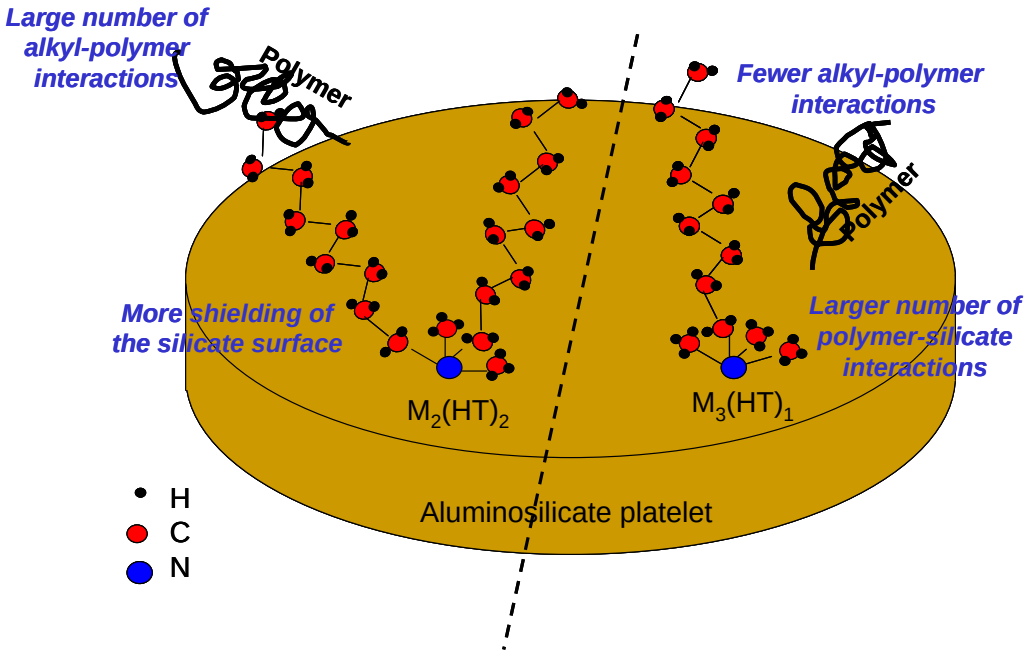

Figure 7.6 Schematic illustration of the proposed differences in interactions between the polymer and the organoclay in the case of a one-tailed organoclay ($M_3(HT)_1$), and a two-tailed organoclay ($M_2(HT)_2$).

Effect of hydroxy-ethyl versus methyl groups on organoclay exfoliation

Figure 7.7 shows TEM micrographs for nanocomposites based on organoclays with and without 2-hydroxy-ethyl substituents, i.e., $(HE)_2M_1T_1$ and M_3T_1. The micrographs expressly reveal a partially exfoliated morphology for the $(HE)_2M_1T_1$ based nanocomposites and an unexfoliated structure for the M_3T_1 based composites. The mechanical properties of the two types of nanocomposites parallel the TEM results. Figure 7.8(a) shows that the organoclay from $(HE)_2M_1T_1$ surfactant leads to much higher levels of reinforcement than that from the M_3T_1 surfactant. The yield strength data, Figure 7.8(b) and the elongation at break data, Figure 7.8(c), agree well with the modulus data and electron micrographs.

The above analysis allows us to conclude that hydroxy-ethyl groups leads to better exfoliation of the clays in this matrix, which again is the opposite of what is seen in nylon 6 based nanocomposites. The differences in morphology and mechanical properties between the composites of the two organoclays are surprisingly large and unprecedented. The improved exfoliation in the case of the $(HE)_2M_1T_1$ organoclay in this matrix could be the combined effect of (i) the favorable chemical interactions between the hydroxyl groups of the surfactant and the ionic or acid groups of the polymer and (ii) reduction of the unfavorable polymer-silicate interactions. The larger hydroxy-ethyl groups occupy more space than the methyl substituents. In addition, the –OH moiety may prefer to reside flat on the surface due to attraction to oxygen atoms on the clay as shown in Figure 7.9. Larger shielding of the clay surface by $(HE)_2M_1T_1$ surfactant, reduces the polymer-clay contact area and, thus, leads to improved exfoliation.

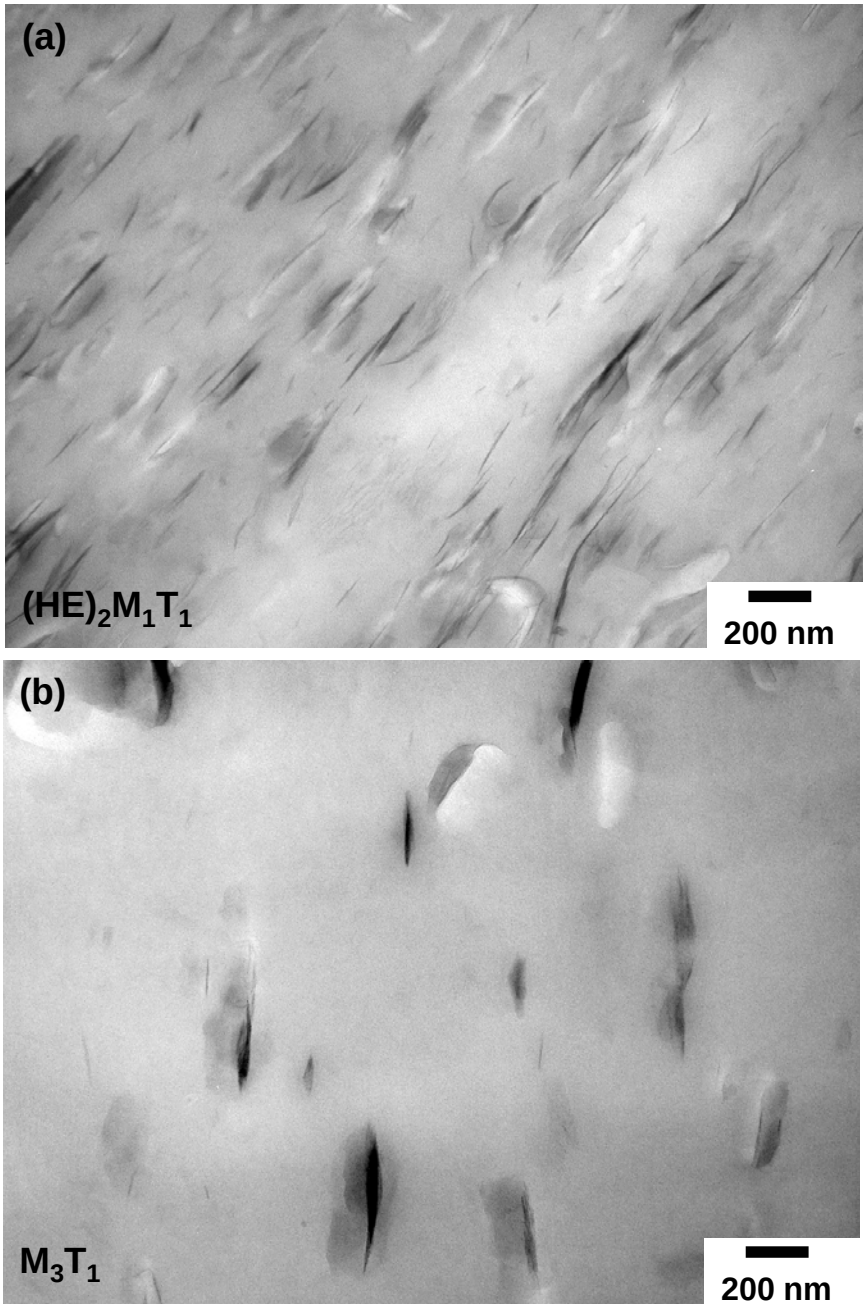

Figure 7.7 TEM micrographs showing the morphology of nanocomposites formed from poly(ethylene-co-methacrylic acid) ionomer and the organoclays $(HE)_2M_1T_1$ and M_3T_1. The concentration of MMT in both cases is 5.0 wt%.

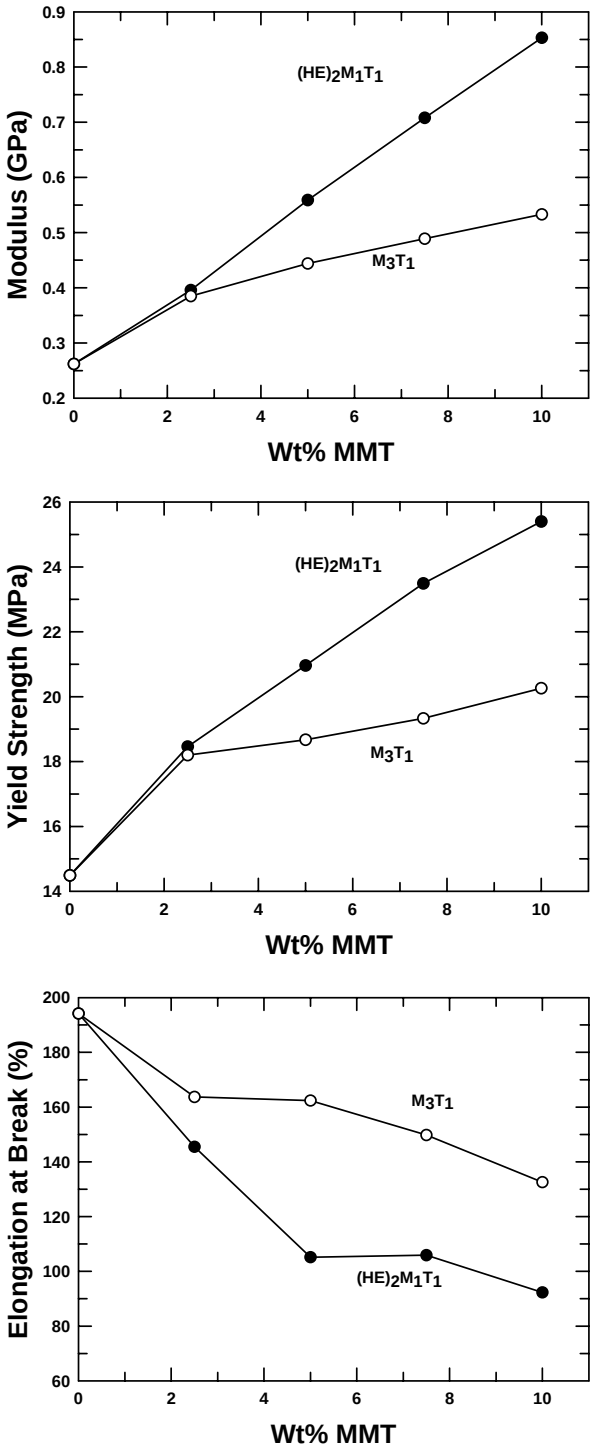

Figure 7.8 (a) Tensile modulus, (b) yield strength, and (c) elongation at break of nanocomposites of poly(ethylene-co-methacrylic acid) ionomer showing the effect of 2-hydroxy-ethyl versus methyl groups on nanocomposite mechanical properties.

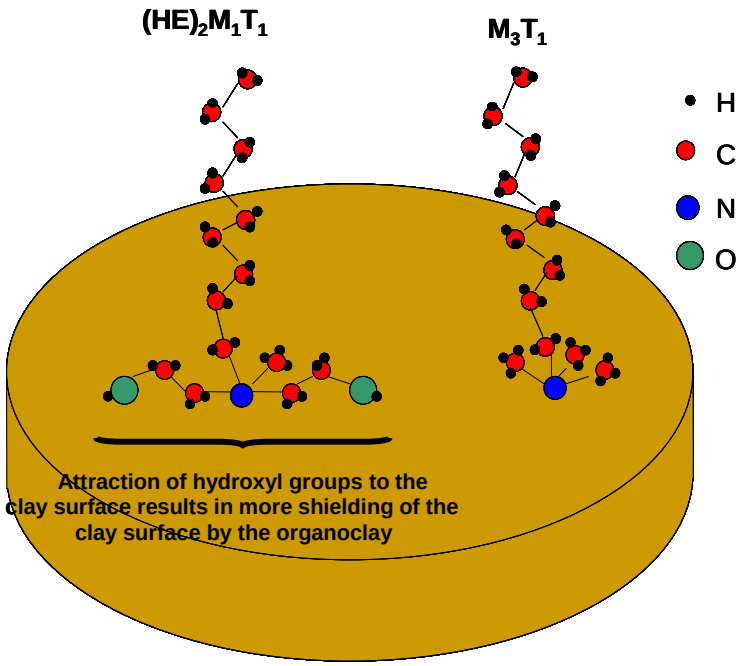

Figure 7.9 Schematic illustration of proposed interactions between the silicate surface and the amine surfactants in the case of $(HE)_2M_1T_1$ and M_3T_1 organoclays.

Effect of the length of the surfactant alkyl tail on organoclay exfoliation

The TEM micrographs in Figure 7.10 provide comparison between the morphology of nanocomposites prepared from organoclays with two different tail lengths. Although, both $(HE)_2M_1T_1$ and $(HE)_2M_1C^*_1$ clays contain the favorable hydroxy-ethyl substituent, the $(HE)_2M_1T_1$ clay, which is predominantly comprised of C_{18} chains, leads to much higher levels of platelet exfoliation than $(HE)_2M_1C^*_1$, which is comprised mainly of C_{12} chains. The mechanical property data are in congruence with the TEM analysis. The tensile moduli of the $(HE)_2M_1T_1$ based composites are about 20-70% higher than that of $(HE)_2M_1C^*_1$ based composites, with the differences being more pronounced at higher MMT concentrations as seen in Figure 7.11(a). The yield strength (Figure 7.11(b)), and the ductility data (Figure 7.11(c)) agree well with the modulus trends.

These observations lead to the conclusion that surfactants with longer alkyl tails are better at exfoliating montmorillonite clays than those with a shorter alkyl tails. The shorter C_{12} tails of $(HE)_2M_1C^*_1$ organoclay result in a lower shielding efficiency and smaller inter-platelet distances as compared to $(HE)_2M_1T_1$ which evidently leads to lower levels of exfoliation.

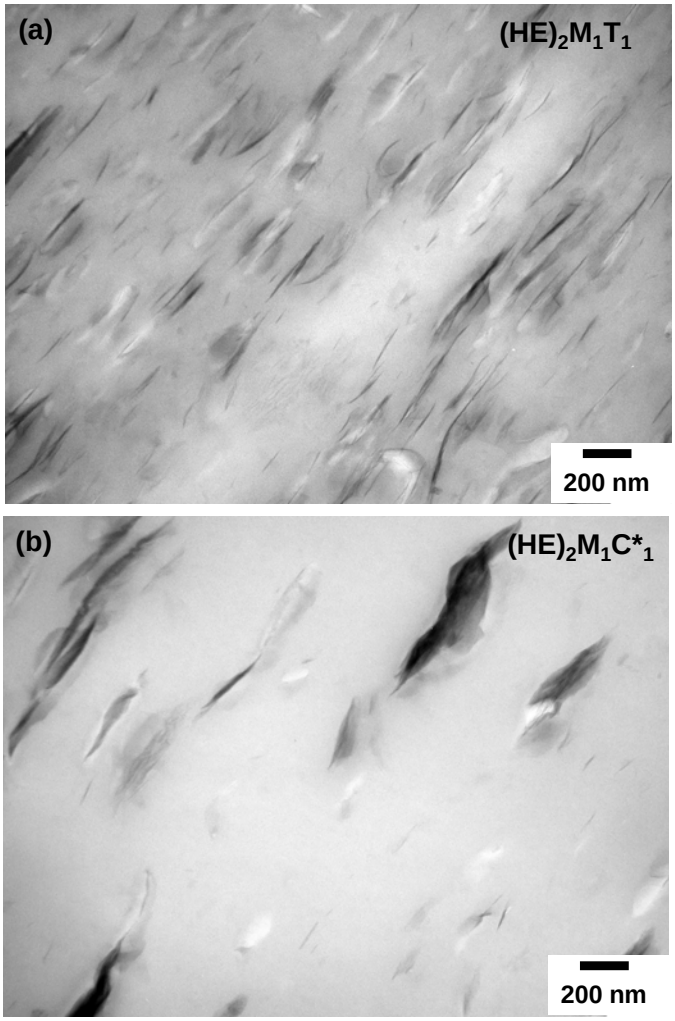

Figure 7.10 TEM micrographs showing the morphology of nanocomposites formed from poly(ethylene-co-methacrylic acid) ionomer and the organoclays $(HE)_2M_1T_1$ and $(HE)_2M_1C^*_1$. The concentration of MMT in both cases is 5.0 wt%.

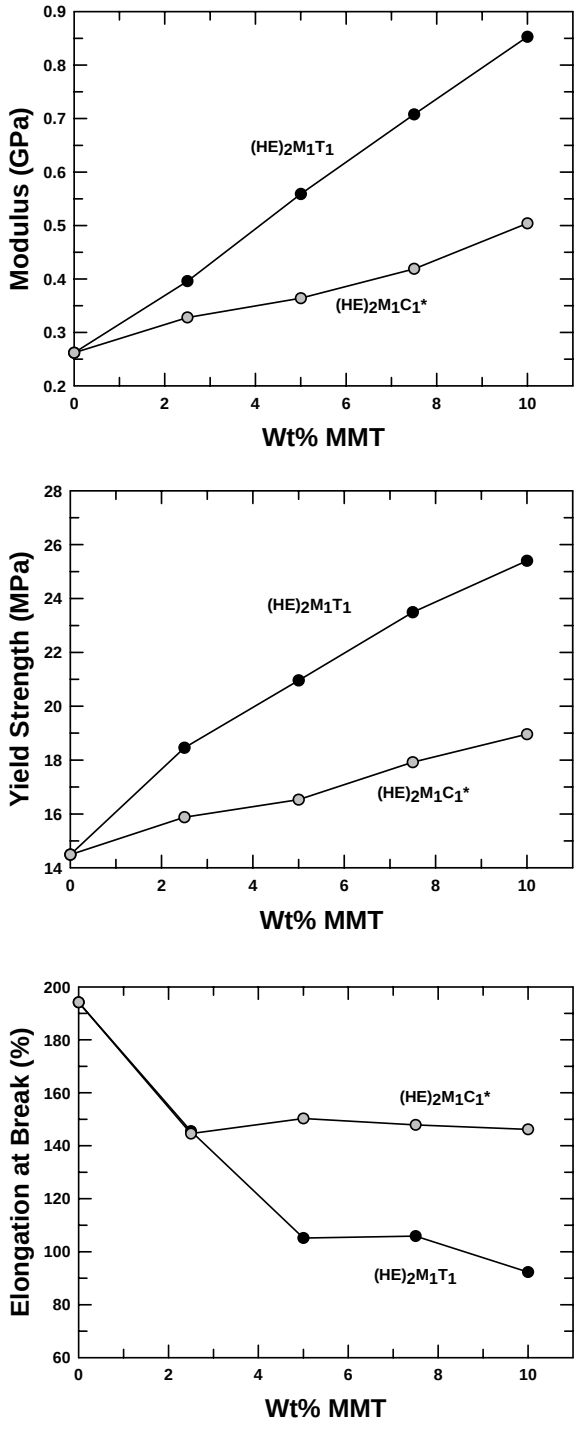

Figure 7.11 (a) Tensile modulus, (b) yield strength, and (c) elongation at break of nanocomposites of poly(ethylene-co-methacrylic acid) ionomer showing the effect of the length of the alkyl tail on nanocomposite mechanical properties.

Effect of the level of organic loading on clay exfoliation (MER comparison)

TEM micrographs of the nanocomposites formed from $M_2(HT)_2$-95 and $M_2(HT)_2$-140, respectively, are shown in Figure 7.12. In both cases a partially exfoliated morphology consisting of individual silicate platelets along with stacks containing two to five platelets is seen. The mechanical properties, however, do provide a clearer and more meaningful distinction between the two organoclays. As seen in Figure 7.13(a), the improvement in modulus values achieved with the over-exchanged clay, $M_2(HT)_2$-140, is roughly 10-15% more than that achieved with $M_2(HT)_2$ -95. This trend is the opposite of what is seen in nylon 6 composites. It appears that the increased alkyl-ionomer interactions and higher inter-platelet distances resulting from the over-exchange of the surfactant helps in improving exfoliation in this matrix. Chemical interchanges between the Na^+ cation of the ionomer and the amine cation of the freely available surfactant could also be contributing to this effect. The improvement in yield strength also follows a similar trend except at high organoclay concentrations, where the yield strength for $M_2(HT)_2$-140 based composites is lower than that of $M_2(HT)_2$ -95 based composites (Figure 7.13(b)). We believe this to be a result of a weaker clay-polymer interface caused by the excessive surfactant available at higher organoclay concentrations. Further discussions on clay-matrix adhesion are made in section 5.

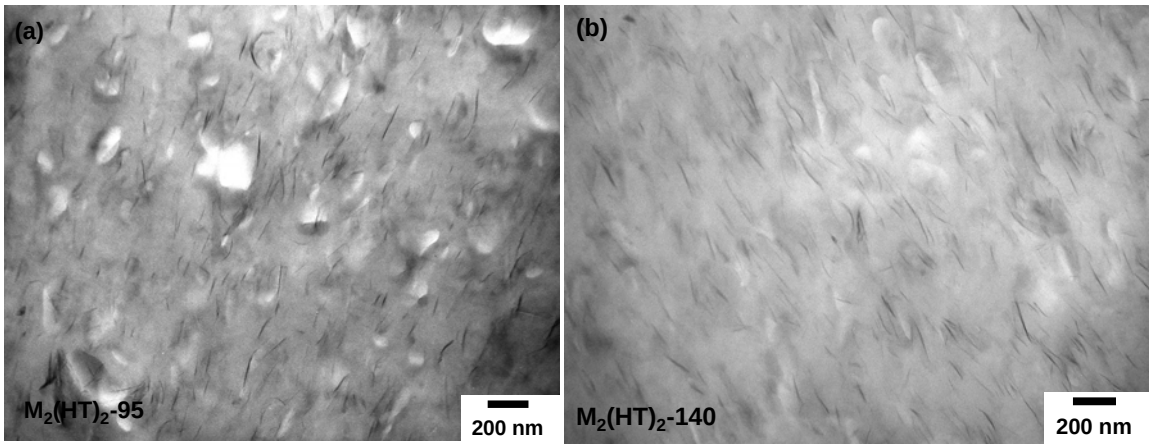

Figure 7.12 TEM micrographs showing the morphology of nanocomposites formed from poly(ethylene-co-methacrylic acid) ionomer and the organoclays $M_2(HT)_2$-95 and $M_2(HT)_2$-140. The concentration of MMT in both cases is 2.5 wt%.

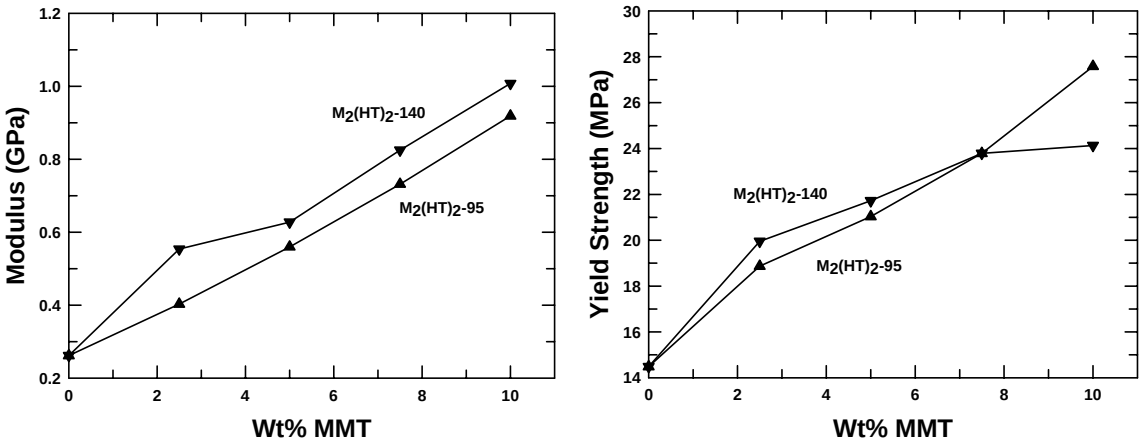

Figure 7.13 (a) Tensile modulus, (b) yield strength, and (c) elongation at break of poly(ethylene-co-methacrylic acid) ionomer showing the effect of MER loading on nanocomposite mechanical properties.

Saturated tallow effects

The long alkyl tails on the surfactants are made from natural oils that contain a certain level of unsaturation. This unsaturation may lead to undesired chemical reactions like matrix degradation [10] at the high temperatures used in melt processing. To examine these effects, nanocomposites based on the saturated and unsaturated form of tallow, $M_3(HT)_1$ and M_3T_1, respectively, were compared against each other. As shown in Figure 7.14, the TEM micrographs show no significant differences in the morphology of the two composites. In both cases, the micrographs reveal similar unaltered clay stacks. The mechanical property values of the two nanocomposites are also similar. Modulus results shown in Figure 7.15(a) reveal a slight advantage for the unsaturated clay at low MMT levels. The yield strength results, seen in Figure 7.15(b), are nearly the same for the two composites. Based on these results, it appears that neither the nanocomposite structure nor its mechanical properties are much affected by the hydrogenation of the tallow double bonds for this system.

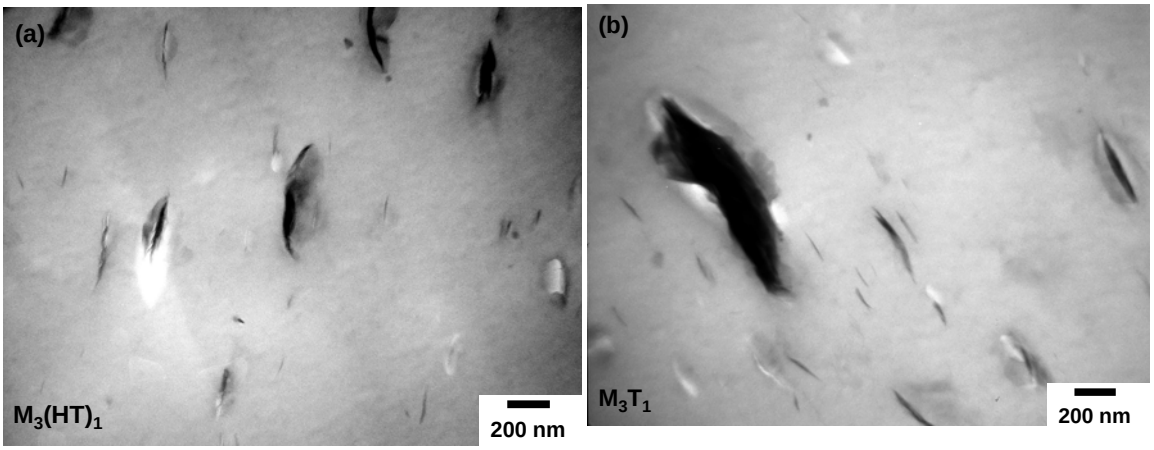

Figure 7.14 TEM micrographs showing the morphology of nanocomposites formed from poly(ethylene-co-methacrylic acid) ionomer and the organoclays $M_3(HT)_1$ and M_3T_1. The concentration of MMT in both cases is 2.5 wt%.

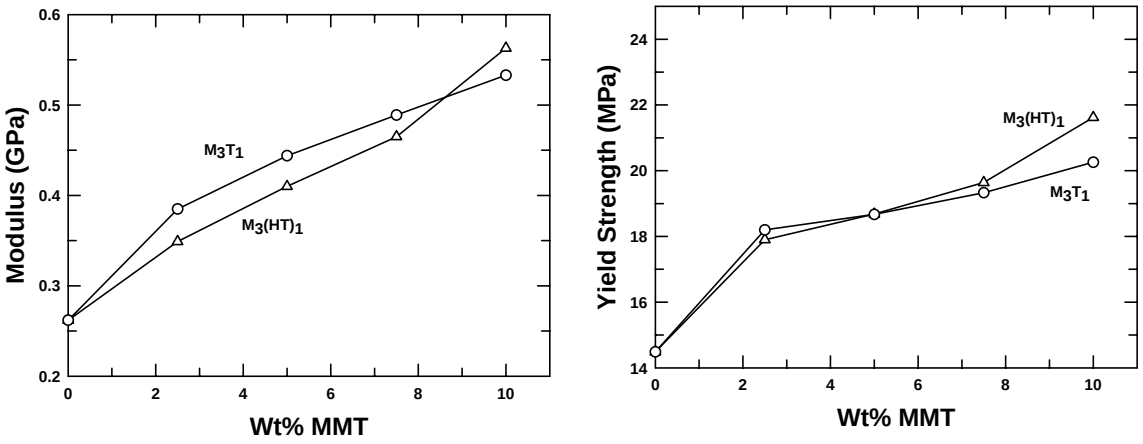

Figure 7.15 (a) Tensile modulus and (b) yield strength of nanocomposites of poly(ethylene-co-methacrylic acid) ionomer showing the effect of alkyl saturation on nanocomposite mechanical properties.

Effect of quaternary vs. tertiary ammonium treatments

Figure 7.16 compares the mechanical properties of nanocomposites made from an organoclay with a quaternary amine, $M_2(HT)_2$-95 to that with a tertiary amine, $M_1H_1(HT)_2$. Modulus results for the two composites, (Figure 7.16(a)) are similar, although, ($M_2(HT)_2$-95) based composites seem to show slightly higher levels of reinforcement. The yield strength data follow a similar trend, Figure 7.16(b). The use of a quaternary amine over a tertiary amine seems to have no sizable effect on the nanocomposite mechanical properties. The small advantage displayed by $M_2(HT)_2$-95 based composites may be the result of the slightly better shielding ability of the bulkier methyl group as compared to the hydrogen group present in the tertiary amine.

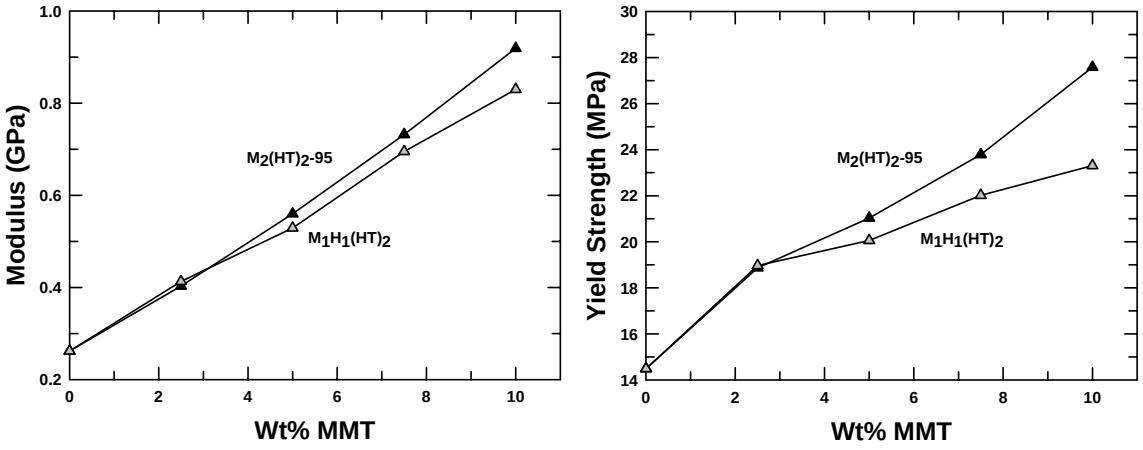

Figure 7.16 (a) Tensile modulus and (b) yield strength of nanocomposites of poly(ethylene-co-methacrylic acid) ionomer showing the effect of quaternary vs. tertiary amines on nanocomposite mechanical properties.

WAXS Analysis

As mentioned in Chapter 2 two sets of samples were prepared to differentiate between the WAXD patterns and, thus, the morphologies of the skin (surface) and the core of the ionomer based nanocomposites. The WAXD patterns of the skin of selected nanocomposites prepared with different organoclays are presented in Figure 7.17. All of these patterns show a distinct peak indicative of the presence of unexfoliated clay tactoids. However, the position of the peaks has shifted in different directions when compared to the WAXD patterns of the organoclays from which they were prepared (Figure 7.18). The peaks of the composites formed from the two-tailed and three-tailed nanocomposites have shifted to higher d-spacings than the organoclays, which according to prevalent understanding suggests the intercalation of polymer within the clay galleries. On the other hand, XRD patterns of nanocomposites prepared from one tailed organoclays revealed a peak that had shifted to the right hand side (lower d-spacings) which could be a result of surfactant degradation. Similar peak shifts to lower d-spacings have been reported for LLDPE [5] and nylon 66 [11] based nanocomposites as well as for highly concentrated masterbatches of nylon 6 nanocomposites [12]. A detailed analysis of organoclay degradation observed in nanocomposites prepared from polyethylene type materials is given in Chapter 8.

Figure 7.19 compares WAXD scans from the core of Izod bars prepared from selected nanocomposites based on different organoclays. A comparison of Figure 7.17 and 7.19 reveals a much lower X-ray scattering intensity from the core samples than from the skin samples; note the more expanded intensity scale in Figure 7.19 than Figure 7.17 and the resulting higher noise to signal ratio. We believe, the high level of platelet

orientation in the skin, resulting from the shear stresses along the walls of the mold during injection molding, than in the core explains these differences. The scans from the core of nanocomposites prepared from $M_2(HT)_2$-95, $M_2(HT)_2$-140, $M_1(C_{16})_3$, $(HE)_2M_1T_1$ organoclays were devoid of any characteristic peaks which is often interpreted as a sign of complete exfoliation. However, we believe this lack of an X-ray peak is the result of a more random orientation of clay particles rather than indicating a more exfoliated morphology; TEM analyses support this hypothesis. X-ray scans of corresponding samples made from $(HE)_2M_1C^*_1$ and $M_3(C_{16})_1$ organoclays have a distinct peak suggesting that these systems have a relatively larger number of unexfoliated clay bundles. This agrees well with the mechanical property and TEM analyses. For a given organoclay, the position of the peak was the same in the skin and the core; however, the height of the peak increased with an increase in the clay concentration.

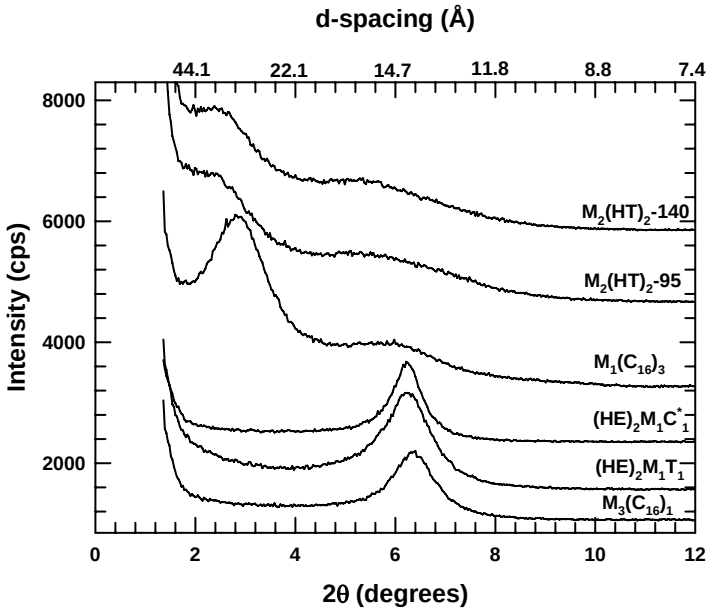

Figure 7.17 WAXD patterns of the skin (surface) of injection molded nanocomposites formed from poly(ethylene-co-methacrylic acid) ionomer and various organoclays. The concentration of MMT in all cases is 5.0 wt%. Curves are shifted vertically for clarity.

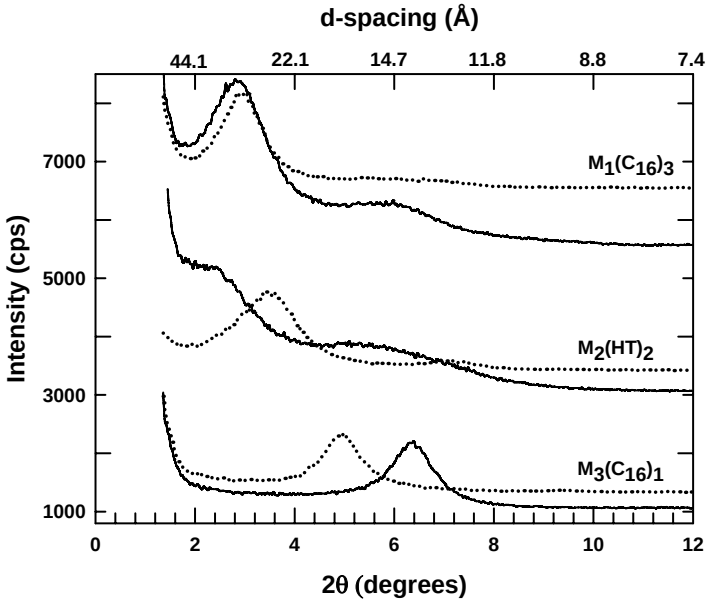

Figure 7.18 WAXD patterns of the skin (surface) of nanocomposites formed from poly(ethylene-co-methacrylic acid) ionomer (full curves) and the corresponding organoclays used to prepare them (dotted curves). The concentration of MMT in all cases is 5.0 wt%. The curves are shifted vertically for clarity.

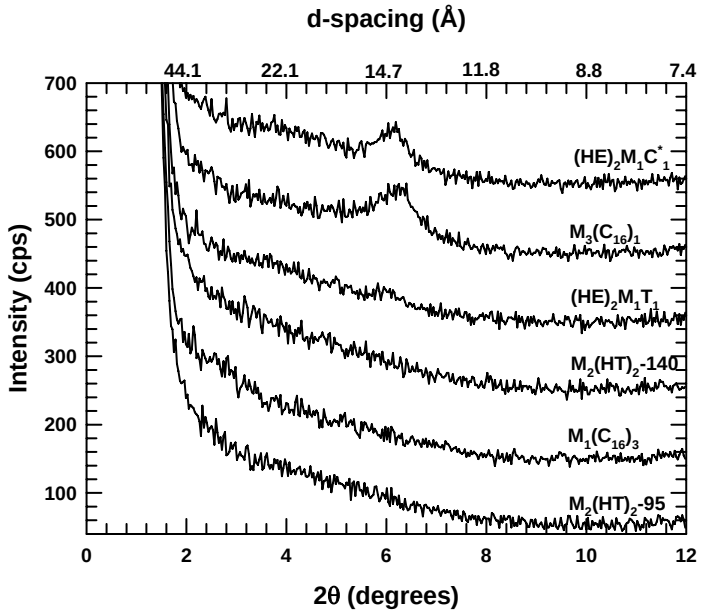

Figure 7.19 WAXD patterns of the core of nanocomposites formed from poly(ethylene-co-methacrylic acid) ionomer and various organoclays. The concentration of MMT in all cases is 5.0 wt%. The curves are shifted vertically for clarity.

Izod Impact measurements

The effects of the clay type and content on room temperature Izod impact behavior of nanocomposites of poly(ethylene-co-methacrylic acid) ionomers are presented in Table 7.1. Although, there is not much difference between the Izod impact values of the gate and far end samples for the neat polymer, the gate end samples are tougher than the far end samples for most nanocomposites. This is the opposite of what has been reported for rubber toughened polyamide blends [13], where the far end samples were found to be tougher than the gate end samples due to differences in the blend morphology at the two ends; rubber particles at the far end were found to be spherical while those at the gate end were highly elongated. In our case, these differences could be a result of possible differences in platelet orientation between the far end and the gate end. To illustrate the current trends, Figure 7.20 shows a plot of the Izod behavior of $(HE)_2M_1T_1$ based nanocomposites versus MMT content. In most cases, the differences between the gate and far end are more pronounced at higher clay concentrations.

For all nanocomposites, toughness as judged by Izod improves with clay addition for low concentrations, but it deteriorates gradually with further increase in clay concentration. The drop in the Izod impact values observed at high clay concentrations is more precipitous in composites that exhibit good clay exfoliation. Since the Izod test measures the energy absorbed during impact, i.e., the area under the resisting force versus displacement curve during the test, as measured using instrumental impact test devices, the values obtained reflect a net result of opposing effects brought by the increased stiffness and reduced ductility. At low clay concentrations, improvements in Izod may reflect the increased stiffness and yield strength of the material which offset the negative

effects brought by the drop in its ductility, i.e., extent of plastic deformation. However, at high clay concentrations, the decreased ductility seems to dominate and toughness decreases.

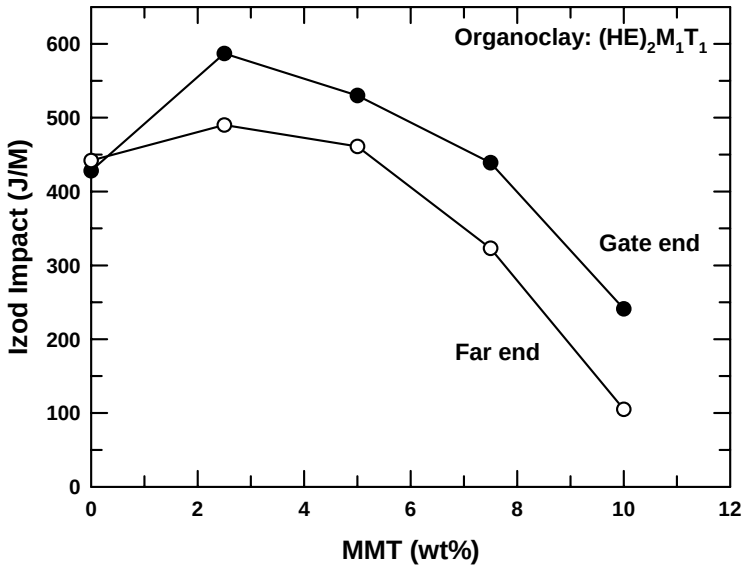

Figure 7.20 Izod impact strength as a function of montmorillonite content for nanocomposites formed from poly(ethylene-co-methacrylic acid) ionomer and $(HE)_2M_1T_1$ organoclay.

DISCUSSION

As described above, a series of polymer-silicate nanocomposites were prepared by melt mixing a sodium ionomer of poly(ethylene-co-methacrylic acid) with ten different organoclays. It should be noted that although some organoclays were exfoliated better than others, none of these nanocomposites exhibited exfoliation levels similar to those seen in nylon 6 nanocomposites. Figure 7.21 shows the relative improvement in matrix stiffness achieved by melt mixing these organoclays with Surlyn® 8945 ionomer.

It is clear that the addition of $M_1(C_{16})_3$ and $M_2(HT)_2$-140 result in the highest improvement in modulus, indicative of their higher levels of exfoliation as compared to the others. On the other hand, most one-tailed organoclays seem to form poorly exfoliated composites. The differences are more pronounced at higher organoclay concentrations, where large agglomerates of the order of a few microns were seen in nanocomposites made from one-tailed organoclays. The use of hydroxy-ethyl instead of methyl substituents clearly results in improved exfoliation. However, as seen in Figure 7.21, the lower reinforcement levels observed in composites formed from $(HE)_2M_1C^*_1$ as compared to those from M_3T_1 indicates that the effect of the shorter alkyl tail length of $(HE)_2M_1C^*_1$ more than negates the favorable effects induced by the hydroxy-ethyl substituents. This suggests that in order to achieve better exfoliation, a longer alkyl tail is more critical than hydroxy-ethyl substitutions.

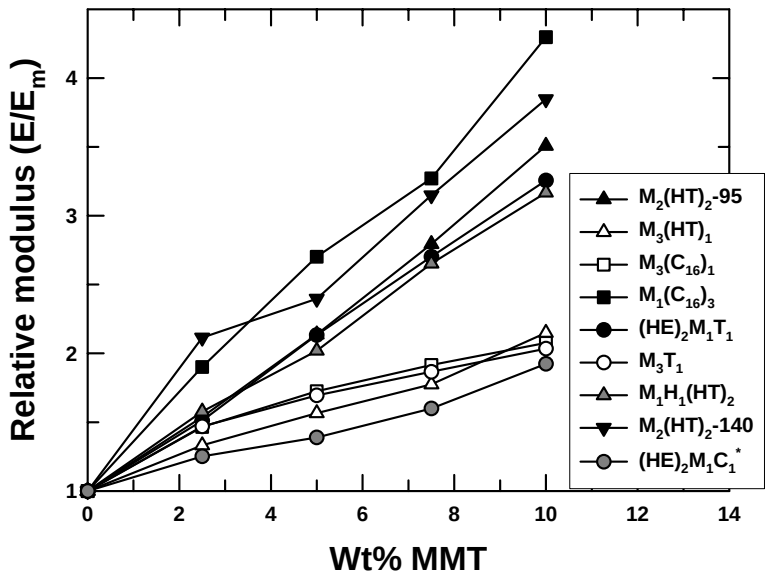

Figure 7.21 Relative modulus (E/E_m) as a function of MMT content for nanocomposites formed from poly(ethylene-co-methacrylic acid) ionomer and various organoclays.

Figure 7.22 shows a plot of the nanocomposite tensile modulus versus the organoclay d-spacing at 2.5 wt% MMT. Clearly, composites made from organoclays with larger d-spacings have higher moduli than composites formed from organoclays with smaller d-spacings. Similar trends were seen at higher clay concentrations. It could be argued that larger d-spacings facilitate easier intercalation of the ionomer within the clay galleries which may subsequently lead to better exfoliation of the clay and, thus, the higher modulus. However, instead of a direct cause and effect relationship, it is quite likely that both the higher stiffness and the larger d-spacings are a result of the higher alkyl content associated with multiple tails, long tails or excess surfactant.

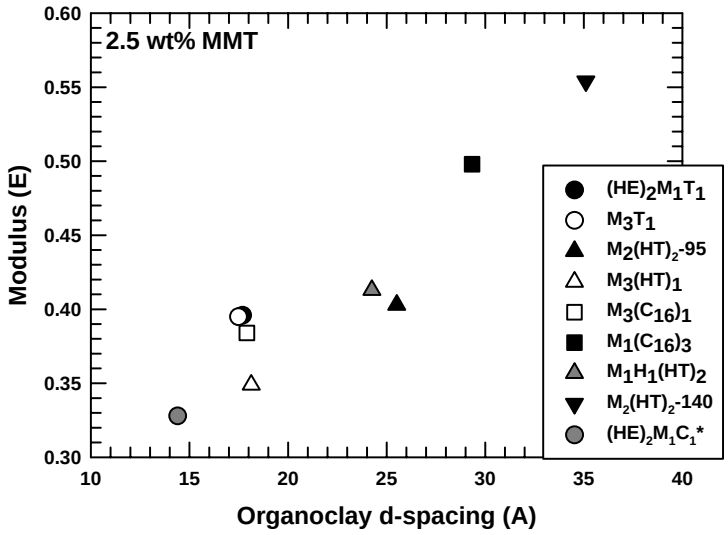

Figure 7.22 Tensile modulus versus organoclay d-spacing for nanocomposites formed from poly(ethylene-co-methacrylic acid) ionomer and various organoclays.

The nanocomposite Izod impact values are plotted against the organoclay d-spacing in Figure 7.23. At low clay concentrations, the Izod impact increases with increasing organoclay d-spacing as seen in Figure 7.23(a). The higher increase in stiffness associated with the larger d-spacings (as shown in Figure 7.22) results in higher

energy absorption for these nanocomposites as compared to nanocomposites prepared from organoclays with smaller d-spacings. At high clay concentrations, the ductility of nanocomposites made from organoclays with large d-spacings, due to better exfoliation, drops dramatically and as a result the Izod impact trend reverses as shown in Figure 7.23(b).

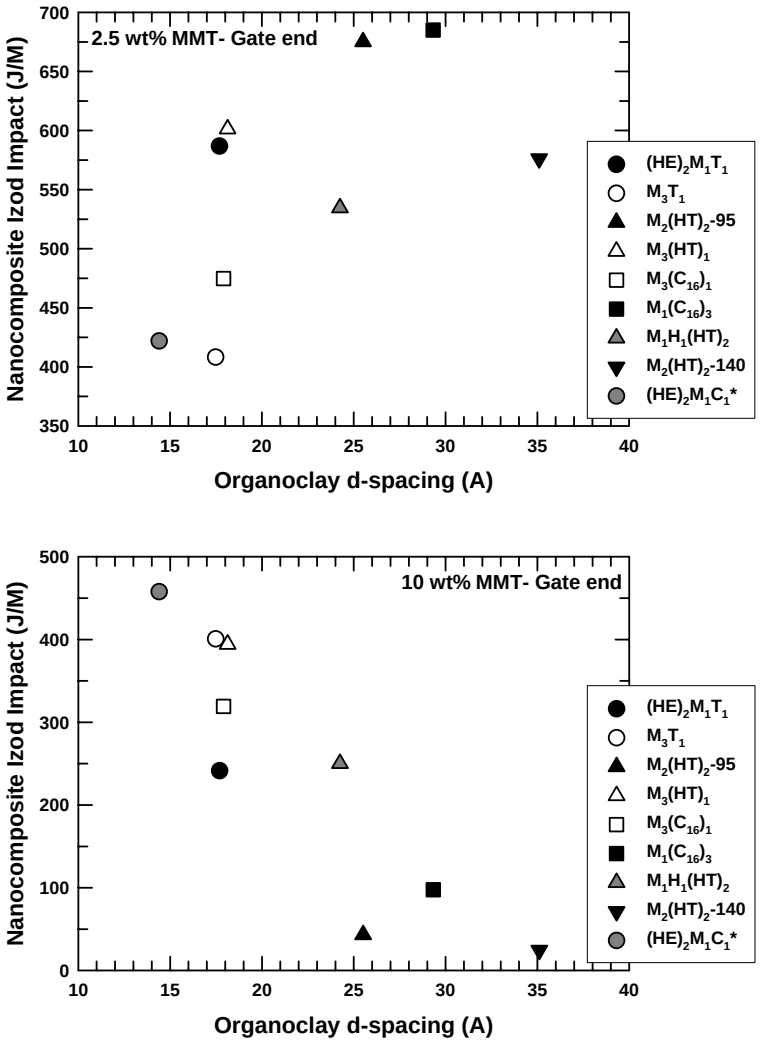

Figure 7.23 Izod impact strength versus organoclay d-spacing for nanocomposites formed from poly(ethylene-co-methacrylic acid) ionomer and various organoclays at (a) 2.5 wt% MMT and (b) 10 wt% MMT

Adequate levels of filler-matrix adhesion are necessary for good performance of conventional composites based on glass or carbon fibers. Polymer-filler interfacial adhesion does not have a significant effect on the tensile modulus of composites, assuming fixed morphology; however, good adhesion is needed to build strength. To study these effects in ionomer-organoclay nanocomposites, we have plotted the yield strength against the modulus of these composites in Figure 7.24. For most of the organoclays, the relationship between yield strength and modulus appears to be about the same which could imply that morphological rather than interfacial adhesion effects dominate in this series of systems. The only exception are nanocomposites formed from $M_2(HT)_2$-140 clays, where at higher organoclay concentrations, the yield strength is lower than expected based on the value of modulus possibly indicating a weaker interface. We believe that the excess surfactant, which may interact well with the polymer but is not ionically bonded to the silica surface, might be a factor in this.

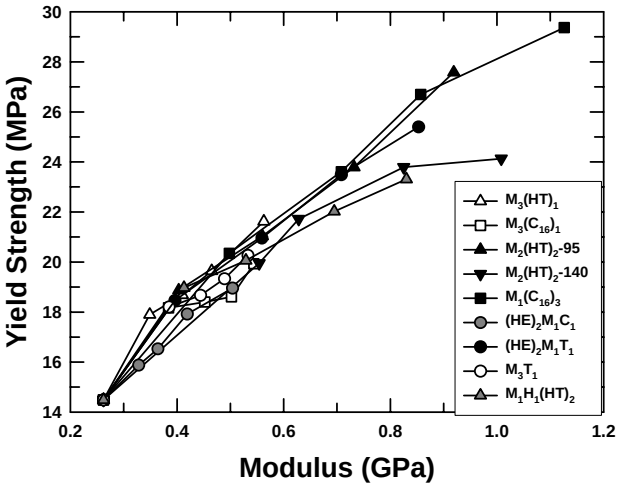

Figure 7.24 Yield strength versus tensile modulus for nanocomposites formed from poly(ethylene-co-methacrylic acid) ionomer and various organoclays

CONCLUSIONS

Structure-property relationships for nanocomposites formed by melt processing from a series of organoclays and poly(ethylene-co-methacrylic acid) ionomers are presented here. The chemical structure of the alkyl ammonium surfactants was systematically varied to determine how specific groups might affect the mechanical properties and morphology of these composites. Four distinct surfactant structural effects have been identified that lead to improved levels of exfoliation and higher stiffness for these nanocomposites: (1) higher number of alkyl tails on the amine rather than one, (2) longer alkyl tails instead of shorter ones, (3) 2-hydroxy-ethyl groups as opposed to methyl groups on the ammonium ion, and (4) excess amount of the amine surfactant on the clay instead of an equivalent amount. Most of these trends are opposite from what has been observed in nylon 6 based nanocomposites [1]. It seems nylon 6 has a higher affinity for the silicate surface than does the poly(ethylene-co-methacrylic acid) ionomer while the latter is less repelled by the alkyl tails than the polyamide. Hence, surfactant structural aspects that lead to more shielding of the silicate surface or increased alkyl material leads to improved exfoliation in the ionomer. These observations are similar to those seen with LDPE [14] and LLDPE [5] based nanocomposites. It should also be noted that, although some organoclays were exfoliated better than others, none of the ionomer-based nanocomposites exhibited exfoliation levels as great as those seen in nylon 6 nanocomposites. Thus, although addition of the acidic and ionic groups (present in ionomers) improves the matrix-polarity and, thus, organoclay exfoliation in polyethylene [14], this does not lead to as favorable polymer-organoclay interactions as

observed for nylon 6 based nanocomposites. Nevertheless, nanocomposites prepared from such ionomers offer promising improvements in performance and may be particularly suitable for barrier applications as shown in Chapter 9.

REFERENCES

[1] Fornes TD, Yoon PJ, Hunter DL, Keskkula H, Paul DR. Polymer 2002;43(22):5915-33.

[2] Yoon PJ, Hunter DL, Paul DR. Polymer 2003;44(18):5323-39.

[3] Stretz HA, Paul DR, Li R, Keskkula H, Cassidy PE. Polymer 2005;46(8):2621-37.

[4] Fornes TD, Hunter DL, Paul DR. Macromolecules 2004;37(5):1793-8.

[5] Hotta S, Paul DR. Polymer 2004;45(22):7639-54.

[6] Nazarenko S, Bensason S, Hiltner A, Baer E. Polymer 1994;35(18):3883-92.

[7] Laraba-Abbes F, Ienny P, Piqules R. Kautschuk Gummi Kunststoffe 1999;52(3):209-14.

[8] Gloaguen JM, Lefebvre JM. Polymer 2001;42(13):5841-7.

[9] Haynes AR, Coates PD. Journal of Materials Science 1996;31(7):1843-55.

[10] Fornes TD, Yoon PJ, Paul DR. Polymer 2003;44(24):7545-56.

[11] Chavarria F, Paul DR. Polymer 2004;Submitted

[12] Shah RK, Paul DR. Polymer 2004;45(9):2991-3000.

[13] Huang JJ, Keskkula H, Paul DR. Polymer 2004;45(12):4203-15.

[14] Shah RK, Paul DR. In preparation

Chapter 8: Organoclay degradation in melt processed polyethylene nanocomposites

As mentioned in Chapter 1, alkyl ammonium surfactants are the most common organic modifiers used to make the naturally occurring hydrophobic montmorillonite clays more organophilic. Unfortunately, these surfactants have low thermal stability and are known to degrade at the high temperatures required for melt processing most polymers. This could possibly affect the level of platelet exfoliation and perhaps interfacial bonding, which influence the physical and mechanical properties of the final nanocomposite. In addition, surfactant decomposition may also result in unwanted side reactions between the decomposition products and the polymer matrix, which could lead to matrix degradation and color formation in nanocomposites [1-4]. Xie et al. [5, 6] have provided an extensive overview of the thermal degradation of alkyl quaternary ammonium modified montmorillonite clay. Their analysis of the degradation products using GC-MS indicated that the initial degradation of the surfactant in an organoclay follows a Hoffmann elimination reaction. VanderHart and Asano [7, 8] estimated from NMR measurements that a considerable portion of the quarternary alkyl ammonium component is depleted during melt processing of nylon 6 nanocomposites. They concluded that the cause of the degradation is a combination of temperature and mechanical shear that is encountered during processing. Since melt processing seems to be one of the most convenient and attractive methods of producing nanocomposites, organoclay degradation during melt mixing has been the subject of recent attention in several laboratories [9-11].

The objective of this study is to examine thermal degradation of the surfactant in various organoclays using thermogravimetric analysis and "in-situ" in melt processed polyethylene-organoclay nanocomposites. As described in Chapter 4, polyethylene, owing to its hydrophobic nature, does not exfoliate organoclays efficiently. As a result, WAXS patterns of PE-organoclay nanocomposites exhibit a distinct peak confirming the presence of clay tactoids. In this work we have characterized the level of organoclay degradation by examining the shift in the position of the WAXS peak of melt processed PE-organoclay nanocomposites. The low melting point of polyethylene allowed us to prepare nanocomposites over a wide range of temperatures (150 °C to 240 °C). The effect of surfactant degradation on the mechanical properties of nanocomposites prepared from one-tailed and two-tailed organoclays was determined by stress-strain analysis. Finally, the thermal stability of the three organoclays with different alkyl contents (number of alkyl tails) are compared by measuring the amount of surfactant lost during thermogravimetric analysis. The surfactant degradation observed while heating the organoclay (without polymer) is also compared to that seen in melt processed nanocomposites.

EXPERIMENTAL

Four commercial grades of LDPE (LD 621, Novapol LF-Y819-A, Novapol LF-0219-A, Novapol LC-0717-A) and three organoclays ($M_3(HT)_1$, $M_2(HT)_2$, $M_3(C_{16})_1$) were used in this study; their specifications are detailed in Chapter 2. The organoclays were carefully chosen to study the thermal stability of surfactants with varying number of alkyl tails. Also, as shown in Chapter 4, in polyethylene type matrices, organic modifiers

with three long alkyl tails lead to higher levels of organoclay dispersion, and hence reinforcement, than those with two alkyl tails, which in turn result in better dispersion than organoclays with one-tail. Thus, the selected three organoclays also allow us to examine surfactant degradation, and its effects, in polyethylene nanocomposites with different morphologies.

Nanocomposites were prepared by melt mixing polymer pellets with organoclay powder in a Haake, co-rotating, intermeshing twin screw extruder using a feed rate of 1200 g/hr. In order to examine the effect of processing temperature on surfactant degradation and mechanical properties of nanocomposites, LDPE (LD 621) was extruded with $M_3(HT)_1$ and $M_2(HT)_2$ organoclays at 150 °C, 165 °C, 180 °C, 200 °C, and 240 °C. The targeted montmorillonite (MMT) content in all nanocomposites was 5 wt%. Of course, such changes in the processing temperature also alter the polymer melt viscosity which could possibly affect organoclay exfoliation in these systems. To isolate the effect of these rheological variations on organoclay dispersion, it was first necessary to characterize the change in melt viscosity over the range of extrusion temperatures mentioned above. This was done in a Tinius Olsen Melt Indexer (Extrusion Plastometer) using a modified ASTM D1238 method. The ASTM standard test method for determining the Melt Index (MI) of the selected grade of polyethylene (LD 621) requires the melt flow rate to be measured at 190 °C under a 2.16 kg load. In our case, we measured the melt flow rate (g/10 min) of the polymer, LD 621 at several temperatures between 150 °C and 250 °C under a fixed load of 2.16 kg. Once the relation between the processing temperature and the melt flow rate of LD 621 was established, three grades of LDPE whose melt indices (MI), determined at the standard temperature of 190 °C,

matched the high, low and intermediate points on the above curve were obtained from Nova Chemicals (Novapol LF-Y819-A, Novapol LF-0219-A, and Novapol LC-0717-A). These three grades of polymer were then extruded with $M_2(HT)_2$ organoclay at 190 °C. Following extrusion, the amount of montmorillonite (MMT) in each nanocomposite was confirmed by incinerating the nanocomposites as described in Chapter 2. To minimize differences in crystallization, all samples (irrespective of extrusion temperature) were injection molded under identical conditions: a barrel temperature of 150 ^{o}C, mold temperature of 45 ^{o}C, injection pressure of 40 bar and holding pressure of 40 bar. The nanocomposites were characterized using WAXS and stress-strain analysis as described in Chapter 2. The data revealed standard deviations of the order of 1-5% for tensile modulus.

Isothermal thermogravimetric analysis (TGA) was conducted on pure organoclays using a Perkin-Elmer TGA7 at 150 °C, 180 °C, 200 °C, 220 °C, and 240 °C under both air and nitrogen atmospheres at a gas flow rate of 50 mL/min. according to ASTM E1131. All organoclays were dried overnight under vacuum at 80 °C prior to thermal analysis.

RESULTS

Organoclay degradation characterized by WAXS analysis

Figure 8.1 (a) shows the WAXS scans of nanocomposites prepared by melt mixing LDPE (LD 621) and $M_3(HT)_1$ organoclay at various temperatures; the presence of a distinct peak indicates incomplete exfoliation of the clay platelets as would be expected.

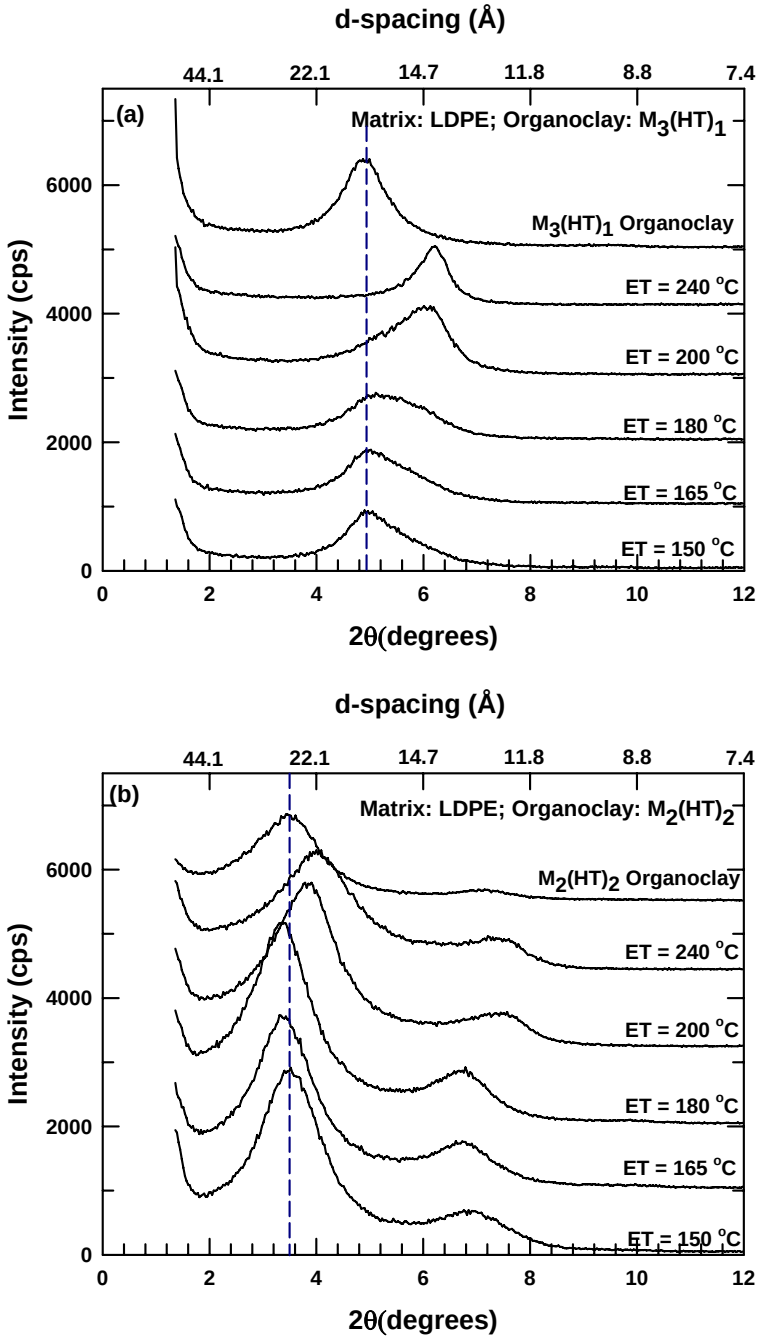

Figure 8.1 WAXS patterns of injection molded samples of LDPE nanocomposites prepared from (a) $M_3(HT)_1$ and (b) $M_2(HT)_2$ organoclays at various extrusion temperatures (ET). X-ray scans of the organoclays are also plotted for comparison. The concentration of MMT in all cases is about 5 wt%. The curves are shifted vertically for clarity.

The WAXS pattern of pristine $M_3(HT)_1$ organoclay, which reveals an intense peak corresponding to a basal spacing of 18 Å, is also included for comparison. It is interesting to note the change in the position of the X-ray scattering intensity peak for the nanocomposites as the processing temperature is increased. For composites extruded at 150 °C and 165 °C, the peak position remains the same as that of the pristine organoclay, which suggests that in these systems the interplatelet distance of the organoclay does not change much during melt processing. The scattering peak for nanocomposites extruded at 180 °C is broader, and shifts a little to the right which denotes a slight decrease in the interplatelet spacing of the organoclay and could be interpreted as the early stages of surfactant degradation resulting in a loss of mass from the organoclay galleries. On increasing the melt processing temperature from 180 °C to 200 °C, there is a distinct shift in the peak position as the organoclay d-spacing is reduced dramatically to ~14 Å. It appears that a significant portion of the surfactant is lost from the clay galleries between 180 °C and 200 °C. On further increasing the processing temperature to 240 °C, the position of the peak does not change much suggesting that the clay galleries do not collapse any further. However, the breadth of the peak reduces which could be construed as more uniform organoclay degradation as compared to that observed in nanocomposites processed at 200 °C.

WAXS scans of nanocomposites prepared by melt mixing LDPE and $M_2(HT)_2$ organoclay at various temperatures are presented in Fig 1(b). As in the case of LDPE-$M_3(HT)_1$ composites, the peak position for LDPE-$M_2(HT)_2$ nanocomposites processed at 150 °C remains the same as that of the pristine organoclay (25.3 Å). The peak shifts to ~23.2 Å when the processing temperature is increased to 200 °C. Increasing the

processing temperature further to 240 °C results in a further decrease in the organoclay d-spacing (~ 22 Å) indicative of an increased loss of mass from the galleries. Careful observation of the WAXS patterns of composites processed at 165 °C and 180 °C reveals a shift to the left relative to that of the pristine organoclay which is often interpreted as a sign of polymer intercalation within the clay galleries. However, we do not think this is the only explanation. The increased d-spacing could also result from intercalation of the low molecular weight oligomers that may be present within the matrix polymer. An alternative explanation derived from studies exploring the density and molecular packing of surfactants within the organoclay galleries should also be considered. Based upon molecular simulations and experimental results, Paul et al. [12] suggested that within an organoclay gallery, the head (nitrogen) groups of the surfactant are essentially tethered to the clay surface while the long hydrocarbon chains tend to adopt a layering structure with disordered conformation. The density of the surfactant in the gallery was determined to be higher than typical of organics of this type which was attributed to the restrictions on molecular motions due to tethering. In the current experiments, as the melt processing temperature increases, the surfactant molecules begin to degrade; however, the alkyl tails which become detached from the ammonium ion may not be immediately extracted from the clay galleries. The detached tails and other degradation products have larger degrees of freedom than surfactant molecules ionically attached to the clay surface. This coupled with the increased energy arising from the higher temperatures could result in some expansion of the organoclay galleries. Why such a shift to the left is observed for nanocomposites based on the $M_2(HT)_2$ organoclay but not the $M_3(HT)_1$ organoclay is not completely understood. The $M_2(HT)_2$ organoclay has a higher mass ratio of intercalated

surfactant to clay than the $M_3(HT)_1$ organoclay (0.55 versus 0.33) . As described later, the two organoclays exhibit different degrees of thermal stability and different levels of exfoliation in LDPE. The effects of these factors on the phenomenon mentioned above have not been fully explored yet. Yoon et al. [13] observed a similar shift to the left in WAXS profiles of pristine $M_2(HT)_2$ organoclay that was heated in a compression molding press in the absence of any polymer.

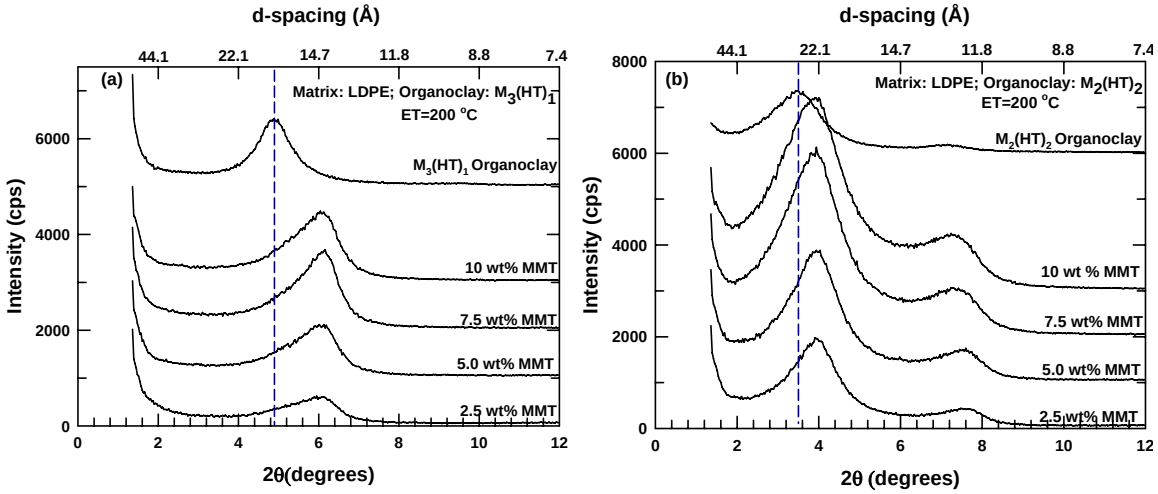

Figure 8.2 WAXD patterns of injection molded samples of LDPE nanocomposites with different montmorillonite contents prepared from (a) $M_3(HT)_1$ and (b) $M_2(HT)_2$ organoclays. The extrusion temperature in all cases is 200 °C. The curves are shifted vertically for clarity.

Figure 8.2 compares the WAXS patterns of nanocomposites prepared from LDPE and varying amounts of organoclay. As expected, for both the $M_3(HT)_1$ and $M_2(HT)_2$ based organoclays, the X-ray scattering intensity increases as the montmorillonite content increases. However, the position of the peak does not change with the organoclay content. Thus, it seems that the extent of surfactant degradation in these nanocomposites is essentially independent of the organoclay content.

Effect of organoclay degradation on mechanical properties

The relative improvement in matrix stiffness achieved by melt mixing LDPE with $M_3(HT)_1$ and $M_2(HT)_2$ organoclays at various temperatures is presented in Figure 8.3. The montmorillonite content of the nanocomposites was controlled between 4.95 and 5.1 wt% (based upon measurement of ash content as described in the Experimental section). Nanocomposites prepared from $M_2(HT)_2$ organoclay exhibit higher levels of reinforcement than those prepared from $M_3(HT)_1$ organoclay at all extrusion temperatures. Similar observations were presented in Chapter 4, where it was determined that the larger the number of alkyl tails on the organic modifier, the higher the level of organoclay exfoliation in polyethylene.

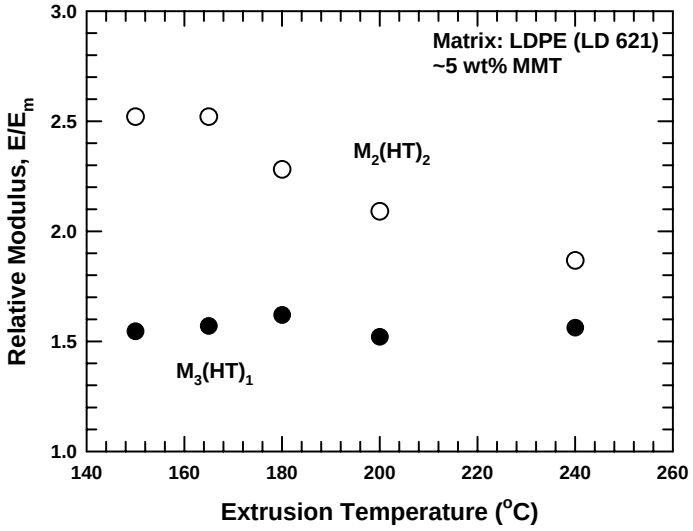

Figure 8.3 Relative modulus (E/E_m) as a function of the extrusion temperature for LDPE (LD 621) nanocomposites prepared from $M_3(HT)_1$ and $M_2(HT)_2$ organoclays. The concentration of MMT in all cases is about 5 wt%.

The tensile modulus of nanocomposites prepared from $M_3(HT)_1$ organoclay seems to be essentially unaffected by the melt processing temperature. It appears that the one-tailed surfactant results in such poor organoclay-polymer interactions that the extent of organoclay dispersion, and hence reinforcement, is independent of the degree of surfactant degradation. On the other hand, the modulus of $M_2(HT)_2$ based nanocomposites drops steadily when the processing temperature is increased beyond 165 °C. As expected, the increase in processing temperature is also accompanied by a drop in the polymer melt viscosity. Our melt processing studies with nylon 6 nanocomposites have revealed that high molecular weight grades of nylon 6 lead to higher levels of exfoliation of organoclays, owing to their higher melt viscosity, than do low molecular weight grades of nylon 6 [14, 15]. Hence, one could argue, that the drop observed in the tensile modulus of LDPE-$M_2(HT)_2$ nanocomposites with the increase in processing temperature might be a result of the reduction in polymer melt viscosity with temperature. To isolate any rheological effects on exfoliation, it was first necessary to characterize the change in melt viscosity over the range of extrusion temperatures mentioned above. As explained in the Experimental section, this was accomplished using a Melt Indexer (Extrusion Plastometer). The melt flow rate (g/10 min) of the polymer, LD 621 was measured at several temperatures between 150 °C and 250 °C under a fixed load of 2.16 kg and the results are presented in Figure 8.4. The curve shows the melt flow rate to increase from 0.25 g/ 10 min. at 150 °C to 6.2 g/10 min. at 240 °C. To account for these changes in melt viscosity, three grades of LDPE with melt indices of 0.75, 2.3 and 7.0 respectively, and similar densities were extruded with the same $M_2(HT)_2$ organoclay at 190 °C. The relative increase in tensile modulus, due to

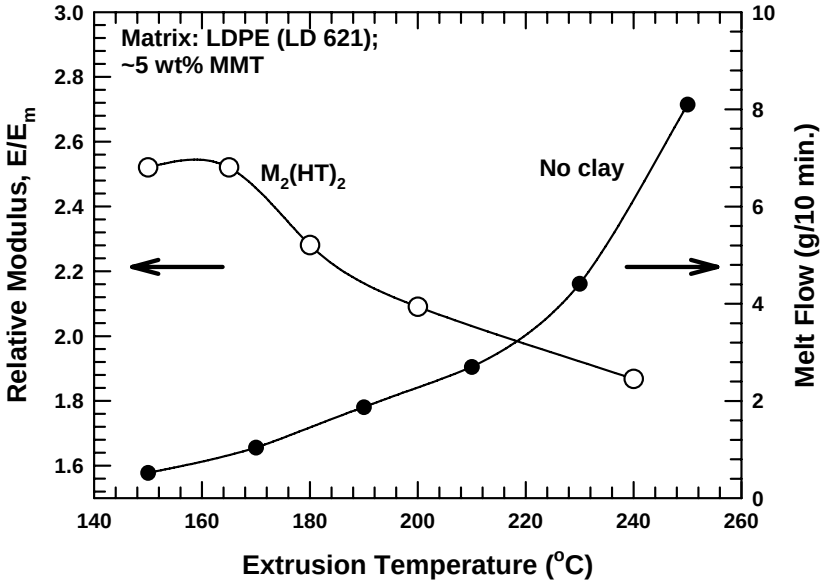

Figure 8.4 Relative modulus (E/E_m) of LD 621- $M_2(HT)_2$ nanocomposites (left axis) is plotted as a function of the extrusion temperature. The data for the melt flow rate of LD 621 (right axis) is plotted against temperature to demonstrate the change in the melt viscosity of the matrix polymer over the same range of temperature.

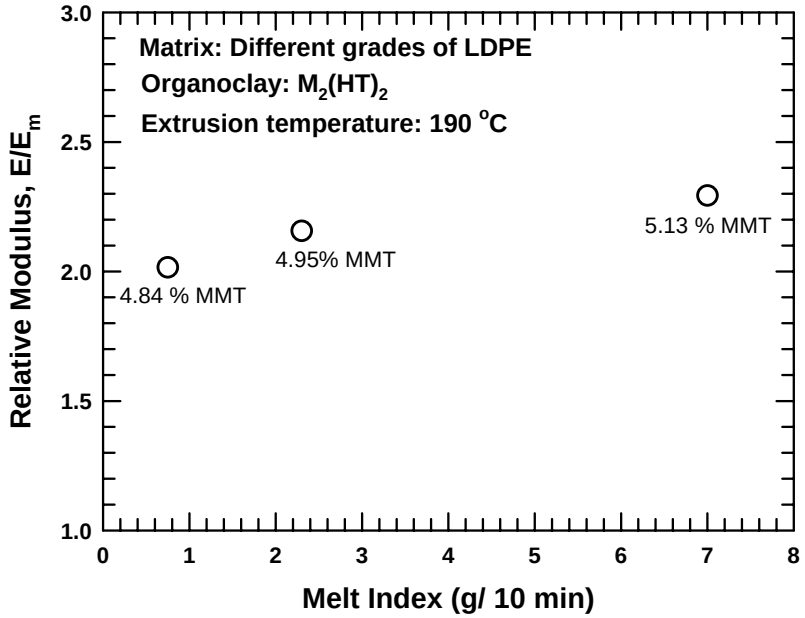

Figure 8.5 Relative modulus (E/E_m) of LDPE-$M_2(HT)_2$ nanocomposites as a function of the melt index of the matrix polymers from which they are formed. Note that there are slight differences in MMT content in the materials that partly account for the trend shown.

reinforcement by the clay, achieved using LDPE resins of different melt indices is presented in Figure 8.5. If the high melt viscosity polymer (within the range mentioned above) caused the improved exfoliation of the selected organoclay, the nanocomposites prepared from Novapol LF-Y819-A (0.75 MI) would have resulted in higher levels of reinforcement than those prepared from Novapol LC-0717-A (7.0 MI). That does not seem to be the case. Although there are minor differences in the montmorillonite content of the nanocomposites (4.84 wt% to 5.13 wt% instead of the targeted 5.0 wt%), it seems that for the MI range mentioned above, the tensile modulus is essentially independent of the polymer melt viscosity, or, if anything, the relative modulus increases with the melt index. Thus, it would be safe to conclude that the drop in the relative modulus of the LDPE-$M_2(HT)_2$ nanocomposites processed at high temperatures (Figure 8.4) is entirely a result of the increased level of surfactant degradation at those temperatures. It appears that the extraction of the organic modifier from the clay galleries and the subsequent reduction of the organoclay d-spacing hampers the ability of LDPE to disperse the $M_2(HT)_2$ organoclay into high aspect ratio particles.

Thermogravimetric analysis (TGA) of pristine organoclays

The thermal stability of the three organoclays with different number of alkyl tails was compared using thermogravimetric analysis. First, the effect of the purge gas on surfactant mass loss was evaluated. Figure 8.6 compares the thermograms of $M_3(HT)_1$ organoclay obtained at 200 °C using nitrogen and air. The data are presented in terms of fractional mass loss of the surfactant rather than the fractional loss of the mass of organoclay. There is slightly more degradation in air than in nitrogen but the difference

between the two curves is relatively small. Thus, the degradation is mainly thermally driven with perhaps a slight oxidative contribution. A previous study [10] reported similar observations during thermogravimetric analysis of a two-tailed organoclay (for T ≤ 200 °C). Since the choice of purge gas used does not significantly affect the amount of surfactant lost, nitrogen gas was arbitrarily chosen as the purge medium for these analyses. Figure 8.7 shows the isothermal plots of mass loss versus time for the one-tailed ($M_3(HT)_1$), two-tailed ($M_2(HT)_2$), and three-tailed ($M_1(C_{16})_3$) organoclays conducted over a wide range of temperatures (150 °C to 240 °C). As expected, for all organoclays, the extent of mass loss increases as the test temperature becomes higher; however, the rate of surfactant loss increases dramatically in going from 200 °C to 220 °C. The rate of mass loss increases even more rapidly when the test temperature is raised to 240 °C. Gelfer et al. [10] noticed a similar trend for two-tailed organoclays. They observed very little surfactant loss between 100 °C and 200 °C. The major weight loss began at 200 °C and continued until 400 °C.

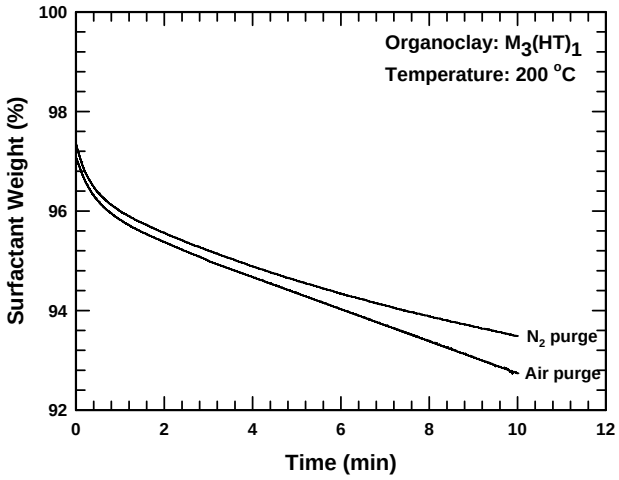

Figure 8.6 Isothermal TGA results for pre-dried $M_3(HT)_1$ organoclay obtained in air and nitrogen at 200 °C.

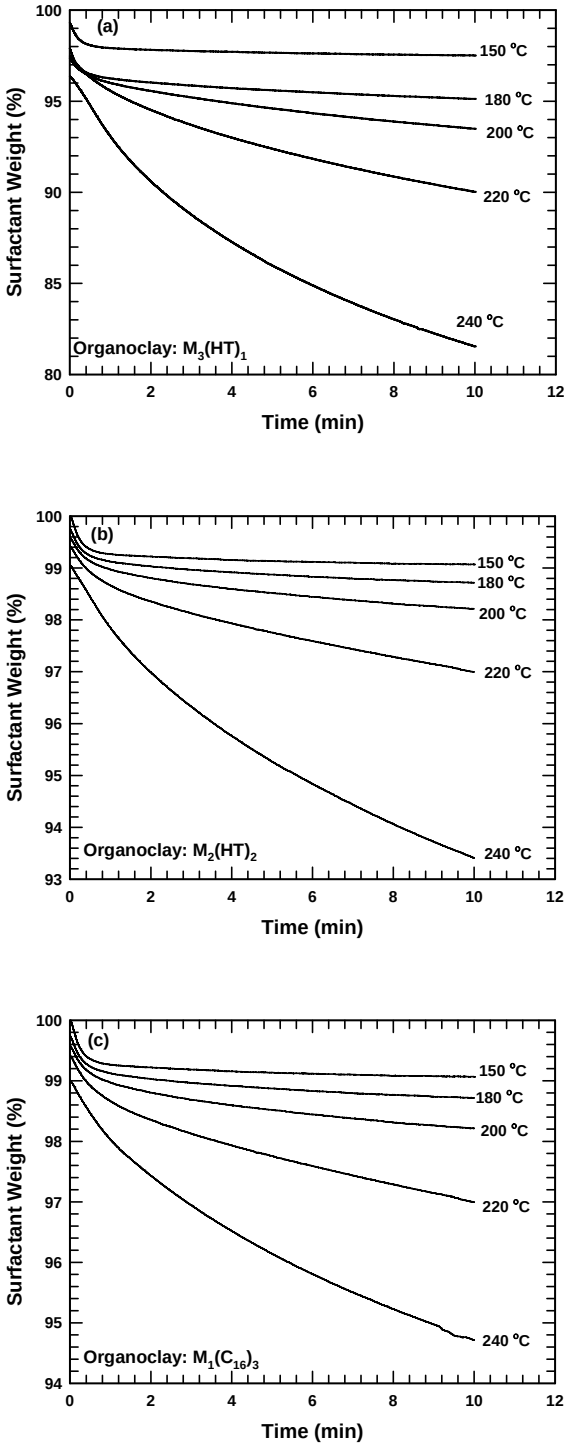

Figure 8.7 Isothermal TGA results of (a) $M_3(HT)_1$, (b) $M_2(HT)_2$ and (c) $M_1(C_{16})_3$ organoclays obtained in nitrogen at various temperatures.

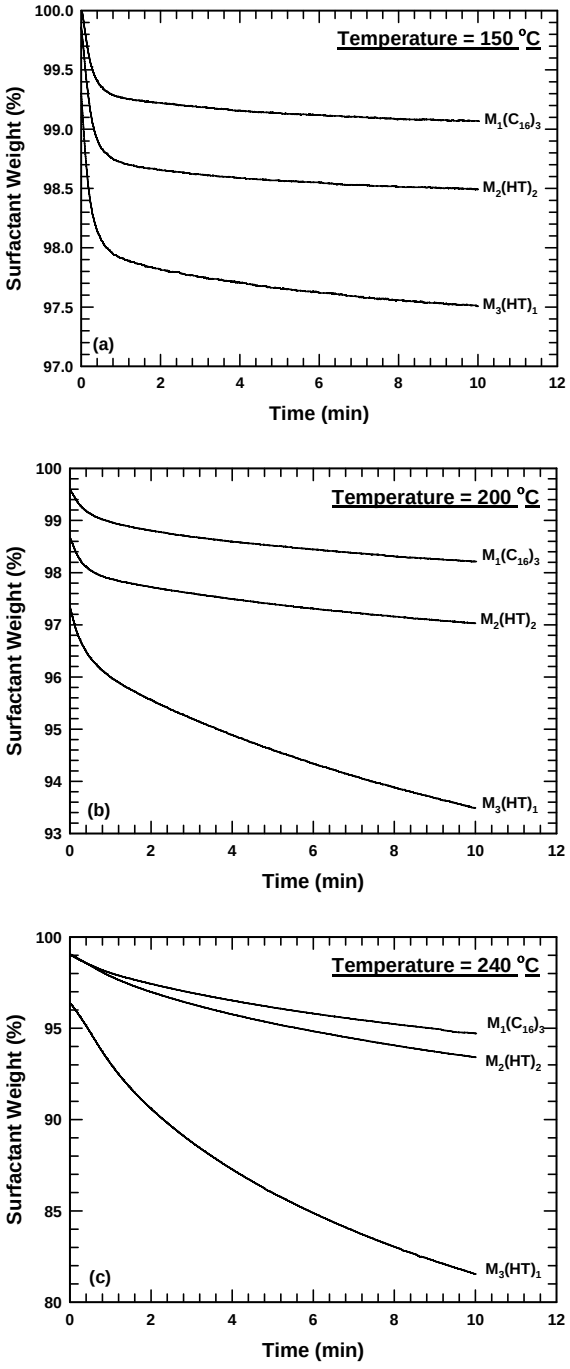

Figure 8.8 Isothermal TGA results showing the weight percent of surfactant loss from $M_3(HT)_1$, $M_2(HT)_2$ and $M_1(C_{16})_3$ organoclays at (a) 150 °C, (b) 200 °C and (c) 240 °C under nitrogen atmosphere.

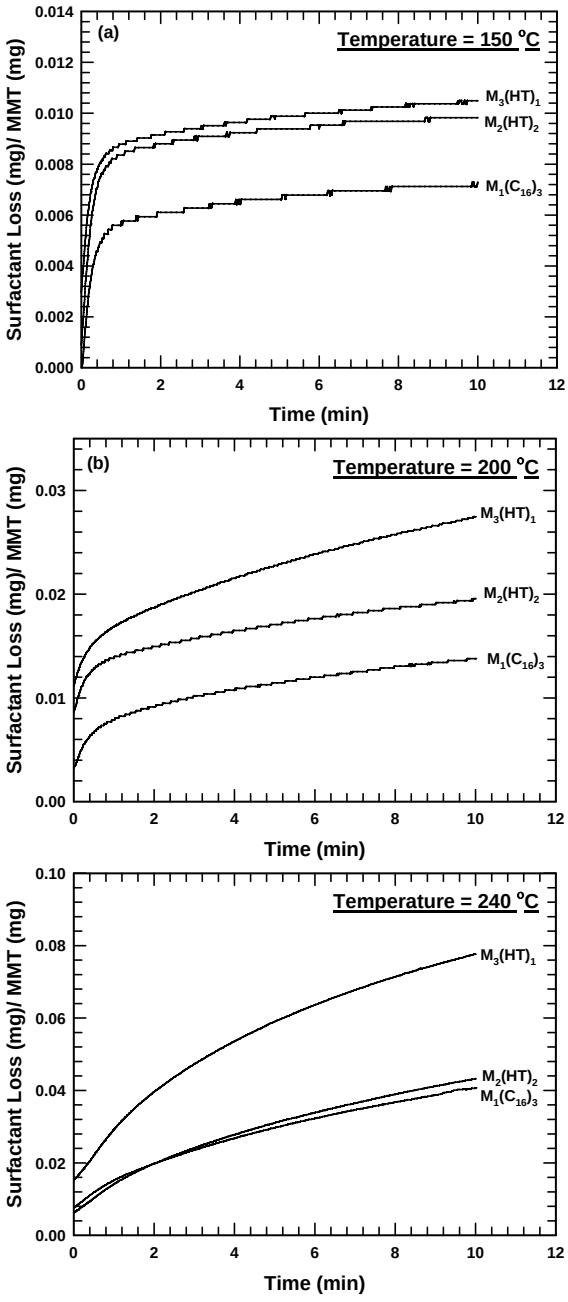

Figure 8.9 Isothermal TGA results showing the absolute mass loss for $M_3(HT)_1$, $M_2(HT)_2$ and $M_1(C_{16})_3$ organoclays at (a) 150 °C, (b) 200 °C and (c) 240 °C under nitrogen atmosphere.

Interestingly, the rate of mass loss for a one-tailed organoclay ($M_3(HT)_1$) is greater than for the multiple-tailed organoclays under the same testing conditions; note the more expanded scales in Figure 8.7(b) and 8.7(c) than in Figure 8.7(a). This is further elucidated in Figure 8.8 where the weight fraction of the surfactant remaining is plotted against time for the three organoclays at 150 °C, 200 °C and 240 °C. At all three temperatures, $M_1(C_{16})_3$ seems to be more thermally stable than $M_2(HT)_2$ which in turn is more stable than $M_3(HT)_1$. The difference between the weight fraction of the surfactant lost in the $M_3(HT)_1$ and the $M_2(HT)_2$ organoclay is much larger than the difference between $M_2(HT)_2$ and $M_1(C_{16})_3$ organoclays. A similar observation was made by Osman et al. [9] while comparing the thermal stability of various organoclays at 200 °C. In their study, organoclays based on dioctadecyldimethylammonium required a longer time to register the same percentage drop in surfactant content than for octadecyltrimethylammonium based organoclays.

It should be remembered that the $M_1(C_{16})_3$ organoclay has a higher organic content than the $M_2(HT)_2$ organoclay which in turn has a higher organic content than the $M_3(HT)_1$ organoclay (see Table 2.2). Thus, a comparison of the reduction in surfactant content in the three given organoclays does not offer a clear comparison of the absolute amount of surfactant leaving the clay galleries during TGA. To resolve this, we have plotted in Figure 8.9 the absolute mass loss normalized by the montmorillonite content of each sample for the three organoclays during isothermal TGA at 150 °C, 200 °C and 240 °C. The trends observed are similar to those presented in Figure 8.8; despite having a larger alkyl content, $M_2(HT)_2$ and $M_1(C_{16})_3$ organoclays lose less mass than the one-

tailed, $M_3(HT)_1$ organoclay. All these observations lead us to the conclusion that organoclays prepared from ammonium-based surfactants with multiple alkyl tails have greater thermal stability than those with a single alkyl tail.

DISCUSSION

The amounts of surfactant lost from $M_3(HT)_1$ organoclay during nanocomposite extrusion and during thermogravimetric analysis of the organoclay at 200 °C and 240 °C are listed in Table 8.1.

Table 8.1 Amount of surfactant loss from $M_3(HT)_1$ organoclay during nanocomposite extrusion and thermogravimetric analysis of the organoclay.

	Melt processing			Thermogravimetric analysis	
Temperature (°C)	WAXD peak position (Å)	Change in peak position[a] (Å)	Surfactant loss[b] (wt%)	Surfactant loss at t = 3.4 min[c] (wt%)	Surfactant loss at t = 10 min (wt%)
200	14.7	3.3	38.4	5.1	7.3
240	14.2	3.8	44.2	12.3	19.4

[a] Calculated using a peak position of 18 Å for pristine $M_3(HT)_1$ organoclay
[b] Based upon a thickness of 9.4 Å for an aluminosilicate platelet, exclusive of the sodium ion [Fornes modelling], and assuming (i) uniform surfactant density between the platelets, and (ii) no polymer intercalation within the clay galleries
[c] The average residence time for the extruder used in this study was 3.4 min [2,20]

The amount of surfactant leaving the clay galleries during nanocomposite extrusion was calculated from the reduction in the d-spacing of the melt processed composites. A few approximations were necessary to allow these calculations. First, the surfactant density was assumed to be uniform across the interplatelet region. It was also assumed that there is no intercalation of LDPE within the $M_3(HT)_1$ organoclay galleries. Based upon the

TEM analysis of LDPE-$M_3(HT)_1$ organoclay nanocomposites presented in Chapter 4, this assumption seems to be appropriate. The average polymer residence time in the extruder used for this study has been determined to be 3.4 minutes [2, 16]. Hence, in order to ensure a fair comparison, surfactant weight loss during thermogravimetric analysis was calculated at 3.4 minutes and 10 minutes using air as purge gas. This comparison is presented graphically in Figure 8.10.

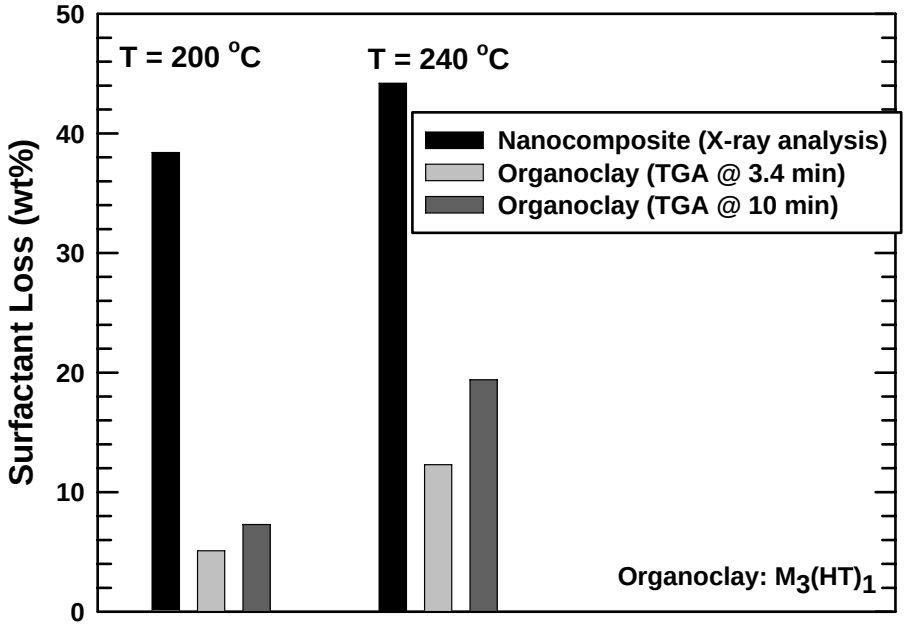

Figure 8.10 Comparison of the surfactant loss from $M_3(HT)_1$ organoclay during nanocomposite extrusion and during thermogravimetric analysis of the organoclay at 200 °C and 240 °C.

The data clearly reveal a larger amount of surfactant loss from the clay galleries during melt processing than during TGA. Xie et al. [5] analyzed the degradation products released during the thermogravimetric analysis of trimethyloctadecyl ammonium chloride organoclays ($M_3(C_{18})_1$) using a GC-MS technique. Their analysis suggested that the initial degradation of the organoclay follows a Hoffman elimination mechanism (shown

below for alkyl ammonium hydroxide) with the release of long chained α-olefins (C16-C18). Alternative schemes for Hoffman elimination reaction for organically modified montmorillonite are also available in the literature [2, 11]. All of them suggest the formation of alpha olefins, amines and other products resulting from the secondary reactions between the degradation products within the organoclay.

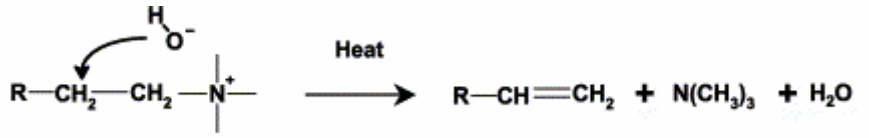

(quaternary ammonium hydroxide) (α-olefin) (amine) (water)

The primary mechanism by which these degradation products leave the clay galleries during TGA would be by evaporation. The vapor pressure of 1-hexadecene at 200 °C and 240 °C is approximately 10 kPa and 35 kPa, respectively, while that for 1-heptadecene is 7.5 kPa and 24 kPa, respectively, and that for 1-octadecene is 4.1 kPa and 15.2 kPa, respectively [17]. For comparison, benzene has a vapor pressure of 15.8 kPa at 30 °C. On the other hand, during melt mixing, evaporation is minimal and the primary mechanism by which the degradation products leave the clay galleries should be dissolution into the matrix polymer. The α-olefins should be readily soluble in polyethylene, and so they are easily extracted from the clay galleries into the matrix polymer. This combined with possibly some effects of the mechanical forces generated during extrusion results in the collapsing of the clay galleries. A comparison of the WAXS patterns of LDPE- nanocomposites to that of pristine tetramethyl ammonium organoclay, M_4 (no alky tails), as shown in Figure 8.11, supports the above theory. After

the elimination of the α-olefins the organoclay d-spacing of the LDPE- $M_3(HT)_1$ nanocomposites approaches that of pristine M_4 organoclay (13.8 Å). X-ray scans of nanocomposites prepared by melt mixing poly(ethylene-co-methacrylic acid) ionomers with one-tailed organoclays at 200 °C exhibit similar patterns [18]. On the other hand the α-olefins may not be as soluble in polypropylene as in polyethylene. This could explain why, under the same processing conditions, the WAXS peak for PP- $M_3(HT)_1$ composites is not shifted as much to the right as for the PE- $M_3(HT)_1$ composites (see Figure 8.11) For the same reasons we would expect WAXS peaks of nanocomposites prepared from polystyrene [19] to not shift as much as those of PE-organoclay composites.

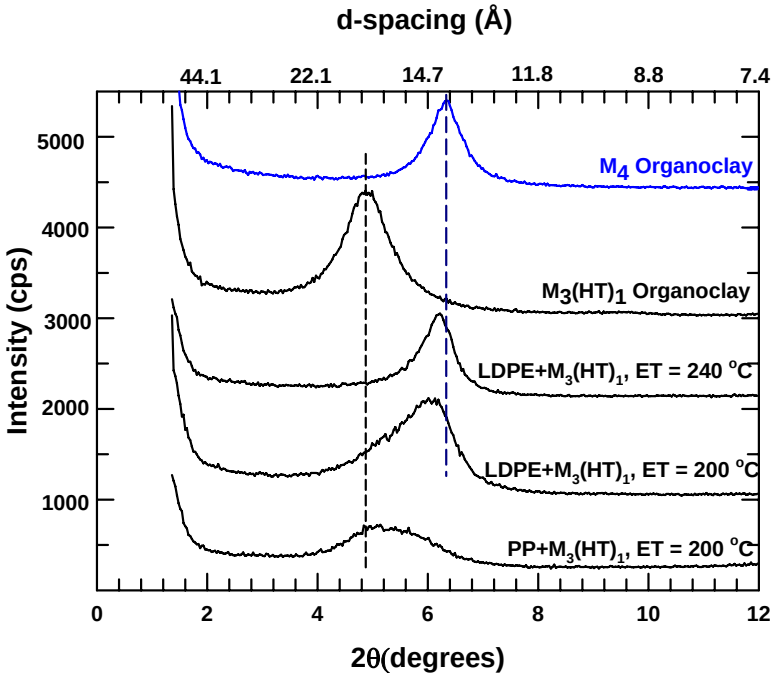

Figure 8.11 WAXD patterns of injection molded samples of LDPE and polypropylene nanocomposites prepared from $M_3(HT)_1$ organoclay at 200 °C and 240 °C. X-ray scans of $M_3(HT)_1$ and M_4 (tetra methyl ammonium) organoclays are plotted for comparison. The concentration of MMT in all cases is about 5 wt%. The curves are shifted vertically for clarity.

CONCLUSIONS

Surfactant degradation in melt processed polyethylene-organoclay nanocomposites was examined using WAXS and thermogravimetric analyses, and its effect on nanocomposite mechanical properties was evaluated using stress-strain analysis. Since polyethylene has a low melting point, it was possible to conduct this examination over a wide range of temperatures (150 °C to 240 °C). The d-spacing from the WAXS peaks for nanocomposites based on both $M_3(HT)_1$ and $M_2(HT)_2$, decreased by 3-4 Å when the processing temperature was raised from 180 °C to 200 °C, thus suggesting a sharp increase in the amount of surfactant leaving the organoclay galleries between these temperatures. The extent of surfactant degradation in the melt processed nanocomposites was determined to be independent of the organoclay content.

The improvement in tensile modulus resulting from melt mixing LDPE with $M_3(HT)_1$ organoclay was much less than for LDPE- $M_2(HT)_2$ nanocomposites, and the modulus seemed to be unaffected by the level of organoclay degradation . On the other hand, the relative modulus (E/E_m) of LDPE- $M_2(HT)_2$ nanocomposites dropped steadily as the processing temperature increased beyond 165 °C. It appears that depletion of organic material from the organoclay galleries by degradation and the resulting reduction in the interplatelet distances restricts the ability of LDPE to exfoliate the $M_2(HT)_2$ organoclay.

Thermogravimetric analysis of $M_3(HT)_1$, $M_2(HT)_2$ and $M_1(C_{16})_3$ organoclays suggest that organoclays based on surfactants with multiple alkyl tails have greater thermal stability than those based on surfactants with a single alkyl tail. The mass of surfactant lost during melt processing of nanocomposites was found to be greater than

during thermogravimetric analysis of organoclays (in the absence of polymer). This could be attributed to the high solubility of the degradation products (predominantly α-olefins) in the polyethylene matrix, thus facilitating an easier removal of these products from the organoclay by extrusion as compared to TGA where the degradation products leave by evaporation.

REFERENCES

[1] Delozier DM, Orwoll RA, Cahoon JF, Johnston NJ, Smith JG, Connell JW. Polymer 2002;43(3):813-22.

[2] Fornes TD, Yoon PJ, Paul DR. Polymer 2003;44(24):7545-56.

[3] Yoon PJ, Hunter DL, Paul DR. Polymer 2003;44(18):5341-54.

[4] Matayabas Jr. JC, Turner SR. In: Polymer-clay nanocomposites, T.J. Pinnavaia and G.W. Beall, editors. Wiley: New York: 2000. p. 207.

[5] Xie W, Gao Z, Pan W-P, Hunter D, Singh A, Vaia R. Chem Mater 2001;13(9):2979-90.

[6] Xie W, Gao Z, Liu K, Pan WP, Vaia R, Hunter D, Singh A. Thermochimica Acta 2001;367-368:339-50.

[7] VanderHart DL, Asano A, Gilman JW. Chem Mater 2001;13(10):3796-809.

[8] VanderHart DL, Asano A, Gilman JW. Macromolecules 2001;34(12):3819-22.

[9] Osman MA, Ploetze M, Suter UW. J Mat Chem 2003;13(9):2359-66.

[10] Gelfer M, Burger C, Fadeev A, Sics I, Chu B, Hsiao BS, Heintz A, Kojo K, Hsu SL, Si M, Rafailovich M. Langmuir 2004;20(9):3746-58.

[11] Davis R, Gilman J, VanderHart D. Polym Degrad Stab 2003;79:111-21.

[12] Paul DR, Zeng QH, Yu AB, Lu GQ. Journal of Colloid and Interface Science 2005;292(2):462-8.

[13] Yoon PJ, Hunter DL, Paul DR. Polymer 2003;44(18):5323-39.

[14] Shah RK, Paul DR. Polymer 2004;45(9):2991-3000.

[15] Fornes TD, Yoon PJ, Keskkula H, Paul DR. Polymer 2001;42(25):9929-40.

[16] Chavarria F, Paul DR. Polymer 2004;45(25):8501-15.

[17] DIPPR, 801, database. (http://dippr.byu.edu/)

[18] Shah RK, Hunter DL, Paul DR. Polymer 2005;46(8):2646-62.

[19] Tanoue S, Utracki LA, Garcia-Rejon A, Tatibouet J, Cole KC, Kamal MR. Polym Eng Sci 2004;44(6):1046-60.

Chapter 9: Blown films of nanocomposites prepared from LDPE and poly(ethylene-co-methacrylic acid) ionomers

After optimizing the organoclay structure and processing conditions, nanocomposites with acceptable levels of organoclay exfoliation were prepared from low density polyethylene (LDPE) and a sodium ionomer of poly(ethylene-co-methacrylic acid). These nanocomposites were then blown into film at various conditions to determine the effect of platelet concentration, exfoliation, and orientation on film performance. Mechanical properties including stiffness, puncture resistance, and resistance to tear propagation were evaluated and these were compared to corresponding properties of unfilled polymer films. Permeability of these films to common atmospheric gases like oxygen, nitrogen and carbon dioxide was also measured using standard testing methods. The details of the experimental methods and the result of these analyses are discussed in this chapter.

EXPERIMENTAL

A commercially available grade of LDPE, Novapol LF-0219A, and a sodium ionomer of poly(ethylene-co-methacrylic acid), Surlyn® 8945 were used in this study. Selected properties of these polymers are included in Table 2.1. As described in Chapter 7, nanocomposites prepared from organoclays with multiple alkyl tails exhibit a more exfoliated morphology than nanocomposites prepared form a one-tailed organoclay. Similar trends were seen for nanocomposites prepared from low density polyethylene (Chapter 4). Also, organoclays with excess amount of the amine surfactant instead of an

equivalent amount exfoliated better in the ionomeric matrix (Chapter 7). Since the three tailed organoclay, $M_1(C_{16})_3$, is an experimental organoclay, and thus, is available only in limited quantities, the over exchanged, two-tailed organoclay, $M_2(HT)_2$-140, was used in this study (See Fig. 2.1 and Table 2.2 for the structure and properties of the organoclays).

The polymers and the organoclay were melt mixed in a Werner-Pfleiderer ZSK25 twin screw co-rotating extruder (D=25 mm, L/D= 48) at 190 °C, using a feed rate of 40 lbs/hr to form nanocomposites with 1 and 3 wt% MMT. The filler and the matrix were added to the extruder using two separate feed-ports. Polymer was fed using an upstream port while the clay was added to the molten polymer using a downstream port. Prior experience [1, 2] has revealed better organoclay exfoliation in nanocomposites formed using such a feeding system, rather than feeding the clay and the polymer together in the upstream region of the extruder, which mainly consists of kneading blocks.

These nanocomposites were then blown into films at 190 °C using a 38 mm Davis Standard extruder fitted with a 10.16 cm Sano Spiral-Mandrel film die, at two different blow-up ratios (BUR), 2:1 and 3:1. The draw down ratio (DDR) was varied to form films with 1 mil, 2 mil, and 3 mil thickness, respectively (1 mil = 25.4 microns). BUR, a term commonly used in describing the processing conditions for blown-films, is the ratio of the diameter of the final film 'tube' to the diameter of the die. DDR, another such term, is a ratio of the final film velocity, i.e., the velocity of the nip roll to the initial polymer velocity (at the die exit). Mathematically, DDR = (Die gap)/ [(film thickness) x (BUR)]. In all, 35 films were blown; it was not possible to blow film from the unfilled ionomer at one condition (3:1 BUR and 7 DDR) as bubble stability could not be maintained. Puncture resistance (dart impact strength), tensile properties, and resistance to tear

propagation of the nanocomposite films in the machine direction (MD) and transverse direction (TD) were evaluated as per ASTM standards D1709, D882, and D1922, respectively, and the properties were compared to those of the corresponding unfilled polymer films. Permeability of the films to O_2, N_2 and CO_2 gases were determined using a constant-volume-variable pressure method as described by Koros et al. [3].

Melt rheological measurements of the nanocomposites were made using an ARES torsional rheometer operated in an oscillatory mode at 190 °C in a nitrogen atmosphere. Compression molded disks (~1.8 – 2.0 mm) were placed between the parallel plates of the rheometer. Once thermal equilibrium was achieved, the disks were squeezed between the parallel plates to 1.6 mm thickness, and the excess material was trimmed prior to the frequency sweep test.

RESULTS

Rheology of nanocomposites

The complex viscosities of the nanocomposites and the unfilled polymers are presented in Fig. 9.1. In both polymers, the melt viscosity increases systematically with increasing clay content. This is consistent with the rheological behavior of polyethylene type nanocomposites reported by Zhong et al [4]. It is interesting to note that the magnitude of viscosity enhancement for the ionomer based nanocomposites is much greater than for the LDPE based nanocomposites. The differences are more pronounced at low frequencies. This is most likely a result of the higher level of organoclay exfoliation [5] in the ionomer based nanocomposites compared to the LDPE based nanocomposites as described in Chapter 4.

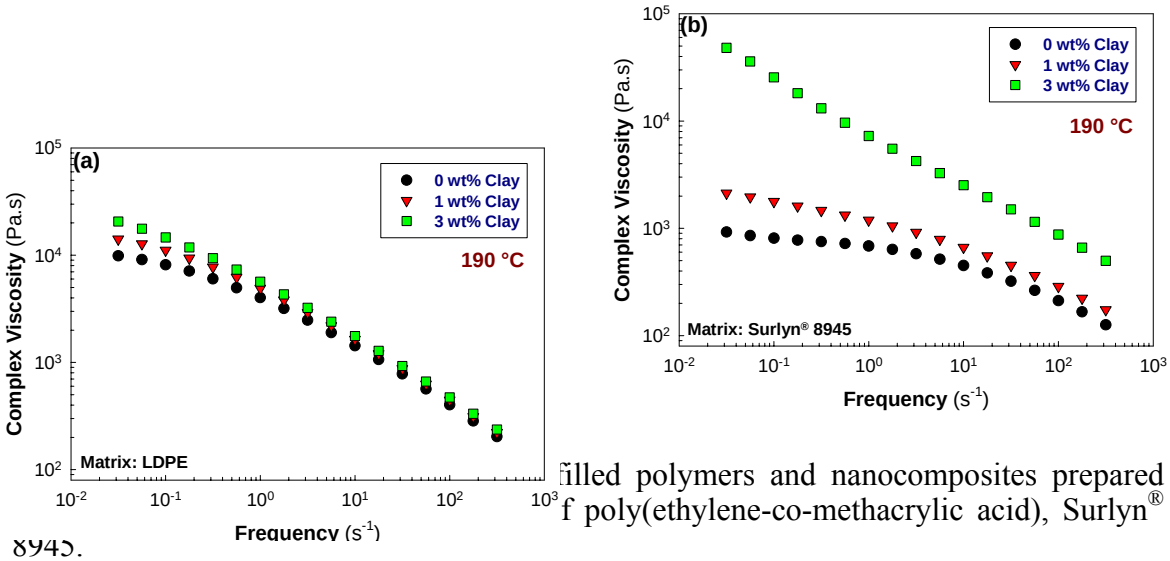

filled polymers and nanocomposites prepared
f poly(ethylene-co-methacrylic acid), Surlyn®
8945.

Visual morphology of blown-films

All of the films had good clarity and surface properties. As expected, samples prepared from the unfilled polymers were colorless, while those prepared from the nanocomposites had a slight yellowish tinge. The films had a smooth texture, which was a significant improvement over previous trials [6] when the samples had a rough, sand-paper like texture. This could be attributed to the acceptable levels of organoclay exfoliation achieved in these nanocomposites resulting from the use of an appropriate organoclay and optimum processing conditions. Films prepared from LDPE and their nanocomposites were free from any visual defects like gels (fish eyes); however, those prepared from the ionomer contained a few gels.

Mechanical properties of blown-films

Selected mechanical properties of the blown-films prepared are listed in Table 9.1

Table 9.1 Selected mechanical properties of the blown-films examined in this study

Film No.	Matrix	MMT (wt%)	BUR	Thickness (mil)	DDR	MD Tear (g)	TD Tear (g)	Dart Impact (g)	Tensile Modulus (MPa)		Break Stress (MPa)		Break Strain (%)	
									MD	TD	MD	TD	MD	TD
1	LDPE	0	2:1	3	10.0	180	148	40	157.8	191.1	16.0	15.0	275.2	564.4
2	LDPE	0	2:1	2	15.0	202	109	42	159.7	191.6	17.9	14.4	221.4	475.2
3	LDPE	0	2:1	1	30.0	362	106	38	184.1	233.6	25.6	12.3	86.3	394.1
4	LDPE	0	3:1	3	6.7	59	126	84	154.5	165.1	15.6	16.4	324.1	502.2
5	LDPE	0	3:1	2	10.0	57	96	87	165.5	172.0	17.4	16.2	251.6	499.0
6	LDPE	0	3:1	1	20.0	104	74	83	188.5	195.2	24.2	15.3	104.4	390.8
7	LDPE	1	2:1	3	10.0	73	152	37	179.5	202.5	17.6	14.6	269.5	541.7
8	LDPE	1	2:1	2	15.0	292	262	45	193.7	229.3	18.7	14.8	171.6	499.2
9	LDPE	1	2:1	1	30.0	290	150	23	212.6	269.2	26.3	11.8	75.5	343.6
10	LDPE	1	3:1	3	6.7	33	113	50	182.2	193.5	15.6	16.1	326.7	529.1
11	LDPE	1	3:1	2	10.0	56	138	72	169.9	200.8	17.0	14.9	228.5	436.1
12	LDPE	1	3:1	1	20.0	43	90	84	202.7	225.8	23.0	14.3	99.6	342.1
13	LDPE	3	2:1	3	10.0	131	181	33	201.8	239.6	17.9	16.4	246.2	600.3
14	LDPE	3	2:1	2	15.0	160	331	35	217.8	268.6	20.0	13.0	139.9	420.5
15	LDPE	3	2:1	1	30.0	11	223	23	236.8	273.2	30.8	11.5	70.7	351.0
16	LDPE	3	3:1	3	6.7	56	144	79	197.6	210.1	15.2	17.4	343.2	512.8
17	LDPE	3	3:1	2	10.0	65	256	59	193.5	199.3	21.7	16.4	222.1	472.9
18	LDPE	3	3:1	1	20.0	84	115	68	219.4	244.5	23.3	14.4	101.4	366.6
19	Ionomer	0	2:1	3	10.0	18	23	274	255.4	261.6	26.9	24.2	252.1	329.5
20	Ionomer	0	2:1	2	15.0	13	23	249	312.5	298.6	29.7	21.0	185.0	253.4
21	Ionomer	0	2:1	1	30.0	9	17	274	252.7	282.3	31.3	19.9	67.4	227.0
22	Ionomer	0	3:1	3	6.7	*	*	*	*	*	*	*	*	*
23	Ionomer	0	3:1	2	10.0	15	16	298	277.0	279.7	24.5	26.5	253.6	275.9
24	Ionomer	0	3:1	1	20.0	17	21	329	296.4	249.4	24.1	26.8	108.0	226.6
25	Ionomer	1	2:1	3	10.0	23	18	250	300.6	302.4	25.8	24.6	238.8	307.2
26	Ionomer	1	2:1	2	15.0	15	19	244	355.2	323.9	27.0	22.5	188.9	251.3
27	Ionomer	1	2:1	1	30.0	9	19	331	335.2	315.5	28.1	20.7	87.5	195.7
28	Ionomer	1	3:1	3	6.7	23	20	164	346.7	348.4	24.3	30.1	275.1	301.7
29	Ionomer	1	3:1	2	10.0	21	17	263	322.2	324.3	25.5	26.6	220.0	241.0
30	Ionomer	1	3:1	1	20.0	15	15	360	326.5	318.8	22.6	24.5	126.6	187.2
31	Ionomer	3	2:1	3	10.0	24	28	196	415.8	385.2	22.8	24.4	251.2	288.9
32	Ionomer	3	2:1	2	15.0	14	21	211	470.3	422.8	26.9	22.3	182.6	232.2
33	Ionomer	3	2:1	1	30.0	11	18	201	440.7	384.2	28.2	19.6	77.3	157.1
34	Ionomer	3	3:1	3	6.7	26	23	178	449.7	434.5	26.7	29.5	266.9	298.2
35	Ionomer	3	3:1	2	10.0	16	17	195	436.1	390.6	24.6	24.6	212.8	236.7
36	Ionomer	3	3:1	1	20.0	14	22	243	432.4	405.4	26.6	22.2	120.4	144.0

* It was not possible to blow film #22, as bubble stability could not be maintained.

Tensile modulus

Tensile moduli data of the blown films prepared from LDPE and its nanocomposites are presented in Fig. 9.2. Similar data for blown films prepared from the Surlyn® ionomer are presented in Fig. 9.3

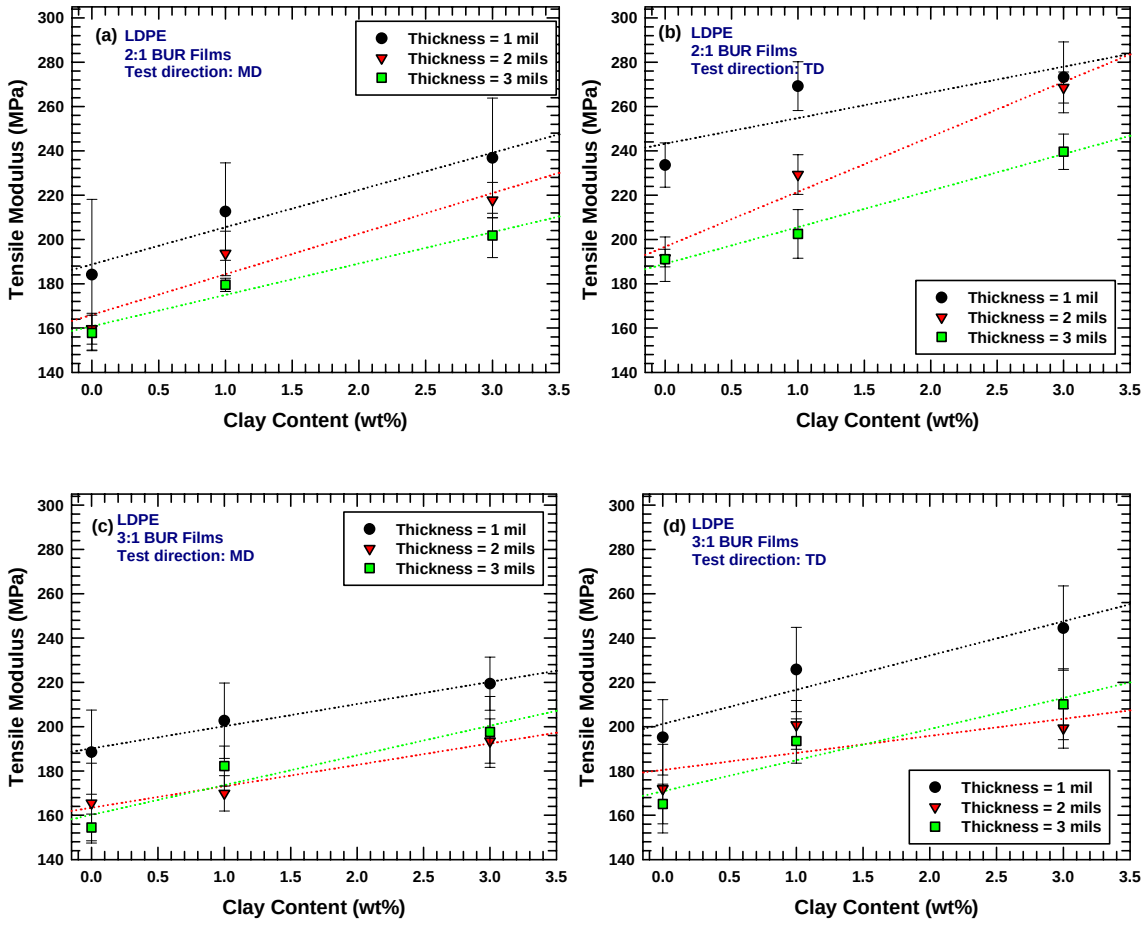

Figure 9.2 Tensile modulus of blown-films prepared from LDPE and $M_2(HT)_2$-140 organoclay plotted as a function of the montmorillonite content: (a) films with 2:1 BUR tested along the machine direction, (b) films with 2:1 BUR tested along the transverse direction, (c) films with 3:1 BUR tested along the machine direction, (d) films with 3:1 BUR tested along the transverse direction. The X-axis has been extended beyond zero in all graphs for clarity. The dotted lines are trend lines (linear regression lines), and are included to serve as visual guides.

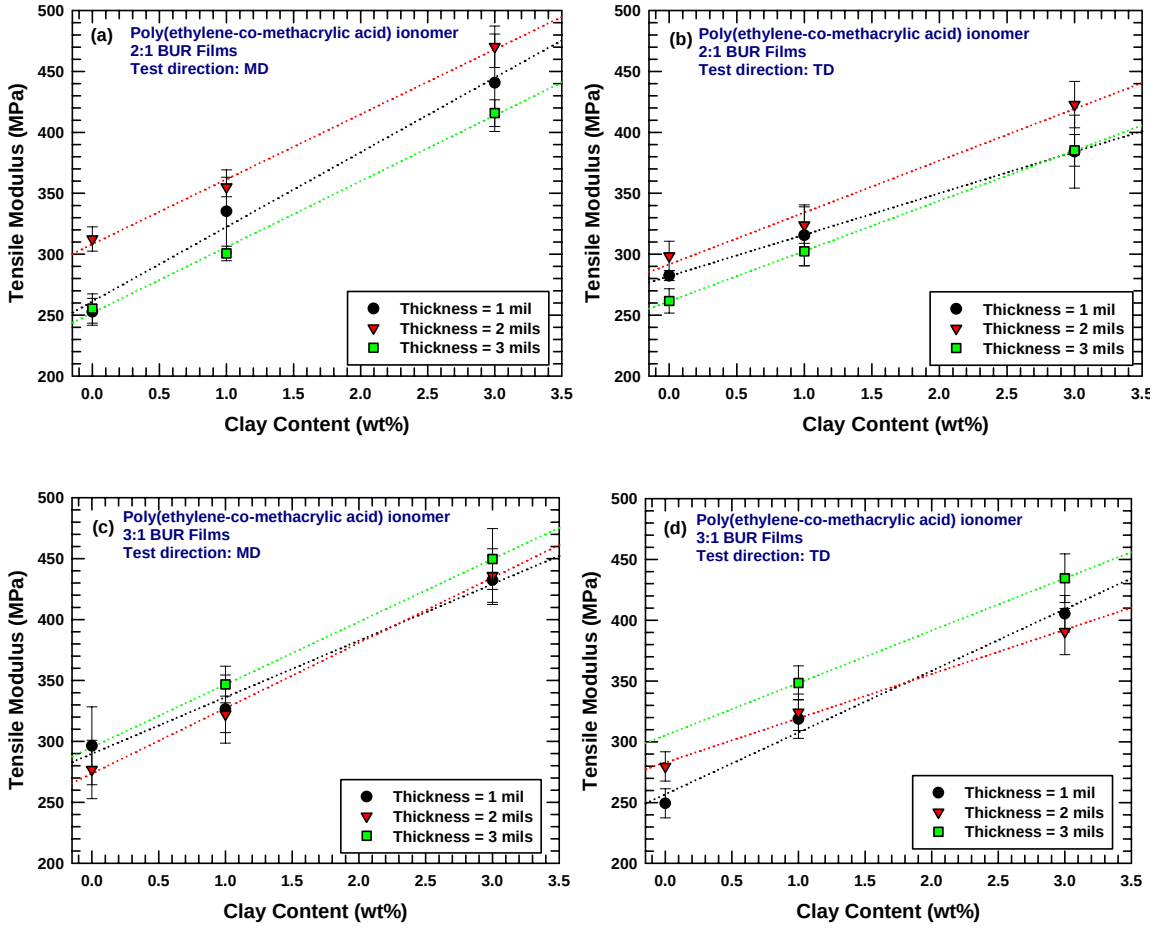

Figure 9.3 Tensile modulus of blown-films prepared from Surlyn® ionomer and $M_2(HT)_2$-140 organoclay plotted as a function of the montmorillonite content: (a) films with 2:1 BUR tested along the machine direction, (b) films with 2:1 BUR tested along the transverse direction, (c) films with 3:1 BUR tested along the machine direction, (d) films with 3:1 BUR tested along the transverse direction. The X-axis has been extended beyond zero in all graphs for clarity. The dotted lines are trend lines (linear regression lines), and are included to serve as visual guides.

As expected [7, 8], for both polymers, tensile modulus increases as the organoclay content increases. The increase in modulus of the films prepared from the ionomer based nanocomposites is significantly higher than that of the LDPE based nanocomposites. This is a result of better organoclay exfoliation in the ionomer than in LDPE as shown in Chapter 4. A numerical comparison between the improvements in modulus exhibited by the nanocomposite films (containing 3 wt% MMT) prepared from LDPE and the ionomer relative to the corresponding films prepared from the unfilled polymer is presented in Table 9.2.

Table 9.2 Improvement in tensile modulus of blown-films prepared from nanocomposites of LDPE and poly(ethylene-co-methacrylic acid) containing 3 wt% MMT relative to modulus of blown films produced using identical processing conditions from the corresponding unfilled polymers.

Thickness (mils)	BUR	LDPE nanocomposite films % Improvements		Ionomer nanocomposite films % Improvements	
		MD	TD	MD	TD
1	2:1	29	17	74	36
2	2:1	36	40	51	42
3	2:1	28	25	63	47
1	3:1	17	23	46	63
2	3:1	17	17	57	40
3	3:1	28	27	30	25

A comparison between Fig. 9.2(a) and 9.2(b) suggests that blown films prepared from unfilled LDPE have a higher tensile modulus along the transverse direction than along the machine direction. On the other hand, such trends are not evident in films prepared from the ionomer (Fig. 9.3). These results could be attributed to the differences between the crystallinity of the two polymers, and orientation of the lamellae in these films. LDPE, although not as crystalline as high density polyethylene (HDPE), is more crystalline than the ionomer. The bulky methacrylic acid groups of the ionomer interfere with the chain folding process, which subsequently results in a lower crystallinity and smaller crystallites compared to the base polyethylene (a morphology which leads to better optical properties, viz., haze, gloss, and clarity for the ionomer). The presence of the ionic clusters may also contribute to this effect. The crystallization of the molecules in a blown film process occurs under the influence of an external strain. This generally results in an oriented morphology, with the long axes of the crystalline lamellae generally oriented perpendicular to the film MD. For polymers such as LDPE, the unit cell 'a' axis is oriented preferentially along the film MD, and such a microstructure is well described by the Keller-Machin "row" structure [9-11]. The orientation of the lamellar long axes perpendicular to the film MD causes the TD modulus to be higher than the MD modulus [12]. On the other hand, for nanocomposites prepared from the ionomer, tensile modulus is slightly higher in the MD than in the TD (opposite of nanocomposites based on LDPE). This is attributable to: (i) very low crystallinity in the ionomer films, and (ii) orientation of the clay platelets/tactoids in the plane of the film. The montmorillonite platelets are not perfectly circular, i.e., they have a major and a minor axis. During the film blowing process, the major axis would tend to get aligned in the machine direction (more so at a

lower BUR than at a higher BUR), and this would result in a higher modulus in the MD than the TD. In LDPE-organoclay composites, the level of organoclay exfoliation is not as great as that in the ionomer. As a result, the contribution of the orientation of the small aspect ratio filler particles towards the tensile modulus of the composite is more than negated by the contribution of the orientation of the crystal lamellae. On the other hand, in ionomer-organoclay nanocomposites, the polymer crstallinity is comparatively lower and the contribution of the orientation of the high aspect ratio clay particles dominates the tensile modulus values.

Another trend that emerges from Fig. 9.2 is that for LDPE based films, modulus increases as the film thickness decreases (increasing draw down ratio). This is true for the unfilled polymer and the nanocomposites. Films prepared from the ionomer or its nanocomposites do not reveal this trend (Fig. 9.3). Once again, this could be attributed to the differences in crystallinity between the two polymers and the consequent influence exerted by the orientation of the crystal lamellae. For LDPE, greater orientation of the crystallites in the plane of the film, resulting from the elongational flow-induced morphology generated during the film-blowing process, improves as the film thickness decreases. The insignificant effect of the film thickness on the tensile modulus of the ionomer based nanocomposites suggests that the orientation of the platelets in the ionomer is not much affected when the film is drawn down to a smaller thickness.

Tensile stress at break

Tensile stress at break of the blown films prepared from LDPE and its nanocomposites are presented in Fig. 9.4. Similar data for blown films prepared from the

Surlyn® ionomer are presented in Fig. 9.5. In general, the ionomer films display greater tensile stress at break compared to the LDPE films. The presence of clay does not appear to change the tensile stress at break (along MD or TD) of the blown films prepared from either polymer.

In most cases, the stress at break in the machine direction is greater than that in the transverse direction. The effects are more pronounced at a lower blow-up ratio, and for the 1 mil thick films. Generally, in LDPE blown films with the "row" structure, the MD stress at break tends to be higher than that along the TD [12]. Because this relates to the preferential orientation of the lamellar long axes perpendicular to the film MD, the differential in the break stress along the MD and TD is greater at lower BUR and for thinner films.

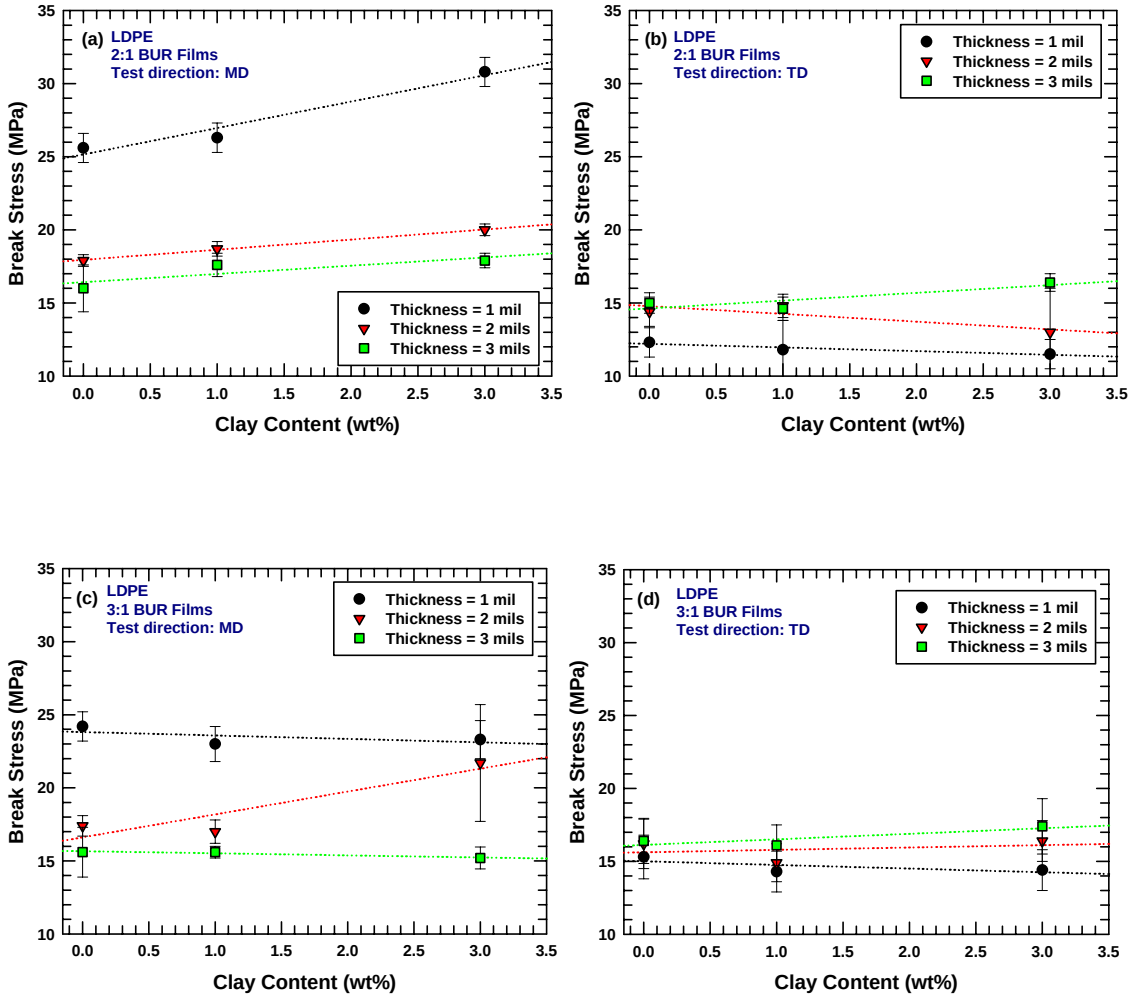

Figure 9.4 Tensile stress at break of blown-films prepared from LDPE and $M_2(HT)_2$-140 organoclay plotted as a function of the montmorillonite content: (a) films with 2:1 BUR tested along the machine direction, (b) films with 2:1 BUR tested along the transverse direction, (c) films with 3:1 BUR tested along the machine direction, (d) films with 3:1 BUR tested along the transverse direction. The X-axis has been extended beyond zero in all graphs for clarity. The dotted lines are trend lines (linear regression lines), and are included to serve as visual guides.

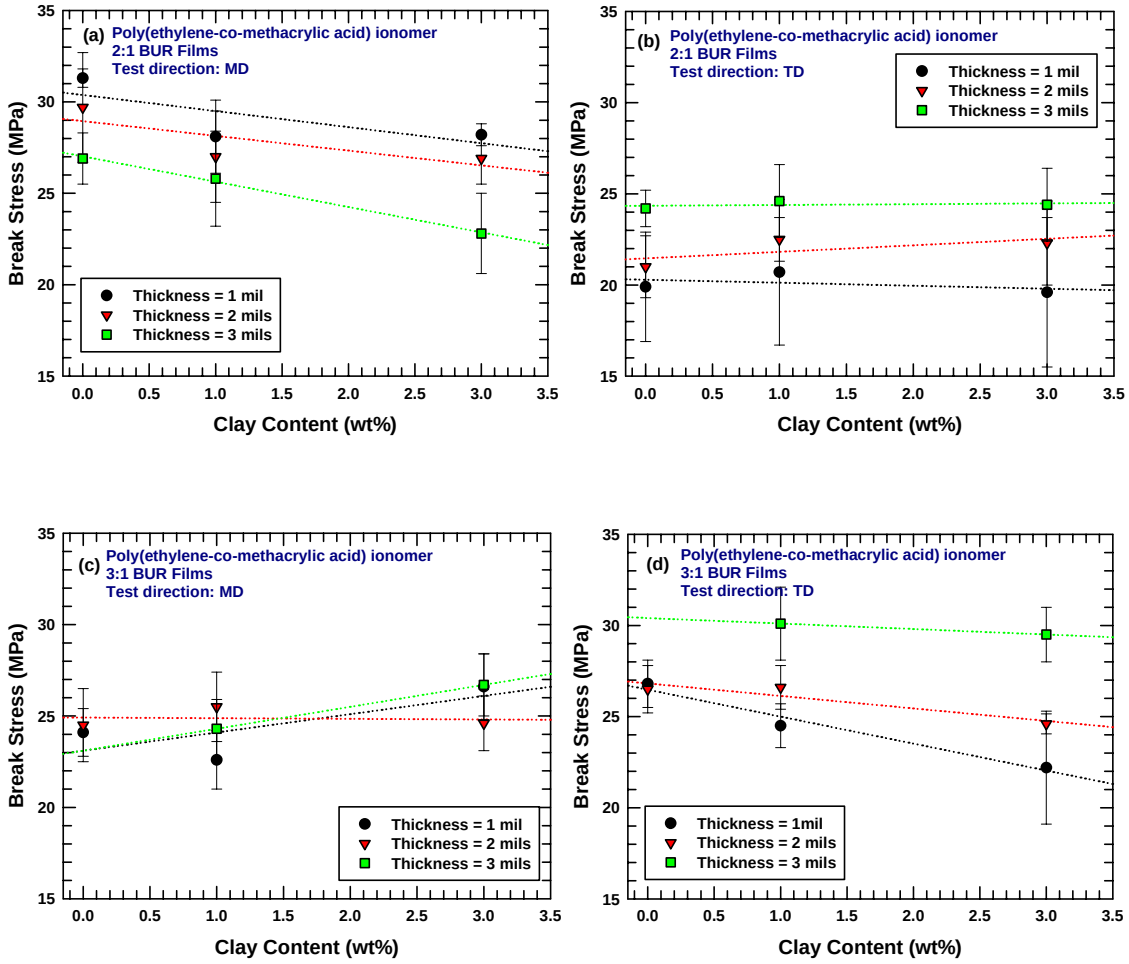

Figure 9.5 Tensile stress at break of blown-films prepared from Surlyn® ionomer and $M_2(HT)_2$-140 organoclay plotted as a function of the montmorillonite content: (a) films with 2:1 BUR tested along the machine direction, (b) films with 2:1 BUR tested along the transverse direction, (c) films with 3:1 BUR tested along the machine direction, (d) films with 3:1 BUR tested along the transverse direction. The X-axis has been extended beyond zero in all graphs for clarity. The dotted lines are trend lines (linear regression lines), and are included to serve as visual guides.

Tensile strain at break

Tensile strain at break of the blown films prepared from LDPE and its nanocomposites are presented in Fig. 9.6. Similar data for blown films prepared from the Surlyn® ionomer are presented in Fig. 9.7. It seems that, the presence of clay does not

affect the tensile strain at break (along MD or TD) of the blown films prepared from either polymer.

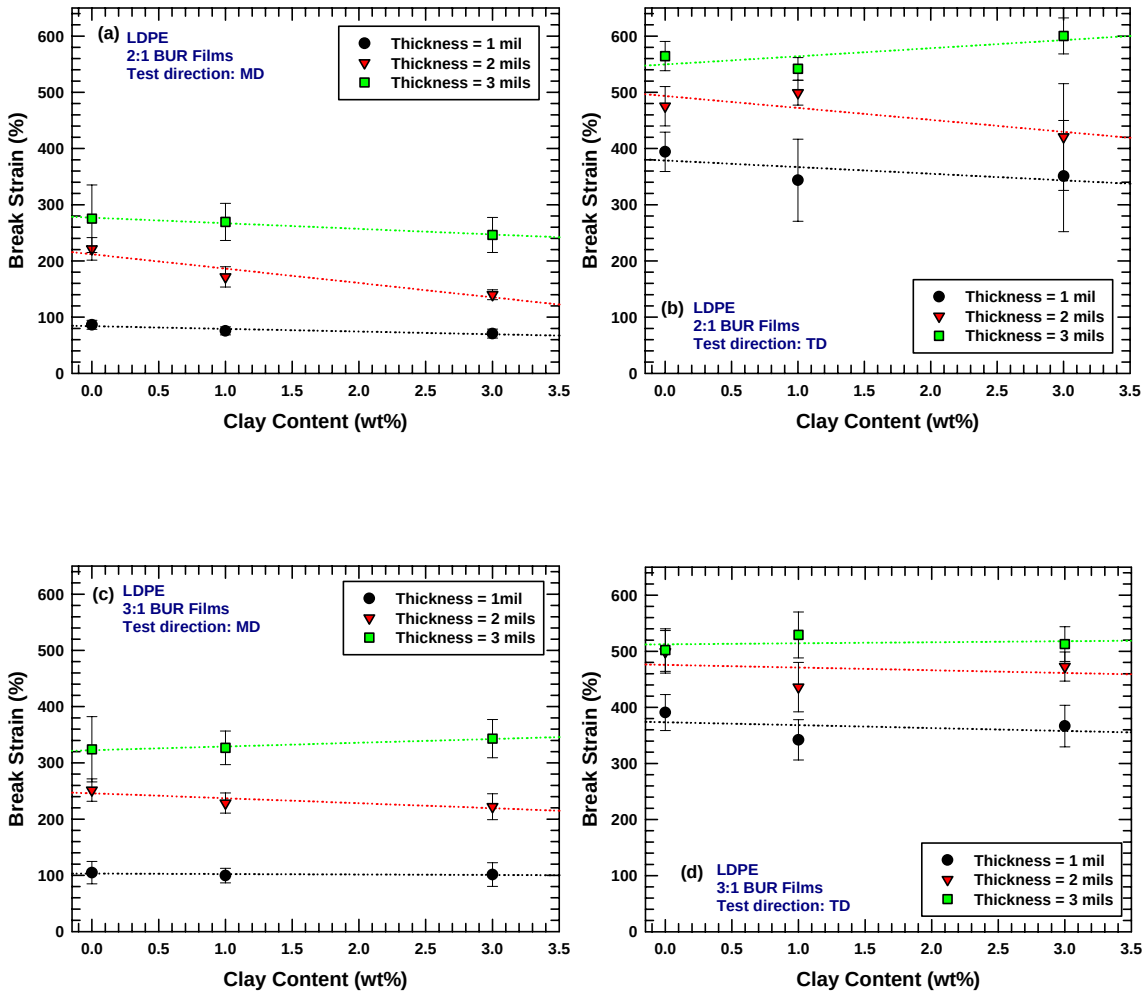

Figure 9.6 Tensile strain at break of blown-films prepared from LDPE and $M_2(HT)_2$-140 organoclay plotted as a function of the montmorillonite content: (a) films with 2:1 BUR tested along the machine direction, (b) films with 2:1 BUR tested along the transverse direction, (c) films with 3:1 BUR tested along the machine direction, (d) films with 3:1 BUR tested along the transverse direction. The X-axis has been extended beyond zero in all graphs for clarity. The dotted lines are trend lines (linear regression lines), and are included to serve as visual guides.

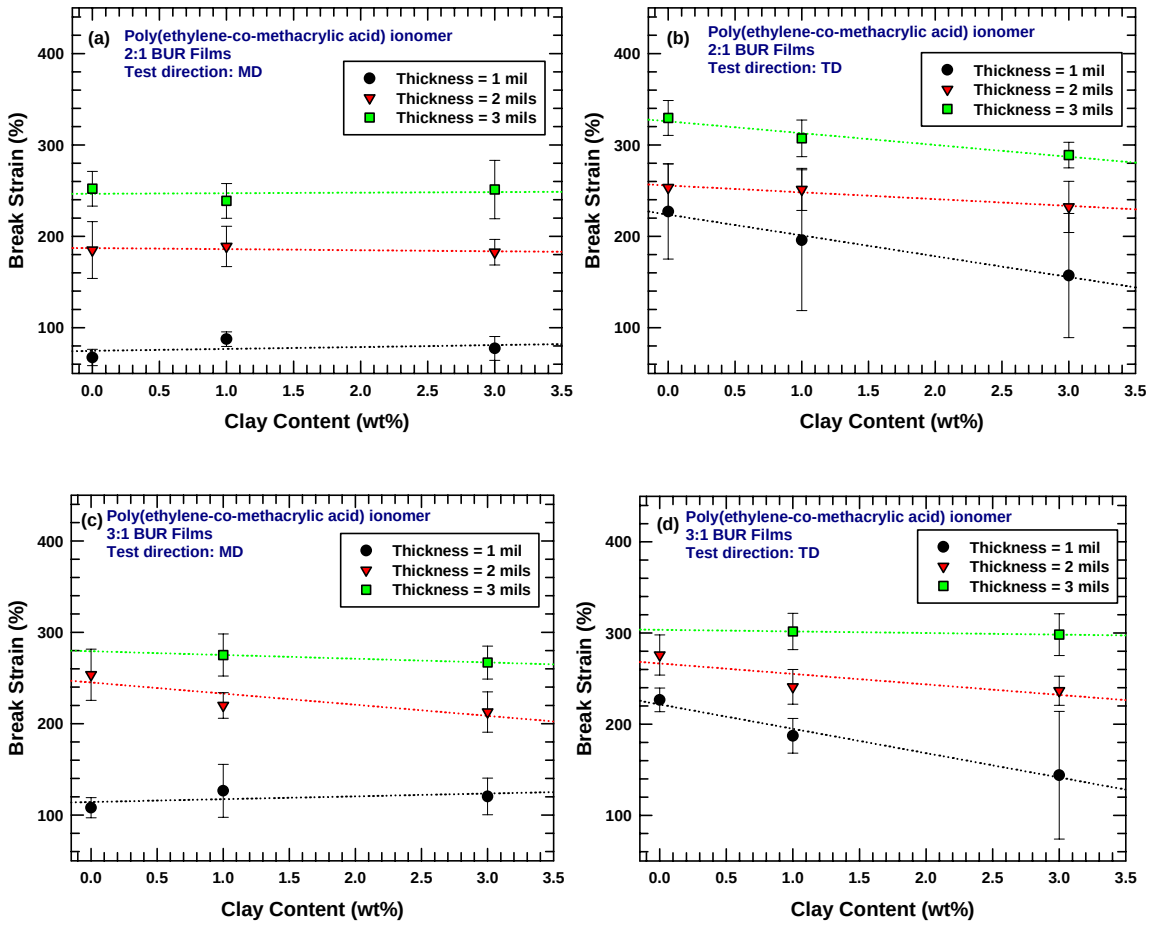

Figure 9.7 Tensile strain at break of blown-films prepared from Surlyn® ionomer and $M_2(HT)_2$-140 organoclay plotted as a function of the montmorillonite content: (a) films with 2:1 BUR tested along the machine direction, (b) films with 2:1 BUR tested along the transverse direction, (c) films with 3:1 BUR tested along the machine direction, (d) films with 3:1 BUR tested along the transverse direction. The X-axis has been extended beyond zero in all graphs for clarity. The dotted lines are trend lines (linear regression lines), and are included to serve as visual guides.

For LDPE and its nanocomposites, the strain at break in the transverse direction is higher than that in the machine direction. The ionomer and its nanocomposites also reveal a similar trend (to a smaller extent). As expected, in all cases the strain at break increases with an increase in the film thickness.

Puncture resistance

Puncture resistance, as measured by dart impact strength, of blown films prepared from LDPE and its nanocomposites are presented in Fig. 9.8. Similar data for blown films prepared from the Surlyn® ionomer are presented in Fig. 9.9. In general, films prepared from the ionomer and its nanocomposites have higher impact strength than corresponding films prepared from LDPE. The addition of clay lowers the dart impact strength of blown films of the two polymers. This may be due to inadequate adhesion between the clay platelets and the polymer.

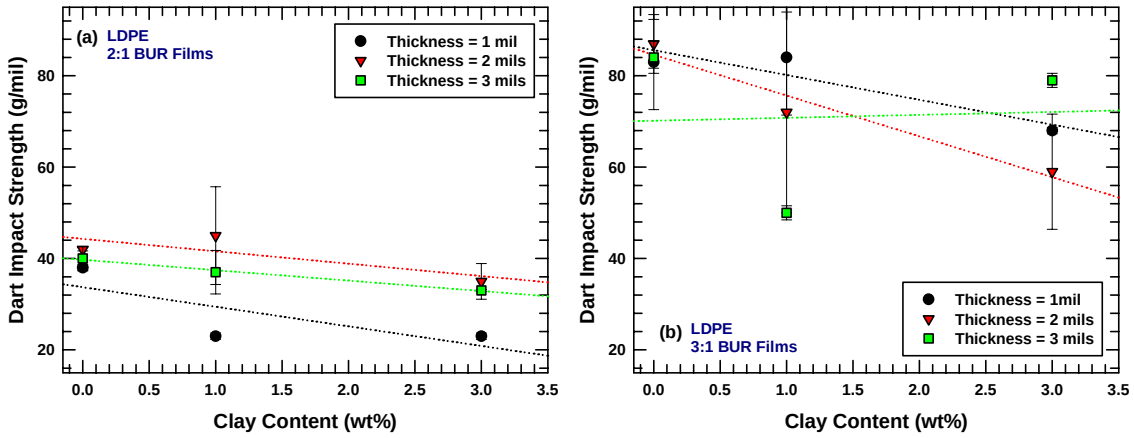

Figure 9.8 Dart impact strength of blown-films prepared from LDPE and $M_2(HT)_2$-140 organoclay plotted as a function of the montmorillonite content: (a) films with 2:1 BUR, (b) films with 3:1 BUR. The X-axis has been extended beyond zero in all graphs for clarity. The dotted lines are trend lines (linear regression lines), and are included to serve as visual guides.

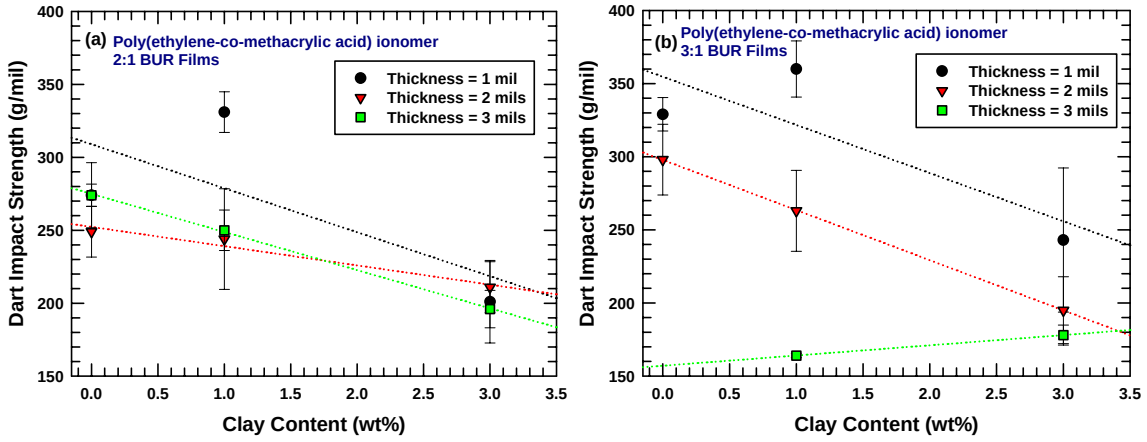

Figure 9.9 Dart impact strength of blown-films prepared from Surlyn® ionomer and $M_2(HT)_2$-140 organoclay plotted as a function of the montmorillonite content: (a) films with 2:1 BUR, (b) films with 3:1 BUR. The X-axis has been extended beyond zero in all graphs for clarity. The dotted lines are trend lines (linear regression lines), and are included to serve as visual guides.

For films prepared from LDPE and its nanocomposites, the dart impact strength for 3:1 BUR films is considerably greater than that of the 2:1 BUR films. Ionomer based films show similar trends but to a lesser extent. These observations could be a result of higher biaxial orientation of the crystallites/ clay platelets in the plane of the film when the BUR is increased from 2:1 to 3:1 [13].

Resistance to tear propagation

The tear resistance, measured along the machine direction and the transverse direction, for the blown films prepared from LDPE and its nanocomposites are presented in Fig. 9.10. Similar data for blown films prepared from the Surlyn® ionomer are presented in Fig. 9.11. One of the most noticeable observations is the difference between the tear strengths of the two polymers (and also their nanocomposites). The ionomer

films display poor tear resistance relative to LDPE films. Although, it is not completely clear as to what would lead to such a difference between the two systems, it could be a consequence of the difference in the crystallinity between the two polymers.

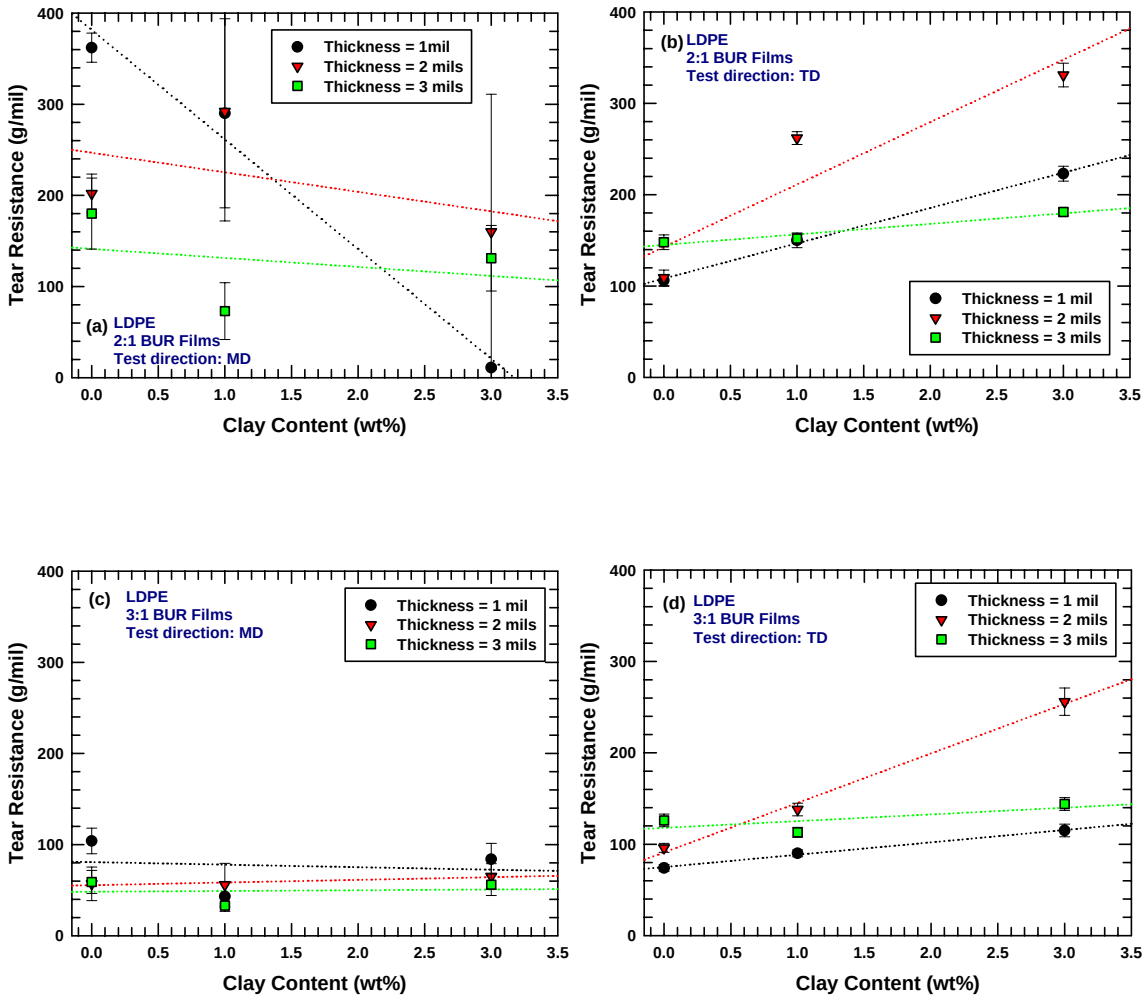

Figure 9.10 Tear strength of blown-films prepared from LDPE and $M_2(HT)_2$-140 organoclay plotted as a function of the montmorillonite content: (a) films with 2:1 BUR tested along the machine direction, (b) films with 2:1 BUR tested along the transverse direction, (c) films with 3:1 BUR tested along the machine direction, (d) films with 3:1 BUR tested along the transverse direction. The X-axis has been extended beyond zero in all graphs for clarity. The dotted lines are trend lines (linear regression lines), and are included to serve as visual guides.

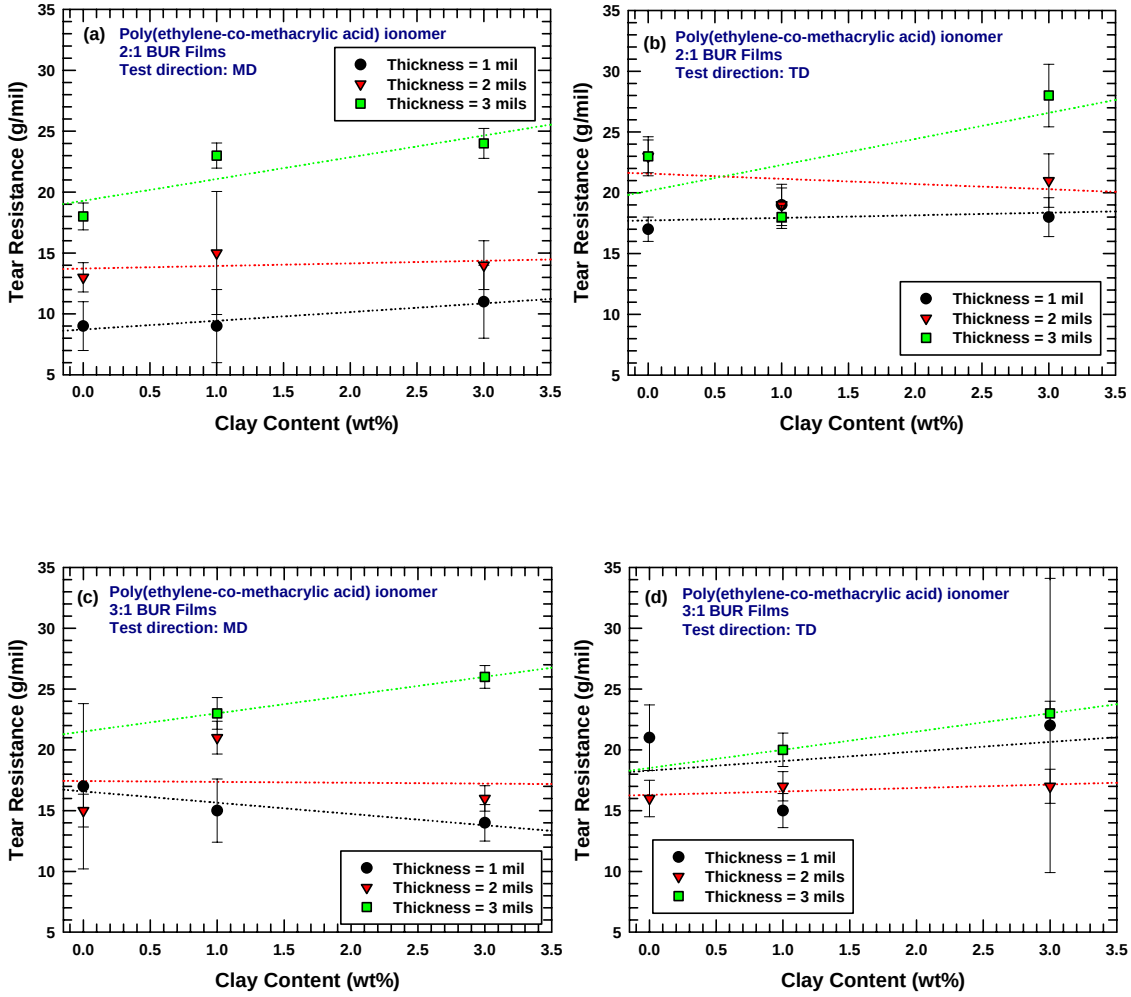

Figure 9.11 Tear strength of blown-films prepared from Surlyn® ionomer and $M_2(HT)_2$-140 organoclay plotted as a function of the montmorillonite content: (a) films with 2:1 BUR tested along the machine direction, (b) films with 2:1 BUR tested along the transverse direction, (c) films with 3:1 BUR tested along the machine direction, (d) films with 3:1 BUR tested along the transverse direction. The X-axis has been extended beyond zero in all graphs for clarity. The dotted lines are trend lines (linear regression lines), and are included to serve as visual guides.

For unfilled LDPE films, the tear resistance is always higher along the MD relative to TD. This difference is more magnified at 2:1 BUR than at 3:1 BUR. This is very likely due to the varying degrees of orientation of the lamellae within the plane of the film. Both MD and TD tear resistance values are higher at 2:1 BUR relative to 3:1 BUR. A deeper insight into the lamellar morphology is required to explain this observation. However, such an investigation is beyond the scope of this study. Nanocomposites prepared from LDPE exhibited similar trends as the unfilled polymer. As the clay content increases, MD tear decreases and TD tear increases. This effect is more dramatic at higher DDR (1 mil thick films) than at lower DDR.

In contrast, tear resistance of films prepared from the ionomer and its nanocomposites seems fairly insensitive to the clay content. There is not much difference between the tear resistance in the machine direction and transverse direction for these films.

Barrier properties

Steady-state gas permeation properties

The measured gas permeability coefficients for selected blown films prepared from nanocomposites of LDPE and Surlyn® 8945 ionomer are tabulated in Table 9.3. The films were carefully chosen such that the effects of clay content and film blowing conditions on the permeability of these membranes to O_2, N_2, and CO_2 gases could be distinctly explored. A comparison between the gas permeabilities of the two unfilled polymer films (film #3 vs. film #21, and film # 6 vs film #24) suggests that blown films prepared from the ionomer have better barrier properties than those prepared from LDPE.

As described earlier, the ionomer has lower crystallinity compared to LDPE, and it is well-known that polymers with lower crystallinity have higher permeability compared to highly crystalline polymers [14]. Thus, it appears that the two observations contradict each other. This disagreement could be explained based on the chemical composition of the two polymers. The unfilled ionomer contains cluster of sodium ions. Thus the polymer by itself could be considered to be a "metal nanocomposite". The metal ions are impermeable to gases, and, thus, improve the gas barrier properties of the ionomer.

Table 9.3 Gas permeability data of selected blown films evaluated in this study

	LDPE films			Permeability [Barrer]				Ionomer films			Permeability [Barrer]		
Film No.	MMT	BUR	Thickness (mil)	O_2	N_2	CO_2	Film No.	MMT	BUR	Thickness (mil)	O_2	N_2	CO_2
3	0	2:1	1	9.302	3.112	38.918	**21**	0	2:1	1	2.967	0.846	11.350
4	0	3:1	3	6.705	2.241	27.515							
5	0	3:1	2	6.348	2.171	27.357							
6	0	3:1	1	9.553	3.110	38.982	**24**	0	3:1	1	2.954	0.814	10.750
12	1	3:1	1	7.525 *0.788*	2.528 *0.813*	31.684 *0.813*	**30**	1	3:1	1	2.458 *0.832*	0.694 *0.852*	9.097 *0.846*
15	3	2:1	1	6.636 *0.713*	2.223 *0.714*	28.090 *0.722*	**33**	3	2:1	1	1.881 *0.634*	0.554 *0.655*	6.950 *0.612*
16	3	3:1	3	5.654 *0.843*	1.985 *0.886*	23.758 *0.863*							
17	3	3:1	2	5.318 *0.838*	1.788 *0.824*	22.485 *0.822*							
18	3	3:1	1	6.597 *0.691*	2.278 *0.732*	28.270 *0.725*	**36**	3	3:1	1	1.765 *0.597*	0.502 *0.616*	6.645 *0.618*

Italicized numbers are the permeabilities of the various gases in nanocomposite films relative to those in the corresponding unfilled polymer films (P/P_o)

The permeability of the two polymers and their nanocomposites was much greater to CO_2 than O_2, which in turn was higher than their permeability to N_2. The differences

between the permeability to various gases stem from the differences in diffusivity and solubility of the gas molecules in the polymer membrane.

Permeability coefficient, P = Diffusivity coefficient, D x Solubility coefficient, S

Diffusivity is governed by the size (critical volume) of a gas molecule. N_2 has a critical volume of 90 cm^3/mole compared to 74 cm^3/mole for O_2 and 94 cm^3/mole for CO_2. There is not a significant difference between the solubilities of N_2 and O_2 [15]. Hence, the membranes have a higher permeability to the oxygen gas compared to nitrogen gas. On the other hand, although the CO_2 molecule is larger than both oxygen and nitrogen, its solubility in the polymer membrane is significantly greater than that of the other two gases [15]. As a result, the polymer membranes have lower barrier resistance to CO_2 than O_2, and N_2.

Gas permeability decreases along with an increase in the organoclay content in both polymers. The relative permeabilities of the various gases in LDPE and ionomer nanocomposite films as a function of the montmorillonite content are presented in Fig. 9.12. As shown below, for a given polymer, at fixed montmorillonite content, there was not a significant difference between the relative permeabilities of the three gases.

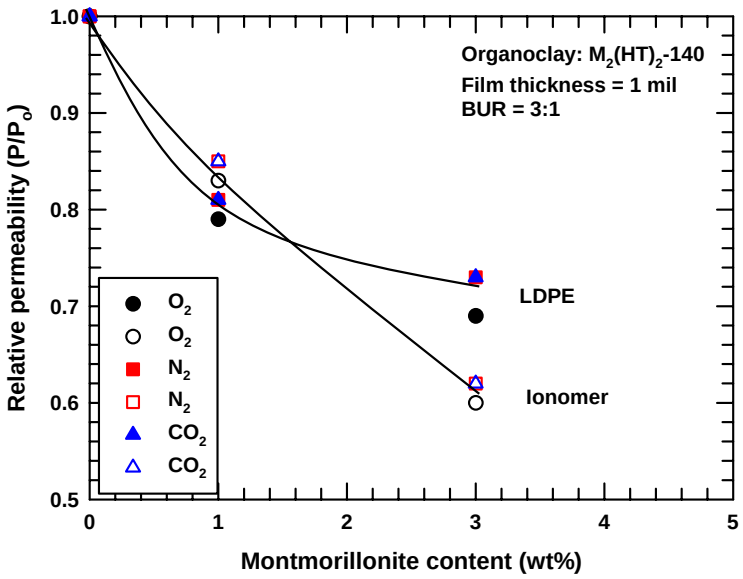

Figure 9.12 Relative permeability (P/P_o) plotted as a function of the montmorillonite content of the nanocomposite films prepared from (a) LDPE, and (b) Surlyn® 8945 ionomer.

The nanocomposite film containing 3 wt% MMT prepared from Surlyn® 8945 ionomer has superior barrier properties compared to corresponding film prepared from LDPE based nanocomposite. Similar trends were seen in blown films prepared using a 2:1 BUR (see Table 9.3). These observations could be attributed to the superior level of organoclay exfoliation achieved in the ionomer compared to LDPE (Chapter 4). However, it is surprising to note the marginally better barrier properties of the LDPE based nanocomposite film containing 1 wt% MMT compared to a similar film prepared from the ionomer based nanocomposite. A possible reason could be small differences in the montmorillonite content of the nanocomposites. As mention in Chapters, 4, 6, and 7, it is not possible to confirm the actual montmorillonite content in nanocomposites

prepared from ionomers using the incineration technique described in Chapter 2. If the montmorillonite content in the ionomer based nanocomposite is slightly lower than that of the LDPE based nanocomposite, it could lead to the anomaly described above.

The effect of the draw down ratio on the barrier properties of blown films prepared from nanocomposites based on LDPE is displayed in Fig. 9.13. It is clear that nanocomposite films with greater DDR have superior gas barrier properties (per unit thickness) compared to those with smaller DDR. This could be attributed to possible greater biaxial orientation of the platelets in the plane of the film during the preparation of thinner films (large DDR) compared to thicker films (small DDR).

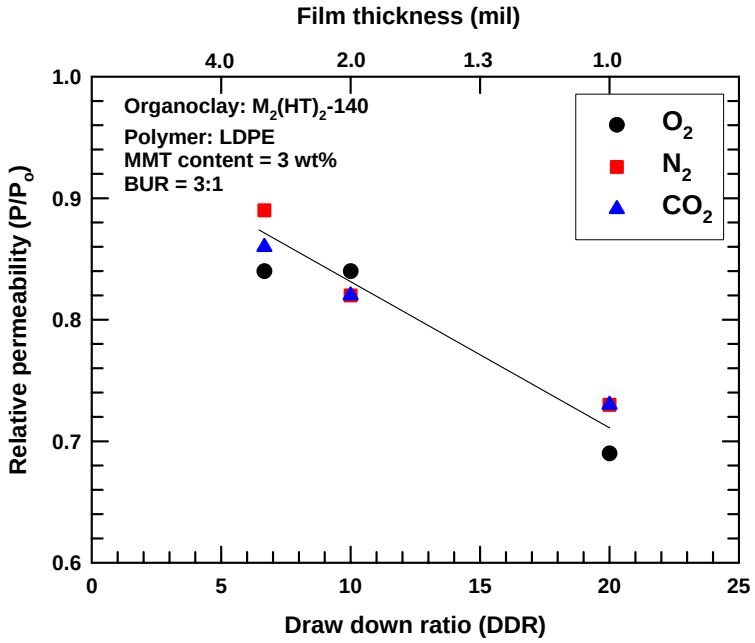

Figure 9.13. Effect of draw down ratio on the barrier properties of blown films prepared from nanocomposites based on LDPE

Comparison of steady-state permeation data with theoretical models

A number of theories have been proposed to correlate the gas permeability of composite membranes to the filler content and geometry [16-24]. In this study, we compare the experimental gas permeation data to that predicted by the Nielsen model [16], and the Cussler regular array model [17]. Both of these theories approximate the filler particles as platelets with finite width, *w*, and thickness, *t*, but infinite length. The mathematical form of these models is presented below:

Nielson model:

$$f^{-1} = \frac{P_0}{P}(1-\phi) = 1 + \alpha\phi / 2$$

Cussler regular array model :

$$f^{-1} = \frac{P_0}{P}(1-\phi) = 1 + (\alpha\phi)^2 / 4$$

Where,

α = particle aspect ratio = *l*/*t*

ø = volume fraction of the particles

f = tortuosity factor = D/D_o

D = gas diffusivity

D_o = gas diffusivity when ø = 0

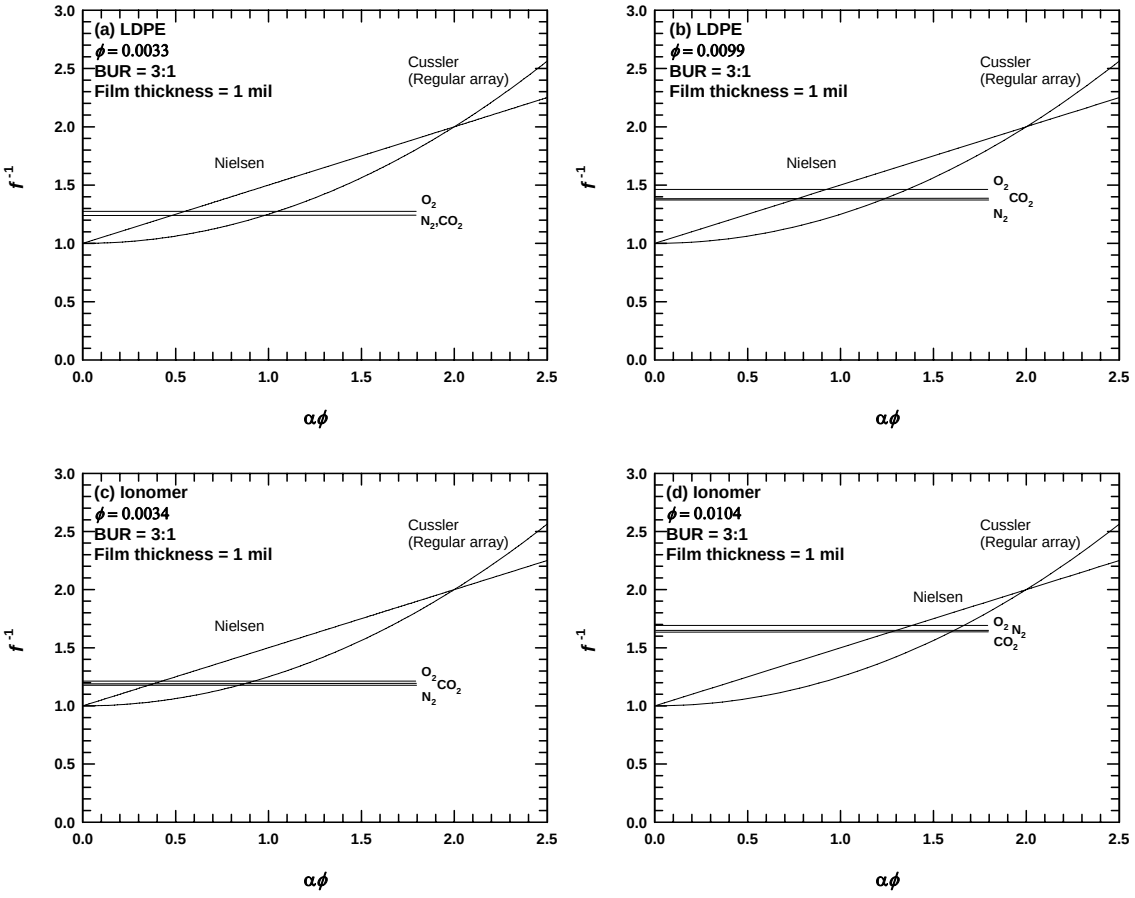

Figure 9.14 The reciprocal tortuosity factor predicted by two theories as a function of αø. Horizontal lines correspond to experimental values for each gas computed from permeability. Plot (a) is for LDPE nanocomposite with a montmorillonite content of ø = 0.0033, plot (b) is for LDPE nanocomposites with a montmorillonite content of ø = 0.0099, plot (c) is for the Surlyn ionomer nanocomposites with a montmorillonite content of ø = 0.0034, and plot (d) is for the Surlyn ionomer nanocomposite with a montmorillonite content of ø = 0.0104.

In Fig. 9.14, we plot the reciprocal quantity, f^{-1}, versus the product αø over the expected range for the two models. Horizontal lines correspond to the experimentally determined value f^{-1} for each gas in each composite membrane. From the known ø, we can determine what α each theory would require in order to predict f^{-1}. In Table 9.4 we show the range of α needed to describe the results for the three gases in each membrane. It is interesting to note that there is not a significant difference between the aspect ratios of the ionomer and LDPE based nanocomposites determined using model calculations. Also, the numbers are significantly larger than the filler aspect ratios of nanocomposites prepared from polyethylene, and Surlyn® 8945 ionomer determined by the particle analysis technique described in Chapters 5 and 6 [25, 26]. Such a discrepancy could be a result of the assumptions [16, 17] built into the permeability models, and the problems associated with the calculation of the particle aspect ratio from TEM micrographs as discussed in Chapter 5.

Table 9.4 Particle aspect ratio calculated by comparison of experimental permeation data with the two composite theories

Polymer	ϕ	**Aspect ratio α**	
		Nielsen	**Cussler (Regular)**
LDPE	0.0033	142 - 165	294 - 317
	0.0099	77 - 93	124 - 137
Ionomer	0.0034	110 - 121	254 - 267
	0.0104	122 - 133	153 - 160

CONCLUSIONS

Mechanical and barrier properties of blown films prepared from nanocomposites based on LDPE and a sodium ionomer of poly(ethylene-co-methacrylic acid) are presented here. The organoclay and processing conditions were carefully chosen to form nanocomposites with acceptable levels of exfoliation. All of films (prepared from unfilled polymer and their nanocomposites) had good clarity and smooth texture. In general, films prepared from nanocomposites based on the ionomer exhibited greater improvement in mechanical and barrier properties over unfilled polymer compared to similar films prepared from nanocomposites based on LDPE. This is due to the greater levels of organoclay exfoliation achieved in the ionomer compared to LDPE.

It was determined that it was possible to improve the stiffness (modulus) of blown LDPE and ionomer films by up to 50% by adding as little as 3 wt% MMT to the polymer without sacrificing much tear strength, puncture resistance or film extensibility. Mechanical properties of films prepared from LDPE and its nanocomposites were more sensitive to processing conditions than those prepared from the ionomer and its nanocomposites. This is because LDPE is more crystalline than the ionomer, and the orientation of the crystal lamellae also plays a role (besides that played by the clay platelets) in the determination of the mechanical properties.

The nanocomposites also offered significant improvements in barrier properties compared to the corresponding unfilled polymer. Gas permeability could be reduced by up to 40% by adding 3 wt% MMT to the polymers. It should be noted, that the permeability of these nanocomposites is not as low as that of current commercial polymers, viz., poly(ethylene vinyl alcohol) [14] used for barrier applications in meat and

fresh food packaging; nevertheless, such nanocomposites could be useful in several niche applications, like the packaging of cereals and cookies/crackers, where moderate improvements in barrier properties are sufficient.

REFERENCES

[1] Hunter DL, *Personal Communication*.

[2] Chavarria F, Paul DR. Under preparation

[3] Koros WJ, Paul DR, Rocha AA. Journal of Polymer Science, Polymer Physics Edition 1976;14(4):687-702.

[4] Zhong Y, De Kee D. Polymer Engineering and Science 2005;45(4):469-77.

[5] Krishnamoorti R, Ren J, Silva AS. J Chem Phys 2001;114(11):4968-73.

[6] Krishnaswamy RK, *Personal communication*.

[7] Shah RK, Hunter DL, Paul DR. Polymer 2005;46(8):2646-62.

[8] Hotta S, Paul DR. Polymer 2004;45(22):7639-54.

[9] Keller A, Kolnaar HWH. Materials Science and Technology 1997;18(Processing of Polymers):189-268.

[10] Krishnaswamy RK. Journal of Polymer Science, Part B: Polymer Physics 2000;38(1):182-93.

[11] Pazur RJ, Purd'homme RE. Macromolecules 1996;29(1):119-28.

[12] Krishnaswamy RK, Lamborn MJ. Polymer Engineering and Science 2000;40(11):2385-96.

[13] Krishnaswamy RK, Sukhadia AM. Journal of Plastic Film & Sheeting 2005;21(2):145-58.

[14] Brandrup J, Immergut EH, Editors. *Polymer Handbook, Fourth Edition*. 1998. 1920 pp.

[15] Ghosal K, Freeman BD. Polymers for Advanced Technologies 1994;5(11):673-97.

[16] Nielsen LE. J Macromol Sci, Part A 1967;1(5):929-42.

[17] Lape NK, Nuxoll EE, Cussler EL. Journal of Membrane Science 2004;236(1-2):29-37.

[18] Perry D, Ward WJ, Cussler EL. Journal of Membrane Science 1989;44(2-3):305-11.

[19] Lape NK, Yang C, Cussler EL. Journal of Membrane Science 2002;209(1):271-82.

[20] Yang C, Smyrl WH, Cussler EL. Journal of Membrane Science 2004;231(1-2):1-12.

[21] Falla WR, Mulski M, Cussler EL. Journal of Membrane Science 1996;119(1):129-38.

[22] Bharadwaj RK. Macromolecules 2001;34(26):9189-92.

[23] Gusev AA, Lusti HR. Advanced Materials (Weinheim, Germany) 2001;13(21):1641-3.

[24] Fredrickson GH, Bicerano J. Journal of Chemical Physics 1999;110(4):2181-8.

[25] Shah RK, Cui L, Williams KL, Bernard B, Paul DR. Accepted by Journal of Applied Polymer Science

[26] Shah RK, Paul DR. Submitted for publication in Macromolecules

Chapter 10: Conclusions and recommendations

Structure property relationships in nanocomposites prepared by melt mixing polymers with organically modified montmorillonite clays were examined in this study. In the initial stages, efforts were concentrated on nylon 6 based nanocomposites; however, later on the focus was shifted to nanocomposites prepared from commercially more attractive polymers like polyethylene. The key to enhanced performance improvements in such nanocomposites lies in the delamination and uniform distribution of the 1-nm thick aluminosilicate platelets in the polymer matrix. Although, several factors play a role in organoclay exfoliation, it is believed to be largely dependent on a complex array of interactions between the polymer matrix and the organoclay. In this regard, nylon 6 and polyethylene represent two opposite extremes of the gamut of polymers. While nylon 6 is one of the few polymers that readily exfoliate montmorillonite based organoclays, organoclay exfoliation is extremely difficult in a non-polar polymer like polyethylene due to the lack of favorable interactions with the polar aluminosilicate clays. Hence, a major part of this investigation was dedicated to improving organoclay exfoliation in polyethylene, and exploring the effects of material chemistry and processing conditions on the morphology and properties of such composites. The main conclusions of this study are summarized below along with recommendations for future work.

CONCLUSIONS

Four different strategies were employed to improve the polarity of the polyethylene matrix, and, thus, its interactions with the organoclay: (i) grafting of maleic anhydride to the polyethylene backbone, (ii) copolymerizing polyethylene monomer with a polar methacrylic acid monomer, (iii) neutralizing some of the acid groups of such ethylene/methacrylic acid copolymers to form ionomers, and (iv) surface modification of the polyethylene particles by subjecting them to a fluoro-oxidation process. All of these modifications helped improve the exfoliation and dispersion of organoclays in polyethylene (Chapters 4 through 6). It should be noted that although some modifications resulted in better exfoliation than others, none of the nanocomposites exhibited exfoliation levels similar to those seen in nylon 6; nevertheless, these nanocomposites offer promising improvements in performance over those of composites prepared from unmodified polyethylene, and may be interesting for several niche applications.

The relationship between the structure of the organic modifier used for preparing the organoclay, and the morphology and properties of nanocomposites was also explored for nanocomposites prepared from polyethylene and the various modifications of polyethylene. It was clear that the interactions between the polyolefin and the organoclay, and, thus, the extent of exfoliation in the polymer are heavily dependent upon the structure of the surfactant [1, 2]. For nanocomposites prepared from ionomers of poly(ethylene-co-methacrylic acid), four distinct surfactant structural effects have been identified that lead to improved levels of exfoliation and higher stiffness: (1) higher number of alkyl tails on the amine rather than one, (2) longer alkyl tails instead of shorter

ones, (3) 2-hydroxy-ethyl groups as opposed to methyl groups on the ammonium ion, and (4) excess amount of the amine surfactant on the clay instead of an equivalent amount. Similar trends were seen in nanocomposites prepared from low density polyethylene, and ethylene/methacrylic acid copolymers, i.e., organoclays with higher number of alkyl tails were exfoliated much better than organoclays with a single alkyl tail. These trends are opposite from those for nylon 6 based nanocomposites [3]. It seems nylon 6 has a higher affinity for the silicate surface than does the polyolefin while the latter is less repelled by the alkyl tails than the polyamide. Hence, surfactant structural aspects that lead to more shielding of the silicate surface or increased alkyl material leads to improved exfoliation in these polymers.

The degradation of the alkyl ammonium surfactants used to prepare the organoclays was examined using WAXS and thermogravimetric analyses, and its effect on nanocomposite mechanical properties was evaluated using stress-strain analysis. Since polyethylene has a low melting point, it was possible to conduct this examination over a wide range of temperatures (150 °C to 240 °C). Results of WAXS analysis of nanocomposites prepared from LDPE suggest that the bulk of the surfactant loss from the organoclay galleries occurs between 180 °C to 200 °C. The relative modulus (E/E_m) of LDPE- $M_2(HT)_2$-95 nanocomposites dropped steadily as the processing temperature increased beyond 165 °C. It appears that depletion of organic material from the organoclay galleries by degradation and the resulting reduction in the interplatelet distances restricts the ability of LDPE to exfoliate the $M_2(HT)_2$-95 organoclay. Thermogravimetric analysis of $M_3(HT)_1$, $M_2(HT)_2$-95 and $M_1(C_{16})_3$ organoclays suggest that organoclays based on surfactants with multiple alkyl tails have greater thermal

stability than those based on surfactants with a single alkyl tail. A comparison between the mass of surfactant lost during melt processing of nanocomposites, and during thermogravimetric analysis of organoclays (in the absence of polymer) indicated a greater mass loss in the former compared to the latter. This could be attributed to the high solubility of the degradation products (predominantly α-olefins) in the polyethylene matrix, thus facilitating an easier removal of these products from the organoclay by extrusion as compared to TGA where the degradation products leave by evaporation.

Once the surfactant structure and processing conditions were optimized, blown films were prepared from LDPE and a sodium ionomer of poly(ethylene-co-methacrylic acid) under a variety of conditions to determine the effect of platelet concentration, exfoliation, and orientation on film performance. All of the films had good clarity and smooth texture. In general, films prepared from nanocomposites based on the ionomer exhibited greater improvements in mechanical and barrier properties over unfilled polymer compared to similar films prepared from nanocomposites based on LDPE. This is due to the greater exfoliation achieved in the ionomer compared to LDPE. In some nanocomposites prepared from the ionomer, the stiffness was improved by as much as 50% by adding as little as 3 wt% MMT. The same clay concentration also resulted in a reduction of up to 40% in gas permeability and 50% in moisture permeability. As mentioned earlier, although, these improvements in barrier properties seem impressive, the permeability of these nanocomposites is still significantly higher than that of current commercial polymers, viz., poly(ethylene-vinyl alcohol), EVOH, used for enhancing the barrier properties in meat and fresh food packaging [4]; nevertheless, such nanocomposites could be useful in several specific applications, where moderate

improvements in barrier properties are sufficient. This work also paves the way for additional research work to further enhance the barrier properties of the current barrier materials like EVOH by melt mixing them with organoclays.

RECOMMENDATIONS

Modifications of polyethylene

As mentioned above, the four different matrix modifications employed to improve polyethylene-organoclay interactions resulted in a significant improvement in organoclay exfoliation. The results are promising and lead into a number of technically and commercially significant directions. Few of the obvious questions that emerge from the above study are that, what is the correlation between the improvements in exfoliation / properties, and the level of modification? What are the limits on the level of such modifications, i.e., what are the technical and economic constraints? To what extent do such modifications affect the melt rheology, crystallinity, and other properties of such polymers? As mentioned in Chapter 6, one of the important goals is to use such modified polymers as compatibilizers to prepare polyethylene nanocomposites on a commercial scale. From a technical standpoint this requires the miscibility of such polymers in unmodified polyethylene. If this miscibility exists, then highly concentrated masterbatches, with high levels of exfoliation, could be prepared from such modified polyethylenes and subsequently diluted down with unmodified polyethylene (while preserving exfoliation). On the other hand, if such miscibility does not exist, then the resulting composites will exhibit a two-phase morphology comprising of domains of the "compatibilizer" (containing exfoliated platelets) in the macro-phase, polyethylene. Such

composites would be of very limited utility. Hence, although it would be interesting to map out the effect of the level of modification (maleic anhydride content, fluoro-oxygenation treatment, etc.) on organoclay exfoliation, it would be necessary to test the miscibility of all such modified polymers with polyethylene.

Another logical question that arises from this work is that, are there any other chemical methods by which polyethylene could be made more compatible with organoclays? Copolymerizing ethylene with vinyl acetate (EVA copolymers) offers an interesting option. Although, a significant amount of work has been done in EVA-organoclay nanocomposites [5-9], it would be interesting to compare the levels of exfoliation achieved in such nanocomposites with that achieved in the polymers evaluated in this study.

Organoclay structure

As described above, polyethylene exfoliates organoclays with multiple alkyl tails much more efficiently than organoclays with a single alkyl tail. This trend is the opposite of that for nylon 6 based nanocomposites [3]. The rationale presented for this discrepancy is that nylon 6 is more polar than polyethylene, and so has a higher affinity for the polar surface of the aluminosilicate clay than the aliphatic alkyl tail; on the other hand polyethylene has a higher affinity for the alkyl tails compared to the polar clay, and so surfactants with multiple alkyl tails which offer greater alkyl-polymer interactions result in better exfoliation. It is interesting to note that, although, all grades of modified polyethylene examined in this study (maleic anhydride grafted polyethylene, ethylene-methacrylic acid copolymers, and their ionomers) increased the polarity of the base

polyethylene, they displayed trends similar to polyethylene in this regard. As a matter of fact, in the study examining the effect of organoclay structure on the morphology of nanocomposites prepared from the sodium ionomer (Chapter 7) all of the trends are opposite of those for nylon 6 [10]. This raises an interesting question: if we raise the polarity of polyethylene beyond a certain critical level, would these trends get reversed (be more nylon-like)? If yes, what is that level? If no, what other factors play a role in the determination of the optimum interactions between the organoclay and a polymer. Some other studies from this lab have reported anomalous behavior of the hydroxy-ethyl based organoclay ($(HE)_2M_1T_1$, Cloisite® 30B) in this regard [11, 12]. The interactions between the hydroxyl group and the clay are suspected to be responsible for such behavior.

The eventual goal is the design of a mathematical model that takes into consideration most of the chemical and thermodynamic interactions between a polymer and an organoclay, and, thus, help determine the ideal organoclay (surfactant treatment) for use with any particular polymer.

Processability

During the course of this study, it was determined that it is best to melt process these nanocomposites at temperatures lower than 180 °C to minimize the negative effects resulting from the degradation of the quaternary ammonium surfactants (Chapter 8). However, most polymers have melting points above 180 °C, and so it is not possible to implement this recommendation. Even in the case of polyethylene, in order to maintain an acceptable throughput rate, the normal processing temperature ranges from 180 °C to

240 °C (depending upon the melt viscosity). In such a case, the use of alternative surfactants based on imidazolium [13-17] or phosphonium [18-20] should be explored.

The design of the screw is equally critical in the formation of well-exfoliated nanocomposites. Dennis et al. [21] reported that the screw design and the changes in extruder residence time, back mixing, and shear intensity associated with it could significantly affect the delamination and dispersion of organoclay in nylon 6. A similar study for polyethylene based nanocomposites is warranted.

Morphology of the base (unmodified) polyethylene

Seemingly insignificant structural variations in polymers tend to affect their exfoliation efficiency [22-24]. As described in Chapter 3, and in previous research [22], high molecular weight grades of nylon 6 tend to exfoliate organoclays more efficiently than low molecular weight grades of nylon 6. The concentration of end groups (acid vs. amine) also affects the morphology and mechanical properties of the nanocomposites formed from nylon 6 [24]. Polyethylene, although, chemically simpler than nylon 6, is morphologically much more diverse than the polyamide. Besides differences in molecular weight and polydispersity, there could be a number of variations associated with the side chain branching, such as, the extent of side chain branching and the type of side chain branching i.e., short chain branching (SCB) vs. long chain branching (LCB). Even in polyethylene with SCB, differences exist based upon the type of the SCB (1-butene, 1-hexene, 1-octene, etc.) In addition to these, the distribution of branching across the molecular weight distribution could also result in differences in morphology, i.e., two polymers might have the same type and amount of side chain branching, however, in one

polymer, the branching is mostly on the high molecular weight chains, while in the other, branching is mostly on the low molecular weight chains. Carefully designed experiments to explore the effects of these aspects of molecular architecture on the organoclay exfoliation efficiency of polyethylene could prove useful as well as insightful.

REFERENCES

[1] Shah RK, Hunter DL, Paul DR. Polymer 2005;46(8):2646-62.

[2] Hotta S, Paul DR. Polymer 2004;45(22):7639-54.

[3] Fornes TD, Hunter DL, Paul DR. Macromolecules 2004;37(5):1793-8.

[4] Brandrup J, Immergut EH, Editors. *Polymer Handbook, Fourth Edition*. 1998. 1920 pp.

[5] Cser F, Bhattacharya SN. Journal of Applied Polymer Science 2003;90(11):3026-31.

[6] Zhang Wa, Chen D, Zhao Q, Fang Ye. Polymer 2003;44(26):7953-61.

[7] Tang Y, Hu Y, Wang J, Zong R, Gui Z, Chen Z, Zhuang Y, Fan W. Journal of Applied Polymer Science 2004;91(4):2416-21.

[8] La Mantia FP, Lo Verso S, Dintcheva NT. Macromolecular Materials and Engineering 2002;287(12):909-14.

[9] Alexandre M, Beyer G, Henrist C, Cloots R, Rulmont A, Jerome R, Dubois P. Macromolecular Rapid Communications 2001;22(8):643-6.

[10] Fornes TD, Yoon PJ, Hunter DL, Keskkula H, Paul DR. Polymer 2002;43(22):5915-33.

[11] Paul DR, Zeng QH, Yu AB, Lu GQ. Journal of Colloid and Interface Science 2005;292(2):462-8.

[12] Chavarria F, Paul DR. Under preparation

[13] Awad WH, Gilman JW, Nyden M, Harris RH, Sutto TE, Callahan J, Trulove PC, DeLong HC, Fox DM. Thermochimica Acta 2004;409(1):3-11.

[14] Bottino FA, Fabbri E, Fragala IL, Malandrino G, Orestano A, Pilati F, Pollicino A. Macromolecular Rapid Communications 2003;24(18):1079-84.

[15] Davis CH, Mathias LJ, Gilman JW, Schiraldi DA, Shields JR, Trulove P, Sutto TE, Delong HC. Journal of Polymer Science, Part B: Polymer Physics 2002;40(23):2661-6.

[16] Gilman JW, Awad WH, Davis RD, Shields J, Harris RH, Jr., Davis C, Morgan AB, Sutto TE, Callahan J, Trulove PC, DeLong HC. Chemistry of Materials 2002;14(9):3776-85.

[17] Wang ZM, Chung TC, Gilman JW, Manias E. Journal of Polymer Science, Part B: Polymer Physics 2003;41(24):3173-87.

[18] Zhu J, Morgan AB, Lamelas FJ, Wilkie CA. Chemistry of Materials 2001;13(10):3774-80.

[19] Kim MH, Park CI, Choi WM, Lee JW, Lim JG, Park OO, Kim JM. Journal of Applied Polymer Science 2004;92(4):2144-50.

[20] Maiti P, Yamada K, Okamoto M, Ueda K, Okamoto K. Chemistry of Materials 2002;14(11):4654-61.

[21] Dennis HR, Hunter DL, Chang D, Kim S, White JL, Cho JW, Paul DR. Polymer 2001;42(23):9513-22.

[22] Fornes TD, Yoon PJ, Keskkula H, Paul DR. Polymer 2001;42(25):9929-40.

[23] Fornes TD, Paul DR. Macromolecules 2004;37(20):7698-709.

[24] Fornes TD. Ph.D. Thesis, The University of Texas at Austin, 2003.

Bibliography

Alexandre M, Beyer G, Henrist C, Cloots R, Rulmont A, Jerome R, Dubois P. Macromolecular Rapid Communications 2001;22(8):643-6.

Alexandre M, Dubois P. Mater Sci Eng, R 2000;R28(1-2):1-63.

Alvero R, Alba MD, Castro MA, Trillo JM. Journal of Physical Chemistry 1994;98(32):7848-53.

Awad WH, Gilman JW, Nyden M, Harris RH, Sutto TE, Callahan J, Trulove PC, DeLong HC, Fox DM. Thermochimica Acta 2004;409(1):3-11.

Barber GD, Bellman SP, Moore RB. Annual Technical Conference - Society of Plastics Engineers 2003;61st(Vol. 2):1369-73.

Barber GD, Calhoun BH, Moore RB. Polymer 2005;46(17):6706-14.

Barber GD, Carter CM, Moore RB. Annual Technical Conference - Society of Plastics Engineers 2000;58th(Vol. 3):3763-7.

Barber GD, Moore RB. Polymeric Materials Science and Engineering 2000;82:241-2.

Bharadwaj RK. Macromolecules 2001;34(26):9189-92.

Bottino FA, Fabbri E, Fragala IL, Malandrino G, Orestano A, Pilati F, Pollicino A. Macromolecular Rapid Communications 2003;24(18):1079-84.

Brandrup J, Immergut EH, Editors. *Polymer Handbook, Fourth Edition*. 1998. 1920 pp.

Calvet R, Prost R. Clays and Clay Minerals, Proceedings of the Conference 1971;19(3):187-91.

Carrado KA, Xu L. Chem Mater 1998;10(5):1440-5.

Chavarria F, Paul DR. Polymer 2004;45(25):8501-15.

Chisholm BJ, Moore RB, Barber G, Khouri F, Hempstead A, Larsen M, Olson E, Kelley J, Balch G, Caraher J. Macromolecules 2002;35(14):5508-16.

Christiani BR, Maxfield M. United States Patent 5747560; 1998. [Assigned to Allied Signal]

Cser F, Bhattacharya SN. Journal of Applied Polymer Science 2003;90(11):3026-31.

Davis CH, Mathias LJ, Gilman JW, Schiraldi DA, Shields JR, Trulove P, Sutto TE, Delong HC. Journal of Polymer Science, Part B: Polymer Physics 2002;40(23):2661-6.

Davis R, Gilman J, VanderHart D. Polym Degrad Stab 2003;79:111-21.

Delozier DM, Orwoll RA, Cahoon JF, Johnston NJ, Smith JG, Connell JW. Polymer 2002;43(3):813-22.

Dennis HR, Hunter DL, Chang D, Kim S, White JL, Cho JW, Paul DR. Plast Eng 2001;57(1):56-60.

Dennis HR, Hunter DL, Chang D, Kim S, White JL, Cho JW, Paul DR. Polymer 2001;42(23):9513-22.

Ding R-d, Newell C. US Patent 6,861,481; 2005. [Assigned to Solvay Engineered Polymers, Inc. (Grand Prairie, TX)]

Editors. Modern Plastics 2005;(September 2005)

Emmerich K, Madsen FT, Kahr G. Clays and Clay Minerals 1999;47(5):591-604.

Emmerich K, Plotze M, Kahr G. Applied Clay Science 2001;19(1-6):143-54.

Falla WR, Mulski M, Cussler EL. Journal of Membrane Science 1996;119(1):129-38.

Fornes TD. Ph.D. Thesis, The University of Texas at Austin, 2003.

Fornes TD, Hunter DL, Paul DR. Macromolecules 2004;37(5):1793-8.

Fornes TD, Paul DR. Polymer 2003;44(17):4993-5013.

Fornes TD, Paul DR. Macromolecules 2004;37(20):7698-709.

Fornes TD, Yoon PJ, Hunter DL, Keskkula H, Paul DR. Polymer 2002;43(22):5915-33.

Fornes TD, Yoon PJ, Keskkula H, Paul DR. Polymer 2001;42(25):9929-40.

Fornes TD, Yoon PJ, Keskkula H, Paul DR. Polymer 2002;43(7):2121-2.

Fornes TD, Yoon PJ, Paul DR. Polymer 2003;44(24):7545-56.

Fornes TD, Yoon PJ, Paul DR. Polymer 2003;44(24):7545-56.

Fredrickson GH, Bicerano J. Journal of Chemical Physics 1999;110(4):2181-8.

Garces JM, Moll DJ, Bicerano J, Fibiger R, McLeod DG. Adv Mater (Weinheim, Ger) 2000;12(23):1835-9.

Gelfer M, Burger C, Fadeev A, Sics I, Chu B, Hsiao BS, Heintz A, Kojo K, Hsu SL, Si M, Rafailovich M. Langmuir 2004;20(9):3746-58.

Ghosal K, Freeman BD. Polymers for Advanced Technologies 1994;5(11):673-97.

Gilman JW. Appl Clay Sci 1999;15(1-2):31-49.

Gilman JW, Awad WH, Davis RD, Shields J, Harris RH, Jr., Davis C, Morgan AB, Sutto TE, Callahan J, Trulove PC, DeLong HC. Chemistry of Materials 2002;14(9):3776-85.

Gloaguen JM, Lefebvre JM. Polymer 2001;42(13):5841-7.

Gregar KC, Winans RE, Botto RE. US Patent 5308808; 1994. [Assigned to (United States Dept. of Energy, USA).]

Gu A, Kuo S-W, Chang F-C. J Appl Polym Sci 2001;79(10):1902-10.

Gusev AA, Lusti HR. Advanced Materials (Weinheim, Germany) 2001;13(21):1641-3.

Halpin JC, Finlayson KM, Ashton JE. *Primer on composite materials analysis*. 2nd , rev. / ed. 1992, Lancaster, Pa.: Technomic Pub. Co. xi, 227.

Halpin JC, Kardos JL. Polymer Engineering and Science 1976;16(5):344-52.

Hasegawa N, Kawakado M, Usuki A, Okada A. JP Patent 97-152854; 1998. [Assigned to (Toyota Central Research and Development Laboratories, Inc., Japan).]

Hasegawa N, Kawasumi M, Kato M, Usuki A, Okada A. J Appl Polym Sci 1998;67(1):87-92.

Hasegawa N, Okamoto H, Kawasumi M, Kato M, Tsukigase A, Usuki A. Macromol Mater Eng 2000;280(281):76-9.

Haynes AR, Coates PD. Journal of Materials Science 1996;31(7):1843-55.

Hofmann U, Klemen R. Z anorg Chem 1950;262:95-9.

Hotta S, Paul DR. Polymer 2004;45(22):7639-54.

Huang J-C, Zhu Z-k, Yin J, Qian X-f, Sun Y-Y. Polymer 2001;42(3):873-7.

Huang JJ, Keskkula H, Paul DR. Polymer 2004;45(12):4203-15.

Hunter DL, *Personal Communication*.

Kawasumi M, Kohzaki M, Kojima Y, Okada A, Kamigaito O. United States Patent 4810734; 1989. [Assigned to Toyota Motor Co., Japan]

Keller A, Kolnaar HWH. Materials Science and Technology 1997;18(Processing of Polymers):189-268.

Kim MH, Park CI, Choi WM, Lee JW, Lim JG, Park OO, Kim JM. Journal of Applied Polymer Science 2004;92(4):2144-50.

Kobayashi T, Takahashi T, Monma T, Kurosaka K, Arai T. WO Patent 9731973; 1997. [Assigned to (E. I. Du Pont de Nemours & Co., USA; Kunimine Industries Co., Ltd.).]

Kojima Y, Usuki A, Kawasumi M, Okada A, Kurauchi T, Kamigaito O. J Polym Sci, Part A: Polym Chem 1993;31(7):1755-8.

Kojima Y, Usuki A, Kawasumi M, Okada A, Kurauchi T, Kamigaito O. J Appl Polym Sci 1993;49(7):1259-64.

Koros WJ, Paul DR, Rocha AA. Journal of Polymer Science, Polymer Physics Edition 1976;14(4):687-702.

Kovarova L, Kalendova A, Malac J, Vaculik J, Malac Z, Simonik J. Annual Technical Conference - Society of Plastics Engineers 2002;60th(Vol. 2):2291-5.

Krishanmoorti R, Giannelis EP. Polym Mater Sci Eng 1996;75:46-7.

Krishnamoorti R, Ren J, Silva AS. J Chem Phys 2001;114(11):4968-73.

Krishnaswamy RK, *Personal communication*.

Krishnaswamy RK. Journal of Polymer Science, Part B: Polymer Physics 2000;38(1):182-93.

Krishnaswamy RK, Lamborn MJ. Polymer Engineering and Science 2000;40(11):2385-96.

Krishnaswamy RK, Sukhadia AM. Journal of Plastic Film & Sheeting 2005;21(2):145-58.

La Mantia FP, Lo Verso S, Dintcheva NT. Macromolecular Materials and Engineering 2002;287(12):909-14.

Lan T, Pinnavaia TJ. Chem Mater 1994;6(12):2216-19.

Laraba-Abbes F, Ienny P, Piqules R. Kautschuk Gummi Kunststoffe 1999;52(3):209-14.

Lee DC, Jang LW. J Appl Polym Sci 1996;61(7):1117-22.

Lee DC, Jang LW. J Appl Polym Sci 1998;68(12):1997-2005.

Lee H-s, Fasulo PD, Rodgers WR, Paul DR. Polymer 2005;46(25):11673-89.

Li X, Wang C-y, Fang L, Liu L-z. Harbin Ligong Daxue Xuebao 2003;8(2):90-3.

Lincoln DM, Vaia RA, Sanders JH, Phillips SD, Cutler JN, Cerbus CA. Polym Mater Sci Eng 2000;82:230-1.

Liu L, Qi Z, Zhu X. J Appl Polym Sci 1999;71(7):1133-38.

Madejova J, Bujdak J, Gates WP, Komadel P. Clay Minerals 1996;31(2):233-41.

Madejova J, Bujdak J, Petit S, Komadel P. Clay Minerals 2000;35(5):739-51.

Maiti P, Yamada K, Okamoto M, Ueda K, Okamoto K. Chemistry of Materials 2002;14(11):4654-61.

Matayabas Jr. JC, Turner SR. In: Polymer-clay nanocomposites, T.J. Pinnavaia and G.W. Beall, editors. Wiley: New York: 2000. p. 207.

Messersmith PB, Giannelis EP. J Polym Sci, Part A: Polym Chem 1995;33(7):1047-57.

Nielsen LE. J Macromol Sci, Part A 1967;1(5):929-42.

Okada A, Fukushima Y, Kawasumi M, Inagaki S, Usuki A, Sugiyami S, Kurauchi T, Kamigaito O. United States Patent 4739007; 1988. [Assigned to Toyota Motor Co., Japan]

Osman MA, Ploetze M, Suter UW. J Mat Chem 2003;13(9):2359-66.

Paul DR, Zeng QH, Yu AB, Lu GQ. Journal of Colloid and Interface Science 2005;292(2):462-8.

Pazur RJ, Purd'homme RE. Macromolecules 1996;29(1):119-28.

Perry D, Ward WJ, Cussler EL. Journal of Membrane Science 1989;44(2-3):305-11.

Register RA, *Personal communication*.

Rose J. Modern Plastics 2001;(October 2001):37.

Shah RK, Hunter DL, Paul DR. Polymer 2005;46(8):2646-62.

Shah RK, Paul DR. Polymer 2004;45(9):2991-3000.

Sinha Ray S, Okamoto M. Progress in Polymer Science 2003;28(11):1539-641.

Stackhouse S, Coveney PV. Journal of Physical Chemistry B 2002;106(48):12470-7.

Start PR, Mauritz KA. Journal of Polymer Science, Part B: Polymer Physics 2003;41(13):1563-71.

Stretz HA, Paul DR, Cassidy PE. Polymer 2005;46(11):3818-30.

Stretz HA, Paul DR, Li R, Keskkula H, Cassidy PE. Polymer 2005;46(8):2621-37.

Tang Y, Hu Y, Wang J, Zong R, Gui Z, Chen Z, Zhuang Y, Fan W. Journal of Applied Polymer Science 2004;91(4):2416-21.

Tanoue S, Utracki LA, Garcia-Rejon A, Tatibouet J, Cole KC, Kamal MR. Polymer Engineering and Science 2004;44(6):1046-60.

Tant MR, Mauritz KA, Wilkes GL, Editors. *Ionomers: Synthesis, Structure, Properties and Applications*. 1997. 514 pp.

Theng BKG, Hayashi S, Soma M, Seyama H. Clays and Clay Minerals 1997;45(5):718-23.

Torkelson JM, Lebovitz A, Kasimatis K, Khait K. US Patent 2003-701067, 2005096422; 2005. [Assigned to (Material Sciences Corporation, USA)]

Torkelson JM, Lebovitz AH, Kasimatis K, Khait K. WO Patent 2003-US34892, 2004043663; 2004. [Assigned to (Material Sciences Corporation, USA)]

Usuki A, Koiwai A, Kojima Y, Kawasumi M, Okada A, Kurauchi T, Kamigaito O. J Appl Polym Sci 1995;55(1):119-23.

Usuki A, Kojima Y, Kawasumi M, Okada A, Fukushima Y, Kurauchi T, Kamigaito O. J Mater Res 1993;8(5):1179-84.

Vaia RA, Ishii H, Giannelis EP. Chem Mater 1993;5(12):1694-6.

Vaia RA, Price G, Ruth PN, Nguyen HT, Lichtenhan J. Appl Clay Sci 1999;15(1-2):67-92.

Van Olphen H. *An introduction to clay colloid chemistry: for clay technologists, geologists, and soil scientists*. 2nd ed. 1977, New York: Wiley. xviii, 318.

VanderHart DL, Asano A, Gilman JW. Macromolecules 2001;34(12):3819-22.

VanderHart DL, Asano A, Gilman JW. Chem Mater 2001;13(10):3796-809.

Wang Z, Pinnavaia TJ. Chem Mater 1998;10(12):3769-71.

Wang ZM, Chung TC, Gilman JW, Manias E. Journal of Polymer Science, Part B: Polymer Physics 2003;41(24):3173-87.

Weimer MW, Chen H, Giannelis EP, Sogah DY. J Am Chem Soc 1999;121(7):1615-6.

Williams J, Purnell JH, Ballantine JA. Catalysis Letters 1991;9(1-2):115-19.

Winey KI, *Personal communication*.

Xie W, Gao Z, Liu K, Pan WP, Vaia R, Hunter D, Singh A. Thermochimica Acta 2001;367-368:339-50.

Xie W, Gao Z, Pan W-P, Hunter D, Singh A, Vaia R. Chem Mater 2001;13(9):2979-90.

Yang C, Smyrl WH, Cussler EL. Journal of Membrane Science 2004;231(1-2):1-12.

Yano K, Usuki A, Okada A, Kurauchi T, Kamigaito O. J Polym Sci, Part A: Polym Chem 1993;31(10):2493-8.

Yoon PJ, Fornes TD, Paul DR. Polymer 2002;43(25):6727-41.

Yoon PJ, Hunter DL, Paul DR. Polymer 2003;44(18):5341-54.

Yoon PJ, Hunter DL, Paul DR. Polymer 2003;44(18):5323-39.

Zhang Wa, Chen D, Zhao Q, Fang Ye. Polymer 2003;44(26):7953-61.

Zhong Y, De Kee D. Polymer Engineering and Science 2005;45(4):469-77.

Zhu J, Morgan AB, Lamelas FJ, Wilkie CA. Chemistry of Materials 2001;13(10):3774-80.

Internet references:

DIPPR, 801 database. (http://dippr.byu.edu/)

Technical Information (http://www2dupontcom/Surlyn/en_US/uses_apps), E. I. du Pont de Nemours and Company.

Vita

Rhutesh Kishorkant Shah was born in Cincinnati, Ohio on November 8, 1971 to Kishorkant and Prafulbala Shah. He received his Bachelors degree in Chemical Engineering from Gujarat University, India in 1994. Soon thereafter, he joined the Department of Chemical Engineering at Michigan State University as a graduate student where he conducted research on environment friendly biodegradable polymers. In 1996, after completing his M.S. education, he joined the Polymers and Materials Division of Phillips Petroleum Company in Bartlesville, Oklahoma as a Research and Development Engineer. In the year 2000, following a merger between Phillips Petroleum Company and Chevron Corporation, he was moved to the newly formed Chevron Phillips Chemical Company as a Program Leader. He resigned from this position in August 2001 to reenter graduate school at The University of Texas at Austin.

Permanent address: 10307 Morado Cove, #204
Austin, TX 78759

This dissertation was typed by the author.